

Diss. ETH No. 17058

Reliability Considerations of Future Energy Systems: Multi-Carrier Systems and the Effect of Energy Storage

A dissertation submitted to the
SWISS FEDERAL INSTITUTE OF TECHNOLOGY
ZURICH

for the degree of
Doctor of Technical Sciences

presented by
GAUDENZ ALESCH KOEPPPEL
Dipl. El.-Ing. ETH
born May 28, 1976
citizen of Germany and Switzerland

accepted on the recommendation of
Prof. Dr. Göran Andersson, examiner
Prof. Dr. Arne Holen, co-examiner

2007

Preface

This thesis documents the results of my research performed at the Power Systems Laboratory of the Swiss Federal Institute of Technology (ETH) Zurich from September 2002 to the end of 2006.

First of all I would like to express my gratitude to Prof. Dr. Göran Andersson for giving me the opportunity to write my thesis as a member of his research group. I am particularly grateful both for his patience and flexibility as well as for the granted freedom to also explore thesis-unrelated areas of energy systems.

Special thanks go to Prof. Dr. Arne Holen for being the co-examiner of my thesis. I additionally want to thank him for the hospitality I always experienced during my visits in Trondheim.

I very much appreciated the various inspiring and motivating discussions with Magnus Korpås from Trondheim. I want to thank him both for proofreading part II of my thesis as well as for introducing me to various aspects of Norwegian culture.

The opportunity to assist the lectures of Dieter Reichelt was a welcome diversion from my research and I got to learn many new things. I very much enjoyed this collaboration.

I also want to thank my officemates Thilo Krause and Turhan Demiray and all my colleagues and friends for various enjoyable discussions, dinners and board game evenings.

Finally and most of all I thank my family for their interest, patience and support.

Contents

Preface	iii
List of Acronyms	xi
Abstract	xiii
Kurzfassung	xv
1 Introduction	1
1.1 Background and Motivation	1
1.2 Contributions	4
1.3 Outline of the Thesis	5
1.4 List of Publications	6
I Reliability Modelling of Multi-Carrier Energy Systems	7
2 Modelling of Multi-Carrier Energy Systems	9
2.1 Introduction	9
2.2 The Energy Hub Modelling Concept	11
3 Reliability Modelling of Multi-Carrier Energy Systems	15
3.1 Modelling Basics and Assumptions	15
3.1.1 Component modelling	16
3.1.2 Introductory example	17
3.2 Output Availability as a Function of the Hub Components	21

3.2.1	Failure and repair rate matrices	22
3.2.2	Derivation of a general calculation procedure . .	23
3.2.3	Procedure for determining the expected reliability of supply	26
3.2.4	Application example	27
3.3	Reliability Models for a Complete Energy Hub	30
3.3.1	Expected reliability of supply	30
3.3.2	Expected energy not supplied (EENS)	36
3.3.3	Application example continued	42
3.4	Discussion of Special Cases	48
3.4.1	Several converters for one coupling	48
3.4.2	Impact of the supplying infrastructures	50
3.5	An Alternative Approach Using Kronecker Products and Sums	51
4	Modelling the Impact of Energy Storage on the Relia- bility of Supply	57
4.1	Markov Approach for Energy Storage Devices	57
4.1.1	Markov properties	59
4.1.2	Failure and repair rates of a storage device . . .	59
4.1.3	Modelling conditions	61
4.1.4	The discrete storage model	63
4.1.5	Sensitivity of the model to the level of discretisation	64
4.1.6	Using the storage for peak loads	70
4.2	Extended Reliability Model for Multi-Carrier Energy Sys- tems	71
4.2.1	Reliability model with storage for back-up	72
4.2.2	Application example	81
4.2.3	Reliability model with storage for back-up and peak supply	83
4.3	Application Example	90
5	Sensitivity Analyses and Conclusion	101
5.1	Sensitivity Analyses	101

5.1.1	Model specific sensitivities	102
5.1.2	Hub specific sensitivities	108
5.2	Directions for Further Work	112
5.3	Conclusion	113

II Improving Network Infeed Reliability of Non-Dispatchable Generators Using Energy Storage 115

6	Combining Non-Dispatchable Generators with Energy Storage Devices 117
6.1	Introduction 117
6.2	System Layout 120
7	A Generalised Model for Time Series Analyses 123
7.1	Algorithm 123
7.2	Initialisation 125
7.3	Calculation of Forecast 125
7.3.1	Using output power measurement data 126
7.3.2	Using energy source measurement data 128
7.3.3	Time dependent forecast errors 129
7.4	Definition of Infeed Profile 131
7.4.1	Considering non-ideal energy storage devices . . 131
7.4.2	Incorporating the charge level in the planning . . 133
7.4.3	Defining the usage factor 134
7.5	Operation of the Energy Storage 139
8	Analysis Methods 143
8.1	Infeed Fulfilment 143
8.2	Conversion Losses 145
8.3	Infeed Accuracy 146

9	Case Studies	147
9.1	Outline of the Case Studies	147
9.2	Photovoltaic System	148
9.2.1	Characteristics of the time series and definition of the simulation parameters	148
9.2.2	Determination of energy and power capacity	148
9.2.3	Simulations with a perfect forecast	150
9.2.4	Simulations with an imperfect forecast	159
9.2.5	Case study summary	164
9.3	Wind-Turbine System	165
9.3.1	Characteristics of the time series and definition of the simulation parameters	165
9.3.2	Determination of energy and power capacity	166
9.3.3	Simulations with a perfect forecast	168
9.3.4	Simulations with an imperfect forecast	170
9.3.5	Case study summary	182
10	Discussion and Conclusion	185
10.1	Value of the Energy Storage Device	185
10.2	Incorporating Price Signals	189
10.3	Relevance of Time Series Models	195
10.4	Conclusion	200
A	Basic Concepts of Reliability Modelling	205
A.1	Reliability Block Diagrams	205
A.1.1	Series systems	206
A.1.2	Parallel systems	207
A.1.3	Combinations of series and parallel systems	207
A.1.4	Standby redundant systems	209
A.2	Markov Processes	210
A.2.1	Failure and repair rates	212
A.2.2	Transition rate matrix	214

A.2.3 Larger systems	215
B Kronecker Products and Sums	219
C Characteristics of Energy Storage Devices	223
Bibliography	231
Curriculum vitae	233

List of Acronyms

CCGT	Combined Cycle Gas Turbine
CHP	Combined Heat and Power
EENS	Expected Energy Not Supplied
EES	Expected Energy Supplied
EIF	Energy Index of Fulfilment
EIR	Energy Index of Reliability
EIU	Energy Index of Unreliability
EWMA	Exponentially Weighted Moving Average
MCES	Multi-Carrier Energy System
MTTF	Mean Time To Failure
MTTR	Mean Time To Repair
PV	Photovoltaic
RMSE	Root Mean Square Error
UCTE	Union for the Co-ordination of Transmission of Electricity

Abstract

This thesis addresses two different reliability aspects of future energy systems, compiled in two different parts.

Part I of the thesis focuses on reliability calculations in multi-carrier energy systems, i.e. energy systems comprising not only electrical energy but also e.g. chemical and thermal energy. A model for reliability analysis is proposed, based on the energy hub modelling concept, suitable for analysing several energy systems simultaneously. With this model expected reliability of supply and expected energy not supplied, optionally considering load shedding can be calculated. Furthermore, the model can be applied both for systems without energy storage devices and for systems including energy storage devices. To include energy storage devices into the reliability model, a Markov model for energy storage devices was developed. The model allows to use the storage both for back-up supply as well as for peak load supply.

The multi-carrier reliability model is verified with alternative reliability calculation methods. Furthermore, the applicability of the storage model and the complete multi-carrier reliability model is demonstrated with several examples and sensitivity analyses.

Major findings are that interconnections between the different energy carriers are beneficial, in particular for reducing expected energy not supplied. This is true for all involved energy carriers, as long as the ratings of the loads and installed components are similar. Otherwise, the systems with larger ratings improve the reliability characteristics of the other energy carriers, however these systems do not benefit from the interconnections.

Part II of the thesis addresses the network infeed reliability of non-dispatchable generators, in particular photovoltaic and wind based systems. A major issue with the generation from renewable energy sources is the limited accuracy of the production forecasts. It is proposed to combine the non-dispatchable generator with an energy storage device at the point of network infeed, with the purpose of the energy storage device to compensate deviations between forecasted and actual generation. This measure is supposed to increase both the reliability of the infeed forecast and the value of the generator.

A time series based modelling procedure is proposed, suited for application with measurements from different types of non-dispatchable generators. This modelling procedure is applied in two case studies, using measurement data from a 500 kW photovoltaic installation as well as using wind speed measurements of a 2 MW wind turbine. The performance of the systems is analysed with a set of proposed analysis procedures. Both case studies show the applicability of the proposed methods. Moreover, both case studies identify that energy storage devices can considerably improve the network infeed reliability. The required energy capacities depend on the rated output of the generator and are thus comparatively high in the case of the wind turbine.

For the simulation of different forecast error magnitudes, both constant and forecast horizon dependent, a new approach for forecast simulations was chosen and successfully implemented. In addition, a procedure for determining the value of the energy storage device is proposed, based on reduced balancing penalties incurred. Furthermore, it is shown that price signals can be included to shift the infeed to high price periods. Closing, the validity of time series analyses is discussed.

Kurzfassung

Diese Dissertation widmet sich in zwei Teilen unterschiedlichen Aspekten der Zuverlässigkeit in zukünftigen Energieversorgungssystemen.

Teil I der Dissertation befasst sich mit Verfügbarkeitsberechnungen in Energieversorgungssystemen, die neben elektrischer Energie auch chemische und thermische Energie übertragen und verteilen. Basierend auf dem Energy Hub Ansatz, der die gleichzeitige Analyse mehrerer Energieträger ermöglicht, wird ein Verfahren zur Berechnung der Verfügbarkeit entwickelt. Mit diesem Zuverlässigkeitsmodell können die erwartete Versorgungszuverlässigkeit sowie die erwartete Menge nicht-versorgter Energie berechnet werden. Zudem können Energiesysteme modelliert werden, die Energiespeicher beinhalten. Zu diesem Zweck wurde ein Markov-basiertes Modell für Energiespeicher entwickelt, wobei der Speicher sowohl als Back-up – zur Überbrückung bei Zuleitungsausfällen – wie auch zur Abdeckung von Spitzenlasten eingesetzt werden kann.

Die Anwendung des Zuverlässigkeitsmodells sowie nur des Speichermodells wird mit verschiedenen Beispielen und Sensitivitätsanalysen demonstriert. Zudem wird die korrekte Funktionsweise des kompletten Modells mit alternativen Berechnungsmethoden schrittweise verifiziert.

Neben der demonstrierten Anwendbarkeit der Modelle ist eine weitere Erkenntnis, dass Konversionen zwischen den verschiedenen Energieträgern einen positiven Einfluss auf die Versorgungsverfügbarkeit haben, insbesondere zur Reduzierung der erwarteten Menge nicht-versorgter Energie. Wenn die jeweiligen Lasten und installierten Übertragungsleistungen ähnlich dimensioniert sind, gilt diese Erkenntnis für alle drei betrachteten Energiesysteme. Vergleichsweise grösser dimensionierte Systeme profitieren zwar nicht von den Verbindungen zu den anderen Energieträgern, beeinflussen jedoch deren Zuverlässigkeit positiv.

Teil II der Dissertation befasst sich mit der Zuverlässigkeit der Netzeinspeisung durch nicht-steuerbare Erzeuger, insbesondere durch Photovoltaikanlagen und Windturbinen. Ein wichtiger Aspekt bei der Erzeugung aus erneuerbaren Energiequellen ist die Ungenauigkeit der Netzeinspeisungsprognosen. Es wird deshalb vorgeschlagen, den nicht-steuerbaren Erzeuger am Einspeiseknoten mit einem Energiespeicher zu kombinieren. Dabei hat der Energiespeicher die Aufgabe, Differenzen zwischen der prognostizierten und der effektiven Einspeisung zu kompensieren. Die Zuverlässigkeit der Einspeiseprognose sowie der Wert des Erzeugers erhöhen sich durch diese Massnahme.

Zu diesem Zweck wird ein Zeitreihen-basiertes Model vorgeschlagen, welches sich auf verschiedene Typen von nicht-steuerbaren Erzeugern anwenden lässt. Der Algorithmus wird in zwei Fallstudien angewendet, mit Messdaten von einer 500 kW Photovoltaikanlage sowie mit Windgeschwindigkeitsmessungen an einer 2 MW Windturbine. Das Verhalten der Systeme wird mit einer Reihe vorgeschlagener Indizes analysiert und bewertet. Beide Fallstudien demonstrieren die Anwendbarkeit der vorgeschlagenen Methoden. Ausserdem resultiert aus beiden Fallstudien, dass Energiespeicher die Zuverlässigkeit der Netzeinspeisung deutlich erhöhen können. Die dazu nötigen Energiekapazitäten hängen von der installierten Leistung der Generatoren ab und sind deshalb im Fall der Windturbine beträchtlich.

Zur Simulation verschiedener Prognosefehler, sowohl konstanter wie auch Zeithorizont-abhängiger Art, wird ein neuer Ansatz entwickelt und erfolgreich implementiert. Des Weiteren wird eine Methode zur monetären Bewertung des Speichers vorgeschlagen, basierend auf eingesparten Regenergiekosten. Ausserdem wird die Verwendung von Preiskurven diskutiert, zur Konzentration der Netzeinspeisung auf Stunden mit höheren Preisen. Schliesslich wird die Relevanz und Aussagekraft von Zeitreihenanalysen diskutiert.

Chapter 1

Introduction

1.1 Background and Motivation

Most of today's energy infrastructures evolved during the second half of the 20th century. The then available power station technology showed significant economies of scale, which is why it was often cost-efficient to commission particularly large, centrally located power stations. Network infrastructures were designed accordingly, such that the generated electricity could be transmitted and distributed with little losses to the end-user. The appropriate level of reliability of supply was guaranteed through the hierarchic and redundant layout of the network and by maintaining an appropriate spinning reserve on the production side. Along with the centrally coordinated dispatching, these operation concepts resulted in the required availability of supply at the customer.

In recent years however, circumstances and operating conditions have been changing and it is arguable whether the established topologies and procedures are suitable for keeping the desired level of reliability of supply. The apparent changes and trends are of regulatory, technical and economic nature, resulting in different new conditions both on the production side as well as on the transmission and distribution and on the consumer side.

Some of these changes have been triggered by the regulatory decision to liberalise electricity markets in different parts of the world. It is a fundamental requirement for the liberalisation of electricity markets and

for a fair competition to establish that all interested parties can participate on the market. Thus, the guaranteed and unrestricted third-party network access is implied in the regulatory framework of the individual market concepts. Realising the right to participate became possible because of various developments in the area of generation technologies. On the one hand, so-called microturbines have matured, with a power spectrum ranging from a few kW up to some hundred kW, meant for individual homes and smaller businesses. Microturbines convert natural gas into electrical and thermal energy and provide its owners the possibility to self-supply demand and to feed any surplus generation back into the network whenever appropriate [1].

On the other hand, important developments took place in the area of the so-called combined-cycle gas-turbine (CCGT) technology. CCGTs convert gas into electricity and heat with overall efficiencies of up to 60%, their power spectrum ranging from some dozens of MW up to several hundred MW. This technology is particularly characterised by low economies of scale and enables thus municipal utilities or industrial companies to participate on the market at justifiable conditions [2, 3]. Compared with conventional large-scale thermal power stations such as nuclear, CCGTs have quite short authorisation and construction times and are also discussed as alternatives when eventually replacing ageing thermal power stations. Altogether, the guaranteed third-party access, facilitating an increasing amount of gas-fired power stations, indirectly leads to an increasing dependency on gas infrastructures.

The question can be raised if and to what extent a dependence and interchangeability between the electricity and the gas infrastructures establish and whether load peaks will be transferred between both networks. Negative effects of such a situation were already experienced in the past winter 2005/06 in the United Kingdom [4]: because of extraordinary low temperatures, a gas supply shortage occurred, resulting in high electricity prices [5]. Nevertheless, the possibility to supply a load directly or indirectly (through conversion) from other independent supply systems offers redundancy effects. The influence of these redundancy effects on the reliability of supply will be subject of the first part of this thesis.

Besides thermal power stations, technologies for the conversion of energy from renewable sources have matured, in particular wind-turbines and photovoltaic systems. The commissioning of such systems became feasible particularly because of governmental subsidy programs, estab-

lished for low emission policies and environmental concerns [6], but also enabled because of the third-party access rule.

The major difficulty with energy from wind and sun is the predictability of their production and their network infeed. Large wind parks are being planned and built in coastal and remote locations with good wind conditions but often comparatively low loads. Long-distance load flows are resulting because energy from remote wind power production areas has to be transported to regions with a high electricity demand.

As a consequence of the limited predictability of the production from wind-turbines, unexpected network loading and even congestions can establish. Particularly photovoltaic systems are installed in lower voltage level networks, resulting in power flows and directions not considered when the networks were built, requiring adapted protection schemes [7]. Wind-turbines on the other hand initiate power flows in high voltage level networks, the reason why the 2005 annual report of the UCTE (Union for the Co-ordination of Transmission of Electricity) identifies wind-power as a major challenge of coming years [8].

The difficulty of wind speed forecasts is particularly the timing of wind speed changes and requires the network operator to have back-up generation at hand for compensating forecast errors. Hence, generators are operating in throttled or no-load mode to quickly come online to maintain the power balance in the network, hence guaranteeing the required level of reliability. Ideally however, the infeed accuracy or reliability of non-dispatchable generators would be optimised prior to the network infeed. In order to identify the possibilities and limitations of using energy storage devices for this purpose, the second part of this thesis investigates different types of non-dispatchable generators and the requirements for increasing their network infeed accuracy.

This dissertation thus investigates two aspects of reliability in future energy systems. One aspect is the influence of the increased interdependence between energy carriers, as a consequence of more local conversions, in particular gas-fired power stations, on the reliability of supply. The other aspect concerns the generation side, where the infeed reliability of non-dispatchable generators is investigated and the opportunities offered by energy storage options. Both aspects concern reliability aspects of future energy systems but focus and applied models are different. They are therefore dealt with in individual parts, both containing specific introductions into the respective fields.

1.2 Contributions

In the area of multi-carrier energy systems, the main contributions can be identified as follows:

- A model is proposed for the analysis of reliability of supply in multi-carrier energy systems. The algorithm allows to determine reliability of supply and expected energy not supplied as functions of the existing conversions and their reliability characteristics. The method is suited for numerical and symbolical applications, and it can be integrated in an optimal power flow algorithm, optimising for reliability of supply.
- A Markov model for energy storage devices is proposed, suitable for storage devices providing back-up as well as peak supply. The model is integrated into the reliability model for multi-carrier energy systems, giving a comprehensive reliability calculation method.
- Examples are discussed, identifying the influence of distinct conversions and connections.

In the area of non-dispatchable generators combined with energy storage devices, the following contributions can be identified:

- A model for time series analyses is proposed and applied, suitable for any type of non-dispatchable generator. The procedure contains a new approach for the simulation of different forecast errors, helping to identify the relation between forecast error magnitude and infeed accuracy.
- New insights concerning the feasibility of using energy storage for increasing the infeed accuracy of non-dispatchable generators are found and discussed.
- Potential income improvements from using the energy storage and the validity of time series based methods for the analysis of wind and solar based generation are discussed.

1.3 Outline of the Thesis

The thesis is divided into the following sections, with separate introductions for each parts.

Part I: Reliability Modelling of Multi-Carrier Energy Systems

Chapter 2 contains the introduction to part I and to the modelling of multi-carrier energy systems. The energy hub modelling concept is introduced, suited for various studies in multi-carrier energy systems.

Chapter 3 presents the detailed reliability model, based on the approach discussed in chapter 2. The developed tool can be used for calculations of availability and of expected energy not supplied.

Chapter 4 extends the reliability model with procedures for modelling the influence of energy storage possibilities.

Chapter 5 is the last chapter of part I containing sensitivity analyses and the conclusion for part I.

Part II: Improving Network Infeed Reliability of Non-Dispatchable Generators Using Energy Storage

Chapter 6 introduces the subject of combining non-dispatchable generators with energy storage devices and outlines the investigation framework and target.

Chapter 7 presents the general modelling approach and discusses algorithm elements in detail.

Chapter 8 presents several analysis methods used for evaluating the simulation results and for determining different sensitivities.

Chapter 9 contains two case studies using the simulation and analysis methods presented in chapters 7 and 8.

Chapter 10 contains the discussion of various aspects of the model and the case studies as well as the conclusion for part II of the thesis.

Appendix A introduces reliability modelling concepts.

Appendix B gives an overview of Kronecker products and sums.

Appendix C briefly discusses the general charge and discharge modelling approach for energy storage devices.

1.4 List of Publications

1. G. Koepfel: *Distributed Generation - Literature Review and Outline of the Swiss Situation*,
Technical report, Power Systems Laboratory, Zurich, Nov 2003
2. G. Koepfel, M. Geidl and G. Andersson: *Value of Storage Devices in Congestion Constrained Distribution Networks*,
Proceedings of the 4th IEEE International Conference on Power System Technology, PowerCon 2004, Singapore, 21-24 Nov 2004
3. G. Koepfel et al.: *Die Vision eines zukünftigen Energieversorgungsnetzwerkes* ,
Bulletin SEV/AES 19/05, Zurich, 2005
4. G. Koepfel and M. Korpås: *Using Storage Devices for Compensating Uncertainties Caused by Non-Dispatchable Generators*,
Proceedings of the 9th International Conference on Probabilistic Methods Applied to Power Systems, PMAPS 2006, Stockholm, Sweden, 11-15 June 2006
5. G. Koepfel and G. Andersson: *The Influence of Combined Power, Gas, and Thermal Networks on the Reliability of Supply*,
Proceedings of the 6th International World Energy System Conference, WESC 2006, Turin, Italy, 10-12 July 2006
6. G. Koepfel and M. Korpås: *Increasing the Network In-feed Accuracy of Wind Turbines with Energy Storage Devices*,
Proceedings of the 6th International World Energy System Conference, WESC 2006, Turin, Italy, 10-12 July 2006

Part I

RELIABILITY MODELLING OF MULTI-CARRIER ENERGY SYSTEMS

Chapter 2

Modelling of Multi-Carrier Energy Systems

This chapter contains the introduction for part I, giving an overview of the modelling of multi-carrier energy systems. Energy systems comprising electrical, chemical and thermal energy are discussed and a short overview of conversion technologies is given. Following, a conceptual approach for the combined modelling of multi-carrier energy systems is presented, serving as the basis for the remainder of part I.

2.1 Introduction

Traditionally, the infrastructures for the supply of electrical, chemical and thermal energy have been treated separately. In most cases, both the topologies and the operation strategies have been developed independently of one another and in some regions or cities, they are also maintained by individual companies. Various developments, however, indicate an increasing mutual dependence and competition between these three infrastructures. This trend is particularly driven by the increasing number of gas-fired power stations, converting natural gas into electricity and thermal energy [9]. Different technologies exist, both for small-scale and large-scale applications, indicating possible interdependencies of the energy carriers on transmission and distribution levels.

The technology for small-scale applications, starting in the few kW range – thus suited for individual houses and small offices – is yet maturing, whereas the technology for large-scale applications with up to several hundred MW of installed capacity is already well established [9]. Particularly the combined cycle gas turbines (CCGT) play a major role in this context, installations being discussed and already taking place in various countries. The technology of CCGTs allows building medium-sized power stations that are at least as cost-efficient as conventional thermal and hydro power stations with their large economies of scale [9]. The comparatively shorter construction and amortisation times as well as their higher operational flexibility is often also claimed to technologically having made possible the liberalisation of the power markets [10].

Gas-fired power stations basically establish a coupling between the chemical and the electrical infrastructures, resulting in a certain interchangeability and redundancy between these two energy carriers. At certain times it might be financially attractive to generate electricity from gas instead of consuming directly from the electrical network, e.g. during peak hours. Or there could be situations, where it is favourable to make use of the short-term storage flexibility, inherent in the gas network. Hence, it is likely that peaks from the electrical network will be migrated to the gas network, resulting in a more intensively and differently used gas network. If, at some point in the future, a hydrogen economy would establish, fuel cells would provide the equivalent coupling, with electrolysers establishing even a bidirectional coupling between electrical and chemical energy. Similar interdependencies can be identified between electrical and thermal networks as well as between chemical and thermal networks, when considering e.g. hot water boilers or combined heat and power (CHP) conversions.

Consequently, investigations concerning new and future energy systems should integrate electrical as well as chemical and thermal energy. The usefulness of such a combined or integrated analysis has already been recognised in a few recent publications [11, 12, 13, 14, 15, 16], focusing mostly on energy flow optimisation aspects and on modelling similarities. However, besides potential economic benefits from a combined power flow optimisation, a major benefit can be identified in the area of reliability of supply. A gas-fired power station or an electrical boiler does not only introduce an interdependence between two energy systems. Because of the coupling established by the converter, the load

can be supplied from several independent infrastructures, which is beneficial in terms of redundancy.

The first part of the thesis presents and discusses a method, which has been developed for the analysis of the reliability of supply in multi-carrier energy systems. The method allows to determine the reliability of supply as a function of the reliability characteristics of the existing conversions. It will be used to investigate the potential benefits of the redundancy effects and to what extent they influence the availability of supply. Furthermore, the method is applied to analyse whether a certain overall reliability of supply can be maintained despite less favourable reliability characteristics of particular components. Such investigations are important both for maintenance considerations – assuming the maintenance frequency to affect the reliability characteristics – and for discussions concerning the benefit of distributed generation.

The next section introduces a conceptual modelling approach suited for multi-carrier energy systems. The subsequent chapter 3 is based on this approach, introducing a method for reliability analyses in multi-carrier energy systems. Chapter 4 discusses a Markov approach for reliability modelling of energy storage devices, used to complement the model from chapter 3. The last chapter of this part (chapter 5) presents sensitivity analyses, performed with the developed methods. The conclusion for part I is included in this chapter as well.

2.2 The Energy Hub Modelling Concept

The term 'multi-carrier energy system' can be applied for any energy system containing more than one energy carrier, from oil to wood chips or compressed air. Throughout this thesis however, the term is used to refer to systems exclusively containing electrical, chemical and thermal energy carriers. These are the energy carriers consumed by most end-users and – when looking at distributed generation technologies – they represent infrastructures with large mutual substitution potentials. Various conversion technologies exist, providing conversions between all three forms of energy. The following table 2.1 gives an informative but non-comprehensive overview of existing and upcoming conversion technologies.

From a system point of view, a unit like a gas-fired power station or an electric boiler is simply a converter, converting one form of energy

from \rightarrow to	electrical	chemical	thermal
electrical	power electronics converters transformer	electrolysis batteries	electric boiler heat pump
chemical	fuel cell CCGT	reformer	gas furnace fuel cell CCGT
thermal	thermovoltaics Stirling engine steam turbine	silicate storage	heat exchanger

Table 2.1: Overview of existing and upcoming conversion technologies.

into one or several other forms of energy. In this context it does not matter, with which technology a conversion is performed but simply that a conversion can take place. In order to have a simple formulation for these conversions, the so-called energy hub modelling concept has been developed [12, 17].

According to this modelling concept, any network participant is represented by the energy conversion it is performing. The general form of an energy hub is thus a multi-port, with several inputs and several outputs, representing the energy carriers. Between the ports, the different energy carriers are converted into each other, depending on the available converters. Figure 2.1 shows the general two-port form of an energy hub, with all possible conversions displayed, i.e. for example the expression 'e-c' representing the electrical-chemical conversion.

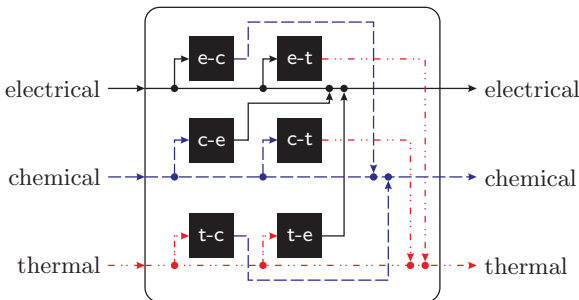


Figure 2.1: Standard representation of a two-port energy hub providing conversions between electrical, chemical and thermal energy.

The energy hub modelling concept has been developed primarily for optimisation of the involved energy flows. In this respect, the crucial characteristic representing the conversion is the efficiency of the conversion. The conversion of e.g. the electrical-chemical converter can then be described with the corresponding efficiency η_{ec} , relating the steady state chemical output load L_c with the electrical input power P_e :

$$L_c = \eta_{ec} \cdot P_e \quad (2.1)$$

Because of energy conservation laws, as discussed in [12], the conversion efficiency has to be multiplied with a so-called dispatch factor ν , which represents the topology. This dispatch factor satisfies $0 \leq \nu \leq 1$ and defines how the power flow from one input is distributed to the different converters. Without the dispatch factor, it could happen that the dispatching of the converters results in a power requirement exceeding the rated network capacities and the energy conservation laws would be violated. As an example, the chemical energy carrier can be used to both supply a gas-fired turbine and a further chemical load. The flow then is separated such that ν_c times the rated capacity serves the gas-fired turbine and $(1 - \nu_c)$ times the rated capacity supplies the load. Following this approach, the so-called coupling matrix \mathbf{C} can be defined, relating each input of the energy hub with each output. This matrix is shown in figure 2.2, corresponding to figure 2.1. The input energy carriers are assigned to the columns and the output carriers to the rows.

As outlined, the entries of the coupling matrix consist of the respective conversion efficiencies weighted with dispatch factors, as soon as one energy carrier is supplying more than one converter or output.

$$\begin{array}{c}
 \text{electrical} \\
 \text{chemical} \\
 \text{thermal}
 \end{array}
 \begin{array}{c}
 \text{electrical} \\
 \text{chemical} \\
 \text{thermal}
 \end{array}
 \begin{bmatrix}
 c_{ee} & c_{ce} & c_{te} \\
 c_{ec} & c_{cc} & c_{tc} \\
 c_{et} & c_{ct} & c_{tt}
 \end{bmatrix}$$

Figure 2.2: Coupling matrix for the energy hub from figure 2.1, providing conversions between electrical, chemical and thermal energy carriers.

The individual power flows P_α at the input of the hub, with α representing the respective energy carriers, can be defined as:

$$\vec{P} = \begin{bmatrix} P_e \\ P_c \\ P_t \end{bmatrix} \quad (2.2)$$

The subscripts 'e', 'c' and 't' stand for *electrical*, *chemical* and *thermal*, respectively. Accordingly, the output or loads L_α of the hub can be represented as:

$$\vec{L} = \begin{bmatrix} L_e \\ L_c \\ L_t \end{bmatrix} \quad (2.3)$$

The coupling matrix \mathbf{C} from figure 2.2 consequently allows relating or coupling both power vectors with each other [12]:

$$\vec{L} = \mathbf{C} \cdot \vec{P} \quad (2.4)$$

$$\begin{bmatrix} L_e \\ L_c \\ L_t \end{bmatrix} = \begin{bmatrix} c_{ee} & c_{ce} & c_{te} \\ c_{ec} & c_{cc} & c_{tc} \\ c_{et} & c_{ct} & c_{tt} \end{bmatrix} \cdot \begin{bmatrix} P_e \\ P_c \\ P_t \end{bmatrix}$$

The relation in equation (2.4) allows performing power flow analyses with given networks, optimising the consumption depending on the installed converters and e.g. price information for the individual energy carriers. It also allows optimisation of matrix elements for given loads and power flows, i.e. performing a structural or topological optimisation. Another useful property of the energy hub modelling approach is that all components in a network can be represented with it. Transmission lines for example do not directly perform a conversion but they are associated with certain transmission losses. They can consequently be represented with a transmission efficiency at the corresponding diagonal entry [12].

The subsequent chapters are based on the above energy hub modelling approach. However, instead of representing a network participant with its conversion efficiencies, it will be described with its reliability characteristics. Consequently, instead of optimal power flow calculations, the model will be used for availability calculations.

Chapter 3

Reliability Modelling of Multi-Carrier Energy Systems

In this chapter, a model is developed for the analysis and calculation of reliability aspects in multi-carrier energy systems. The chapter starts by introducing the basic reliability modelling approach and presents the perception of reliability within the energy hub framework. A simple example is used to develop the general modelling procedure. This modelling procedure is then generalized and stated for a general energy hub. The resulting method can be used for both analytical and numerical calculations and it can be used as target function for optimisations.

3.1 Modelling Basics and Assumptions

The most simple form of an energy hub is a load, which is supplied directly from the corresponding energy carrier and indirectly through a converter, converting energy from a second energy carrier. This results in redundancy effects for the load, assuming it can be supplied by either connection during certain periods. Because of this additional supply path, i.e. the converter, an increased level of reliability of supply can be expected intuitively. To analyse these expected benefits, a model is needed, considering the characteristics of the different energy carriers. So far however, only few studies on the subject of reliability modelling in multi-carrier energy systems have been published [14, 15]. Thus,

a method for the combined analysis of reliability aspects is proposed throughout this chapter, based on reliability models for power systems. Such models have been the subject of many books [18, 19, 20, 21] and various publications, summarised in structured bibliographies [22, 23, 24]. Chapter 5, containing the sensitivity analyses, will then apply the method and further outline and discuss the various advantages and disadvantages.

3.1.1 Component modelling

For the reliability analysis, it is assumed that all connections and converters within an energy hub can be represented as single units, no matter of how many processes they physically consist. All considered components are assumed to behave as stationary Markov processes (see appendix A.2¹) and each component is either in an operating state or in a failed state; intermediate or standby states are not considered. Furthermore, the components are repairable and as good as new after a repair. According to A.2, a component thus stays in the operating state until a failure occurs. The component then transits to the failed state, where it resides until it has been repaired, returning back to the operating state. This behaviour can be illustrated as in figure 3.1.

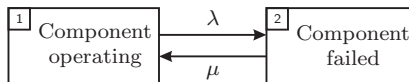


Figure 3.1: Representation of a single component with failure rate λ and repair rate μ .

According to figure 3.1, the transition from the operating state to the failed state happens with the so-called failure rate λ . The rate λ is defined as the reciprocal of the mean time to failure (MTTF). Analogously, the repairing takes place with the associated repair rate μ , being the reciprocal of the mean time to repair (MTTR). Both transition rates are usually expressed relative to the duration of a year. As outlined in appendix A, the steady-state probability R_1 of being in the operating

¹A short introduction to the main reliability models and procedures applied in this thesis is contained in appendix A, entitled 'Basic Concepts of Reliability Modelling'.

state – i.e. the availability of the component – is defined as:

$$R_1 = \frac{\mu}{\mu + \lambda} \quad (3.1)$$

The sum of all state probabilities is equal to 1 and hence the unavailability $Q = R_2$ – corresponding to the probability of residing in state 2 – must satisfy:

$$R_2 = 1 - R_1 = \frac{\lambda}{\mu + \lambda} \quad (3.2)$$

3.1.2 Introductory example

In the context of multi-carrier energy systems, conversions between two energy carriers result in a certain dependence but also provide the option to supply a load from either network. Figure 3.2 illustrates this with a small example.

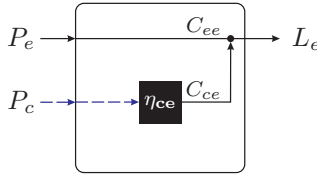


Figure 3.2: Example of an energy hub, corresponding to equation (3.3). The electrical load L_e is supplied directly through an electrical-electrical connection C_{ee} and indirectly through a chemical-electrical connection C_{ce} .

An electrical load is connected to the electrical infrastructure but it can also be supplied from a gas-fired turbine. This constellation can be represented with an energy hub and the associated coupling matrix, as shown in equation (3.3):

$$\mathbf{C} = \begin{bmatrix} \eta_{ee} & \eta_{ce} & 0 \\ 0 & 0 & 0 \\ 0 & 0 & 0 \end{bmatrix} \quad (3.3)$$

The capacity of the gas-fired turbine is designated as C_{ce} and associated with the conversion efficiency η_{ce} . Consequently, if the gas-fired turbine

is operating at the rated output, the demand from the chemical network P_c satisfies $P_c = C_{ce} \cdot \eta_{ce}^{-1}$. The electrical connection has a rated capacity of C_{ee} and is associated with the transmission efficiency η_{ee} . All other connections and lines are considered dimensionless and the supply lines are considered ideal. The load is supplied redundantly as long as the load demand satisfies $L_e \leq C_{ce}$ and $L_e \leq C_{ee}$.

Reliability block diagram approach

Using reliability block diagrams, as introduced in appendix A, this situation can be displayed as in figure 3.3. The term R_{ee} corresponds to the probability of an operating electrical connection and the term R_{ce} likewise corresponds to the probability of a working chemical-electrical connection. Assuming redundant supply, the availability of supply $R_{e_{out}}$ for the electrical output L_e then satisfies:

$$R_{e_{out}} = R_{ee} + R_{ce} - R_{ee}R_{ce} \quad (3.4)$$

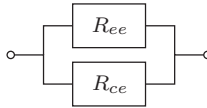


Figure 3.3: Reliability block diagram for the energy hub in figure 3.2.

As outlined, both the electrical line and the chemical-electrical converter are treated as one component each. Thus, failure and repair rates can be introduced, as depicted in the component models in figure 3.4.



Figure 3.4: Component models for the example in figure 3.2.

The availability of supply $R_{e_{out}}$ at the electrical output can now be determined as a function of the failure and repair rates of the associated components, using equations (3.1), (3.2) and (3.4):

$$\begin{aligned} R_{e_{out}} &= \frac{\mu_{ee}}{\mu_{ee} + \lambda_{ee}} + \frac{\mu_{ce}}{\mu_{ce} + \lambda_{ce}} - \frac{\mu_{ee}}{\mu_{ee} + \lambda_{ee}} \cdot \frac{\mu_{ce}}{\mu_{ce} + \lambda_{ce}} \\ &= \frac{\mu_{ee}\mu_{ce} + \mu_{ee}\lambda_{ce} + \lambda_{ee}\mu_{ce}}{(\mu_{ee} + \lambda_{ee})(\mu_{ce} + \lambda_{ce})} \end{aligned} \quad (3.5)$$

State space diagram approach

The same result can be obtained by combining the two components from figure 3.4 to construct the state space diagram of the supply situation (figure 3.5). The symbol '✓' represents an operating connection and '×' a failed state.

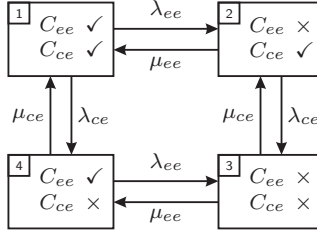


Figure 3.5: State space diagram for the example in figure 3.2.

Applying the technique described in appendix A.2.2 leads to the probabilities of residing in the respective states:

$$\begin{aligned}
 R_1 &= \frac{\mu_{ee}\mu_{ce}}{(\mu_{ee} + \lambda_{ee})(\mu_{ce} + \lambda_{ce})} \\
 R_2 &= \frac{\lambda_{ee}\mu_{ce}}{(\mu_{ee} + \lambda_{ee})(\mu_{ce} + \lambda_{ce})} \\
 R_3 &= \frac{\lambda_{ee}\lambda_{ce}}{(\mu_{ee} + \lambda_{ee})(\mu_{ce} + \lambda_{ce})} \\
 R_4 &= \frac{\mu_{ee}\lambda_{ce}}{(\mu_{ee} + \lambda_{ee})(\mu_{ce} + \lambda_{ce})}
 \end{aligned} \tag{3.6}$$

As long as at least one of both components is operating, the load can be supplied. The availability is thus found as the sum of the probabilities of residing in either state 1, 2 or 4, which is equal to equation (3.5):

$$R_{e_{out}} = R_1 + R_2 + R_4 \tag{3.7}$$

Variable load

The results obtained so far are valid as long as the load L_e stays below the rated capacities of both components C_{ee} and C_{ce} , respectively. If

this assumption does not hold true, the load demand $L_e(t)$ has to be compared with the installed capacities during every time interval t to determine whether a parallel or a series supply situation exists. Using the state space diagram from figure 3.5, the probability of supply can be determined rather straight forward.

Different supply scenarios are conceivable, assuming $C_{ee} > C_{ce}$:

$$\begin{aligned} L_e(t) \leq C_{ce} &: & R_{e_{out}} &= R_1 + R_2 + R_4 \\ C_{ce} < L_e(t) \leq C_{ee} &: & R_{e_{out}} &= R_1 + R_4 \\ L_e(t) \leq C_{ee} + C_{ce} &: & R_{e_{out}} &= R_1 \end{aligned}$$

Similar relations can be identified for cases where $C_{ce} > C_{ee}$:

$$\begin{aligned} L_e(t) \leq C_{ee} &: & R_{e_{out}} &= R_1 + R_2 + R_4 \\ C_{ee} < L_e(t) \leq C_{ce} &: & R_{e_{out}} &= R_1 + R_2 \\ L_e(t) \leq C_{ee} + C_{ce} &: & R_{e_{out}} &= R_1 \end{aligned}$$

If the load demand $L_e(t)$ lies between the installed capacities of both connections (e.g. $C_{ee} < L_e(t) \leq C_{ce}$), the smaller rated connection (C_{ee}) does not contribute in terms of reliability improvement. It is however conceivable that the smaller rated connection (C_{ee}) will take over the supply of partial loads in case of a failure of the sufficiently sized connection (C_{ce}). Partial load shedding would still occur but the expected energy not supplied would be reduced. This operation strategy will be the subject later-on, in section 3.3.2. For now, expected energy not supplied is not discussed further.

Obviously, state 1 of the state space diagram is a supplying state as long as the load is smaller than the capacity of any or both connections together. States 2 and 4 are supplying states as long as $L_e \leq C_{ce}$ or $L_e \leq C_{ee}$, respectively. To summarise these relations in one expression, the following auxiliary variables have to be defined using boolean logics:

$$\begin{aligned} a(t) &= \begin{cases} 1, & L_e(t) \leq (C_{ee} + C_{ce}) \\ 0, & else \end{cases} \\ b(t) &= \begin{cases} 1, & L_e(t) \leq C_{ce} \\ 0, & else \end{cases} \\ c(t) &= \begin{cases} 1, & L_e(t) \leq C_{ee} \\ 0, & else \end{cases} \end{aligned} \quad (3.8)$$

Consequently, variable a is true when at least one of the variables b or c is true. The availability of supply $R_{e_{out}}$ at any time interval t can then be defined as follows, valid for any relations of L_e , C_{ee} and C_{ce} :

$$R_{e_{out}}(t) = R_1 \cdot a(t) + R_2 \cdot b(t) + R_4 \cdot c(t) \quad (3.9)$$

Analogously, the probability of failure could be found as follows, with $\neg a(t)$ implying both $\neg b(t)$ and $\neg c(t)$:

$$Q_{e_{out}}(t) = R_1 \cdot \neg a(t) + R_2 \cdot \neg b(t) + R_3 + R_4 \cdot \neg c(t) \quad (3.10)$$

This closes the example, used for introducing the applied reliability principles and the modelling procedure. The same approach as in equation (3.9) will now be developed for a general energy hub.

3.2 Output Availability as a Function of the Hub Components

The example in the previous section introduced the general approach applied in the reliability model for multi-carrier energy systems. Other approaches are possible, using reliability block diagrams or using the concept of generation outage tables [20]. The approach developed in this thesis however is particularly suited for numerical and symbolic calculations, which in turn is useful for sensitivity analyses. Furthermore, the approach follows the hub matrix notation. In this section, the procedure applied for the example in figure 3.2 is generalised, first focusing on one output only. Afterwards, the model is postulated for hubs with three outputs.

For the general form of the model, the supplying networks are assumed to be 100% reliable. This allows to focus on the influence of the converting elements and to identify benefits of an energy hub. Later-on, the model will be complemented with non-ideal supply infrastructures to incorporate the different failure behaviour of the individual infrastructures. Furthermore, it is assumed that only one converter exists between two energy carriers. This assumption will be discussed as well later-on.

3.2.1 Failure and repair rate matrices

In figure 3.4 the component models for the electrical-electrical connection C_{ee} and for the chemical-electrical connection C_{ce} are displayed. For each connection, the failure rate and the repair rate have been stated. Following the energy hub approach it is thus possible to define a failure rate matrix $\mathbf{\Lambda}$ and a repair rate matrix \mathbf{M} , containing the failure and repair rates of all couplings:

$$\mathbf{\Lambda} = \begin{bmatrix} \lambda_{ee} & \lambda_{ce} & \lambda_{te} \\ \lambda_{ec} & \lambda_{cc} & \lambda_{tc} \\ \lambda_{et} & \lambda_{ct} & \lambda_{tt} \end{bmatrix} \quad (3.11)$$

$$\mathbf{M} = \begin{bmatrix} \mu_{ee} & \mu_{ce} & \mu_{te} \\ \mu_{ec} & \mu_{cc} & \mu_{tc} \\ \mu_{et} & \mu_{ct} & \mu_{tt} \end{bmatrix} \quad (3.12)$$

The matrix elements correspond to the failure and repair rates of the associated coupling. The conversions provided by the energy hub are thus reduced to their reliability characteristics. Each coupling is treated as one process, no matter how many elements it consists of physically. The corresponding matrix in equation (2.4) directly relates the power flows at the input with those at the output. In the context of probabilities, however, no similar direct relations between input and output reliability were found, implying equations (3.11), (3.12). Hence, an algorithm is developed, for which the matrix representation of the failure and repair rates is well suited. Sometimes, not all possible couplings will be occupied. These particular connections are defined to have a failure rate $\lambda = 0$ and a repair rate $\mu = 1$; these values have no physical meaning, but they are necessary for the algorithm to properly perform, as will be seen later-on.

The reliability of a conversion from energy carrier α to energy carrier β ($\alpha, \beta \in [e, c, t]$) can be defined using equations (3.1) and (3.2). The term $R_{\alpha\beta}$ corresponds to the probability of a working conversion from α to β and $Q_{\alpha\beta}$ consequently to the probability of a failed conversion:

$$R_{\alpha\beta} = \frac{\mu_{\alpha\beta}}{\mu_{\alpha\beta} + \lambda_{\alpha\beta}} \quad (3.13)$$

$$Q_{\alpha\beta} = \frac{\lambda_{\alpha\beta}}{\mu_{\alpha\beta} + \lambda_{\alpha\beta}} \quad (3.14)$$

3.2.2 Derivation of a general calculation procedure

Similar to the earlier discussed example, the state space diagram for the supply of output L_α can be defined. For the remainder of this section, the index ' α ' serves as placeholder for any of the three possible hub loads, representing the electrical, chemical and thermal energy carriers. The availability of supply at output L_α of the energy hub depends both on a direct connection as well as on two indirect connections. Hence, the state space diagram for the supply of L_α consists of $2^3 = 8$ states, with the involved connections $C_{e\alpha}$, $C_{c\alpha}$ and $C_{t\alpha}$, displayed in figure 3.6.

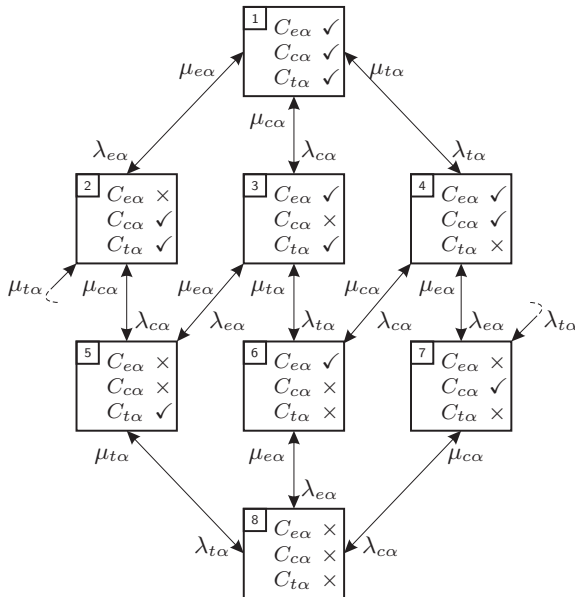


Figure 3.6: State space diagram for the supply of output L_α from inputs P_e , P_c and P_t through the connections $C_{e\alpha}$, $C_{c\alpha}$ and $C_{t\alpha}$.

Again, as in the example discussed earlier, successful supply depends on the relation between the momentary load and the installed capacities of the individual connections. The increased amount of components results in more supply situations with parallel, series and combined configurations (see figure 3.7 for a complete overview). Analysing these different configurations separately however is not useful, which is why the same procedure as in equations (3.8) and (3.9) is applied.

The state probabilities can be found according to A.2.3 as:

$$R_{1\alpha} = \frac{\mu_{e\alpha}\mu_{c\alpha}\mu_{t\alpha}}{(\mu_{e\alpha} + \lambda_{e\alpha})(\mu_{c\alpha} + \lambda_{c\alpha})(\mu_{t\alpha} + \lambda_{t\alpha})}$$

$$R_{2\alpha} = \frac{\lambda_{e\alpha}\mu_{c\alpha}\mu_{t\alpha}}{(\mu_{e\alpha} + \lambda_{e\alpha})(\mu_{c\alpha} + \lambda_{c\alpha})(\mu_{t\alpha} + \lambda_{t\alpha})}$$

$$R_{3\alpha} = \frac{\mu_{e\alpha}\lambda_{c\alpha}\mu_{t\alpha}}{(\mu_{e\alpha} + \lambda_{e\alpha})(\mu_{c\alpha} + \lambda_{c\alpha})(\mu_{t\alpha} + \lambda_{t\alpha})}$$

$$R_{4\alpha} = \frac{\mu_{e\alpha}\mu_{c\alpha}\lambda_{t\alpha}}{(\mu_{e\alpha} + \lambda_{e\alpha})(\mu_{c\alpha} + \lambda_{c\alpha})(\mu_{t\alpha} + \lambda_{t\alpha})}$$

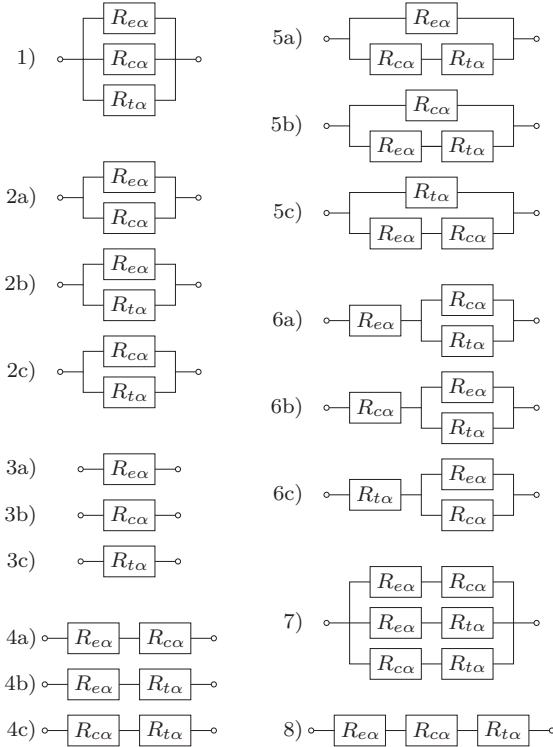


Figure 3.7: Reliability block diagrams for the supply of output α from the electrical, chemical and thermal inputs, $\alpha \in [e, c, t]$.

$$\begin{aligned}
 R_{5\alpha} &= \frac{\lambda_{e\alpha} \lambda_{c\alpha} \mu_{t\alpha}}{(\mu_{e\alpha} + \lambda_{e\alpha})(\mu_{c\alpha} + \lambda_{c\alpha})(\mu_{t\alpha} + \lambda_{t\alpha})} \\
 R_{6\alpha} &= \frac{\mu_{e\alpha} \lambda_{c\alpha} \lambda_{t\alpha}}{(\mu_{e\alpha} + \lambda_{e\alpha})(\mu_{c\alpha} + \lambda_{c\alpha})(\mu_{t\alpha} + \lambda_{t\alpha})} \\
 R_{7\alpha} &= \frac{\lambda_{e\alpha} \mu_{c\alpha} \lambda_{t\alpha}}{(\mu_{e\alpha} + \lambda_{e\alpha})(\mu_{c\alpha} + \lambda_{c\alpha})(\mu_{t\alpha} + \lambda_{t\alpha})} \\
 R_{8\alpha} &= \frac{\lambda_{e\alpha} \lambda_{c\alpha} \lambda_{t\alpha}}{(\mu_{e\alpha} + \lambda_{e\alpha})(\mu_{c\alpha} + \lambda_{c\alpha})(\mu_{t\alpha} + \lambda_{t\alpha})} \tag{3.15}
 \end{aligned}$$

For later use, the individual probabilities can be combined and written as vector $\vec{R}_\alpha = [R_{1\alpha}, R_{2\alpha}, R_{3\alpha}, R_{4\alpha}, R_{5\alpha}, R_{6\alpha}, R_{7\alpha}, R_{8\alpha}]^T$. Entry $\vec{R}_\alpha(3)$ then e.g. corresponds to the probability of residing in state 3.

Similar to equation (3.9), the probability of being supplied can be expressed with one equation. This equation holds true for any load and any installed capacities $C_{e\alpha}$, $C_{c\alpha}$ and $C_{t\alpha}$. To state this equation, the following boolean variables are defined for every time period t :

$$\begin{aligned}
 a(t) &= \begin{cases} 1, & L_\alpha(t) \leq (C_{e\alpha} + C_{c\alpha} + C_{t\alpha}) \\ 0, & \text{else} \end{cases} \\
 b(t) &= \begin{cases} 1, & L_\alpha(t) \leq (C_{c\alpha} + C_{t\alpha}) \\ 0, & \text{else} \end{cases} \\
 c(t) &= \begin{cases} 1, & L_\alpha(t) \leq (C_{e\alpha} + C_{t\alpha}) \\ 0, & \text{else} \end{cases} \\
 d(t) &= \begin{cases} 1, & L_\alpha(t) \leq (C_{e\alpha} + C_{c\alpha}) \\ 0, & \text{else} \end{cases} \\
 e(t) &= \begin{cases} 1, & L_\alpha(t) \leq C_{t\alpha} \\ 0, & \text{else} \end{cases} \\
 f(t) &= \begin{cases} 1, & L_\alpha(t) \leq C_{e\alpha} \\ 0, & \text{else} \end{cases} \\
 g(t) &= \begin{cases} 1, & L_\alpha(t) \leq C_{c\alpha} \\ 0, & \text{else} \end{cases} \tag{3.16}
 \end{aligned}$$

The probability of a successful supply of load $L_\alpha(t)$ can then be calculated for every period t as:

$$\begin{aligned}
 R_{\alpha_{out}}(t) &= \vec{R}_\alpha(1) \cdot a(t) + \vec{R}_\alpha(2) \cdot b(t) + \vec{R}_\alpha(3) \cdot c(t) + \vec{R}_\alpha(4) \cdot d(t) \\
 &\quad + \vec{R}_\alpha(5) \cdot e(t) + \vec{R}_\alpha(6) \cdot f(t) + \vec{R}_\alpha(7) \cdot g(t) \tag{3.17}
 \end{aligned}$$

Equation (3.17) basically compiles the information from the state space diagram in figure 3.6. For instance, state 3 is a supplying state as long as either $C_{e\alpha}$, $C_{t\alpha}$ or both contemporaneously ($C_{e\alpha} + C_{t\alpha}$) are capable of supplying the load. These conditions correspond with the variables $f(t)$, $e(t)$ or $c(t)$ being true and thus equal to one. Both $e(t)$ and $f(t)$ imply $c(t)$, which is why it is sufficient to multiply $\vec{R}_\alpha(3)$ with $c(t)$.

Similar to the state probabilities, the multiplication coefficients in equation (3.17) can be combined in a row vector $\vec{F}_\alpha(t)$:

$$\vec{F}_\alpha(t) = [a(t) \quad b(t) \quad c(t) \quad d(t) \quad e(t) \quad f(t) \quad g(t) \quad 0] \quad (3.18)$$

This allows writing the probability of a successful supply $R_{\alpha_{out}}(t)$ at time t as the following scalar product:

$$R_{\alpha_{out}}(t) = \vec{F}_\alpha(t) \cdot \vec{R}_\alpha \quad (3.19)$$

The modelling procedure so far can be described as follows: vector \vec{R}_α contains the individual constant state probabilities for each state of the state space diagram in figure 3.6. The row vector $\vec{F}_\alpha(t)$ contains the boolean variables relating the momentary load $L_\alpha(t)$ with the capacities of the different connections. Hence, to incorporate a varying load, vector $\vec{F}_\alpha(t)$ has to be redefined for every time period t , in order to reflect the momentary supply situation. The associated momentary level of reliability of supply $R_{\alpha_{out}}(t)$ then is found as the sum of the probabilities of all states that are supplying states for the momentary load $L_\alpha(t)$. These supplying states in turn are defined through the entries of $\vec{F}_\alpha(t)$.

3.2.3 Procedure for determining the expected reliability of supply

For a given load curve – which can be a duration curve or a sequential load representation – and a given hub configuration, i.e. known $C_{e\alpha}$, $C_{c\alpha}$ and $C_{t\alpha}$, the average expected reliability of supply $R_{\alpha_{out}}$ for a certain observation duration T can be defined according to the following procedure. The observation period T is defined to consist of n intervals of duration Δt , hence $n \cdot \Delta t = T$. Intervals Δt are expressed relative to an hour, e.g. 5 min intervals result in $\Delta t = \frac{1}{12}$ h.

- (1) Determine the reliability characteristics of the hub components and define matrices $\mathbf{\Lambda}$ and \mathbf{M} .
- (2) Determine the state probability vector \vec{R}_α .
- (3) Determine the boolean variables $a(t)$ to $g(t)$ for every interval of the load curve of length n and store them in the $n \times 8$ matrix \mathbf{F}_α (equations (3.16) and (3.18)). Row t of \mathbf{F}_α corresponds to $\vec{F}_\alpha(t)$, with $t \in [1, \dots, n]$.
- (4) Determine the weight of every state probability by summing up matrix \mathbf{F}_α column-wise and by dividing by the length n . This results in the 1×8 array \vec{G}_α , containing entries between 0 and 1:

$$\vec{G}_\alpha = \frac{1}{n} \left[\sum_{t=1}^n \mathbf{F}_\alpha(t, 1) \quad \sum_{t=1}^n \mathbf{F}_\alpha(t, 2) \quad \dots \quad \sum_{t=1}^n \mathbf{F}_\alpha(t, 8) \right] \quad (3.20)$$

- (5) Calculate the expected reliability of supply $R_{\alpha_{out}}$ for load L_α as:

$$R_{\alpha_{out}} = \vec{G}_\alpha \cdot \vec{R}_\alpha \quad (3.21)$$

This procedure results in the average availability of supply during the period covered by the load curve. The following paragraphs contain a short application example, illustrating the use of the suggested procedure. Afterwards, the algorithm is postulated for all three outputs, followed by a procedure for the calculation of expected energy not supplied.

3.2.4 Application example

This subsection contains a short example, demonstrating the use of the suggested procedure for calculating the expected reliability of supply. The example considers an electrical load (i.e. $\alpha = e$), which is supplied from the electrical, chemical and thermal network. Figure 3.8 shows the German standard weekday electrical load profile for a small business, scaled to a total annual consumption of 20 MWh [25]. The load curve consists of $n = 96$ intervals, each with 15 min duration.

The electrical-electrical connection is rated $C_{ee} = 10$ kW, the chemical-electrical connection satisfies $C_{ce} = 2$ kW and the thermal-electrical

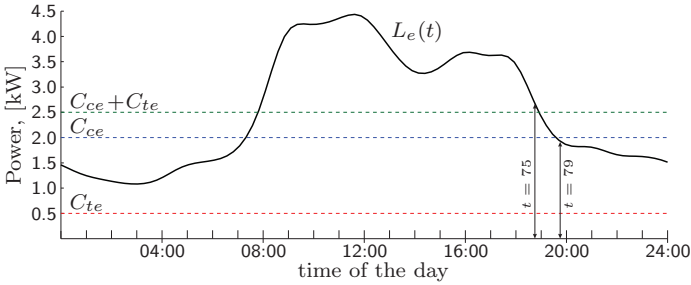


Figure 3.8: Load curve of an electrical load L_e supplied with an energy hub.

connection $C_{te} = 0.5$ kW [26, 27, 28]. The failure and repair rate matrices are defined as:

$$\mathbf{\Lambda} = \begin{bmatrix} 0.5 & 1.5 & 1.5 \\ 0 & 0 & 0 \\ 0 & 0 & 0 \end{bmatrix}$$

$$\mathbf{M} = \begin{bmatrix} 4380 & 365 & 365 \\ 1 & 1 & 1 \\ 1 & 1 & 1 \end{bmatrix}$$

Thus, the chemical-electrical and the thermal-electrical converter fail three times as much as the electrical-electrical connection. Furthermore, their repair needs 12 times as long, i.e. 24 h. Using equation (3.15) and the matrix entries (e.g. λ_{ce} corresponds to $\mathbf{\Lambda}(1,2)$), the corresponding state probability vector \vec{R}_e is found as:

$$\vec{R}_e = \begin{bmatrix} 0.99171800206280 \\ 0.00011320981759 \\ 0.00407555343313 \\ 0.00407555343313 \\ 0.00000046524583 \\ 0.00001674884973 \\ 0.00000046524583 \\ 0.00000000191197 \end{bmatrix}$$

It is obvious from figure 3.8 that the converters (C_{ce} and C_{te}) only contribute during periods where $L_e(t) \leq 2.5$ kW. Furthermore, the thermal-

electrical converter is not powerful enough to supply the load by itself at all. An excerpt of matrix \mathbf{F}_e shows the different state probability weights between 18:45 and 20:00. During time steps 76 to 78, i.e. 19:00 to 19:45, for a short time, a redundant supply situation exists, which can only persist as long as C_{ce} and C_{te} are operating. After 19:45 the load has decreased further, such that C_{ce} can maintain the redundant supply on its own, not anymore requiring C_{te} :

$$\mathbf{F}_e = \begin{bmatrix} \cdot & \cdot & \cdot & \cdot & \cdot & \cdot & \cdot & \cdot & \cdot \\ 1 & 0 & 1 & 1 & 0 & 1 & 0 & 0 & \cdot \\ 1 & 1 & 1 & 1 & 0 & 1 & 0 & 0 & \cdot \\ 1 & 1 & 1 & 1 & 0 & 1 & 0 & 0 & \cdot \\ 1 & 1 & 1 & 1 & 0 & 1 & 0 & 0 & \cdot \\ 1 & 1 & 1 & 1 & 0 & 1 & 1 & 0 & \cdot \\ \cdot & \cdot & \cdot & \cdot & \cdot & \cdot & \cdot & \cdot & \cdot \end{bmatrix} \begin{matrix} \cdot \\ t=75 \\ t=76 \\ t=77 \\ t=78 \\ t=79 \\ \cdot \end{matrix}$$

This excerpt shows that state 1 is always a supplying state. Furthermore, as long as $L_e(t) > 2.5$ kW, states 3, 4 and 6 are supplying as well (compare also with figure 3.6). Then, from time step 76 to 78, additionally state 2 is a supplying state: C_{ee} is down, but $C_{ce} + C_{te}$ can supply the load. After time step 78, state 7 also becomes a supplying state. Summing up matrix \mathbf{F}_e , following the before outlined procedure, results in row vector \vec{G}_e with the average state frequencies:

$$\vec{G}_e = \left[1 \quad \frac{52}{96} \quad 1 \quad 1 \quad 0 \quad 1 \quad \frac{47}{96} \quad 0 \right]$$

The availability of supply at the electrical output is finally found with equation (3.21):

$$R_{e_{out}} = \vec{G}_e \cdot \vec{R}_e = 0.999947$$

The availability of supply without the energy hub, i.e. considering only the electrical supply, equals $R_{ee} = 0.999886$. This corresponds to an annual outage duration of 59.99 min. With the energy hub, i.e. considering the converters from the chemical and the thermal networks, the expected annual outage duration is reduced to 27.64 min.

3.3 Reliability Models for a Complete Energy Hub

This section contains the general reliability model suited for an arbitrary energy hub. The model is basically the extension of the above developed procedure to three outputs and it is based as well on state space diagrams as displayed in figure 3.6. Different state space diagrams are possible, but then the associated equations and vector entries have to be changed accordingly.

Theoretically, the hub with 6 converters and 3 connections could be represented with one large state space diagram, containing $2^{3 \times 3} = 512$ states. However, unless one converter has two different outputs, as e.g. a combined heat and power, most system states will be independent of each other and could be combined again. This is why it was decided to work with three individual state space diagrams for each output, following the same form. Thus, the state space diagram in figure 3.6 is applied for all outputs. Only the indices of the connections have to be replaced accordingly, with $\alpha \in [e, c, t]$. The same holds true for the failure and repair rates.

It is important to note that this approach still allows the consideration of converters with more than one output. As each converter is treated as one single unit, it is assumed that e.g. for a CHP the reliability characteristics for both conversions are identical: $\lambda_{ce} = \lambda_{ct}$ and $\mu_{ce} = \mu_{ct}$.

3.3.1 Expected reliability of supply

The procedure suggested in section 3.2.3 is restated here, valid for the complete hub and in more detail, showing the necessary extensions. Generally, in all matrices needed and defined throughout this procedure, the first row or column, where appropriate, is always assigned to the electrical energy carrier, the second one to the chemical and the third one to the thermal energy carrier. Furthermore, the algorithm is noted in matrix notation where possible, indicating the modelling approach for programs like Matlab[®]. As before, the modelling focuses only on the hub components so far, assuming the supplying networks to be 100% reliable. This assumption will be discussed in section 3.4.2.

Procedure for calculating expected reliability of supply

- (1) Determine the reliability characteristics of the hub components and define matrices $\mathbf{\Lambda}$ and \mathbf{M} :

$$\mathbf{\Lambda} = \begin{bmatrix} \lambda_{ee} & \lambda_{ce} & \lambda_{te} \\ \lambda_{ec} & \lambda_{cc} & \lambda_{tc} \\ \lambda_{et} & \lambda_{ct} & \lambda_{tt} \end{bmatrix}; \quad \mathbf{M} = \begin{bmatrix} \mu_{ee} & \mu_{ce} & \mu_{te} \\ \mu_{ec} & \mu_{cc} & \mu_{tc} \\ \mu_{et} & \mu_{ct} & \mu_{tt} \end{bmatrix} \quad (3.22)$$

- (2) Determine the connection capacities of the hub and define the connection matrix $\hat{\zeta}$:

$$\hat{\zeta} = \begin{bmatrix} C_{ee} & C_{ce} & C_{te} \\ C_{ec} & C_{cc} & C_{tc} \\ C_{et} & C_{ct} & C_{tt} \end{bmatrix} \quad (3.23)$$

A converter with several outputs was defined to have identical failure and repair rates for all conversions it is providing. The connection capacities are however not necessarily identical. The thermal capacity of e.g. a CHP usually differs from the electrical capacity; C_{ce} is not necessarily equal to C_{te} .

- (3) Define the $n \times 3$ load curve matrix \mathbf{L} , column-wise containing the loads for every time step t of the observation period of length n with $t \in [1, \dots, n]$. For example, $\mathbf{L}(5, 3)$ contains the level of the thermal load in the fifth interval:

$$\mathbf{L} = [\vec{L}_e \quad \vec{L}_c \quad \vec{L}_t] \quad (3.24)$$

- (4) Determine the 8×3 state probability matrix \mathbf{R} , which contains the state probabilities for the individual state space diagrams, i.e. the individual hub output:

$$\mathbf{R} = [\vec{R}_e \quad \vec{R}_c \quad \vec{R}_t] \quad (3.25)$$

With $j \in [1, 2, 3]$ representing the electrical, chemical and thermal outputs, e.g. $\mathbf{R}(7, j)$ hence corresponds to the probability of residing in state 7 for output j , according to figure 3.6. Using the failure rate and repair rate matrices, this probability is given as follows, according to equation (3.15):

$$\mathbf{R}(7, j) = \frac{\mathbf{\Lambda}(j, 1)\mathbf{M}(j, 2)\mathbf{\Lambda}(j, 3)}{(\mathbf{\Lambda}(j, 1) + \mathbf{M}(j, 1)) \cdot (\mathbf{\Lambda}(j, 2) + \mathbf{M}(j, 2)) \cdot (\mathbf{\Lambda}(j, 3) + \mathbf{M}(j, 3))}$$

As mentioned before, an energy hub might not have converters at all possible couplings and the non-existent couplings are defined to have $\lambda = 0$ and $\mu = 1$. These values have no physical meaning but they ensure not to end up with entries of \mathbf{R} with a denominator equal to 0.

- (5) Determine for each time step t the boolean variables, relating the connection capacities $\boldsymbol{\zeta}$ and the momentary loads \mathbf{L} (equation (3.16)):

$$\begin{aligned}
 a(t, j) &= \mathbf{L}(t, j) \leq (\boldsymbol{\zeta}(j, 1) + \boldsymbol{\zeta}(j, 2) + \boldsymbol{\zeta}(j, 3)) \\
 b(t, j) &= \mathbf{L}(t, j) \leq (\boldsymbol{\zeta}(j, 2) + \boldsymbol{\zeta}(j, 3)) \\
 c(t, j) &= \mathbf{L}(t, j) \leq (\boldsymbol{\zeta}(j, 1) + \boldsymbol{\zeta}(j, 3)) \\
 d(t, j) &= \mathbf{L}(t, j) \leq (\boldsymbol{\zeta}(j, 1) + \boldsymbol{\zeta}(j, 2)) \\
 e(t, j) &= \mathbf{L}(t, j) \leq \boldsymbol{\zeta}(j, 3) \\
 f(t, j) &= \mathbf{L}(t, j) \leq \boldsymbol{\zeta}(j, 1) \\
 g(t, j) &= \mathbf{L}(t, j) \leq \boldsymbol{\zeta}(j, 2)
 \end{aligned} \tag{3.26}$$

- (6) Determine the $3 \times 8 \times n$ factor matrix \mathbf{F} , according to equation (3.18), using the boolean matrices defined in step (5):

$$\begin{aligned}
 \mathbf{F}(j, 1, t) &= a(t, j) \\
 \mathbf{F}(j, 2, t) &= b(t, j) \\
 \mathbf{F}(j, 3, t) &= c(t, j) \\
 \mathbf{F}(j, 4, t) &= d(t, j) \\
 \mathbf{F}(j, 5, t) &= e(t, j) \\
 \mathbf{F}(j, 6, t) &= f(t, j) \\
 \mathbf{F}(j, 7, t) &= g(t, j) \\
 \mathbf{F}(j, 8, t) &= 0
 \end{aligned} \tag{3.27}$$

- (7) Calculate the weight of the probabilities of residing in the individual states by summing up matrix \mathbf{F} along the third dimension, resulting in the 3×8 weighting matrix \mathbf{G} :

$$\mathbf{G} = \frac{1}{n} \begin{bmatrix} \sum_{t=1}^n \mathbf{F}(1, 1, t) & \sum_{t=1}^n \mathbf{F}(1, 2, t) & \cdots & \sum_{t=1}^n \mathbf{F}(1, 8, t) \\ \sum_{t=1}^n \mathbf{F}(2, 1, t) & \sum_{t=1}^n \mathbf{F}(2, 2, t) & \cdots & \sum_{t=1}^n \mathbf{F}(2, 8, t) \\ \sum_{t=1}^n \mathbf{F}(3, 1, t) & \sum_{t=1}^n \mathbf{F}(3, 2, t) & \cdots & \sum_{t=1}^n \mathbf{F}(3, 8, t) \end{bmatrix} \tag{3.28}$$

- (8) The reliability of supply for all three loads of the energy hub results as the diagonal elements from a multiplication of the weighting matrix with the state probability matrix:

$$\vec{R}_{out} = \begin{bmatrix} R_{e_{out}} \\ R_{c_{out}} \\ R_{t_{out}} \end{bmatrix} = \begin{bmatrix} (\mathbf{G} \cdot \mathbf{R})_{(1,1)} \\ (\mathbf{G} \cdot \mathbf{R})_{(2,2)} \\ (\mathbf{G} \cdot \mathbf{R})_{(3,3)} \end{bmatrix} \quad (3.29)$$

Summarising, this algorithm analyses the load curves in every time step and determines the supplying states. At the end of the algorithm the occurrence of the individual states is counted and weighted relative to the total load curve duration. The sum of the weighted state probabilities then results in the individual availabilities of supply for each energy carrier. In other words, matrices \mathbf{A} and \mathbf{M} are used to define the state probability matrix \mathbf{R} and the connection matrix $\mathbf{\zeta}$ is used together with the load matrix \mathbf{L} to define the factor matrix \mathbf{F} . Multiplying \mathbf{R} with \mathbf{F} then gives the probability of supply in each time interval.

So far, the capacities of the converters have been assumed constant. However, the effectively available converter capacity depends on the loading of the hub input, supplying the converters [17]. The input capacities are assumed equal to the capacities of the associated direct connections and the directly connected loads are assumed to have supply priority. Hence, if one of these loads gets close to the rated capacity of the direct connection, it can happen that the converters cannot be operated at their rated capacity. The following scenario illustrates this. The thermal input is assumed to supply three different connections: the direct thermal connection with $C_{tt} = 15$ kW, the thermal-electrical connection with $C_{te} = 2$ kW and the thermal-chemical connection with $C_{tc} = 1$ kW. Accordingly, the hub input capacity is as well at 15 kW, equal to C_{tt} . Thus, if all three connections would be operating at their limits, the demand would sum up to 18 kW, exceeding the supply capacity of the thermal hub input. Consequently, as soon as the thermal load L_t exceeds 12 kW, a priority rule comes active, defining which converters to dispatch. If the load is at e.g. $L_t = 14$ kW either the thermal-electrical connection has to be set to zero with $C_{te} = 0$ kW, guaranteeing the rated operation of the thermal-chemical connection, or both connections are reduced to half of the available supply capacity with $C_{te} = 0.5$ kW and $C_{tc} = 0.5$ kW. On the other hand, if the chemical load would be at e.g. $L_c = 6$ kW and the electrical load only at $L_e = 1$ kW, setting $C_{tc} = 0$ kW would allow to define $C_{te} = 1$ kW,

achieving a redundant supply of the electrical load. Of course, also the direct connection could be reduced, ensuring the rated supply of both converters. Obviously, different criteria, e.g. economic criteria or security of supply, can be used when defining the dispatch policy.

Below, one possible approach is presented, redefining the capacities for every time step. The directly supplied load has priority and the remaining supply capacity is distributed among the converters. If both of the neighbouring supply systems are in normal operation, i.e. the direct connection can supply the load by itself, the remaining margin is distributed evenly. Otherwise, the remaining capacity is allocated according to the demand of the neighbouring systems. Sometimes, a converter will not be able to contribute to reliability of supply because its disposable capacity is too small. However, in case of an outage, such a converter can still supply a partial load. This is the reason why any available margin is always allocated to the existing converters, useful for expected energy not supplied analyses.

Hence, before continuing with step (5) in the procedure, determining the supplying states, the matrix ζ has to be defined for each time step t . As long as the following conditions hold true – checking whether all loads and converters could be supplied without exceeding any limits – the rated capacities could be maintained and the matrix ζ stays unchanged:

$$\begin{aligned} C_{ee} - L_e(t) - C_{ec} - C_{et} &\geq 0 \\ C_{cc} - L_c(t) - C_{ce} - C_{ct} &\geq 0 \\ C_{tt} - L_t(t) - C_{te} - C_{tc} &\geq 0 \end{aligned} \quad (3.30)$$

If any of these conditions is violated, ζ has to be adjusted. The procedure for doing so is explained below, referring to the line numbers of a pseudocode segment on the next page. The procedure is identical for all three hub outputs but described here for the electrical output only:

- 1-3: Calculate the remaining supply capacities, considered as margin m_α , available for supplying the converters.
- 4-6: If m_α is negative, the energy carrier α cannot supply the load at its output, requiring support from the other energy carriers. The variable d_α is defined true if this is the case.
- 7-9: Check whether the electrical hub input can provide support to the other energy carriers. If no margin is left, set the concerned converter

capacities to 0, with ζ_{tmp} being a temporary variable. In this interval, the converters from the electrical network are inoperable.

10: The margin is positive, i.e. the electrical load is below the rated capacity of the direct connection and a portion of the hub's electrical input capacity is available for supplying the converters.

11-21: If the chemical and the thermal network have negative margins, they both require support to supply their loads. The electrical supply mar-

Algorithm 1 Determination of momentary converter capacities

```

1:  $m_e = \zeta(1, 1) - L_e(t)$ 
2:  $m_c = \zeta(2, 2) - L_c(t)$ 
3:  $m_t = \zeta(3, 3) - L_t(t)$ 
4:  $d_e = m_e < 0$ 
5:  $d_c = m_c < 0$ 
6:  $d_t = m_t < 0$ 

7: if  $m_e \leq 0$  then
8:    $\zeta_{tmp}(2, 1) = 0$ 
9:    $\zeta_{tmp}(3, 1) = 0$ 
10: else
11:   if  $d_c = 1$  and  $d_t = 1$  then
12:     if  $\text{abs}(m_c) \leq 0.5 \cdot m_e$  then
13:        $\zeta_{tmp}(2, 1) = \min(\zeta(2, 1), \text{abs}(m_c))$ 
14:        $\zeta_{tmp}(3, 1) = \min(\zeta(3, 1), m_e - \text{abs}(m_c))$ 
15:     else if  $\text{abs}(m_t) \leq 0.5 \cdot m_e$  then
16:        $\zeta_{tmp}(2, 1) = \min(\zeta(2, 1), m_e - \text{abs}(m_t))$ 
17:        $\zeta_{tmp}(3, 1) = \min(\zeta(3, 1), \text{abs}(m_t))$ 
18:     else
19:        $\zeta_{tmp}(2, 1) = \min(\zeta(2, 1), 0.5 \cdot m_e)$ 
20:        $\zeta_{tmp}(3, 1) = \min(\zeta(3, 1), 0.5 \cdot m_e)$ 
21:     end if
22:   else
23:      $\zeta_{tmp}(2, 1) = \min(\zeta(2, 1), 0.5 \cdot m_e \cdot (d_c + (1 - d_t)))$ 
24:      $\zeta_{tmp}(3, 1) = \min(\zeta(3, 1), 0.5 \cdot m_e \cdot ((1 - d_c) + d_t))$ 
25:   end if
26:   if  $\zeta_{tmp}(2, 1) < \zeta(2, 1)$  and  $(\zeta_{tmp}(2, 1) + \zeta_{tmp}(3, 1)) < m_e$  then
27:      $\zeta_{tmp}(2, 1) = \min(\zeta(2, 1), m_e - \zeta_{tmp}(3, 1))$ 
28:   else if  $\zeta_{tmp}(3, 1) < \zeta(3, 1)$  and  $(\zeta_{tmp}(2, 1) + \zeta_{tmp}(3, 1)) < m_e$  then
29:      $\zeta_{tmp}(3, 1) = \min(\zeta(3, 1), m_e - \zeta_{tmp}(2, 1))$ 
30:   end if
31: end if

```

gin is split evenly to both energy carriers. If one of the two energy carriers however requires less than half, the remaining amount is provided to the energy carrier with more load at risk. In any case, the corrected supply capacity cannot exceed the rated converter capacity, which is why a $\min()$ query is included. If both the chemical and the thermal network require more than half of the available electrical supply margin, the margin is split up equally.

- 22-25: Either only one of the two neighbouring systems has a support requirement or none of both. If none of the other systems requires support, the remaining capacity is split up evenly to both converters. Hence, these converters might not contribute to reliability of supply but in case of partial load shedding they could supply certain loads. If only one of both neighbouring system requires support, it is defined to get the whole available margin – as long as it does not exceed the rated converter capacity.
- 26-30: For certain constellations, it can happen that some converters are below their rated capacity albeit some supply margin is still available. If this is the case, the remaining capacity is again distributed according to the needs. With this algorithm, the electrical-chemical converter is prioritised, as its margin is checked and possibly adjusted first.

The temporary ζ_{tmp} , containing the adjusted capacities, is now used to calculate the boolean variables in step (5) of the reliability calculation procedure. The procedure will be applied later-on in an example in section 4.3, after storage devices have been included into the modelling procedure as well.

3.3.2 Expected energy not supplied (EENS)

The algorithm presented in the previous section calculates the availability of supply at the three outputs of an energy hub. Sometimes, it is however more important to know the amount of energy that could not be supplied, the so-called expected energy not supplied (EENS). Looking at the example in figure 3.8 shows that a failure of the electrical supply during the peak period would still allow a certain base load to be supplied, as long as the chemical-electrical and the thermal-electrical converter are still operating. Thus, only a part of the load has to be shed, which has an influence on calculations of expected energy not supplied. In this section, this issue is discussed and a modelling procedure is postulated.

Two different approaches are developed for investigating expected energy not supplied. Which approach to use depends on the type of load supplied, as load shedding sometimes is not appropriate. If the load is e.g. an industrial process, a loss of load most certainly results in a loss of production and supplying part loads will probably not be helpful. Modelling the supply of such a load, incorporating load shedding, thus makes little sense. On the other hand, if the hub supplies e.g. a residential area with many individual houses, load shedding would mean that some of the houses or some loads in the houses can still be supplied. A similar effect occurs when looking at distributed generation: in case of a failure of the main supply system, the distributed generator can probably still supply a certain base load. The use of load shedding thus results in a reduction of EENS. This reduction corresponds to a certain value that can be put in relation to the expenses for being able to perform load shedding. These expenses are e.g. the cost for the converter or the cost for the information infrastructure, required for deciding which loads when to dis- and reconnect.

EENS without load shedding

In the case where load shedding is not considered useful, a failure of the supply means total loss of load. The expected energy not supplied $N_{\alpha_{nls}}(t)$ at time interval t thus corresponds to the momentary load demand $L_{\alpha}(t)$ multiplied with the probability of failure. This momentary probability of failure $Q_{\alpha_{out}}(t)$ adds up to unity with the probability of being operating $R_{\alpha_{out}}(t)$ and the definition for EENS at time t can be identified as:

$$N_{\alpha_{nls}}(t) = \Delta t \cdot (1 - R_{\alpha_{out}}(t)) \cdot L_{\alpha}(t) \quad (3.31)$$

The time interval duration Δt has to be applied in order to express EENS in [Wh]. The probability of being operating at time t is defined as in equation (3.19), with $\vec{F}_{\alpha}(t)$ containing the boolean variables:

$$R_{\alpha_{out}}(t) = \vec{F}_{\alpha}(t) \cdot \vec{R}_{\alpha} \quad (3.32)$$

The expected energy not supplied $N_{\alpha_{nls}}$ for the total observation period T consequently can be found as:

$$N_{\alpha_{nls}} = \Delta t \cdot \sum_{t=1}^n \left(1 - \vec{F}_{\alpha}(t) \cdot \vec{R}_{\alpha} \right) \cdot L_{\alpha}(t) \quad (3.33)$$

For the calculation of EENS of a general energy hub, the $3 \times n$ matrix \mathbf{Q} can be defined, containing the probability of failure for every time step $t \in [1, 2, \dots, n]$ for all energy carriers:

$$\mathbf{Q} = \begin{bmatrix} 1 - \sum_{i=1}^8 \mathbf{F}(1, i, 1) \cdot \mathbf{R}(i, 1) & \cdots & 1 - \sum_{i=1}^8 \mathbf{F}(1, i, n) \cdot \mathbf{R}(i, 1) \\ 1 - \sum_{i=1}^8 \mathbf{F}(2, i, 1) \cdot \mathbf{R}(i, 2) & \cdots & 1 - \sum_{i=1}^8 \mathbf{F}(2, i, n) \cdot \mathbf{R}(i, 2) \\ 1 - \sum_{i=1}^8 \mathbf{F}(3, i, 1) \cdot \mathbf{R}(i, 3) & \cdots & 1 - \sum_{i=1}^8 \mathbf{F}(3, i, n) \cdot \mathbf{R}(i, 3) \end{bmatrix} \quad (3.34)$$

The individual values of EENS of the respective energy carriers can then be found as the diagonal entries of the matrix resulting from the multiplication of \mathbf{Q} with the load matrix \mathbf{L} :

$$\vec{N}_{nls} = \begin{bmatrix} N_{e_{nls}} \\ N_{c_{nls}} \\ N_{t_{nls}} \end{bmatrix} = \Delta t \cdot \begin{bmatrix} (\mathbf{Q} \cdot \mathbf{L})_{(1,1)} \\ (\mathbf{Q} \cdot \mathbf{L})_{(2,2)} \\ (\mathbf{Q} \cdot \mathbf{L})_{(3,3)} \end{bmatrix} \quad (3.35)$$

This procedure will be applied in section 3.3.3 to calculate the EENS for the example discussed in section 3.2.4. Section 3.3.3 will also outline the use of the method presented in the next paragraphs and put the results in relation to each other, indicating the benefit of considering load shedding. Furthermore, the results will be verified with an alternative, more intuitive and stepwise calculation.

EENS with load shedding

This section discusses an approach for calculating EENS considering load shedding and its fundamentals are illustrated based on the example from section 3.2.4. The electrical load L_e is supplied through three connections C_{ee} , C_{ce} and C_{te} . Their capacities satisfy $C_{te} < C_{ce} < (C_{ce} + C_{te}) < C_{ee}$ and between 08:00 and 18:45, only the direct electrical connection C_{ee} is able to supply the full load L_e (see the load curve in figure 3.8). Following the state space diagram in figure 3.6, the supplying states are states 1, 3, 4 and 6. If the electrical connection fails, the energy hub can only supply a load that satisfies $L_{e_{shed}} = C_{ce} + C_{te}$ and state 2 is the supplying state. Either the chemical-electrical or the thermal-electrical connection could now still fail, resulting in $L_{e_{shed}} = C_{te}$ (state 5) or $L_{e_{shed}} = C_{ce}$ (state 7), respectively.

The expected energy not supplied can be evaluated by calculating the conditional probabilities for different supply levels and by summing up all possible situations. This can be achieved in an elegant way by using the state space diagram from figure 3.6. The probability of each state already is expressed as a conditional probability. For instance the probability R_{5e} of state 5 corresponds to an operating thermal-electrical connection given that both the electrical-electrical and the chemical-electrical connection have failed. Hence, if the system is residing in state 5, being the only supplying state left, the expected energy supplied (EES) corresponds to $R_{e5} \cdot C_{te}$ with $L_{e_{shed}}(t) = C_{te}$. EENS is then found as the difference between the load and the expected supplied energy $(1 - R_{e5}) \cdot C_{te}$.

This approach can be extended to all states of the state space diagram. For this purpose it must be known for every time step, what each state's supply capacity is. Considering the aforementioned reasoning, the momentary supply capacities of the converters depend on the directly connected loads. At this point, hence, the momentary valid connection capacity matrix $\zeta(t)$ has to be determined. For all states of the state space diagram, the maximum supply capacities can then be derived and stored in the vector $\vec{S}_\alpha(t)$, using the corresponding elements from matrix $\zeta(t)$. The entries of this vector are the momentary disposable supply capacities of each state, corresponding to the sum of all connections that are considered operating in the respective state:

$$\vec{S}_\alpha(t) = \begin{bmatrix} C_{e\alpha} + C_{c\alpha} + C_{t\alpha} \\ C_{c\alpha} + C_{t\alpha} \\ C_{e\alpha} + C_{t\alpha} \\ C_{e\alpha} + C_{c\alpha} \\ C_{t\alpha} \\ C_{e\alpha} \\ C_{c\alpha} \\ 0 \end{bmatrix} \quad (3.36)$$

For the calculation of EENS it is necessary to check whether the load $L_\alpha(t)$ is smaller than the supply capacity of a state. For instance, if the load equals 7 kW and the maximum supply capacity of a state is 10 kW, EENS for that state has to be calculated considering the actual load of 7 kW and not the suppliable load of 10 kW. The boolean variables defined in equation (3.16) indicate for all states whether their supply capacity is below or above the momentary load. Row vector $\vec{F}_\alpha(t)$,

defined in equation (3.18), contains these boolean variables for every time step t . It is defined to add up to unity with row vector $\vec{F}_{\alpha_{not}}(t)$:

$$\vec{F}_{\alpha_{not}}(t) = [-a(t) \quad -b(t) \quad -c(t) \quad -d(t) \quad -e(t) \quad -f(t) \quad -g(t) \quad 1] \quad (3.37)$$

These can be used to define the 1×8 row vector $\vec{V}_{\alpha}(t)$, containing not the maximum possible but the momentary supply capacities:

$$\vec{V}_{\alpha}(t)^T = \begin{bmatrix} F_{\alpha_{not}}(t, 1) \cdot \vec{S}_{\alpha}(1) + F_{\alpha}(t, 1) \cdot L_{\alpha}(t) \\ F_{\alpha_{not}}(t, 2) \cdot \vec{S}_{\alpha}(2) + F_{\alpha}(t, 2) \cdot L_{\alpha}(t) \\ F_{\alpha_{not}}(t, 3) \cdot \vec{S}_{\alpha}(3) + F_{\alpha}(t, 3) \cdot L_{\alpha}(t) \\ F_{\alpha_{not}}(t, 4) \cdot \vec{S}_{\alpha}(4) + F_{\alpha}(t, 4) \cdot L_{\alpha}(t) \\ F_{\alpha_{not}}(t, 5) \cdot \vec{S}_{\alpha}(5) + F_{\alpha}(t, 5) \cdot L_{\alpha}(t) \\ F_{\alpha_{not}}(t, 6) \cdot \vec{S}_{\alpha}(6) + F_{\alpha}(t, 6) \cdot L_{\alpha}(t) \\ F_{\alpha_{not}}(t, 7) \cdot \vec{S}_{\alpha}(7) + F_{\alpha}(t, 7) \cdot L_{\alpha}(t) \\ F_{\alpha_{not}}(t, 8) \cdot \vec{S}_{\alpha}(8) + F_{\alpha}(t, 8) \cdot L_{\alpha}(t) \end{bmatrix} \quad (3.38)$$

The entries of vector $\vec{V}_{\alpha}(t)$ thus represent the capacities each state is or could be supplying to serve the load $L_{\alpha}(t)$ at time t . All states are operating with a certain probability, as defined in the state probability vector $\vec{R}_{\alpha}(t)$. The expected energy supplied results as the sum of all state capacities multiplied with their corresponding probability. EENS then corresponds to the difference between the momentary load $L_{\alpha}(t)$ and the expected energy supplied:

$$N_{\alpha_{is}}(t) = \Delta t \cdot \left(L_{\alpha}(t) - \vec{V}_{\alpha}(t) \cdot \vec{R}_{\alpha} \right) \quad (3.39)$$

The expected energy not supplied for the observation period of length $T = n \cdot \Delta t$ is then defined as:

$$N_{\alpha_{is}} = \Delta t \cdot \sum_{t=1}^n \left(L_{\alpha}(t) - \vec{V}_{\alpha}(t) \cdot \vec{R}_{\alpha} \right) \quad (3.40)$$

As before, the algorithm can be derived and stated for a general energy hub. The $8 \times 3 \times n$ matrix \mathbf{S} contains the momentary supply capacities for all states for the three individual outputs, analogous to equation (3.36):

$$\mathbf{S} = [\vec{S}_e \quad \vec{S}_c \quad \vec{S}_t] \quad (3.41)$$

The $3 \times 8 \times n$ matrix \mathbf{F}_{not} is defined to add up to unity with the factor matrix \mathbf{F} :

$$\mathbf{F}_{not}(j, i, t) = -\mathbf{F}(j, i, t) \quad (3.42)$$

The entries of the $3 \times 8 \times n$ matrix $\mathbf{V}(t)$ contain the momentary supply capacities and are defined as follows, with $i \in [1, \dots, 8]$ representing the states and $j \in [1, 2, 3]$ the individual energy carriers:

$$\mathbf{V}(j, i, t) = \mathbf{F}_{not}(j, i, t) \cdot \mathbf{S}(i, j, t) + \mathbf{F}(j, i, t) \cdot \mathbf{L}(t, j) \quad (3.43)$$

The expected energy supplied for every time interval t can be derived as an $n \times 3$ matrix:

$$\mathbf{E}(t) = \left[\begin{array}{ccc} \sum_{i=1}^8 \mathbf{V}(1, i, t) \cdot \mathbf{R}(i, 1) & \cdots & \sum_{i=1}^8 \mathbf{V}(3, i, t) \cdot \mathbf{R}(i, 3) \end{array} \right] \quad (3.44)$$

Expected energy not supplied is then given by the following definition:

$$\vec{N}_{ts} = \begin{bmatrix} N_{e_{ts}} \\ N_{c_{ts}} \\ N_{t_{ts}} \end{bmatrix} = \Delta t \cdot \begin{bmatrix} \sum_{t=1}^n \mathbf{L}(t, 1) - \mathbf{E}(t, 1) \\ \sum_{t=1}^n \mathbf{L}(t, 2) - \mathbf{E}(t, 2) \\ \sum_{t=1}^n \mathbf{L}(t, 3) - \mathbf{E}(t, 3) \end{bmatrix} \quad (3.45)$$

The definitions contained in equations (3.35) and (3.45) each result in three values, giving EENS without and with load shedding at the output of an energy hub. The case without load shedding is somewhat simpler as it is sufficient to determine the probability of failure of supply for every interval t and to multiply this probability of failure with the momentary load demand. The sum over the whole observation period then gives the expected energy not supplied. If load shedding is incorporated, it must be calculated how much of the load is expected to be supplied by each individual state of the state space diagram. This expected supply in turn is compared with the momentary load in every time interval and the sum of the differences then results as the expected energy not supplied.

3.3.3 Application example continued

This section continues the example from section 3.2.4 and calculates EENS with and without load shedding. It serves as application example for both EENS methods and at the same time verifies the soundness of the results by applying a second, more illustrative method. Figure 3.9 repeats the load curve used in the example, shown before in figure 3.8.

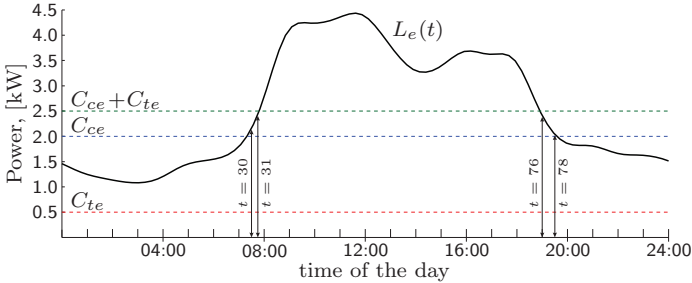


Figure 3.9: Load curve of an electrical load L_e supplied with an energy hub.

EENS without load shedding

Following the approach for a general energy hub, the $1 \times n$ matrix \mathbf{Q} can be defined to contain the probabilities of failure for every time step t , according to equation (3.34). The EENS per day then results as the product of \mathbf{Q} and the $n \times 1$ matrix containing the load curve \mathbf{L} (equation (3.35)):

$$N_{e_{nts}} = 4.6957 \text{ Wh}$$

The total energy demand over one day results as the sum of the load curve and equals:

$$\Delta t \sum_{t=1}^n \mathbf{L}(t) = 61.1995 \text{ kWh}$$

The expected energy not supplied without the energy hub, i.e. only considering the electrical connection, results as:

$$\frac{\lambda_{ee}}{\mu_{ee} + \lambda_{ee}} \cdot \Delta t \cdot \sum_{t=1}^n \mathbf{L}(t) = 6.9854 \text{ Wh}$$

The presence of an energy hub, i.e. the possibility to also supply the electrical load through C_{ce} and through C_{te} , results in a reduction of EENS from 6.99 Wh per day to 4.70 Wh per day. This reduction of EENS by 33% is remarkable as the energy hub only contributes to the supply during low load periods.

EENS with load shedding

The expected energy not supplied is expected to further reduce in case of load shedding; partial loads can still be supplied, however with a lower probability. This expectation is investigated by applying the calculation procedure discussed on pages 38ff.

The supply capacities are summarised in the 8×1 matrix \mathbf{S} (equation (3.36)). Matrix \mathbf{S} is static, as the supplying converters are assumed to always be at their rated capacity:

$$\mathbf{S} = \begin{bmatrix} 12.5 \\ 2.5 \\ 10.5 \\ 12.0 \\ 0.5 \\ 10.0 \\ 2.0 \\ 0.0 \end{bmatrix}$$

An excerpt of matrix \mathbf{V} is displayed below, corresponding to matrix \mathbf{F}_e on page 29:

$$\mathbf{V} = \begin{bmatrix} \cdot & \cdot & \cdot & \cdot & \cdot & \cdot & \cdot & \cdot & \cdot \\ 2740 & 2500 & 2740 & 2740 & 500 & 2740 & 2000 & 0 & 75 \\ 2466 & 2466 & 2466 & 2466 & 500 & 2466 & 2000 & 0 & 76 \\ 2242 & 2242 & 2242 & 2242 & 500 & 2242 & 2000 & 0 & 77 \\ 2068 & 2068 & 2068 & 2068 & 500 & 2068 & 2000 & 0 & 78 \\ 1946 & 1946 & 1946 & 1946 & 500 & 1946 & 1946 & 0 & 79 \\ \cdot & \cdot & \cdot & \cdot & \cdot & \cdot & \cdot & \cdot & \cdot \end{bmatrix}$$

Obviously, states 1, 3, 4 and 6 are able to supply the full load, which is equal to $L_e(t = 75) = 2740$ W. States 2, 5 and 7 however can only supply partial loads equal to the capacity of the corresponding connections. Later-on, at $t = 79$, the load has reduced such that it can also be supplied by the chemical-electrical converter. Hence, in terms of reliability

of supply, states 1, 2, 3, 4, 6 and 7 can now supply the load. State 5 only can supply a part load equal to the capacity of the thermal-electrical converter $C_{te} = 0.5$ kW. Expected energy supplied thus equals the sum of the individual probabilities of residing in states 1, 2, 3, 4, 6 and 7, multiplied with the momentary load of $\mathbf{L}(t = 79) = 1948$ W. In case of failure of both the electrical and the chemical-electrical connection, state 5 would still be able to supply a part load of 500 W with a certain probability. These reasonings hold true as long as both the chemical and the thermal hub input are able to supply the converters accordingly. If, however, e.g. the thermal network would be at its limit, the thermal-electrical converter would not operate and state 5 would have a supply capacity of 0 kW. This eventuality is considered in the algorithm described on page 35, defining the momentary converter capacities.

Applying equations (3.44) and (3.45) gives the corresponding EENS as:

$$N_{e_{ts}} = 1.5655 \text{ Wh}$$

Incorporating load shedding results in a significantly lower EENS, compared with the case without load shedding. Considering partial load shedding thus reduces EENS from 4.70 Wh by 66% to 1.57 Wh per day. Hence, the true value of the energy hub is defined as the EENS reduction by 5.42 Wh per day. The monetary value this would correspond to depends on the type of load and the cost resulting from such an outage.

Model verification with alternative calculation procedures

The results obtained so far will be verified with alternative calculation approaches for both cases, i.e. EENS with and without load shedding.

EENS not including load shedding In the case of no load shedding, EENS is defined as the difference between the load demand L_e and the expected load supply, being the product of the probability of being operating $R_{e_{out}}(t)$ and the load demand L_e . The probability of being operating $R_{e_{out}}$ can be found by looking at the load curve in figure 3.9.

Using reliability block diagrams, as introduced in appendix A, the supply configuration can be separated into several groups, as shown in table 3.1. The corresponding illustrations are also depicted in figure 3.7 as 2a), 5a) and 3a), respectively.

time	segments	block diagram	$R_{e_{out}}$
00:00 - 07:15	$t \in [1, \dots, 29]$	$C_{ee} \vee C_{ce}$	$R_{ee} + R_{ce} - R_{ee}R_{ce}$
07:30 - 07:45	$t \in [30, 31]$	$C_{ee} \vee (C_{ce} \wedge C_{te})$	$R_{ee} + R_{ce}R_{te} - R_{ee}R_{ce}R_{te}$
08:00 - 18:45	$t \in [32, \dots, 75]$	C_{ee}	R_{ee}
19:00 - 19:30	$t \in [76, \dots, 78]$	$C_{ee} \vee (C_{ce} \wedge C_{te})$	$R_{ee} + R_{ce}R_{te} - R_{ee}R_{ce}R_{te}$
19:45 - 00:00	$t \in [79, \dots, 96]$	$C_{ee} \vee C_{ce}$	$R_{ee} + R_{ce} - R_{ee}R_{ce}$

Table 3.1: Supply configurations for load curve in figure 3.9.

With this information, EENS can be calculated as displayed in equation (3.46). Basically, the equation iterates through the load curve and multiplies the momentary load demand with the momentary probability of supply. The difference to the load demand corresponds to the expected energy not served and is identical to the result obtained above:

$$\begin{aligned}
 N_{e_{nls}} &= \Delta t \cdot \left[\sum_{t=1}^{96} L_e(t) - \sum_{t=1}^{29} (R_{ee} + R_{ce} - R_{ee}R_{ce}) \cdot L_e(t) \right. \\
 &\quad - \sum_{t=30}^{31} (R_{ee} + R_{ce}R_{te} - R_{ee}R_{ce}R_{te}) \cdot L_e(t) \\
 &\quad - \sum_{t=32}^{75} R_{ee} \cdot L_e(t) \\
 &\quad - \sum_{t=76}^{78} (R_{ee} + R_{ce}R_{te} - R_{ee}R_{ce}R_{te}) \cdot L_e(t) \\
 &\quad \left. - \sum_{t=79}^{96} (R_{ee} + R_{ce} - R_{ee}R_{ce}) \cdot L_e(t) \right] \\
 &= 4.6957 \text{ Wh} \tag{3.46}
 \end{aligned}$$

Equation (3.46) consequently verifies the soundness of the procedure contained in equations (3.34) and (3.35).

EENS including load shedding The calculation of expected energy not supplied considering partial load shedding is not as straightforward and uses conditional probabilities. However, as the three networks are not considered dependent, conditional probabilities can just be multiplied [19]. The load curve in figure 3.9 can be separated into several horizontal

layers, each with a different reliability configuration. The sum of the EENS of each layer then equals the sum of the total EENS. During the whole duration covered by the load curve, a base load of $C_{te} = 500$ W can be supplied. All three connections are capable of supplying this load individually and hence a doubly redundant supply situation exists. EENS for this load can be calculated as the probability of failure of supply, multiplied with C_{te} :

$$\Delta t \cdot \sum_{t=1}^{96} C_{te} \cdot Q_{ee} Q_{ce} Q_{te} \quad (3.47)$$

The next layer concerns all loads between the smallest capacity (C_{te}) and the next smallest capacity (C_{ce}). To be able to calculate this contribution, a temporary load curve has to be introduced, limited by a cap equal to C_{ce} and a floor equal to C_{te} :

$$L_{e_{tmp1}}(t) = \begin{cases} C_{ce} & L_e(t) > C_{ce} \\ L_e(t) & C_{te} \leq L_e(t) \leq C_{ce} \\ C_{te} & else \end{cases}$$

This load in turn can be supplied both from the electrical-electrical and the chemical-electrical connection. The status of the thermal-electrical connection is without influence on this supply situation:

$$\Delta t \cdot \sum_{t=1}^{96} (L_{e_{tmp1}}(t) - C_{te}) \cdot Q_{ee} Q_{ce} \quad (3.48)$$

The third layer consists of all load levels between the capacity of the chemical-electrical converter C_{ce} and the sum of the capacities ($C_{ce} + C_{te}$). Again, the load curve has to be defined according to these limits:

$$L_{e_{tmp2}}(t) = \begin{cases} C_{ce} + C_{te} & L_e(t) > C_{ce} + C_{te} \\ L_e(t) & C_{ce} \leq L_e(t) \leq C_{ce} + C_{te} \\ C_{ce} & else \end{cases}$$

This load can be supplied by both the electrical-electrical connection and the joint operation of the chemical-electrical and the thermal-electrical connections:

$$\Delta t \cdot \sum_{t=1}^{96} (L_{e_{tmp2}}(t) - C_{ce}) \cdot Q_{ee} (Q_{ce} + Q_{te} - Q_{ce} Q_{te}) \quad (3.49)$$

The last layer in the underlying example is the portion of the load that exceeds the capacities of the additional converters. Hence, the following load curve can be defined:

$$L_{e_{tmp3}}(t) = \begin{cases} C_{ce} + C_{te} & L_e(t) \leq C_{ce} + C_{te} \\ L_e(t) & \text{else} \end{cases}$$

The corresponding EENS only depends on the probability of failure of the electrical-electrical connection:

$$\Delta t \cdot \sum_{t=1}^{96} (L_{e_{tmp3}}(t) - C_{ce} - C_{te}) \cdot Q_{ee} \quad (3.50)$$

The total EENS for one day is finally found as the sum of the EENS of the individual layers:

$$\begin{aligned} N_{els} &= \Delta t \cdot \left[\sum_{t=1}^{96} C_{te} \cdot Q_{ee} Q_{ce} Q_{te} \right. \\ &\quad + \sum_{t=1}^{96} (L_{e_{tmp1}}(t) - C_{te}) \cdot Q_{ee} Q_{ce} \\ &\quad + \sum_{t=1}^{96} (L_{e_{tmp2}}(t) - C_{ce}) \cdot Q_{ee} (Q_{ce} + Q_{te} - Q_{ce} Q_{te}) \\ &\quad \left. + \sum_{t=1}^{96} (L_{e_{tmp3}}(t) - C_{ce} - C_{te}) \cdot Q_{ee} \right] \\ &= 1.5655 \text{ Wh} \end{aligned} \quad (3.51)$$

The result is identical to the result obtained with the method presented in equations (3.41) and (3.45). This closes the example, illustrating the applicability and verifying the methods.

Besides, if all elements in matrix \mathbf{F}_{not} in equation (3.42) are set to zero, the resulting EENS corresponds to the case without load shedding considered. Matrix \mathbf{F}_{not} concerns all states, which are not capable of supplying the effective load and hence only contribute in the case of partial load shedding. This result was therefore expected and confirms the consistency of the approach.

3.4 Discussion of Special Cases

So far, the subject of the combined reliability modelling in multi-carrier energy systems has been introduced. The general modelling approach was developed using an energy hub with only one converter in addition to the direct supply. Based on this, the overall modelling procedure for one output was stated and elaborated. Section 3.3 postulated the modelling procedure for a complete energy hub, containing three direct connection and 6 converters, i.e. indirect connections. The models were complemented with two algorithms for calculating expected energy not supplied. All models so far have been based on some assumptions, which will be shortly discussed in this section.

3.4.1 Several converters for one coupling

It is theoretically possible that an energy hub represents a situation with several converters, establishing couplings between the same two energy carriers. An example would be an energy hub with a gas furnace and a CHP, thus two converters converting chemical energy into thermal energy. Figure 3.10 illustrates this symbolically for the coupling from chemical to electrical. The question addressed here is thus how to incorporate this special case into the earlier stated procedures.

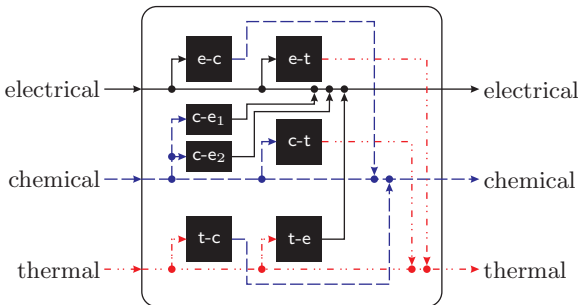


Figure 3.10: Modelling approach for incorporating two converters coupling the same energy carriers, shown with the example of two converters from chemical to electrical.

This situation can be modelled by combining all considered converters and treating them as one component. In that case, their common con-

version capacity and the corresponding reliability characteristics need to be determined, in order to be included in the above discussed models. The involved converters can form either a series or a parallel system or a combination of both.

If they form a series system, the connection capacity of the combined connection equals the sum of the individual converter capacities. In the case of two components, the series system can be represented as one component with the following characteristics [19]:

$$C_{series} = C_1 + C_2 \quad (3.52)$$

$$\lambda_{series} = \lambda_1 + \lambda_2 \quad (3.53)$$

$$\mu_{series} = \frac{\mu_1 \mu_2 (\lambda_1 + \lambda_2)}{\lambda_1 \lambda_2 + \lambda_1 \mu_2 + \mu_1 \lambda_2} \quad (3.54)$$

If the involved converters form a parallel system, the joint capacity equals the smallest capacity of all involved components. For two components, the reliability characteristics of the parallel combined component are defined as:

$$C_{parallel} = \min(C_1, C_2) \quad (3.55)$$

$$\lambda_{parallel} = \frac{\lambda_1 \lambda_2 (\mu_1 + \mu_2)}{\mu_1 \mu_2 + \lambda_1 \mu_2 + \mu_1 \lambda_2} \quad (3.56)$$

$$\mu_{parallel} = \mu_1 + \mu_2 \quad (3.57)$$

Equations (3.52) to (3.57) can be extended to suit with the actual number of converters, using reliability block diagram concepts from appendix A. This gives the failure and repair rate of the combined coupling. The associated capacity, however, might not be represented correctly. Even in the two component case, the true contribution will be missing in EENS calculations. In the case of the series configuration, the failure of one component results in a total failure of this coupling. This is invalid, as the coupling capacity is just reduced to the capacity of the remaining converters. In the parallel configuration, in turn, the coupling capacity is only equal to the capacity of the smaller rated converter, hence not taking into account the supply potential of the larger rated converter. Equations (3.52) to (3.57) can also be applied if the influence of two direct connections is to be investigated.

Hence, to model the behaviour of the considered coupling accurately, it is necessary to derive a separate state space diagram for the affected

converters and to extend the earlier presented model with it. Each additional converter results in a doubling of the states. This results in a larger state space diagram but also in more accurate results. The presented procedure can be adjusted accordingly, but the trade-off is evident. However, one approach – keeping the effort limited – would be the application of Kronecker sums and products, as suggested in [18]. Kronecker sums are explained in appendix B and will be applied in section 3.5, providing an alternative approach for the definition of some matrices and vectors applied in the procedures discussed in section 3.3.

Nevertheless, representing converters providing the same coupling with a detailed model, within the suggested procedure, will change the corresponding matrix dimensions. The failure rate and repair rate matrices have to be extended to provide corresponding entries for the additional conversions from e.g. chemical to electrical, as illustrated in figure 3.10. Consequently, e.g. the third row or column might not anymore be associated with the thermal hub components.

3.4.2 Impact of the supplying infrastructures

So far, the supplying infrastructures have been assumed to be 100% reliable. This is also often the approach in other reliability calculations, allowing to focus on the hub itself. However, the chemical and the thermal network have characteristics that differ significantly from the electrical network and to fully cover the effect of a combined multi-carrier analysis, it should be possible to incorporate these networks if desired.

Each of the supplying infrastructures is treated as one component with failure and repair rate. The probabilities of being operating can thus be defined according to equation 3.1, with the subscripts explicitly identifying the supplying systems:

$$R_{el} = \frac{\mu_{el}}{\mu_{el} + \lambda_{el}} \quad (3.58)$$

$$R_{ch} = \frac{\mu_{ch}}{\mu_{ch} + \lambda_{ch}} \quad (3.59)$$

$$R_{th} = \frac{\mu_{th}}{\mu_{th} + \lambda_{th}} \quad (3.60)$$

In terms of reliability, the supplying infrastructures form a series system with the respective components in the energy hub. Consequently, the

characteristics of the supplying system can be incorporated into the failure rate and repair rate matrices, using equations (3.53) and (3.54):

$$\mathbf{\Lambda} = \begin{bmatrix} \lambda_{el} + \lambda_{ee} & \lambda_{ch} + \lambda_{ce} & \lambda_{th} + \lambda_{te} \\ \lambda_{el} + \lambda_{ec} & \lambda_{ch} + \lambda_{cc} & \lambda_{th} + \lambda_{ct} \\ \lambda_{el} + \lambda_{et} & \lambda_{ch} + \lambda_{ct} & \lambda_{th} + \lambda_{tt} \end{bmatrix}$$

$$\mathbf{M} = \begin{bmatrix} \frac{\mu_{el}\mu_{ee}(\lambda_{el}+\lambda_{ee})}{\lambda_{el}\lambda_{ee}+\lambda_{el}\mu_{ee}+\mu_{el}\lambda_{ee}} & \frac{\mu_{ch}\mu_{ce}(\lambda_{ch}+\lambda_{ce})}{\lambda_{ch}\lambda_{ce}+\lambda_{ch}\mu_{ce}+\mu_{ch}\lambda_{ce}} & \frac{\mu_{th}\mu_{te}(\lambda_{th}+\lambda_{te})}{\lambda_{th}\lambda_{te}+\lambda_{th}\mu_{te}+\mu_{th}\lambda_{te}} \\ \frac{\mu_{el}\mu_{ce}(\lambda_{el}+\lambda_{ce})}{\lambda_{el}\lambda_{ce}+\lambda_{el}\mu_{ce}+\mu_{el}\lambda_{ce}} & \frac{\mu_{ch}\mu_{cc}(\lambda_{ch}+\lambda_{cc})}{\lambda_{ch}\lambda_{cc}+\lambda_{ch}\mu_{cc}+\mu_{ch}\lambda_{cc}} & \frac{\mu_{th}\mu_{tc}(\lambda_{th}+\lambda_{tc})}{\lambda_{th}\lambda_{tc}+\lambda_{th}\mu_{tc}+\mu_{th}\lambda_{tc}} \\ \frac{\mu_{el}\mu_{te}(\lambda_{el}+\lambda_{te})}{\lambda_{el}\lambda_{te}+\lambda_{el}\mu_{te}+\mu_{el}\lambda_{te}} & \frac{\mu_{ch}\mu_{ct}(\lambda_{ch}+\lambda_{ct})}{\lambda_{ch}\lambda_{ct}+\lambda_{ch}\mu_{ct}+\mu_{ch}\lambda_{ct}} & \frac{\mu_{th}\mu_{tt}(\lambda_{th}+\lambda_{tt})}{\lambda_{th}\lambda_{tt}+\lambda_{th}\mu_{tt}+\mu_{th}\lambda_{tt}} \end{bmatrix}$$

The entries of these matrices do not only represent the converter but the supplying system as well. The capacities of the individual couplings are assumed not to be concerned by this, i.e. the supplying systems' capacities exceed the capacities of the respective converters and have no restricting effect.

3.5 An Alternative Approach Using Kronecker Products and Sums

Sometimes, complex systems can be split into independent modules, which can be treated as individual Markov processes. These independent modules can be analysed by constructing the appropriate state space diagrams and defining the corresponding transition rate matrix and steady-state probability vectors. The resulting matrices and vectors can then again be combined, using Kronecker sums and products [18]. The main concepts are discussed in appendix B and are applied here to the procedures from sections 3.3.1 and 3.3.2.

When defining the expected reliability of supply, as in section 3.3.1, the supply of each output is modelled as a state space diagram. The state space diagram consists of 8 states, representing all possible combinations of the three involved connections (one direct and two indirect connections). This is not a complex system, but it is still illustrative to apply Kronecker products to reproduce the procedure. Furthermore, the subsequent chapter, applying Kronecker products to incorporate

energy storage devices, can build on the presented approach. Hence, this section illustrates how to apply this approach for one hub output, equally valid for any hub output.

For this purpose, the supply with the three different energy carriers is assumed to be independent and the individual state space diagrams can be found as illustrated in figure 3.11.

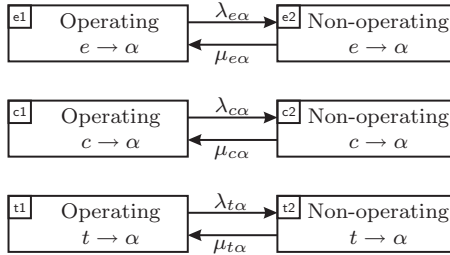


Figure 3.11: Individual state space diagrams for the three supply paths for one energy hub output α .

The states $e1$, $c1$ and $t1$ are the operating states for each connection. The transition rate matrix $\mathbf{A}_{e\alpha}$ and the steady-state probability vector $\vec{P}_{e\alpha}$ for the $e \rightarrow \alpha$ connection are given as follows, with appendix A.2:

$$\vec{P}_{e\alpha} \cdot \mathbf{A}_{e\alpha} = [P_{e_1} \quad P_{e_2}] \cdot \begin{bmatrix} -\lambda_{e\alpha} & \lambda_{e\alpha} \\ \mu_{e\alpha} & -\mu_{e\alpha} \end{bmatrix} = 0 \quad (3.61)$$

The transition rate matrix and the associated state probability vector for the $c \rightarrow \alpha$ and $t \rightarrow \alpha$ connections are defined analogously.

Following the Kronecker approach, the transition rate matrix \mathbf{A}_α , representing the combined state space diagram, is given as²:

$$\mathbf{A}_\alpha = \mathbf{A}_{e\alpha} \oplus \mathbf{A}_{c\alpha} \oplus \mathbf{A}_{t\alpha} \quad (3.62)$$

The corresponding state probability vector \vec{P}_α is given accordingly as:

$$\vec{P}_\alpha = \vec{P}_{e\alpha} \otimes \vec{P}_{c\alpha} \otimes \vec{P}_{t\alpha} \quad (3.63)$$

²A Kronecker sum is represented with \oplus and a Kronecker product with \otimes .

The entries of \vec{P}_α result as follows, with the subscript $\alpha 2$ identifying the failed state of component $e\alpha$, corresponding to figure 3.11:

$$\vec{P}_\alpha^T = \begin{bmatrix} P_{e1}P_{c1}P_{t1} \\ P_{e1}P_{c1}P_{t2} \\ P_{e1}P_{c2}P_{t1} \\ P_{e1}P_{c2}P_{t2} \\ P_{e2}P_{c1}P_{t1} \\ P_{e2}P_{c1}P_{t2} \\ P_{e2}P_{c2}P_{t1} \\ P_{e2}P_{c2}P_{t2} \end{bmatrix} \quad (3.64)$$

Compared with the state space diagram developed earlier, in figure 3.6, some states are defined differently. For instance state 4 in figure 3.6 corresponds not to $\vec{P}_\alpha(4)$ but to $\vec{P}_\alpha(2)$. However, following the Kronecker approach, as outlined here, will lead to the same results because the states are consistent with the transition rate matrix \mathbf{A}_α . The combined system now satisfies:

$$\vec{P}_\alpha \cdot \mathbf{A}_\alpha = 0 \quad (3.65)$$

Thus, instead of solving the combined system, the state space diagram of each component is solved separately, according to equation (3.61) and appendix A.2. The resulting state probability vectors $\vec{P}_{\alpha,\beta}$ are then combined as in equation (3.63), resulting in \vec{P}_α . Instead of solving one large linear equation system, several small systems are solved and the results are combined with the Kronecker approach.

Returning to the procedure outlined in section 3.3.1, shows that the resulting \vec{P}_α corresponds to \vec{R}_α , required in step (4), for the definition of matrix \mathbf{R} . According to (3.25) on page 31, this matrix contains the three vectors with the state probabilities for each hub output. To fit within the procedure from section 3.3.1, the failure and repair rates in equation (3.61) can be defined using the corresponding entries of the failure rate and repair rate matrices $\mathbf{\Lambda}$ and \mathbf{M} , given in equation 3.22 in step (1) of the procedure.

Following this procedure, the next step is to define the factor matrix \mathbf{F} , which identifies the supplying states in each time interval. Earlier, boolean variables were defined in an intermediate step, relating the load with the supply capacities of each state. The then used definitions

however correspond to the state space diagram in figure 3.6 and do not comply with the state definition given by \mathbf{A}_α and \vec{P}_α . Besides, the intermediate step was rather of illustrative purpose and the factor matrix \mathbf{F} can be defined directly.

For this purpose, the momentary supply capacities of each state have to be identified. For each state space diagram in figure 3.11, a matrix $\Gamma_{\alpha\beta}$ can be defined, containing the supply capacity of each state in the corresponding diagonal element. With e.g. $C_{e\alpha}$ denoting the power rating of the connection from electrical to energy carrier α , this results in the matrices:

$$\Gamma_{e\alpha} = \begin{bmatrix} C_{e\alpha} & 0 \\ 0 & 0 \end{bmatrix} \quad (3.66)$$

$$\Gamma_{c\alpha} = \begin{bmatrix} C_{c\alpha} & 0 \\ 0 & 0 \end{bmatrix} \quad (3.67)$$

$$\Gamma_{t\alpha} = \begin{bmatrix} C_{t\alpha} & 0 \\ 0 & 0 \end{bmatrix} \quad (3.68)$$

Hence, $\Gamma_{c\alpha}(1, 1)$ corresponds to state e1 of the connection $c \rightarrow \alpha$, supplying a power equal to $C_{c\alpha}$. These three matrices can now be combined using Kronecker sums to give the $8 \times 8 \times n$ matrix Γ_α :

$$\Gamma_\alpha = \Gamma_{e\alpha} \oplus \Gamma_{c\alpha} \oplus \Gamma_{t\alpha} \quad (3.69)$$

Matrix Γ_α is a diagonal matrix and the entries correspond to the supply capacity of each state. This matrix has to be defined in every time interval to consider possibly reduced ratings of converters, as discussed in section 3.3.1. Because of the application of Kronecker sums, these capacities are consistent with the states defined in \mathbf{A}_α and \vec{P}_α . That means, $\Gamma_\alpha(3, 3, t)$ corresponds to the supply capacity of state 3 during interval t . Relating these supply capacities with the momentary load L results in matrix \mathbf{F} , using boolean expressions as follows, with $j \in [1, 2, 3]$ and α representing the three energy carriers:

$$\mathbf{F}(j, 1, t) = \mathbf{L}(t, j) \leq \Gamma_\alpha(1, 1, t)$$

$$\mathbf{F}(j, 2, t) = \mathbf{L}(t, j) \leq \Gamma_\alpha(2, 2, t)$$

$$\mathbf{F}(j, 3, t) = \mathbf{L}(t, j) \leq \Gamma_\alpha(3, 3, t)$$

$$\mathbf{F}(j, 4, t) = \mathbf{L}(t, j) \leq \Gamma_\alpha(4, 4, t)$$

$$\mathbf{F}(j, 5, t) = \mathbf{L}(t, j) \leq \Gamma_\alpha(5, 5, t)$$

$$\begin{aligned}
\mathbf{F}(j, 6, t) &= \mathbf{L}(t, j) \leq \Gamma_\alpha(6, 6, t) \\
\mathbf{F}(j, 7, t) &= \mathbf{L}(t, j) \leq \Gamma_\alpha(7, 7, t) \\
\mathbf{F}(j, 8, t) &= 0
\end{aligned} \tag{3.70}$$

Analogous to the transition rates, it is possible to define the matrices $\Gamma_{e\alpha}$, $\Gamma_{c\alpha}$ and $\Gamma_{t\alpha}$ using the corresponding entries from matrix $\boldsymbol{\zeta}$, defined earlier in equation (3.23) in step (2). Matrix \mathbf{R} and matrix \mathbf{F} are consistent, as they both were defined directly or indirectly, through matrix $\mathbf{\Gamma}$, with Kronecker products. Hence, the calculation of expected reliability of supply can be now finished, proceeding with step (7) on page 32.

The calculation of EENS can be performed as outlined before. If load shedding is considered, it is required to define matrix \mathbf{S} , as discussed on page 39, containing the supply capacities of each state in each interval. This information is already contained in matrix Γ_α and thus, \mathbf{S} can be defined as:

$$\mathbf{S}(t) = \begin{bmatrix} \Gamma_e(1, 1, t) & \Gamma_c(1, 1, t) & \Gamma_t(1, 1, t) \\ \Gamma_e(2, 2, t) & \Gamma_c(2, 2, t) & \Gamma_t(2, 2, t) \\ \vdots & \vdots & \vdots \\ \Gamma_e(8, 8, t) & \Gamma_c(8, 8, t) & \Gamma_t(8, 8, t) \end{bmatrix} \tag{3.71}$$

This closes the introduction to applying Kronecker products to the suggested calculation procedures. As mentioned, this approach will be used later-on, in the next chapter, to calculate the expected reliability of supply and EENS for energy hubs containing energy storage devices.

Chapter 4

Modelling the Impact of Energy Storage on the Reliability of Supply

This chapter extends the presented reliability model in order to incorporate energy storage devices. First, a general modelling approach is presented, which allows to represent storage devices as systems with failure and repair rates. This approach is then used to include storage devices into the previously introduced multi-carrier reliability model. In addition, the chapter contains extended application examples.

4.1 Markov Approach for Energy Storage Devices

Energy storage devices generally serve two major purposes. They can be charged to provide additional energy in peak load periods and they can be charged to provide emergency or back-up energy in case of supply outages. Both applications have a positive influence on the reliability of supply, either by delaying supply outages or by preventing load shedding, imminent because of loads exceeding the rated supply capacity. In both cases, the storage can be regarded as an assisting system taking over or supporting in cases of emergency.

These operation modes exist in all three considered energy systems and can be generally understood as illustrated in figure 4.1. This figure symbolically shows the operation of a charged storage, which is to supply energy in case it is needed. The operation of the switch is considered to be ideal, i.e. 100% reliable and lossless. However, this switch could be modelled to incorporate certain failure probabilities concerned with e.g. the charging of the storage device, using concepts from appendix A.1.4.

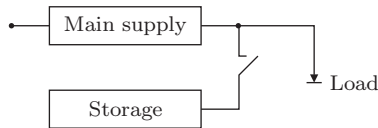


Figure 4.1: Symbolic illustration of the general operation of a charged energy storage device.

Using reliability block diagrams, as described in appendix A, the contributions for the case of peak shaving and the case of bridging supply outages have to be modelled differently. In the case of peak shaving, the storage device is necessary to be able to supply the load; it hence forms a series system with the main supply, as shown in figure 4.2a). If the energy storage is used to bridge supply outages, it can be considered to form a parallel system with the main supply, as in figure 4.2b). This configuration is however only valid as long as the power rating of the storage is capable of supplying the full load.

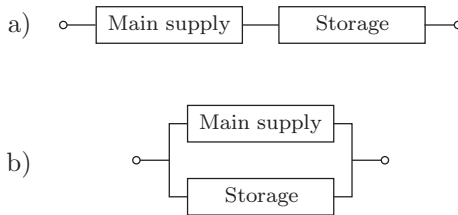


Figure 4.2: Reliability block diagram representation of a supply system containing an energy storage device.

The following subsections present an approach for modelling the behaviour of the energy storage device as a Markov process. This allows to extend the previously introduced reliability model with storage devices and to investigate potential benefits.

4.1.1 Markov properties

The reliability model presented in chapter 3 is based on Markov processes, as discussed in the appendix A. Hence, in order to include storage devices into this model, a way had to be found to describe storage devices as Markov processes. A process must show two properties to be considered as a Markov process, see appendix A.2. These properties can be described qualitatively as follows:

- The process does not have a memory. The future development is independent of past developments and only depends on the present state.
- The process must be stationary. The probability of a transition from one state to the other is independent of the time; it is the same at all times in the past and in the future.

Accordingly, the Markov approach is applicable to those systems whose behaviour can be described with a probability distribution function that is characterised by a constant failure rate [19]. Only then the probability of transit from one state to the other remains constant for all time periods. Hence, it must be assured that this transition probability is not a function of the overall process time [18]. As stored energy, charge or discharge power and time are mutually dependent and influencing each other, some restrictions had to be introduced to be able to satisfy the Markov properties. These restrictions can be best discussed by looking at the definition of the failure and repair rates of energy storage devices.

4.1.2 Failure and repair rates of a storage device

Generally, a storage device can be said to fail operation as soon as it is completely discharged. The failure rate λ_{st} of the storage can thus be considered to be equivalent to the mean time to failure (MTTF) of the storage. The mean time to failure, in turn, can be expressed as a function of the average power demand \bar{P}_{load} of the load as well as of the stored energy $E_{st}(t)$ and the discharge efficiency η_{dch} . The stored energy $E_{st}(t)$ satisfies $0 \leq E_{st}(t) \leq E_{st}$, with E_{st} being the rated capacity of the storage. The MTTF consequently corresponds to the time duration

the storage device can supply the load; after this duration, the storage device fails operation:

$$\text{MTTF} = \frac{E_{st}(t)}{\overline{P}_{load}} \cdot \eta_{dch} \quad (4.1)$$

$$\overline{P}_{load} = \frac{1}{T} \int_{t=0}^T P_{load}(t) \cdot dt$$

Failure rates are commonly expressed as 'failures per year' and with MTTF usually being expressed in hours, the storage failure rate λ_{st} can then be defined as [18]:

$$\lambda_{st} = \frac{1}{\text{MTTF}} = \frac{1}{\text{MTTF}} \cdot \frac{8760 \text{ h}}{\text{yr}} \quad (4.2)$$

Using equation (4.1) results in the following relation:

$$\lambda_{st} = \frac{\overline{P}_{load}}{E_{st}(t) \cdot \eta_{dch}} \cdot \frac{8760 \text{ h}}{\text{yr}} \quad (4.3)$$

The repair rate μ_{st} of the storage device can be defined analogously. The mean time to repair (MTTR), i.e. the time needed to restore the storage to be fully operable, is a function of the storage capacity E_{st} , the charge efficiency η_{ch} and the average charge power \overline{P}_{charge} . MTTR then equals the time needed to fully recharge the energy storage device:

$$\text{MTTR} = \frac{E_{st}(t)}{\overline{P}_{charge}} \cdot \frac{1}{\eta_{ch}} \quad (4.4)$$

$$\overline{P}_{charge} = \frac{1}{T} \int_{t=0}^T P_{charge}(t) \cdot dt$$

Relating MTTR to the duration of one year results in the definition of the storage repair rate μ_{st} , equivalent to equation (4.3):

$$\mu_{st} = \frac{\overline{P}_{charge} \cdot \eta_{ch}}{E_{st}(t)} \cdot \frac{8760 \text{ h}}{\text{yr}} \quad (4.5)$$

With this approach, the failure rate is defined by the time needed to discharge the storage device and the repair rate is defined by the time needed to recharge the storage device. However, the charge level of a storage device, both in charging and discharging mode, depends on the process time and the model is therefore not fulfilling the stationarity criterion. It seems that failure and repair rates change continuously, depending on the actual charge level and the charging and discharging power.

4.1.3 Modelling conditions

In order to fulfill the Markov properties, it is thus necessary to introduce certain conditions, under which the model can be applied. These conditions can be found by looking at the definition of the failure and repair rate in equations (4.3) and (4.5), respectively. Both transition rates depend on the charge level of the storage $E_{st}(t)$ and the average power level of the storage activities (\overline{P}_{load} or \overline{P}_{charge}). If these parameters are constant and identical whenever the storage starts operation or is being recharged, the corresponding rates will be constant as well; the modelling approach will be valid.

The following considerations show that these conditions are not as restrictive and unrealistic as they might seem at first and that they often are satisfied without peculiar measures.

Constant load demand: Generally, a storage device fulfills two purposes (see figure 4.2): it can bridge power outages and it can be used to compensate peak load demand. In both cases the power demand of the load can be assumed to be constant for the following reasons. If the storage acts as a back-up, it will take over the supply function whenever the main supply fails. In this case, all non-critical services can be assumed to be turned off immediately; the remaining consumption will cover basic and crucial loads. These vital services are usually known and have equal power demand at all times. Consequently, the load demand can be claimed to be constant. On the other hand – if the storage is used to cover demand peaks, thus acting in addition to the main supply – it is legitimate to assume that possible load fluctuations are dealt with by the main supply and that the demand from the storage is set constant. In both cases, the demand level can further be assumed to be

equal to the rated power output of the storage, presuming the rating of the storage device was chosen to meet a certain expected demand.

A different possibility to assure a constant load demand is to model the storage such that it only starts operation if the load demand is below or equal to the rated output. However, throughout this thesis, the model is applied with measured load curves, containing the average power demand during e.g. 15 min intervals. In other words, the model is applied with a time interval-wise constant load demand.

Constant charge power: The charge power is assumed to be equal to the rated charge power of the storage. Should this assumption result in an overloading of the supply system – as the storage is charged at the same time as loads are supplied – an accordingly lower constant charge power has to be defined.

Constant charge level: The most critical condition is the restriction that the charge level of the storage device is either always at an identical level or empty. This constraint can be alleviated by modelling the storage device to have discrete charge levels. The charge level differences between two states is known and with the charging power being constant, the recharge time is known and constant as well. The storage device is thus divided into several discrete states with corresponding transition rates in-between. This approximation and the associated drawbacks and advantages will be discussed in the subsequent sections. It is important to note that the discretisation should not be mistaken as discretisation of the probability of making a state transition; this would be a violation of the stationarity criterion [20].

With the charge power $P_{charge}(t)$ and the discharge or load power $P_{load}(t)$ being constant and equal to the rated power P_{st} of the storage, the following relations can be identified:

$$\overline{P}_{charge} = P_{charge}(t) = P_{st} \quad (4.6)$$

$$\overline{P}_{load} = P_{load}(t) = P_{st} \quad (4.7)$$

At this point it should be stressed that the failure and repair rate of the storage do not represent physical component outages and repairs. The rates applied only consider the failing and repairing of the storage in terms of becoming discharged and recharged, respectively.

4.1.4 The discrete storage model

Approximating the storage device by assuming discrete charge levels has the advantage that MTTR and MTTF are known, because charge and discharge power are constant (equations (4.6), (4.7)). The approximation is closer to reality the smaller the differences between the respective charge levels are. If the storage device model however is combined with the earlier discussed model (see chapter 3), it will result in an increased amount of additional state spaces, the more exact the approximation is. A trade-off should be established between a detailed model and the associated modelling effort. Figure 4.3 shows a possible discretisation, where the difference between the charge levels equals 10% of the rated charge.

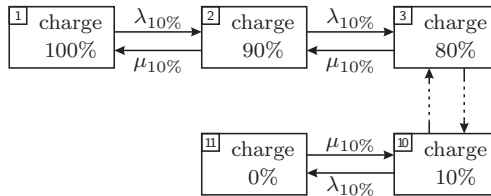


Figure 4.3: Representation of an energy storage device with discrete charge levels.

The discretisation does not have to be linear or uniform, as in this example. The failure and repair rates will then just be different for each transition. This approach could also be used if the modelled storage device technology would have charge and discharge efficiencies that depend strongly on momentary charge level and power; the different transition rates are determined with corresponding efficiencies.

Consider the storage to be modelled as a process $\{X(t), t \geq 0\}$ with continuous time and discrete state space $\mathcal{X} = \{1, 2, \dots, n\}$, i.e. as a continuous-time Markov chain or Markov process. For all times $t \geq 0$ the process then satisfies $X(t) = i, i \in \mathcal{X}$. Let X_i represent all situations where $X(t) = i$. Designating the energy level associated with state X_i as $E_{st}(X_i)$ then allows defining the charge level difference ΔE_{st} in case of a uniform discretisation as:

$$\Delta E_{st} = E_{st}(X_i) - E_{st}(X_{i+1}) = \frac{1}{n-1} \cdot E_{st}, \quad \forall i \in [1, 2, \dots, n-1] \quad (4.8)$$

According to equation (4.3), the corresponding failure rate λ_{st} consequently is defined as:

$$\lambda_{st} = \frac{P_{st}}{\Delta E_{st} \cdot \eta_{dch}} \cdot \frac{8760 \text{ h}}{\text{yr}} \quad (4.9)$$

Likewise, the repair rate μ_{st} can be found with equation (4.3) as:

$$\mu_{st} = \frac{P_{st} \cdot \eta_{ch}}{\Delta E_{st}} \cdot \frac{8760 \text{ h}}{\text{yr}} \quad (4.10)$$

The definitions of equations 4.9 and 4.10 show that failure and repair rate now are constant. It is also obvious from these equations, that any value could be used for ΔE in order to represent other differences in charge level.

4.1.5 Sensitivity of the model to the level of discretisation

Before the integration of the developed storage model into the multi-carrier model, a series of calculations is performed to identify the influence of the discretisation of the storage’s charge level. These investigations will give insights about which level of detail to choose when applying this approach. Figure 4.4 shows the state space diagram of a system consisting of a main connection and an energy storage device, modelled in the most fundamental way, when using the storage only as back-up during outages of the main supply.

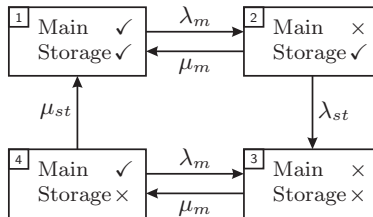


Figure 4.4: State space diagram of a main supply system combined with an energy storage device.

The load is defined to be constant at all times and equal to the rating of the storage output. The storage is thus used to retard and possibly even

bridge outages of the main supply. The failure state is state 3 and will be reached if the main supply cannot be restored before the storage is completely discharged. The state space is designed such that the storage device can only be recharged if the main connection has been restored. Theoretically, it would also be possible to have a transition from state 3 to state 1 directly. One example for such a transition would be a ruptured gas pipeline (physically damaged by e.g. construction work) that is repaired and refilled including a certain linepack, before it is reconnected to the load again. This situation is however not considered here.

The availability of supply can be found as the sum of the steady state probabilities of residing in states 1, 2 and 4. $P_i(t)$ denotes the probability that the process satisfies $X(t) = i$ and thus is the availability of state i at time t . The steady state probability P_i is then defined as (see appendix A):

$$P_i = \lim_{t \rightarrow \infty} P_i(t) \quad (4.11)$$

The up-state probability R can be calculated as:

$$R = P_1 + P_2 + P_4 \quad (4.12)$$

$$R = \frac{\mu_m \cdot (\lambda_{st} \cdot (\lambda_m + \mu_{st}) + \mu_{st} \cdot (\mu_m + \lambda_m))}{(\mu_m + \lambda_m) \cdot (\mu_m \mu_{st} + \mu_{st} \lambda_{st} + \lambda_m \lambda_{st})} \quad (4.13)$$

And the probability for being down is accordingly:

$$Q = P_3 = 1 - R \quad (4.14)$$

$$Q = \frac{\lambda_m \lambda_{st} \cdot (\lambda_m + \mu_{st})}{(\mu_m + \lambda_m) \cdot (\mu_m \mu_{st} + \mu_{st} \lambda_{st} + \lambda_m \lambda_{st})} \quad (4.15)$$

The influence of the failure rate of the storage can be identified with the following numerical example, using the values from table 4.1. The subscript 'm' in this context represents the main supply and the subscript 'st' the storage device. The resulting probability of having no supply is $Q = 0.001981$, corresponding to an annual outage duration of 17.35 h. Without a storage device available, the probability of being not supplied was $Q = 0.002278$, corresponding to an annual outage duration of 19.95 h. The outage duration is thus reduced by approximately 2.6 h.

P_{st}	= 20 kW	E_{st}	= 60 kWh
η_{ch}	= 1	η_{dch}	= 1
$MTTF_m$	= 8760 h	$MTTR_m$	= 20 h
$MTTF_{st}$	= 3 h	$MTTR_{st}$	= 3 h
λ_m	= 1 f/yr	μ_m	= 438 r/yr
λ_{st}	= 2920 f/yr	μ_{st}	= 2920 r/yr

Table 4.1: Numerical values for the example including a main supply and a simple model of an energy storage device.

The state space diagram in figure 4.4 contains a transition from state 2 to state 1, associated with the repair rate for the main supply. State 1 is defined to represent the situation where the main supply is operating and the storage device is fully charged. However, depending on the duration the process stays in state 2, the storage device will be partially discharged and state 1 is not accurately representing the physical state of the system. In order to investigate the difference of the results, a more detailed storage model is applied (figure 4.5), as introduced in section 4.1.4.

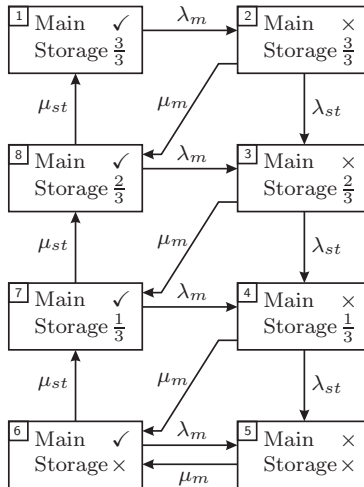


Figure 4.5: State space diagram of a main supply combined with an energy storage device, represented with discrete charge levels.

If the main supply is repaired while the process is in state 2, then a transition occurs into state 8, assuming that the charge level is not at its maximum level anymore and satisfies $E_{st}(t) \geq \frac{2}{3}E_{st}$. This is still a rough approximation to reality, representing the worst case, but more accurate than the model in figure 4.4.

Compared with the values in table 4.1 and according to equations (4.9) and (4.10), the failure and repair rates have to be adjusted, taking into account that the storage capacity is split into three charge levels:

$$\lambda_{st} = \frac{20 \text{ kW}}{\frac{1}{3} \cdot 60 \text{ kWh} \cdot 1} \cdot \frac{8760 \text{ h}}{\text{yr}} = 8760 \text{ f/yr}$$

$$\mu_{st} = \frac{20 \text{ kW} \cdot 1}{\frac{1}{3} \cdot 60 \text{ kWh}} \cdot \frac{8760 \text{ h}}{\text{yr}} = 8760 \text{ r/yr}$$

The load will experience an outage as soon as the process enters state 5. The probability of residing in state 5, i.e. the probability of failure, can be calculated to be $Q = 0.001968$, corresponding to an annual outage duration of 17.24 h. The result is fairly close to the result obtained with the example corresponding to figure 4.4; the difference is 0.11 h.

The transition rate matrix corresponding to figure 4.5 is displayed in equation (4.16). Apart from the first, the last and the fifth row, the matrix is symmetric. It is thus possible to define any level of discretisation and to calculate the corresponding matrix, following the approach for the state space diagram from figure 4.5. The rules for determining the matrix entries are outlined in table 4.2. This symmetry property is used to calculate the sensitivity of the result to the discretisation level, up to steps of 5%.

Figure 4.6 shows the expected annual outage duration for different levels of discretisation. The influence of the more detailed approximation is clearly visible. Modelling the energy storage device to consist of $\Delta E_{st} = \frac{1}{20}E_{st}$ charge steps results in an annual outage of about 17.18 h, compared to approximately 17.27 h for a discretisation with $\Delta E_{st} = \frac{1}{2}E_{st}$, i.e. 50% charge levels. Although the sensitivity is visible, the influence relative to the total outage reduction of 156 min is small.

Figure 4.7 shows both the influence of the discretisation resolution ΔE_{st} and the influence of the rated storage capacity E_{st} . With the load demand being $P_{load} = P_{st} = 20 \text{ kW}$, an energy storage device with a capacity of $E_{st} = 400 \text{ kWh}$ is able to supply the load for 20 h. This duration is equal to the MTTR of the main supply and results in an

$$A = \begin{bmatrix}
 -\lambda_m & \lambda_m & 0 & 0 & 0 & 0 & 0 & 0 & 0 & 0 \\
 0 & -(\mu_m + \lambda_{st}) & \lambda_{st} & 0 & 0 & 0 & 0 & 0 & 0 & \mu_m \\
 0 & 0 & -(\mu_m + \lambda_{st}) & \lambda_{st} & 0 & 0 & \mu_m & 0 & 0 & 0 \\
 0 & 0 & 0 & -(\mu_m + \lambda_{st}) & \lambda_{st} & \mu_m & 0 & 0 & 0 & 0 \\
 0 & 0 & 0 & 0 & -\mu_m & \mu_m & 0 & 0 & 0 & 0 \\
 0 & 0 & 0 & 0 & \lambda_m & -(\lambda_m + \mu_{st}) & \mu_{st} & 0 & 0 & 0 \\
 0 & 0 & 0 & \lambda_m & 0 & 0 & -(\lambda_m + \mu_{st}) & \mu_{st} & 0 & 0 \\
 \mu_{st} & 0 & \lambda_m & 0 & 0 & 0 & 0 & -(\lambda_m + \mu_{st}) & 0 & -(\lambda_m + \mu_{st})
 \end{bmatrix} \quad (4.16)$$

$\delta =$ number of discretisation steps, e.g. 10% steps result in $\delta = 10$

$n = 2 \cdot (\delta + 1) =$ number of system states, with state $(\frac{n}{2} + 1)$ representing the failure state

$i \in [2, 3, \dots, \frac{n}{2}], j \in [\frac{n}{2} + 2, \frac{n}{2} + 3, \dots, n - 1]$

$A(1, 1)$	$= -\lambda_m$	$A(1, 2)$	$= \lambda_m$
$A(n, 1)$	$= \mu_{st}$	$A(n, 3)$	$= \lambda_m$
$A(\frac{n}{2} + 1, \frac{n}{2} + 1)$	$= -\mu_m$	$A(\frac{n}{2} + 1, \frac{n}{2} + 2)$	$= \mu_m$
$A(i, i)$	$= -(\mu_m + \lambda_{st})$	$A(i, i + 1)$	$= \lambda_{st}$
$A(j, j - 1 - 2 \cdot (j - \frac{n}{2} - 2))$	$= \lambda_m$	$A(j, j)$	$= -(\lambda_m + \mu_{st})$
		$A(i, n + 2 - i)$	$= \mu_m$
		$A(j, j + 1)$	$= \mu_{st}$
		$A(n, n)$	$= -(\lambda_m + \mu_{st})$

Table 4.2: Transition rate matrix entries for state space diagrams following the systematics of figure 4.5, with a storage device divided into δ discrete charge level steps; remaining matrix entries are equal to 0.

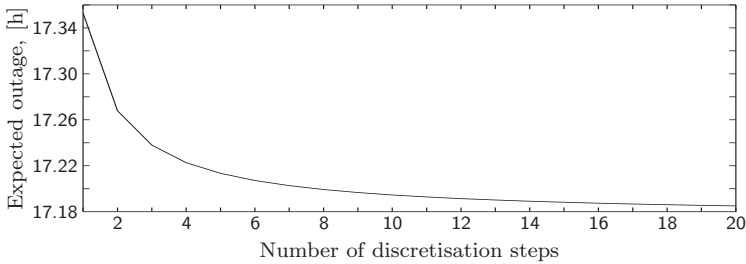


Figure 4.6: Expected annual outage duration as a function of the discretisation steps of the storage device, $E_{st} = 60$ kWh.

expected annual outage duration of approximately 7.5 h. The figure shows also that a more detailed discretisation becomes more influential for larger energy capacities, which is understandable. Thus, the number of discretisation steps should be chosen according to the duration the storage can supply the load. For the cases shown in figure 4.7, a discretisation in steps with $\Delta E_{st} = \frac{1}{5} E_{st}$ is sufficiently accurate – the resulting differences in the expected annual outage become negligible for smaller discretisation steps.

The main connection's repair rate μ_m is assumed identical for all concerned transitions. This reflects the worst case but it avoids introducing

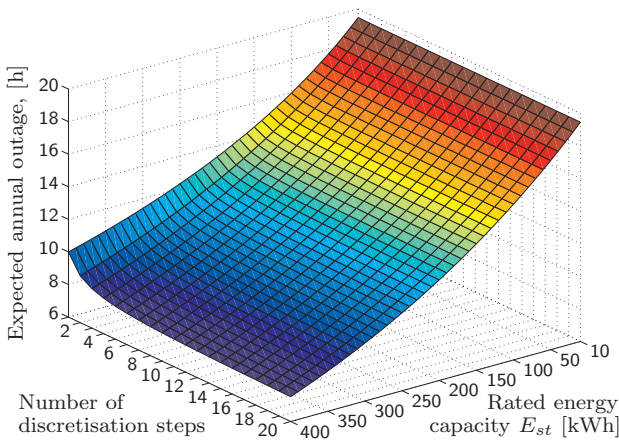


Figure 4.7: Expected annual outage as a function of the discretisation of the storage and of the rated energy capacity E_{st} in [kWh].

path dependent transition rates. This could be questioned for the following reason. If the process resides in state 1, according to figure 4.5, it will probably progress to states 3, 4 and eventually to state 5. One could claim that while discharging the storage, the repairing of the main supply would have already started and consequently the transition rate from state 5 to state 6 should take this into account. In other words, μ_m for that transition should be higher than for the transition from e.g. state 3 to state 8. This would mean that the rate μ_m is path dependent, which in turn is a contradiction to the Markov properties. For this reason, a constant and identical repair rate μ_m is used.

4.1.6 Using the storage for peak loads

Closing, a model is presented for investigating the use of a storage device for both peak shaving and supply outage bridging. The time periods, where peak shaving is necessary, can be identified from the load duration curve. Whenever the load exceeds the rated supply capacity, the storage can be utilized to supply this surplus demand. Hence, the model from figure 4.4 has to be extended, allowing the storage device to be discharged while the main supply is operating. Figure 4.8 shows the suggested model, representing the storage with only one charge level. The rate $r_{L>M}$ designates the rate of the load exceeding the capacity of the main supply and analogously, rate $r_{L\leq M}$ denotes the rate of the load decreasing below the capacity of the main supply.

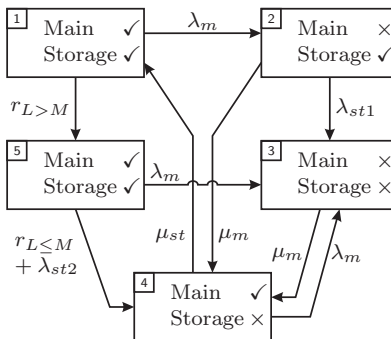


Figure 4.8: State space diagram of a main supply system combined with an energy storage device used for back-up and peak supply.

Thus, states 1 to 4 are identical as before in figure 4.4. Only, when residing in state 2, the repairing of the main supply results in a transition to state 4 and not to state 1, as discussed earlier. This reflects the fact that – because the storage is modelled with one charge level only – state 1 represents a fully charged and ready storage. However, after residing in state 2, the storage device cannot be assumed to be fully charged and state 1 would not represent the true system state. State 5 designates the situation where the storage operates in parallel with the main supply, to cover peaks. If the system resides in state 5 and the load supply fails, the system transits to state 3 and not state 2, again to reflect the storage device’s charge level. The same holds true for the case where the load demand decreases below the capacity of the main supply, the peaking period being finished. The process transits to state 4 in order to first recharge the storage device. This model hence represents a simple approach assuming valid but most likely worst case transition rates.

The failure rates λ_{st1} and λ_{st2} for the storage device are different in the models in figure 4.8, as they depend on the system the model represents. If the model is used within an electrical network, the storage device is a separate device with its own interface and the above stated assumption of constant load demand, both for back-up and peak shaving, can be considered valid and thus $\lambda_{st1} = \lambda_{st2}$. If the model is used for calculating linepack in a gas pipeline, then the discharge ratio of the linepack also depends on the momentary load. The reason for this is the common interface of both the supplying system and the storage device. Hence, $\lambda_{st1} \neq \lambda_{st2}$, taking into account the different volume flows through the compressor.

4.2 Extended Reliability Model for Multi-Carrier Energy Systems

This section uses the Markov model introduced in section 4.1 to complement the energy hub reliability model, discussed in chapter 3. The purpose of doing so is to be able to investigate the reliability implications from having an energy storage device in the energy hub. The storage device is modelled with one charge level only. The sensitivity analysis, displayed in figure 4.7, showed that a higher discretisation would increase the accuracy but the state space diagrams become large

and not easy to grasp. Besides, the general modelling approach does not change for a higher level of discretisation, it will only lead to slightly more accurate result. In fact, the state transition diagram representing the storage with one charge level can be replaced with a state transition matrix corresponding to an arbitrary number of discrete charge levels. Such a transition rate matrix can be constructed by applying the rules from table 4.2.

Figure 4.9 symbolically shows the storage as an explicit component in the hub, even though it could be representing line pack or thermal storage in the pipeline. Also, recalling that the energy hub is merely a conceptual model, the storage device is physically not connected to the direct connection, which is actually rather just a node. Hence, it is assumed that the storage device can supply both the load and the converters even if the direct connection would be non-operating. As before, the connections within the hub are considered ideal but for the designated major connections (converters and direct connections).

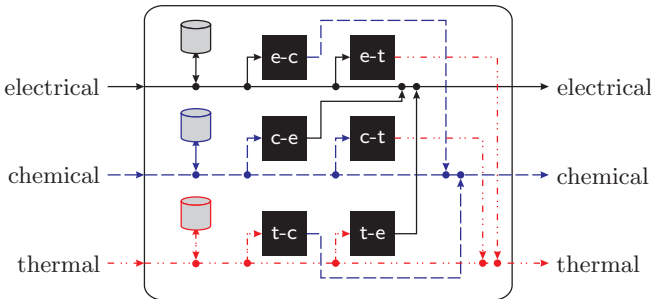


Figure 4.9: Representation of an energy hub with conversions between electrical, chemical and thermal energy and energy storage.

4.2.1 Reliability model with storage for back-up

The focus of this investigation is the reliability of supply at the outputs of the energy hub and in particular the influence of the respective connections and converters. In this context, the storage device is first considered only as back-up device, i.e. used for supply outage bridging; peak-shaving will not be discussed at the moment. However, peak supply plays an certain role when investigating the mutual influence of parallel energy carriers. Section 4.2.3 will discuss this.

If the storage device is only used for back-up purposes, the model is rather simple. Looking first at only one output illustrates this. Focusing e.g. on the electrical output shows that in case of a failure of the direct connection, the electrical storage can still supply the load. If this load is supplied also indirectly through a converter from the chemical system, however, the chemical storage's back-up capability is of no use for the electrical load. This is explained with the following reasoning. The supply of the hub, i.e. up to the hub input, is assumed ideal, as before in chapter 3. Hence, the supply of the chemical-electrical converter is ideal too; as outlined on the previous page, the hub should be understood rather as a node. Therefore, only if the supplying system is considered as well, the chemical storage will have an influence on the electrical output. Otherwise, when looking at the hub proper, the supply is already ideal. Besides this, the crucial element is the chemical-electrical converter itself and back-up supply cannot prevent an outage of this converter. Nor does the non-existence of a storage worsen the converter's reliability characteristics.

The reasoning holds true for all three outputs. Thus, only the energy storage device in parallel to the direct connection can improve the reliability of supply; the reliability of the indirect connections is independent of the respective storage options. Hence, the electrical output of the hub is supplied with the following three systems, illustrated in figure 4.10. As earlier, the expression $C_{\alpha\beta}$ denotes the connection from energy carrier α to energy carrier β , i.e. $\alpha, \beta \in [e, c, t]$. The energy storage device operating with energy carrier α is designated as E_α .

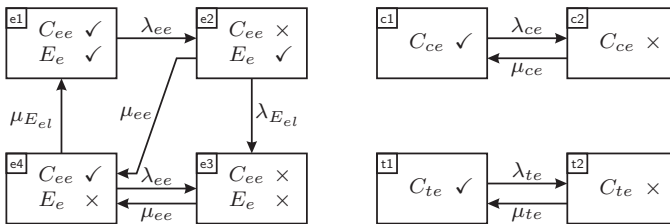


Figure 4.10: State space diagrams of the systems supplying the electrical output.

Assuming the storage device to have the same power rating as the electrical connection C_{ce} , gives the supplying states as states e1, e2, e4, c1 and t1. The three systems in figure 4.10 can furthermore be considered

independent and Kronecker products can be used to derive the state probabilities, as explained in appendix B, based on [18].

Section 3.5 already showed how to apply Kronecker products within the suggested modelling procedure. This approach is used again here, still following the procedures from section 3.3. The general approach is identical but for the changed state probability vector and the associated matrices. First, the altered model elements are discussed and then the complete procedure is restated.

The three supplying systems can each be described with a state probability vector $\vec{P}_{\alpha\beta}$ and a transition matrix $\mathbf{A}_{\alpha\beta}$. Both the chemical and the thermal component follow the form of equation 3.61, the electrical system is described as follows, with the transition rate matrix following the form given in table 4.2:

$$\begin{aligned} \vec{P}_{ee} \cdot \mathbf{A}_{ee} &= 0 & (4.17) \\ \vec{P}_{ee} &= [P_{e1} \quad P_{e2} \quad P_{e3} \quad P_{e4}] \\ \mathbf{A}_{ee} &= \begin{bmatrix} -\lambda_{ee} & \lambda_{ee} & 0 & 0 \\ 0 & -(\mu_{ee} + \lambda_{E_e}) & \lambda_{E_e} & \mu_{ee} \\ 0 & 0 & -\mu_{ee} & \mu_{ee} \\ \mu_{E_e} & 0 & \lambda_{ee} & -(\lambda_{ee} + \mu_{E_e}) \end{bmatrix} \end{aligned}$$

The transition rate matrix of the combined system, i.e. comprising all systems from figure 4.10, is defined as the Kronecker sum of the individual transition rate matrices, giving the 16×16 matrix \mathbf{A}_e :

$$\mathbf{A}_e = \mathbf{A}_{ee} \oplus \mathbf{A}_{ce} \oplus \mathbf{A}_{te} \quad (4.18)$$

The corresponding state probability vector \vec{P}_e is found as the Kronecker product of the individual state probability vectors $\vec{P}_{\alpha e}$:

$$\vec{P}_e = \vec{P}_{ee} \otimes \vec{P}_{ce} \otimes \vec{P}_{te} \quad (4.19)$$

Hence, each state space diagram can be analysed separately and the resulting state probabilities can be combined to give the state probabilities corresponding to matrix \mathbf{A}_e . As outlined in section 3.5, vector \vec{P}_e corresponds to vector \vec{R}_e and satisfies:

$$\vec{P}_e \cdot \mathbf{A}_e = 0 \quad (4.20)$$

Besides the probability of a state, its connection capacity must also be identified. Following the same approach as in section 3.5, the supply capacity matrices $\Gamma_{\alpha\beta}$ can be defined as follows, with C_{E_e} designating the power rating of the storage device:

$$\Gamma_{ee} = \begin{bmatrix} C_{ee} & 0 & 0 & 0 \\ 0 & C_{E_e} & 0 & 0 \\ 0 & 0 & 0 & 0 \\ 0 & 0 & 0 & C_{ee} \end{bmatrix} \quad (4.21)$$

$$\Gamma_{ce} = \begin{bmatrix} C_{ce} & 0 \\ 0 & 0 \end{bmatrix} \quad (4.22)$$

$$\Gamma_{te} = \begin{bmatrix} C_{te} & 0 \\ 0 & 0 \end{bmatrix} \quad (4.23)$$

Although state e1 represents a state with both the main supply and the storage operating, i.e. ready to operate, the capacity is limited to C_{ee} ; the storage device is not defined to operate in parallel. In contrast to the converters, whose actual capacities have to be evaluated in every time step, depending on the disposable capacities of the supplying systems, the storage device's capacity is assumed to be always at the rated level. This also means that the algorithm on page 35 for determining the momentary supply capacities does not have to be changed. The supply capacity of each state can be determined with Kronecker sums as:

$$\Gamma_e = \Gamma_{ee} \oplus \Gamma_{ce} \oplus \Gamma_{te} \quad (4.24)$$

The entries of this diagonal matrix correspond to the supply capacities of each state, as discussed before in section 3.5. The corresponding matrices and vectors for the chemical and thermal output are defined analogously. Before stating the complete procedure for calculating expected reliability of supply, the definition of the failure rate of the storage device has to be discussed again.

As defined in equation (4.9), the failure rate depends on the load demand. As long as the load is constant, the failure rate will thus be constant as well. When analysing a load during a certain period, the load though is most likely changing continuously. If the storage device has to take over the supply because of a failed main connection, the MTTF will change and accordingly the failure rate. However, a Markov process cannot contain time-dependent transition rates. This

contradiction can be solved by using discrete load profiles, being constant during each time interval of e.g. 15 min duration. In each period, the storage failure rate is constant but it changes from period to period. This can be understood as applying different models in each period, depending on the momentary load. With this approach, using discrete load profiles, the Markov conditions are not violated and still, the true benefit of the storage device can be accounted for. For lower loads, the storage device can bridge comparatively longer outages than for higher loads, and this should be considered when calculating EENS or the reliability of supply. The calculation procedure thus has to be adjusted to consider the different state probabilities in each period.

Subsequently, the modified procedure is presented, followed by the procedures for calculating EENS with and without load shedding. Then, the same example as before is applied, focusing only on the electrical output. This is suitable for identifying the benefit because of the energy storage device. A detailed example in section 4.3 will then discuss various aspects of complete energy hubs.

Procedure for calculating expected reliability of supply, including energy storage devices

- (1) Determine the reliability characteristics of the hub components and define matrices $\mathbf{\Lambda}$ and \mathbf{M} :

$$\mathbf{\Lambda} = \begin{bmatrix} \lambda_{ee} & \lambda_{ce} & \lambda_{te} \\ \lambda_{ec} & \lambda_{cc} & \lambda_{tc} \\ \lambda_{et} & \lambda_{ct} & \lambda_{tt} \end{bmatrix}; \quad \mathbf{M} = \begin{bmatrix} \mu_{ee} & \mu_{ce} & \mu_{te} \\ \mu_{ec} & \mu_{cc} & \mu_{tc} \\ \mu_{et} & \mu_{ct} & \mu_{tt} \end{bmatrix} \quad (4.25)$$

- (2) Define the $n \times 3$ load curve matrix \mathbf{L} , column-wise containing the hub output's individual load curves of length n with $t \in [1, \dots, n]$:

$$\mathbf{L} = [\vec{L}_e \quad \vec{L}_c \quad \vec{L}_t] \quad (4.26)$$

- (3) Determine the disposable connection capacities of the hub and define the $3 \times 3 \times n$ connection matrix ζ , using the load profile \mathbf{L} and the converter dispatch policy discussed in section 3.3.1:

$$\zeta(t) = \begin{bmatrix} C_{ee} & C_{ce}(t) & C_{te}(t) \\ C_{ec}(t) & C_{cc} & C_{tc}(t) \\ C_{et}(t) & C_{ct}(t) & C_{tt} \end{bmatrix} \quad (4.27)$$

- (4) Define the static storage characteristics matrix Φ , containing the energy capacity E_α , power rating C_{E_α} and the charge and discharge efficiencies:

$$\Phi = \begin{bmatrix} E_e & C_{E_e} & \eta_{ch_e} & \eta_{dch_e} \\ E_c & C_{E_c} & \eta_{ch_c} & \eta_{dch_c} \\ E_t & C_{E_t} & \eta_{ch_t} & \eta_{dch_t} \end{bmatrix} \quad (4.28)$$

- (5) Define the $3 \times 2 \times n$ storage failure and repair rate matrix Ψ , containing the rates for every time interval t :

$$\Psi(t) = \begin{bmatrix} \lambda_{E_e}(t) & \mu_{E_e} \\ \lambda_{E_c}(t) & \mu_{E_c} \\ \lambda_{E_t}(t) & \mu_{E_t} \end{bmatrix} \quad (4.29)$$

Using both the load curve matrix \mathbf{L} and the storage characteristics matrix Φ , the rates are given with equations (4.9) and (4.10) as:

$$\Psi(t) = \begin{bmatrix} \frac{\min(\mathbf{L}(t,1), \Phi(1,2))}{\Phi(1,1) \cdot \Phi(1,4)} & \frac{\Phi(1,2) \cdot \Phi(1,3)}{\Phi(1,1)} \\ \frac{\min(\mathbf{L}(t,2), \Phi(2,2))}{\Phi(2,1) \cdot \Phi(2,4)} & \frac{\Phi(2,2) \cdot \Phi(2,3)}{\Phi(2,1)} \\ \frac{\min(\mathbf{L}(t,3), \Phi(3,2))}{\Phi(3,1) \cdot \Phi(3,4)} & \frac{\Phi(3,2) \cdot \Phi(3,3)}{\Phi(3,1)} \end{bmatrix} \cdot \frac{8760 \text{ h}}{\text{yr}} \quad (4.30)$$

The discharge power cannot exceed the power rating C_{E_α} , which is why the smaller of both values is used for defining $\lambda_{E_\alpha}(t)$. The charge power is independent of the load and defined constant during all intervals, equal to the rating of the storage device; the resulting repair rate is constant. If the storage device is modelled with discrete charge levels, the number of discretisation steps has to be considered in the denominators. Furthermore, if a denominator is 0 because no energy storage device is installed, the rates are defined to be $\lambda_{E_\alpha}(t) = 0$ and $\mu_{E_\alpha} = 1$, similar to the failure and repair rate matrix entries for non-existent couplings.

- (6) Define the transition rate matrices $\mathbf{A}_{\alpha\beta}$ and the associated state probability vectors $\vec{P}_{\alpha\beta}$. Solve each equation system and use Kronecker products to calculate the resulting state probability vector, analogous to equation (4.19). With the failure rate being interval dependent, the state probabilities become interval dependent as well and have to be calculated for each time step. Combine the resulting state probability vectors in the $16 \times 3 \times n$ state probability matrix \mathbf{R} . This matrix contains the state probabilities for

each time interval t , with $i \in [1, 2, \dots, 16]$ representing the different states and $j \in [1, 2, 3]$ representing the electrical, chemical and thermal outputs:

$$\mathbf{R}(i, j, t) = \begin{bmatrix} \vec{R}_e(1, t) & \vec{R}_c(1, t) & \vec{R}_t(1, t) \\ \vec{R}_e(2, t) & \vec{R}_c(2, t) & \vec{R}_t(2, t) \\ \vdots & \vdots & \vdots \\ \vec{R}_e(16, t) & \vec{R}_c(16, t) & \vec{R}_t(16, t) \end{bmatrix} \quad (4.31)$$

- (7) Define the supply capacity matrices $\Gamma_{\alpha\beta}$ for every time step t , following equations (4.21) to (4.23), and calculate the combined supply capacity matrices Γ_α using Kronecker sums, as in equation (4.24). Summarise the resulting supply capacities with the $16 \times 3 \times n$ matrix $\mathbf{\Gamma}$ as follows:

$$\mathbf{\Gamma}(i, j, t) = \begin{bmatrix} \Gamma_e(1, 1, t) & \Gamma_c(1, 1, t) & \Gamma_t(1, 1, t) \\ \Gamma_e(2, 2, t) & \Gamma_c(2, 2, t) & \Gamma_t(2, 2, t) \\ \vdots & \vdots & \vdots \\ \Gamma_e(16, 16, t) & \Gamma_c(16, 16, t) & \Gamma_t(16, 16, t) \end{bmatrix} \quad (4.32)$$

- (8) Determine the $3 \times 16 \times n$ factor matrix \mathbf{F} , using the supply capacity matrix $\mathbf{\Gamma}$ and boolean expressions:

$$\mathbf{F}(j, i, t) = \begin{bmatrix} \mathbf{L}(t, 1) \leq \Gamma(1, 1, t) & \dots & \mathbf{L}(t, 1) \leq \Gamma(16, 1, t) \\ \mathbf{L}(t, 2) \leq \Gamma(1, 2, t) & \dots & \mathbf{L}(t, 2) \leq \Gamma(16, 2, t) \\ \mathbf{L}(t, 3) \leq \Gamma(1, 3, t) & \dots & \mathbf{L}(t, 3) \leq \Gamma(16, 3, t) \end{bmatrix} \quad (4.33)$$

- (9) Unlike the case without energy storage, the state probabilities are different in each time interval. Therefore, it is not possible to define the average occurrence of each state and to then multiply it with the constant state probability vector. Rather, in each time interval, the $3 \times 16 \times n$ matrix \mathbf{F} , defining whether a state is a supplying state or not, has to be multiplied with the $16 \times 3 \times n$ matrix \mathbf{R} , containing the probability of each state. The diagonal elements of the resulting $3 \times 3 \times n$ matrix give the probability of supply in each time interval t . Hence, summing this product along the third dimension (representing the time) and dividing it through the length of the load curve, results in the reliability of

supply of all three hub outputs, defined as vector \vec{R}_{out} :

$$\vec{R}_{out} = \begin{bmatrix} R_{e_{out}} \\ R_{c_{out}} \\ R_{t_{out}} \end{bmatrix} = \begin{bmatrix} \frac{1}{n} \sum_{t=1}^n \sum_{i=1}^{16} \mathbf{F}(1, i, t) \cdot \mathbf{R}(i, 1, t) \\ \frac{1}{n} \sum_{t=1}^n \sum_{i=1}^{16} \mathbf{F}(2, i, t) \cdot \mathbf{R}(i, 2, t) \\ \frac{1}{n} \sum_{t=1}^n \sum_{i=1}^{16} \mathbf{F}(3, i, t) \cdot \mathbf{R}(i, 3, t) \end{bmatrix} \quad (4.34)$$

This procedure can be summarised as follows. In every time interval, the failure rate for the energy storage device is determined, depending on the time required by the momentary load to discharge the storage. The transition rate matrix elements depend on this load and hence the probabilities of each state. The load profile is used to determine both the momentary capacity of the converters as well as which of the states is a supplying state and which is not. Adding the probabilities of these states results in the reliability of supply for each time interval. Summing up over all time intervals and dividing by the number of time intervals results in the expected availability of supply at each hub output.

EENS without load shedding

Expected energy not supplied (EENS) is calculated similar to before, using matrices \mathbf{F} , \mathbf{R} and the load curves stored in \mathbf{L} . Similar to section 3.3.2, EENS is calculated using the probability of failure in each time interval and multiplying it with the momentary load demand. Analogous to equation (3.34), the $3 \times n$ matrix \mathbf{Q} is defined to contain the probability of failure for each time interval $t \in [1, 2, \dots, n]$:

$$\mathbf{Q} = \begin{bmatrix} 1 - \sum_{i=1}^{16} \mathbf{F}(1, i, 1) \cdot \mathbf{R}(i, 1, 1) & \dots & 1 - \sum_{i=1}^{16} \mathbf{F}(1, i, n) \cdot \mathbf{R}(i, 1, n) \\ 1 - \sum_{i=1}^{16} \mathbf{F}(2, i, 1) \cdot \mathbf{R}(i, 2, 1) & \dots & 1 - \sum_{i=1}^{16} \mathbf{F}(2, i, n) \cdot \mathbf{R}(i, 2, n) \\ 1 - \sum_{i=1}^{16} \mathbf{F}(3, i, 1) \cdot \mathbf{R}(i, 3, 1) & \dots & 1 - \sum_{i=1}^{16} \mathbf{F}(3, i, n) \cdot \mathbf{R}(i, 3, n) \end{bmatrix} \quad (4.35)$$

Considering the duration Δt of one interval t to convert the power demand in energy equivalents, and multiplying \mathbf{Q} with the load curve \mathbf{L} , results in the individual values of EENS for each output, similar to

equation (3.35). The vector \vec{N}_{nls} contains the resulting values, with the index 'nls' identifying EENS with no load shedding considered:

$$\vec{N}_{nls} = \begin{bmatrix} N_{e_{nls}} \\ N_{c_{nls}} \\ N_{t_{nls}} \end{bmatrix} = \Delta t \cdot \begin{bmatrix} \sum_{t=1}^n \mathbf{Q}(1, t) \cdot \mathbf{L}(t, 1) \\ \sum_{t=1}^n \mathbf{Q}(2, t) \cdot \mathbf{L}(t, 2) \\ \sum_{t=1}^n \mathbf{Q}(3, t) \cdot \mathbf{L}(t, 3) \end{bmatrix} \quad (4.36)$$

EENS with load shedding

Considering load shedding when calculating EENS makes sense particularly if some supply paths are only able to supply a partial load. Analogous to section 3.3.2, the general procedure again first defines the supply level of each state; if the state is a supplying state, it supplies the load and if it is not a supplying state it still is able to supply a partial load equal to the state's supply capacity. The sum over all time interval then results in the EENS for each output. The momentary available supply capacities have already been defined above with matrix $\mathbf{\Gamma}$, for defining the factor matrix. To identify those states, which only supply a portion of the load, again the $3 \times 16 \times n$ matrix \mathbf{F}_{not} is defined, adding up to unity in each entry with matrix \mathbf{F} :

$$\mathbf{F}_{not}(j, i, t) = \neg \mathbf{F}(j, i, t) \quad (4.37)$$

Following the approach from section 3.3.2, the $3 \times 16 \times n$ matrix \mathbf{V} is defined, containing the momentary supply capacity of each state for each time interval, with $i \in [1, 2, \dots, 16]$ and $j \in [1, 2, 3]$:

$$\mathbf{V}(j, i, t) = \mathbf{F}_{not}(j, 1, t) \cdot \mathbf{\Gamma}(i, j, t) + \mathbf{F}(j, i, t) \cdot \mathbf{L}(t, j) \quad (4.38)$$

The expected energy supplied can be defined for every time interval t as:

$$\mathbf{E}(t) = \begin{bmatrix} \sum_{i=1}^{16} \mathbf{V}(1, i, t) \cdot \mathbf{R}(i, 1, t) & \cdots & \sum_{i=1}^{16} \mathbf{V}(3, i, t) \cdot \mathbf{R}(i, 3, t) \end{bmatrix} \quad (4.39)$$

The difference between the actual load demand and the expected energy supplied corresponds to the EENS. It can be defined as follows, with

the index 'ls' indicating the case considering load shedding:

$$\vec{N}_{ls} = \begin{bmatrix} N_{e_{ls}} \\ N_{c_{ls}} \\ N_{t_{ls}} \end{bmatrix} = \Delta t \cdot \begin{bmatrix} \frac{1}{n} \sum_{t=1}^n \left(\mathbf{L}(t, 1) - \sum_{i=1}^{16} \mathbf{V}(1, i, t) \cdot \mathbf{R}(i, 1, t) \right) \\ \frac{1}{n} \sum_{t=1}^n \left(\mathbf{L}(t, 2) - \sum_{i=1}^{16} \mathbf{V}(2, i, t) \cdot \mathbf{R}(i, 2, t) \right) \\ \frac{1}{n} \sum_{t=1}^n \left(\mathbf{L}(t, 3) - \sum_{i=1}^{16} \mathbf{V}(3, i, t) \cdot \mathbf{R}(i, 3, t) \right) \end{bmatrix} \quad (4.40)$$

4.2.2 Application example

To show the application and to investigate the benefit from using an energy storage device to bridge supply outages, the procedures defined in the previous section 4.2.1 are applied with the load curve from figure 3.9, redisplayed in figure 4.11.

Following equations (4.25) to (4.34), the different matrices are defined as follows, using the characteristics defined in the example in section 3.2.4¹

$$\Lambda = \begin{bmatrix} 0.5 & 1.5 & 1.5 \\ 0 & 0 & 0 \\ 0 & 0 & 0 \end{bmatrix} \quad \mathbf{M} = \begin{bmatrix} 4380 & 365 & 365 \\ 1 & 1 & 1 \\ 1 & 1 & 1 \end{bmatrix}$$

$$\zeta = \begin{bmatrix} 10000 & 2000 & 500 \\ 0 & 0 & 0 \\ 0 & 0 & 0 \end{bmatrix} \quad \Phi^2 = \begin{bmatrix} 1000 & 2000 & 1 & 1 \\ 0 & 0 & 0 & 0 \\ 0 & 0 & 0 & 0 \end{bmatrix}$$

$$\Psi^3(1) = \begin{bmatrix} 1279 & 8760 \\ 0 & 1 \\ 0 & 1 \end{bmatrix} \quad \Psi^3(2) = \begin{bmatrix} 1228 & 8760 \\ 0 & 1 \\ 0 & 1 \end{bmatrix}$$

Based on these matrices, the procedure can be applied to calculate the expected reliability of supply, following steps (1) to (9) on pages 76 to 79. Doing so, results in the expected reliability of supply as

¹The units of the matrix elements are not explicitly noted as they correspond to the units discussed earlier, when defining the matrices.

²The storage's energy capacity allows to supply a fifth of the rated capacity of the direct connection during half an hour.

³The load in time interval 1 is 1'460 W, resulting in $\lambda_{E_{el}}(1) = 1279$ f/yr, and 1'402 W in time interval 2, resulting in $\lambda_{E_{el}}(1) = 1228$ f/yr. The MTTR of the storage is always 1 h; this corresponds to a repair rate of 8760 r/yr.

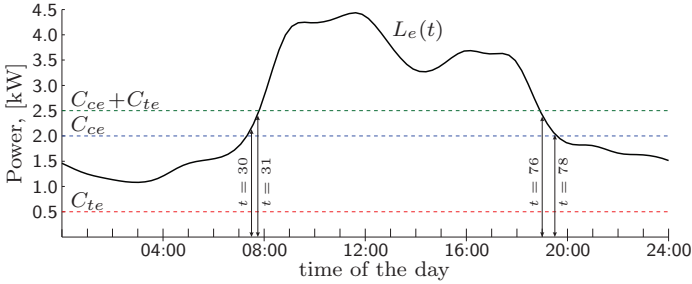


Figure 4.11: Load curve of an electrical load L_e supplied with an energy hub.

$R_{e_{out}} = 0.999958$, corresponding to an expected annual outage duration of 22.14 min. In the case with converters to the other energy carriers but without storage device, the outage duration was determined to be roughly 27.5 min. Hence, the storage device results in a further outage duration reduction of around 20%. EENS without considering load shedding reduces to $N_{nls} = 3.76$ Wh per day. If load shedding is considered, the resulting EENS satisfies $N_{ls} = 1.25$ Wh.

If only the storage device would be present, and no converters from the other energy carriers, the expected reliability would satisfy $R_{e_{out}} = 0.999900$, i.e. an outage duration of 52.45 min. Figure 4.12 shows the different values of the probability of an operating storage for the total load curve duration. During the higher load periods, the limiting factor is the rating of the storage device of 2 kW. During this period, failure and repair rate are identical and the probability of being operating hence is only 50%.

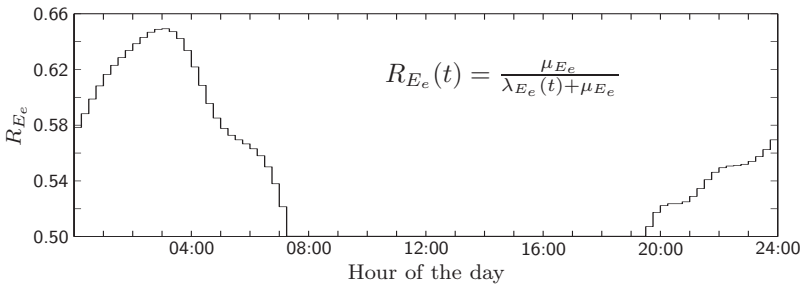


Figure 4.12: Probability of the storage device being operating.

Setting the storage capacity to zero leads to the same results as in the examples in chapter 3. Hence, the extended model is also applicable for the case without storage. Besides, as already mentioned at the beginning of this section, it is possible to represent the storage device with an arbitrary number of discrete charge levels. In state (6), the transition rate matrices for the different supply paths are modelled and then combined using Kronecker products. Hence, it is possible to apply the rules from table 4.2 at this stage and to model the storage as accurately as desired, simply adding the correspondingly larger matrix with the Kronecker approach. The sensitivity of the results towards the storage discretisation will be analysed in section 5.1.1, applying this approach. Before discussing an example with a fully occupied energy hub in section 4.3, a model for using the energy storage device in peak demand situations is discussed.

4.2.3 Reliability model with storage for back-up and peak supply

The models presented so-far considered the storage device to operate as back-up, only in case of an outage of the main supply. Even if both the main supply, i.e. the direct connection, and the storage were operational, the supply capacity of the corresponding state was set equal to the capacity of the direct connection only, see equation (4.21). Intuitively, the necessity of the storage device to provide power for peak loads might be small; the direct connection and the connections to the other energy carriers can be presumed to be dimensioned according to the load. Nevertheless, situations are conceivable where the energy storage is required to cover peaks. These peaks originate not necessarily directly from the load demand at the associated hub output but rather indirectly from the interconnections between the energy carriers. The following scenario illustrates this. The electrical load increases and exceeds the capacity of the main supply. This excess demand can be covered by the electrical storage, the chemical-electrical and/or the thermal-electrical converter. If the chemical-electrical converter would be used, the demand from the chemical network will increase. If the direct chemical load is at a high level as well, it could happen that their combined demand exceeds the power rating of the hub input. At this point, the chemical storage must be used for satisfying the demand peak, thus ensuring the supply of both the chemical load and indirectly

the electrical load. Otherwise, either the direct chemical load would have to be shed or the electrical load cannot anymore be part-supplied through the chemical-electrical converter. In other words, the storage is not only used to supply load peaks at the hub output but to absorb demand peaks at the hub input, keeping the demand from the network below the rated capacity, thus enabling the operation of converters.

The state space diagram for incorporating the peak supply operation mode has been discussed shortly with figure 4.8 in section 4.1.6. States 1 and 5 look similar in this model and the process resides in either one of them, depending on whether the storage is operating for peak supply or whether it is only ready to bridge an outage. Sometimes it is difficult to identify the appropriate transition rate between both states. Another approach is therefore to split the model from figure 4.8 into two models, each appropriate for one operation mode, as indicated with figure 4.13.

As long as the load demands from the converters and the directly connected loads stay below the rated capacities of the respective hub inputs, the storage device is in the back-up operation mode. Thus, the model in figure 4.13a) is used, discussed and successfully applied in section 4.2.1. As soon as the demand at the hub input exceeds the rated capacity, the storage device is required to cover the peak demand; the model in figure 4.13b) becomes valid. As long as the process resides in state 5, a peak demand can be satisfied. If, while residing in state 5, the main supply experiences an outage, the model transits to state 3. As discussed before, the storage device cannot be assumed to still be fully charged. Hence, once the storage device is discharged, the system cannot anymore use the storage; a part of the peak load has to be shed. If the load falls back below the capacity of the main supply, the model in figure

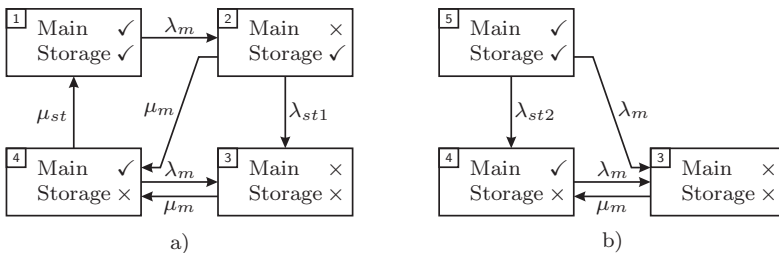


Figure 4.13: State space diagrams for a) back-up operation mode and b) peak supply operation mode.

4.13a) becomes valid again and the storage can be recharged. If the peak periods are short compared with the discharge time of the storage, it might be appropriate to represent the storage device with discrete charge levels. As outlined before, the application of Kronecker products allows to include transition rate matrices representing an arbitrary number of discrete charge levels.

So far, the models were based on steady-state probabilities for all system states, as discussed in appendix A.2. Looking at figure 4.13b) however indicates that the steady-state probability of state 5 will satisfy $P_5 = 0$. No transition leads back to state 5 and thus, for $t \rightarrow \infty$, the process will reside in either state 3 or state 4. Applying the model in the previously introduced calculation procedures would thus be meaningless; the state with the supply capacity of both the direct line and the storage device has a probability of 0 and hence is contributing neither to reliability of supply nor to a reduction of EENS. This is valid for long-term considerations but with load profiles changing every 15 min the storage device could clearly support the supply during certain intervals. This problem would not arise if the model from figure 4.8 would be applied, valid for both operation modes. However, when applying load profiles, which clearly identify whether the storage is required for peak supply or whether it can be used for back-up purposes, it is suitable to have two separate models, to be applied depending on the operation mode.

One solution to this issue would be to use the model from figure 4.13b) and to use Laplace transformations to define the time-dependent probabilities of residing in the individual states [18, 19]. This is however a drawback of the suggested Markov model for storage devices. With a constant discharge efficiency and a constant discharge power, the failure behaviour of the storage device is linear and does not follow the shape of the availability function, displayed in figure A.7. This identifies that the suggested approach of modelling a storage device as a Markov process is only an approximation.

The here chosen solution is to change the model from figure 4.13b) to contain one state, designated for recharging the storage device. Thus, a certain amount of the supply capacity of the direct connection is used for recharging the storage. To the load, this state looks like a derated state with a reduced supply capacity. The state space diagram from figure 4.13b) is changed accordingly, as displayed in figure 4.14. Hence, state 4 is operating with a reduced capacity only, designated by the bracketed check mark.

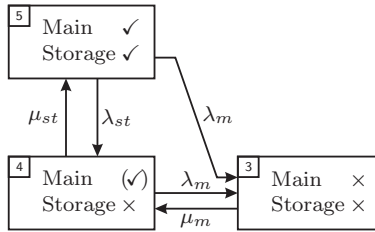


Figure 4.14: State space diagram for peak supply operation mode.

The model is an approximation with a certain trade-off. Without the storage device, all the load demand exceeding the rated hub input capacity would have to be shed. With the storage, the demand peak can be satisfied for a certain time, until the storage is discharged. Then, in turn, a portion of the hub input capacity is used to recharge the storage device. Thus, while residing in state 4, more load has to be shed than if no storage device would be available. The purpose of this model however is to achieve a certain steady-state probability for state 5. Thus, the amount of power used to recharge the storage device could be set relatively small, resulting in state 4 having a supply capacity that is only slightly lower than the rated capacity.

The expected reliability of supply can be calculated using the procedure from before, discussed for the application of the storage device as back-up support. In step (6) of the procedure, Kronecker products are applied to calculate the transition rate matrices and the state probability vectors, using equations (4.18) and (4.19). This calculation has to be performed for every time interval, as the storage device's discharge time depends on the load demand in each period. In this step of the procedure it is thus possible to choose the appropriate state space model. If the load demand is above the rated capacity of the direct connection, the transition rate matrix corresponding to figure 4.14 is applied in the Kronecker multiplication. If the load demand stays below the rated capacity, the transition rate matrix representing figure 4.13a) is applied.

Earlier, it was necessary to identify the momentary available supply capacities of the different converters. If the load was close to the rated capacity of the direct connection, the converters were defined to be turned off or to have a reduced capacity, as discussed on page 35. This

procedure has to be extended to consider that the storage device could be used for peaking. As discussed in the context of the pseudocode segment on page 35, certain assumptions and dispatch priorities have to be considered. In this context, it is assumed again that no economic dispatch is performed, i.e. as long as the loads stay below the maximum capacity of the respective direct connections, the direct connections are supplying the loads. The remaining supply margins are used to power the different converters. As long as this situation holds true, no demand peak exists and the model from figure 4.13a) is applied. If the demand at the hub input however increases – either because of the directly supplied load or because of the converters, supplying loads indirectly – the storage device is required to cover the peak demand at the hub input. In other words, if the maximum supply capacity of a hub input is reached, the storage is required to absorb the hub-internal peak demand. With the direct connection having priority, the storage consequently is used to serve demand from the converters. Hence, the failure rate of the storage has to be added to the failure rate of the concerned converter; this supply path will only persist until either the storage is discharged or the converter has an outage.

Consequently, the procedure from page 35 has to be extended accordingly, taking into account the additional supply capacities. It is recommended to first calculate the available converter and connection capacities without considering the storage. If it is possible to supply all loads, the derived configuration should be chosen and the storage treated as back-up device. Otherwise, the supply capacity is extended by the rated capacity of the storage and the configuration is redefined. Thus, the storage device is primarily used as a back-up device and should only supply peaks in case of emergency. Of course, as mentioned earlier, other dispatch policies are possible.

The resulting connection and converter capacities are used to define the momentary $\Gamma(t)$. Furthermore, the failure rate of the storage device has to be defined. If the storage device is used for back-up supply, the failure rate is defined as in equation (4.30). However, if the storage device is used for peak supply, the discharge demand P_{st_α} from the storage has to be identified as follows:

$$\begin{aligned}
 P_{st_e} &= -(\zeta(1, 1) - L_e(t) - \zeta(2, 1) - \zeta(3, 1)) \\
 P_{st_c} &= -(\zeta(2, 2) - L_c(t) - \zeta(1, 2) - \zeta(3, 2)) \\
 P_{st_t} &= -(\zeta(3, 3) - L_t(t) - \zeta(1, 3) - \zeta(2, 3))
 \end{aligned} \tag{4.41}$$

$$A = \begin{bmatrix} -\lambda_m - \lambda_{st} & \lambda_m & 0 & 0 & 0 & 0 & 0 & \lambda_{st} \\ 0 & -(\mu_m + \lambda_{st}) & \lambda_{st} & 0 & 0 & \mu_m & 0 & 0 \\ 0 & 0 & -(\mu_m + \lambda_{st}) & \lambda_{st} & 0 & 0 & 0 & 0 \\ 0 & 0 & 0 & -\mu_m & \mu_m & 0 & 0 & 0 \\ \mu_{st} & 0 & 0 & \lambda_m & -(\lambda_m + \mu_{st}) & 0 & 0 & 0 \\ 0 & 0 & 0 & \lambda_m & \lambda_{st} & -(\lambda_m + \lambda_{st}) & 0 & 0 \\ 0 & 0 & 0 & \lambda_m & 0 & \lambda_{st} & -(\lambda_m + \lambda_{st}) & 0 \end{bmatrix} \quad (4.42)$$

$\delta =$ number of discretisation steps, e.g. 10% steps result in $\delta = 10$

$n = 2 \cdot \delta + 1 =$ number of system states, with state $(\frac{n-1}{2})$ representing the failure state

$i \in [2, 3, \dots, \frac{n-1}{2}]^\dagger, j \in [\frac{n+1}{2} + 2, \frac{n+1}{2} + 3, \dots, n]^\ddagger; \quad \dagger$ only valid for $n > 3$

$$\begin{array}{l} A(1, 1) = -(\lambda_m + \lambda_{st}) \quad A(1, 2) = \lambda_m \quad A(1, n) = \lambda_{st} \\ A(\frac{n+1}{2}, \frac{n+1}{2}) = -\mu_m \quad A(\frac{n+1}{2}, \frac{n+1}{2} + 1) = \mu_m \\ A(\frac{n+1}{2} + 1, 1) = \mu_{st} \quad A(\frac{n+1}{2} + 1, \frac{n+1}{2}) = \lambda_m \quad A(\frac{n+1}{2} + 1, \frac{n+1}{2} + 1) = -(\lambda_m + \mu_{st}) \\ A(i, i) = -(\mu_m + \lambda_{st}) \quad A(i, i+1) = \lambda_{st} \quad A(i, n+1-i) = \mu_m \\ A(j, 3+n-j) = \lambda_m \quad A(j, j-1) = \lambda_{st} \quad A(j, j) = -(\lambda_m + \lambda_{st}) \end{array}$$

Table 4.3: Transition rate matrix entries for state space diagrams following the systematics of figure 4.15, with a storage device divided into δ discrete charge level steps; remaining matrix entries are equal to 0.

Hence, as long as the resulting values in equation (4.41) are negative, the storage device is not required to peak supply and the model from figure 4.13a) is applied. For those energy carriers where the resulting values are positive, the model from figure 4.14 is applied. The failure rate of the storage device is then given with the corresponding value from equation (4.41) and the rated energy capacity of the storage. As mentioned, this failure rate also affects the converters. If the storage is required for the converters to operate, the storage device's failure rate has to be added to the converters's failure rate; the converter fails operation as soon as the storage is discharged.

It is also possible to use discrete charge levels to represent the energy storage device, as before. As the model is not straightforward, it is displayed in figure 4.15. The resulting transition rate matrix is displayed in equation (4.42) and analogous to table 4.2, it is possible to define a set of rules to create the transition rate matrix valid for any level of discretisation, displayed in table 4.3. The subscript 'm' designates the direct connection and 'st' represents the storage. The derated state is state 5, immediately starting to recharge the storage as soon as it is discharged. It is important to consider that the storage failure rate

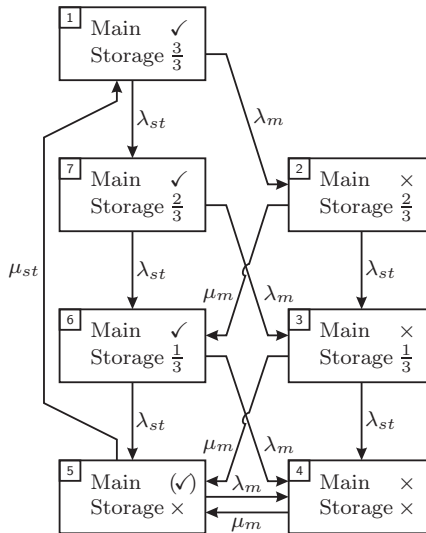


Figure 4.15: State space diagram for peak supply operation mode.

corresponds to discharging a third of the total energy capacity but that the repair rate represents the full recharging in one step.

When applying this model, it is crucial to correctly define the supply capacities, i.e. considering a certain margin for recharging the energy storage device. In chapter 5, an investigation will be performed, analysing the influence of the chosen charge power. The general procedure is identical to equations (4.25) to (4.34), which is why the procedure is not restated here. Besides, the following section contains an application example covering the different special cases and illustrating the discussed concepts in detail.

It is important to note again that during certain time intervals some converters are treated as pure back-up or standby connections. Their rating might be too small to be able to contribute to supplying a load but in case of supply outages, they can supply a partial load. Hence, the supply capacity matrix might suggest loop flows, with converters converting e.g. from the chemical network to the thermal network and vice versa at the same time. However, these converters are merely standby capacities, to start operating in case of imminent loss of load. Besides, the algorithm on page 35, used to defined the momentary supply capacities, ensures that no loop connections can establish.

4.3 Application Example

This section presents a short series of subsequent load levels, intended to indicate how the simulation algorithm works. A fully occupied hub is assumed albeit some conversion path are purely theoretical. Table 4.4 lists the characteristics of all involved components. Most values are educated guesses and chosen such that differences in the results are well recognisable. The direct connections were always assumed to have one failure per year and the indirect connections are assumed to fail 5 times yearly. The mean time to repair was chosen to be one day except for the electrical connection with half a day and for the chemical and thermal networks with 3 days. These values can be used to define matrices $\mathbf{\Lambda}$, \mathbf{M} and $\mathbf{\Phi}$, following steps (1) and (4) on page 76f. The maximum supply capacities at the hub inputs are assumed to be equal to the ratings of the direct connections. Furthermore, to focus on the general algorithm performance, all efficiencies are assumed equal to 100% and the storage devices are modelled with one charge level.

$C_{ee} = 10$ kW	$\lambda_{ee} = 1$ f/yr	$\mu_{ee} = 730$ r/yr
$C_{ce} = 2$ kW	$\lambda_{ce} = 5$ f/yr	$\mu_{ce} = 365$ r/yr
$C_{te} = 0.5$ kW	$\lambda_{te} = 5$ f/yr	$\mu_{te} = 365$ r/yr
$C_{ec} = 2$ kW	$\lambda_{ec} = 5$ f/yr	$\mu_{ec} = 365$ r/yr
$C_{cc} = 8$ kW	$\lambda_{cc} = 1$ f/yr	$\mu_{cc} = 121$ r/yr
$C_{tc} = 6$ kW	$\lambda_{tc} = 5$ f/yr	$\mu_{tc} = 365$ r/yr
$C_{et} = 5$ kW	$\lambda_{et} = 5$ f/yr	$\mu_{et} = 365$ r/yr
$C_{ct} = 5$ kW	$\lambda_{ct} = 5$ f/yr	$\mu_{ct} = 365$ r/yr
$C_{tt} = 15$ kW	$\lambda_{tt} = 1$ f/yr	$\mu_{tt} = 121$ r/yr
$C_{E_e} = 1$ kW	$C_{E_c} = 8$ kW	$C_{E_t} = 15$ kW
$E_e = 2$ kWh	$E_c = 20$ kWh	$E_t = 15$ kWh
$\eta_{che} = 1$	$\eta_{chc} = 1$	$\eta_{cht} = 1$
$\eta_{dch_e} = 1$	$\eta_{dch_c} = 1$	$\eta_{dch_t} = 1$

Table 4.4: Characteristics of the hub components.

To be able to define the further required matrices and vectors, the load profile has to be known. A short load profile has been constructed, to show different aspects of the procedures developed and discussed in section 4.2. The load profile represents the average power demand during half an hour and consists of 6 entries, i.e. the curve covers 3 h. The chemical demand is chosen to be constant while the electrical and the thermal loads increase for a certain period. This constellation allows to analyse the behaviour of both expected reliability of supply and EENS. In particular, it will be seen that the increasing electrical and thermal loads result in reduced supply paths to the chemical load, resulting in larger amounts of EENS.

$$\mathbf{L} = \begin{bmatrix} 7 & 6 & 10 \\ 12 & 6 & 12 \\ 12.5 & 6 & 14 \\ 13 & 6 & 16 \\ 11 & 6 & 10 \\ 9 & 6 & 10 \end{bmatrix} \begin{matrix} t = 1 \\ t = 2 \\ t = 3 \\ t = 4 \\ t = 5 \\ t = 6 \end{matrix}$$

The six time intervals will now be analysed step by step, discussing the consequences from using the chosen dispatch policy rule. Figure 4.16 displays the load profiles from matrix \mathbf{L} , together with the capacities of the direct connections. Obviously, the electrical load is at risk during hours 2 to 5 and the thermal load during hour 4.

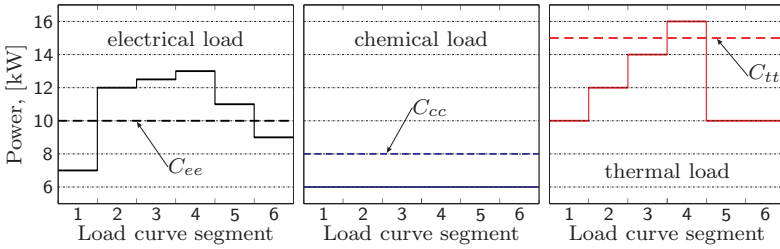


Figure 4.16: Load profiles at the hub outputs and the capacities of the direct connections.

Following the procedure from before, first the connection matrix ζ and the storage failure rate matrix Ψ have to be defined. Using the dispatch policy introduced on page 35 and discussed also in section 4.2, the resulting connection matrix can be derived. Figure 4.17 shows the different disposable converter capacities in a graphical way.

During step 1, each load can be supplied by its own direct supply and the storage devices operate as back-up. The matrix $\Psi(1)$ can thus be defined according to equation (4.30). The model for the direct connections corresponds to figure 4.13a), to be used within the Kronecker summation. The resulting reliability of supply and EENS are found as:

$$R_{out}(1) = \begin{bmatrix} 0.998632 \\ 0.999790 \\ 0.991970 \end{bmatrix}; \quad N_{nls}(1) = \begin{bmatrix} 4.7880 \\ 0.6311 \\ 40.1518 \end{bmatrix} \quad [\text{Wh}]; \quad N_{ls}(1) = \begin{bmatrix} 3.6781 \\ 0.3177 \\ 30.2495 \end{bmatrix} \quad [\text{Wh}]$$

The chemical load can be supplied redundantly with the electrical-chemical and thermal-chemical converters together being able to supply 6 kW. The effect of this is well identifiable from both the reliability of supply and EENS. The performance of the thermal output is considerably lower than those of the other two outputs. The reason for this is the longer repair time, compared with the electrical connection, and the non-existence of a redundant supply, compared with the chemical connection.

In interval 2, the electrical and the thermal load have increased, whereas the electrical load now exceeds the supply capacity of the direct connection. Figure 4.17 shows that the chemical system is henceforth providing the full margin of 2 kW (difference between the rated capacity of the hub input and the chemical load) to the chemical-electrical converter,

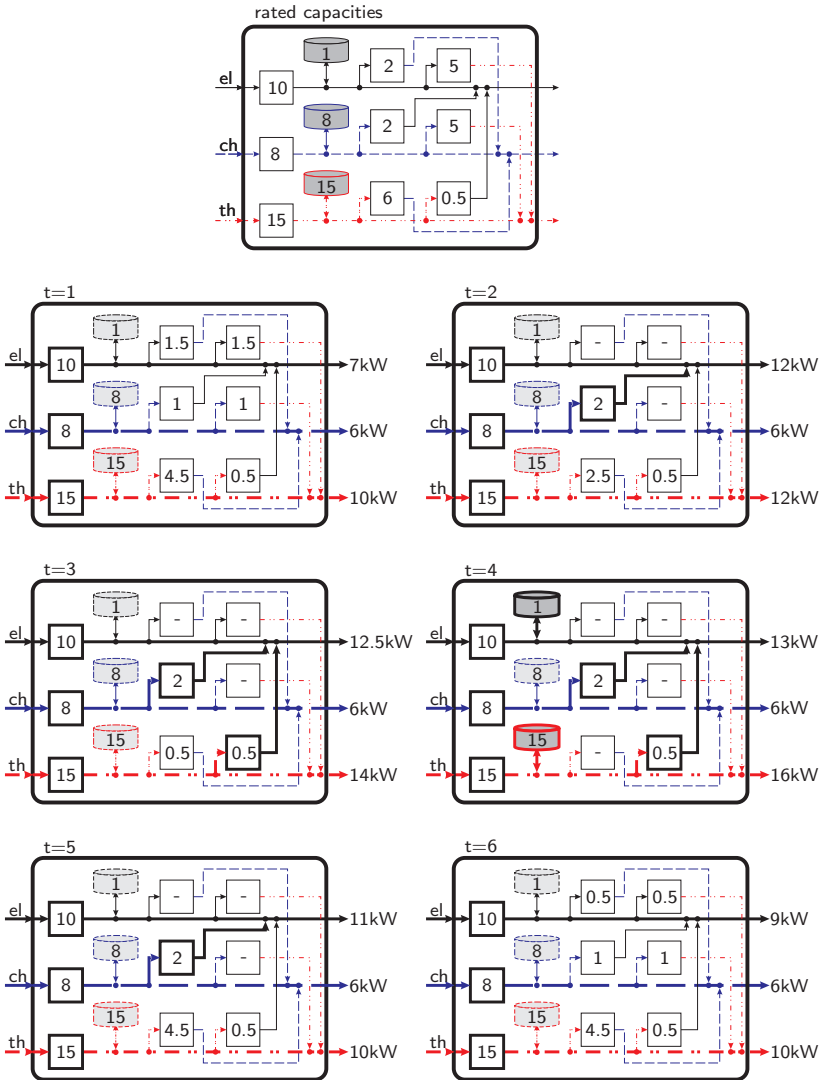


Figure 4.17: Converter capacities during the different time steps.

thus guaranteeing the supply of the electrical load. The electrical storage consequently is not required and can be treated as back-up, using again the model from figure 4.13a). Still, the electrical load's supply now depends on both the direct connection and the chemical-electrical converter, resulting in a reduction of $R_{e_{out}}$:

$$R_{out}(2) = \begin{bmatrix} 0.985137 \\ 0.992164 \\ 0.991942 \end{bmatrix}; \quad N_{nls}(2) = \begin{bmatrix} 89.1781 \\ 23.5081 \\ 48.3457 \end{bmatrix} \text{ [Wh]}; \quad N_{ls}(2) = \begin{bmatrix} 16.5902 \\ 13.8454 \\ 48.3457 \end{bmatrix} \text{ [Wh]}$$

The reliability of supply of the thermal output is slightly decreased as well. The reason for this are not the non-operating converters to the thermal load but the higher load and thus the higher failure rate of the thermal storage, operating as back-up device. Already in time step 1, the converters from the neighbouring system were too small to improve the reliability of supply. Still, both the chemical and the thermal load experience a higher EENS despite not being at risk. The reason for this is the missing support from the electrical network and – in the case of the thermal load – the chemical supply now dispatching all available power to the chemical-electrical converter. With no support from the neighbouring systems, no converter is available to supply a partial load and thus, the thermal load's EENS is independent of load shedding.

During time interval 3, the electrical and the thermal load increase further. According to figure 4.17, the electrical load can still be supplied without requiring the electrical storage device to peak. However, the load supply now depends on three components: the direct electrical connection and both converters from the chemical and the thermal network, respectively. Because of the increased thermal load, the support for the thermal-chemical converter has to be further reduced. This is visible in the increasing EENS for the chemical load:

$$R_{out}(3) = \begin{bmatrix} 0.971824 \\ 0.992164 \\ 0.991923 \end{bmatrix}; \quad N_{nls}(3) = \begin{bmatrix} 176.0980 \\ 23.5081 \\ 56.5404 \end{bmatrix} \text{ [Wh]}; \quad N_{ls}(3) = \begin{bmatrix} 23.6341 \\ 21.5756 \\ 56.5404 \end{bmatrix} \text{ [Wh]}$$

If load shedding is not considered, the electrical load risks a comparatively high EENS. As mentioned, all three supply paths have to be operating to supply the load and hence the probability of supply equals the product of the probability of supply of each supply path. Still, if load shedding is considered, the electrical load is actually less at risk than

the thermal load, having no support from the neighbouring systems at all. EENS of the thermal load rises further, with the storage failure rate increasing proportionally to the load demand, now at $L_t(3) = 14$ kW.

Advancing to time interval 4 shows that, besides the electrical load, the thermal load exceeds its rated supply capacity as well. If no storage device would be present, the 2 kW available from the chemical input would be split evenly to both systems. This would result in unsupplied load at the electrical output. The electrical load supply would be short by 2 kW and the thermal load supply would be exactly at the required 16 kW. Thus, only the electrical load is at risk and the storage could be used to supply the demand peak. Unfortunately, the electrical storage is rated 1 kW only and so the electrical load supply is still short by 1 kW. This is why the chemical network is providing all of its available margin to the chemical-electrical converter, thereby requiring the thermal system to utilize its own storage. According to figure 4.17, the thermal storage is also providing power to the thermal-electrical converter. This is meaningful, as the thermal storage is rated 15 kWh and only has to supply a load demand of 1 kW, respectively 1.5 kW including the converter. The MTTF of the thermal storage results with 10 h and MTTF of the electrical storage is at 4 h, following this dispatch policy. Obviously, providing energy to the thermal-electrical converter increases the overall survival time of the loads connected to the hub.

Both the electrical-electrical and the thermal-thermal connection are using the storage for peak supply. It is thus necessary to apply the model from figure 4.14 and to calculate the storage failure rate using equation (4.41). During time step 3, the thermal storage was ready to provide back-up for a load of 14 kW. The resulting failure rate was $\lambda_{E_t} = 8176$ f/yr. Hence, MTTF was only a little bit more than an hour, which is true with $E_t = 15$ kWh stored energy and an energy demand of $L_t(3) = 14$ kW. With the storage device now in peak supply mode, the demand from the storage has reduced to $P_{st_t} = 1.5$ kW, giving a failure rate of $\lambda_{E_t} = 876$ f/yr. On the other hand, the chosen model contains a derated state with a reduced supply capacity. The connection capacity matrix Γ_{tt} in time steps 3 and 4 result as follows, with the entries in [kW]:

$$\Gamma_{tt}(3) = \begin{bmatrix} 15 & 0 & 0 & 0 \\ 0 & 15 & 0 & 0 \\ 0 & 0 & 0 & 0 \\ 0 & 0 & 0 & 15 \end{bmatrix}; \quad \Gamma_{tt}(4) = \begin{bmatrix} 30 & 0 & 0 \\ 0 & 0 & 0 \\ 0 & 0 & 11.25 \end{bmatrix}$$

Hence, the derated state uses one quarter of the installed capacity to recharge the storage device. The repair rate thus is equal to $\mu_{E_t} = 2190$ r/yr, as it takes exactly 4 h to recharge the storage. Similar observations can be made for the electrical-electrical connection, where the load demand from the storage decreased from 10 kW in the back-up mode to 0.5 kW in the peak supply mode. Hence, the transition rate matrices for the supply of the electrical and the thermal load are changed, taking into account the changed models for the direct connections. The transition rate matrix for the electrical load, however, has to be changed further. The thermal-electrical converter can only operate as long as the thermal storage is available and, thus, the transition rate matrix \mathbf{A}_{te} has to be adjusted; it is necessary to combine the failure and repair rates as discussed with equation (3.52) for two components forming a series system:

$$\mathbf{A}_{te}(t = 3) = \begin{bmatrix} -5 & 5 \\ 365 & 365 \end{bmatrix}; \quad \mathbf{A}_{te}(t = 4) = \begin{bmatrix} -881 & 881 \\ 2158 & -2158 \end{bmatrix}$$

The expected reliability of supply and EENS during time step 4 are finally found as:

$$R_{out}(4) = \begin{bmatrix} 0.656658 \\ 0.992164 \\ 0.708200 \end{bmatrix}; \quad N_{nls}(4) = \begin{bmatrix} 2231.7227 \\ 23.5081 \\ 2334.4006 \end{bmatrix} \text{ [Wh]}; \quad N_{is}(4) = \begin{bmatrix} 168.1962 \\ 23.5081 \\ 739.1317 \end{bmatrix} \text{ [Wh]}$$

As expected, the reliability of supply both for the electrical and the thermal load is drastically reduced. Nevertheless, without the storage device present – or the converters from the other energy carriers – the probability would be 0 for both loads. Due to the energy hub, i.e. the interconnections between the energy carriers, both loads can be supplied albeit with a poor reliability. EENS for the chemical load is independent of load shedding; no converters are available to supply partial loads and hence, an outage of the chemical connection results in total loss of load. In that respect, the electrical load profits most from the neighbouring systems, having a considerably lower value for EENS when implying load shedding. The EENS of the thermal load shows that the possibility of partial load supply, while residing in the derated state, results in an outage reduction of roughly two thirds compared with the case with no load shedding.

In time step 5, the thermal load has reduced and is not anymore at risk, while the electrical load still requires support. The resulting converter

capacities are displayed in figure 4.17, showing that the thermal system is almost providing a redundant supply for the chemical load again. Although this will not improve the reliability of supply of the chemical load, it will improve EENS. The storage devices are not anymore required and each load is supplied with the model from figure 4.13a). The different values result as:

$$R_{out}(5) = \begin{bmatrix} 0.985137 \\ 0.992164 \\ 0.991970 \end{bmatrix}; \quad N_{nls}(5) = \begin{bmatrix} 81.7465 \\ 23.5081 \\ 40.1518 \end{bmatrix} \text{ [Wh]}; \quad N_{ls}(5) = \begin{bmatrix} 9.1587 \\ 6.1153 \\ 40.1518 \end{bmatrix} \text{ [Wh]}$$

In time step 6, finally, also the electrical load has decreased again and all loads can be supplied again with the direct connections only. The given load levels are still close the rated capacities of the respective direct connections and the converters are only allocated comparatively small capacities. Hence, the reliability of supply is not affected by the converters but they lead to decreased amounts of EENS, particularly when considering load shedding:

$$R_{out}(6) = \begin{bmatrix} 0.998632 \\ 0.992164 \\ 0.991970 \end{bmatrix}; \quad N_{nls}(6) = \begin{bmatrix} 6.1560 \\ 23.5081 \\ 40.1518 \end{bmatrix} \text{ [Wh]}; \quad N_{ls}(6) = \begin{bmatrix} 5.0462 \\ 4.1827 \\ 34.2104 \end{bmatrix} \text{ [Wh]}$$

Finally, the average expected reliability of supply and overall EENS are found as:

$$R_{out} = \begin{bmatrix} 0.932670 \\ 0.993435 \\ 0.944662 \end{bmatrix}; \quad N_{nls} = \begin{bmatrix} 2589.6893 \\ 118.1716 \\ 2559.7420 \end{bmatrix} \text{ [Wh]}; \quad N_{ls} = \begin{bmatrix} 226.3035 \\ 69.5448 \\ 948.6295 \end{bmatrix} \text{ [Wh]}$$

While the chemical load's expected reliability of supply profits from the redundant supply during the first time interval, both the electrical and the thermal load show the considerable influence of those periods, where the load exceeds the rated capacity. If a direct connection is rated barely larger than the corresponding load, only a little margin is disposable to be allocated to the converters. This is the case both in the electrical and the chemical system. Consequently, little capacity is available for partial supply of the thermal load, experiencing a considerable amount of EENS despite load shedding.

If no energy storage devices would be installed, the following values can be found:

$$R_{out} = \begin{bmatrix} 0.823227 \\ 0.993132 \\ 0.989569 \end{bmatrix}; \quad N_{nls} = \begin{bmatrix} 6857.9666 \\ 123.6109 \\ 402.3039 \end{bmatrix}; \quad N_{ls} = \begin{bmatrix} 1072.1925 \\ 72.7459 \\ 281.5685 \end{bmatrix}$$

Obviously, the electrical load and the chemical load profit from the energy storage devices, particularly in terms of reliability of supply. Interestingly, however, the presence of the storage devices seems to be disadvantageous for the thermal load. The reason for this is the chemical system providing the remaining supply capacity mostly to the electrical load because the thermal system can also use its storage device. However, the thermal storage device is relatively small compared with the average thermal load. Thus, without the storage device the chemical surplus would be split evenly to the electrical and the thermal load during time step 4. This would result in an outage of the electrical load but the thermal load could just be maintained. In both cases, i.e. with and without storage device, the thermal load requires two components during time step 4 in order to operate, the direct connection and either the chemical-thermal converter or the storage device in peaking mode. The chemical-thermal converter has a better reliability characteristic than the thermal storage and thus a higher reliability of supply and a lower EENS result with this configuration.

It is also possible to use the storage devices only as back-up devices. In this case, the following values results:

$$R_{out} = \begin{bmatrix} 0.823227 \\ 0.992164 \\ 0.989714 \end{bmatrix}; \quad N_{nls} = \begin{bmatrix} 6857.9666 \\ 141.0487 \\ 397.2560 \end{bmatrix}; \quad N_{ls} = \begin{bmatrix} 1071.6064 \\ 115.9257 \\ 276.8924 \end{bmatrix}$$

Again, such an operation mode is beneficial only for the thermal system. Obviously, comparatively larger rated systems – as it is the case with the thermal supply compared with the other two energy carriers – hardly profit from the interconnections. Their resources are used to also supply the other systems and at the same time, their ratings are too large for the other energy carriers to in turn provide significant support. This is visible particularly from the EENS values.

It is also interesting to note that the results from the calculations with no storage and with storage for back-up supply only are almost identical.

This comes from the models developed for the storage device. The failure and repair rates are defined through the discharge and charge time and hence, the reliability characteristics are significantly worse than those of the other connections and components. The influence of the storage is small if used for back-up only. In peaking mode, as discussed above in the context of time step 4, the load demand from the storage only concerns the amount of power exceeding the connection capacity. Consequently, the load demand from the storage is smaller, than in the back-up mode, and the failure rate decreases proportionally, resulting in a higher availability of the storage device itself.

Just to give an impression of the situation with neither interconnections nor storage devices, the corresponding results are displayed here:

$$R_{out} = \begin{bmatrix} 0.332877 \\ 0.991803 \\ 0.826503 \end{bmatrix}; \quad N_{nls} = \begin{bmatrix} 24260.9439 \\ 147.5410 \\ 8229.5082 \end{bmatrix} \text{ [Wh]}; \quad N_{ls} = \begin{bmatrix} 4288.3037 \\ 147.5410 \\ 790.984 \end{bmatrix} \text{ [Wh]}$$

The benefit of interconnections is obvious, particularly for those loads that exceed the rated capacity of their direct connections. It must however be stressed that the chosen load curve and hub characteristics were intended to illustrate the performance of the algorithm, in particular with higher loads; in these situations – in terms of reliability – the benefits of an energy hub are most profound.

This closes the example, showing the performance of various algorithm elements. The purpose of the example was to both demonstrate the applicability of all so far discussed algorithms as well as to illustrate the benefits of having interconnections between the energy carriers. However the example also shows that the coordination can become quite complex, depending on various factors such as how the storage devices are prioritised or which loads are more important than others. In particular, the investigation showed that the operation of storage devices is not necessarily beneficial for all considered loads, whereas this depends as well on the dispatch priority. In this respect, the example also indicated, even if not explicitly discussed, that various dispatch policies are possible. The following chapter focuses in particular on the sensitivity of the models themselves, identifying possible drawbacks of the models. It additionally investigates the sensitivity towards certain converter parameters and it contains the conclusion for this part of the thesis.

Chapter 5

Sensitivity Analyses and Conclusion

This chapter is the last chapter of part I of the thesis. It contains different analyses using the procedures developed throughout the previous chapters. The focus lies on analysing the behaviour of the model itself. In addition, some investigations are performed to identify the influence of different parameters and to show the spectrum of possible analyses. The chapter closes with indications for further work and a conclusion.

5.1 Sensitivity Analyses

The applicability of the developed models and procedures has already been demonstrated with examples and verified throughout chapters 3 and 4. Therefore, this section will focus on applying the models to analyse different sensitivities. At this point it is necessary to stress that results obtained with the models also depend on the structure and assumptions implied in the models themselves. This holds true for any model but it is useful to be kept in mind. Hence, the following analyses will point out sensitivities and conclusions, but they must always be understood to also partly represent the way the model was defined. For this purpose, first some model specific analyses are performed to identify the accuracy of the models. Analysing the influence of the model definitions allows to derive appropriate model parameters, concerning e.g.

the discretisation of the energy storage device. Then, using these conditions, some analyses are performed, investigating energy hub specific characteristics.

5.1.1 Model specific sensitivities

The general modelling approach is based on state-of-the-art reliability calculations, using state space diagrams and assuming Markov processes. This method is well established and investigating model specific sensitivities in that respect is not necessary. However, the suggested Markov model for storage devices is based on a set of assumptions, which should be analysed. Three different analyses will be performed. First, the influence of interval-wise adjusting the failure rate is analysed. Then the impact of discrete charge levels is investigated, both for the application of the storage for back-up and for peak supply. The third and last model specific analysis concerns the derated state that had to be introduced when using the storage for peak supply. Due to this derated state, a transition could be introduced, preventing the model from having states with zero steady-state probabilities.

Interval-wise adjusted storage failure rate

For analysing the influence of interval-wise adjusting the failure rate of the storage device, it is sufficient to focus on one hub output. For this purpose, the earlier applied electrical load curve has been chosen, redisplayed in figure 5.1. The load curve covers one day and consists of 15 min measurements, hence in total 96 time segments.

The relevant characteristics are given in table 5.1, whereas a different energy capacity than before was chosen. The momentary failure rate of the storage device depends on the load demand from the storage

$C_{ee} = 10$ kW	$\lambda_{ee} = 0.5$ f/yr	$\mu_{ee} = 4380$ r/yr
$C_{ce} = 2$ kW	$\lambda_{ce} = 1.5$ f/yr	$\mu_{ce} = 365$ r/yr
$C_{te} = 0.5$ kW	$\lambda_{te} = 1.5$ f/yr	$\mu_{te} = 365$ r/yr
$C_{E_{el}} = 10$ kW	$\emptyset \lambda_{E_{el}} = 2234$ f/yr	$\mu_{E_{el}} = 8760$ r/yr
$E_{el} = 10$ kWh	$\eta_{ch_{el}} = 1$	$\eta_{dch_{el}} = 1$

Table 5.1: Characteristics of the hub components.

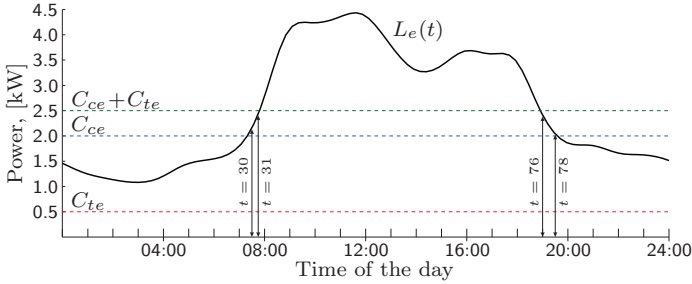


Figure 5.1: Load curve of an electrical load L_e supplied with an energy hub.

device. If the load demand exceeds the rated power capacity of the storage interface, this interface rating is the limiting factor, as discussed in the context of equation (4.30). Therefore, the storage power rating was chosen large enough, to be able to analyse the impact of interval-wise adjusting the failure rate; the load curve is never below 1 kW and using a storage with this rating would be meaningless for this particular analysis. The resulting average failure rate is displayed in table 5.1.

The advantage of using an average failure rate concerns the computation time. This average failure rate could be evaluated at the beginning of the simulation, using the average load demand, and thus would not have to be recalculated in every time step. The same holds true for the state probabilities, depending on these failure rates. If the storage device is used for peak-supply, it is obvious that the failure rate has to be calculated in every interval, depending on the dispatching of the available converters. However, when using for back-up purposes only, the trade-off between accuracy and computation effort is worth to be analysed. Figure 5.2 shows the evolution of both the interval-wise adjusted failure rate and the failure rate resulting from using the average load demand.

With the interval-wise adjusted failure rate $\lambda_{E_{el}}(t)$, an expected reliability of supply of $R_{e_{out}} = 0.999978$ results, identical to an expected outage duration of 11.74 min. Using the average failure rate of $\lambda_{E_{el}} = 2234$ f/yr gives an expected reliability of supply of $R_{e_{out}} = 0.999982$, equal to an expected outage duration of 9.34 min. Looking at EENS gives $N_{nls} = 2.02$ Wh and $N_{ls} = 0.68$ Wh with the adjusted failure rate and $N_{nls} = 1.59$ Wh and $N_{ls} = 0.53$ Wh with the constant failure rate.

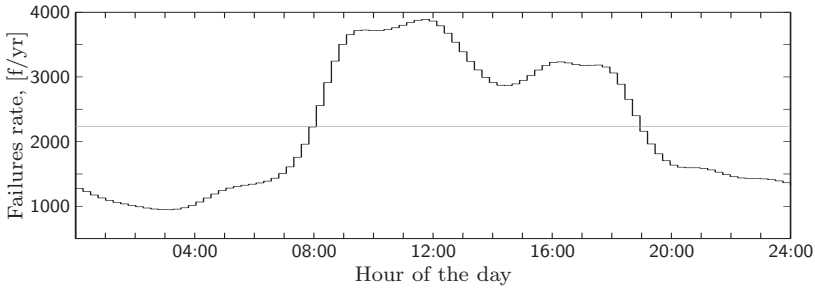


Figure 5.2: Interval-wise adjusted and constant storage failure rate for $C_{E_{el}} = 10$ kW.

Using a constant failure rate obviously overestimates the performance of the system. Particularly during high load periods, the adjusted failure rate is significantly higher and results in higher fractions of EENS and a lower reliability of supply.

Charge level discretisation

The second investigation concerns the discretisation of the energy storage device and can be understood as the continuation of the analysis displayed in figures 4.6 and 4.7. That analysis showed a certain dependency on the charge level discretisation, also indicating that a discretisation with about five discrete charge levels is sufficient. Similar to before, the discretisation is increased from 1 step up to 20 steps, i.e. up to one state representing 5% of the total charge. The corresponding state space diagram is analogous to figure 4.5 and created using the rules from table 4.2. The application of Kronecker products facilitates this investigation significantly, as all the other matrices remain unchanged and can simply be added in the Kronecker summation. The resulting expected reliability of supply $R_{e_{out}}$ is displayed in figure 5.3 and the resulting EENS, with load shedding considered, is displayed in figure 5.4. The storage rating has been reduced to $C_{E_{el}} = 1$ kW and the capacity to $E_{el} = 1$ kWh, having a rated power capacity between the chemical-electrical and the thermal-electrical converter.

Obviously, the earlier discovered sensitivity also exists when including the storage model in the energy hub reliability model. Both the reliability of supply and EENS asymptotically approach steady values for

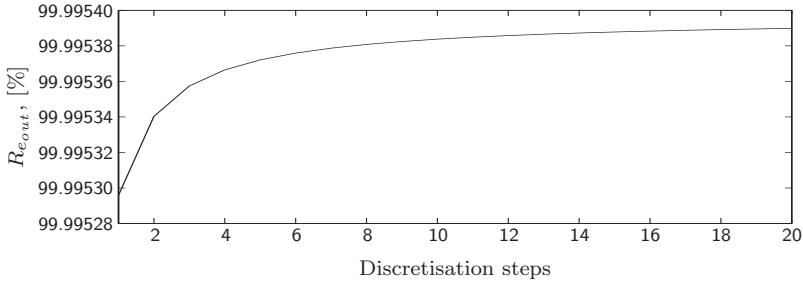


Figure 5.3: Expected reliability of supply as a function of the discretisation steps of the storage device, back-up mode.

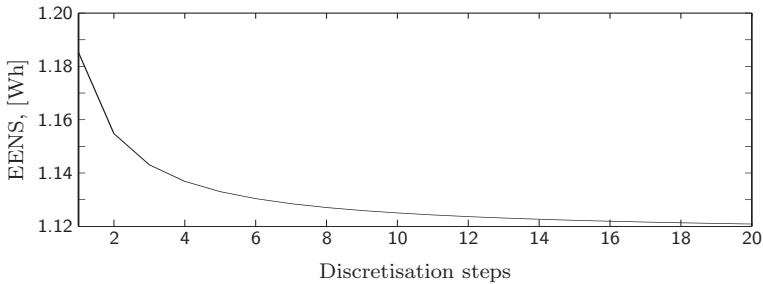


Figure 5.4: EENS with load shedding considered as a function of the discretisation steps of the storage device, back-up mode.

an increased number of discrete charge levels. Looking at the resolution of the ordinates shows however that the differences are rather small and that a discretisation of the charge level into five to ten steps is sufficiently accurate, as already indicated in section 4.1.5.

A similar analysis is performed with the peak load model for the storage device, depicted in figure 4.15. Table 4.3 contains the rules for creating the transition rate matrix corresponding to a state space diagram with an arbitrary number of discrete charge levels. The influence of the number of charge levels is analysed by looking at one time interval only. Again, the electrical load is investigated, with the converter capacities and the storage device being rated identical to before. The load is assumed to be at 13.5 kW and thus, the storage is required to be able to supply the load, with $C_{ee} = 10$ kW, $C_{ce} = 2$ kW, $C_{te} = 0.5$ kW and $C_{E_e} = 1$ kW. The derated state is assumed to have a capacity of 9 kW,

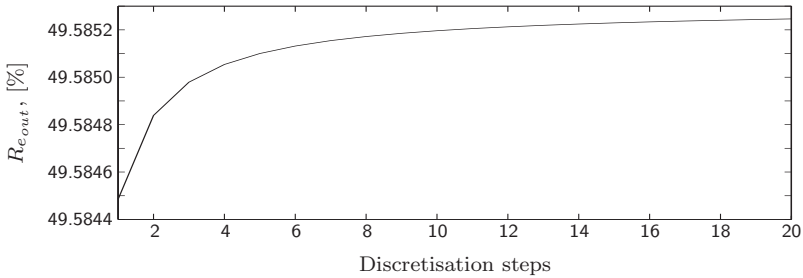


Figure 5.5: Expected reliability of supply as a function of the discretisation steps of the storage device, peak supply mode.

hence recharging the storage device with 1 kW within 1 h. The expected reliability of supply is displayed in figure 5.5 and EENS considering load shedding is displayed in figure 5.6.

The influence of the discretisation is visible as well, whereas the resolution of the ordinate is different to before. The results seem to be somewhat more sensitive than when the back-up model is applied. It is however important to note that the investigations concerning the back-up model were performed for a varying load curve, with some time segments containing a redundantly supplied load. Nevertheless, independent of the ordinate resolution it can be stated that a certain influence exists and it can be concluded that charge levels of approximately 20% seem to be a reasonable choice.

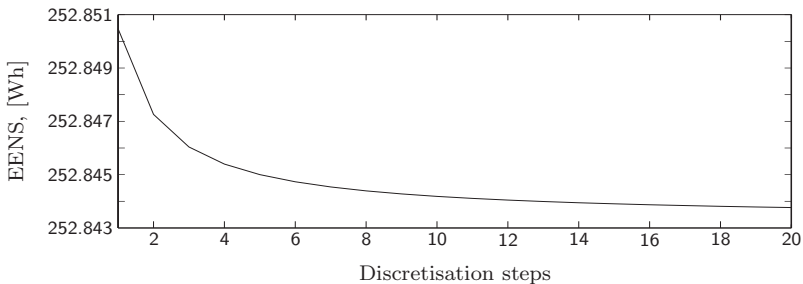


Figure 5.6: EENS with load shedding considered as a function of the discretisation steps of the storage device, peak supply mode.

Recharge power of the derated state

As mentioned, figures 5.5 and 5.6 were calculated assuming a recharge power of 1 kW, giving a recharge duration of 1 h, i.e. a repair rate of $\mu_{E_e} = 8760$ r/yr. The disadvantage is that during this hour, only 9 kW are available from the direct electrical connection. Thus, there is a certain trade-off between a high recharge power, giving a short recharge time, and having a lower supply capacity of the derated state. The following figure 5.7 shows the influence of both the level of discretisation and the influence of the charge power available during the derated state.

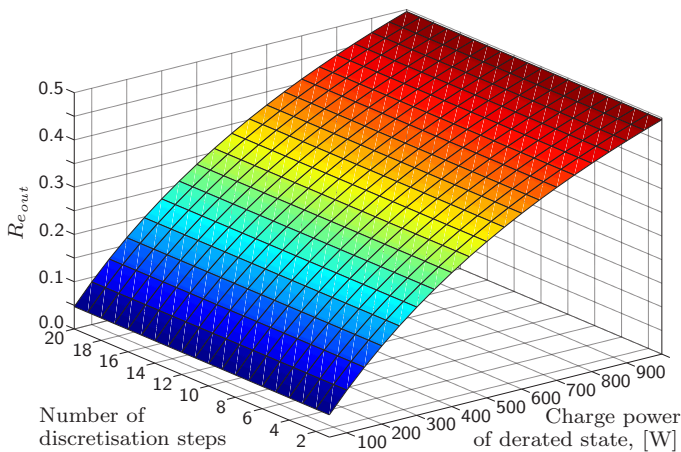


Figure 5.7: Expected reliability of supply for different storage charge levels and different charge power values; storage in peak mode.

The figure shows a clear influence of the charge power. Obviously, the lower the repair rate, i.e. the lower the charge power, the poorer the performance of the storage device. Thus, it is beneficial to choose a relatively high recharging power. The derated state has a lower capacity but the resulting repair rate is comparatively high, guaranteeing a soon transition to the recharged state.

This closes the model specific analyses. It can be concluded that it is appropriate to model the storage with a certain number of discrete charge levels. Furthermore, when using the storage for peak supply modelling, the derated state, meant for recharging the storage, should provide a considerably high recharge power.

5.1.2 Hub specific sensitivities

Section 4.3 already discussed several aspects of different components concerning the overall reliability of supply. The example also illustrated the mutual influencing and indicated the spectrum of analysis possible with the model. This section contains a few analyses concerning different parameters and aspects of the energy hub, complementing the findings from section 4.3. The focus is again on one hub output only, as this allows to identify the major dependencies. Besides, a complete energy hub is based on many assumptions, such that the expressiveness of analyses is limited, in particular for deriving general dependencies.

Influence of the storage capacity

This first hub specific analysis concerns the relation between the energy capacity and power rating of the storage, relative to the capacities of the available converters.

If the storage device would be comparatively larger than the converters from the neighbouring networks, the influence of these converters is expected to be small. This analysis therefore concerns the influence of

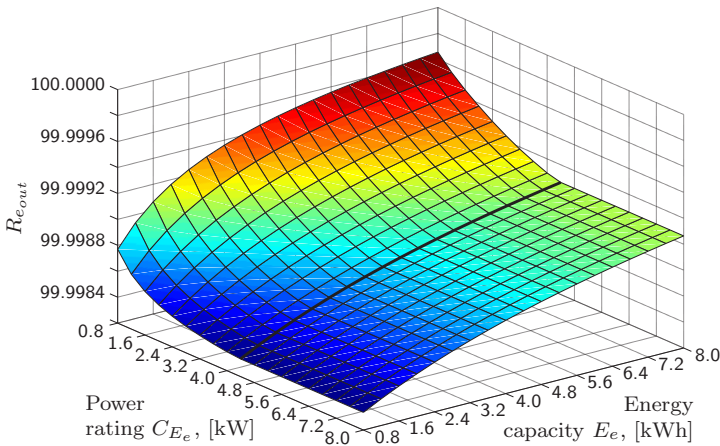


Figure 5.8: Expected reliability of supply for different E_e and C_{E_e} , storage in back-up mode; line representing the maximum load at 4.44 kW.

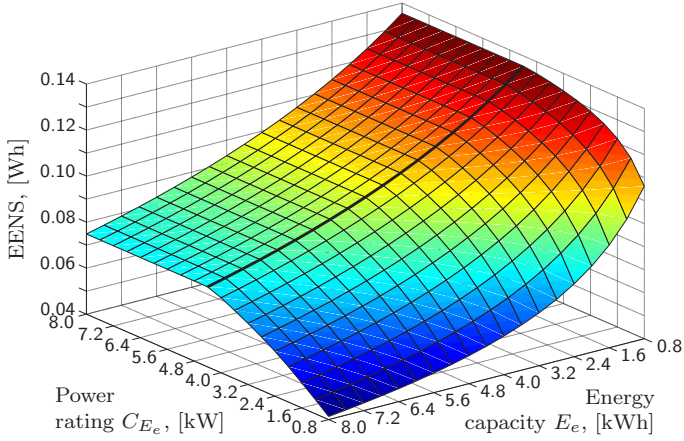


Figure 5.9: EENS for different E_e and C_{E_e} , storage in back-up mode; line representing the maximum load at 4.44 kW.

the storage energy capacity and power rating, relative to the capacity of converters from the other networks. For this purpose, the load curve from figure 5.1 was used again, with $C_{ee} = 10$ kW, $C_{ce} = 4$ kW and $C_{te} = 0$ kW. The chemical-electrical converter thus provides a redundant supply for most load intervals. The electrical storage device is varied with $C_{E_e} \in [0.8, 1.2, \dots, 8]$ kW and $E_e \in [0.8, 1.2, \dots, 8]$ kWh. The resulting reliability of supply is displayed in figure 5.8 and EENS in figure 5.9.

Both figures show how the energy capacity E_e of the storage device has an influence on the result, independent of the power rating of the storage. The larger the capacity of the storage the longer it takes for discharging, independent of the power rating. The figures also show that a comparatively low power rating has a beneficial effect. The failure rate of the storage is defined through the load demand and the power rating. If the load demand is higher than the power rating, the power rating is the limiting factor. For ratings above approximately $C_{E_e} \geq 4$ kW, the failure rate is thus always defined by the load demand, resulting in a λ_{E_e} independent of C_{E_e} . However, for lower ratings, the limiting factor is the storage interface rating, resulting in a lower failure rate as the storage is discharging slower with the smaller discharge power. The lower failure rate is beneficial, as the state with an operating storage has a higher probability albeit a lower supply capacity.

Influence of the converter failure rates

This section investigates the importance of the failure rate of the converters from the chemical and the thermal networks. The question addressed is how unfavourable the reliability characteristics could be, with the converters still improving the reliability of supply. Figure 5.10 shows the expected annual outage duration as a function of the two converter's failure rates. The chosen capacities correspond to table 5.1, except for the storage device, which is rated with $C_{E_e} = 1$ kW and $E_e = 1$ kWh.

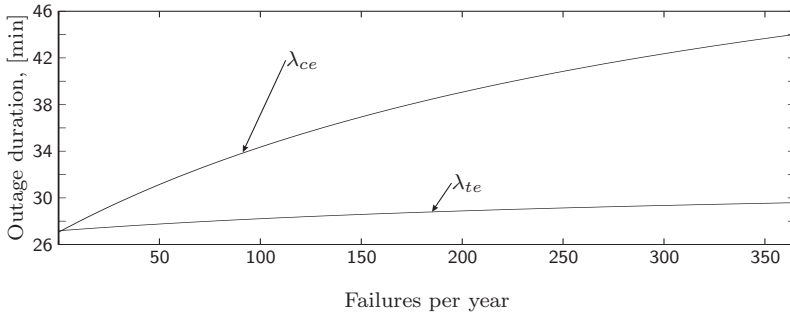


Figure 5.10: Expected outage duration in minutes for different failure rates of the chemical-electrical and the thermal-electrical converter.

The general sensitivity is visible, the larger capacity of the chemical-electrical converter being responsible for its larger influence. The expected outage duration without energy hub was calculated to be exactly 59.99 min. Hence, even if the chemical-electrical converter would fail once a week, the outage duration could be reduced to roughly half than before. This result is interesting in so far as both converters only contribute to the reliability of supply during lower load hours. This analysis also raises the question whether the failure rate of the direct connection could be allowed to increase because of the additional supply paths. The next subsection concerns this aspect.

Failure tolerance of the direct connection

Distributed generation is sometimes claimed to allow for postponing network enhancements or to even make them superfluous [7]. The assumption behind this claim is that potentially existing distribution network

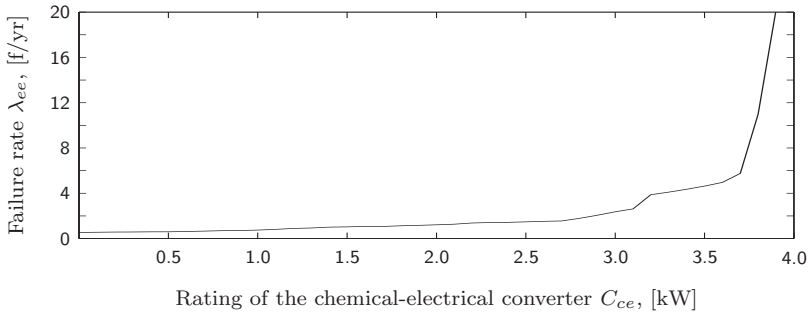


Figure 5.11: Maximum allowable failure rate for the direct electrical connection for an increasing chemical-electrical converter and a targeted annual outage duration of 1 h.

congestions can be alleviated by locally generating a certain amount of power. This results in a reduction of the demand from the network and hence, the network enhancement is not necessary anymore or at least not for the moment. In terms of reliability, a higher loaded connection can be understood to be more at risk to fail. Hence, it is analysed in this paragraph to what extent a higher failure rate of the electrical connection can be allowed, because of the converters from the other networks. Without these converters and the storage device, the expected annual outage duration was found to be roughly 1 h. The question thus is if the additional converters allow to actually have a higher failure rate of the electrical connection without risking a annual outage duration higher than 1 h. Figure 5.11 shows the maximum allowable failure rate λ_{ee} for the direct connection for different capacities of the chemical-electrical converter.

The figure shows that the failure rate of the electrical connection could increase with an increasing chemical-electrical converter capacity. Obviously, the more the chemical-electrical converter can supply the load by its own, the higher the failure rate λ_{ee} can be. As soon as the capacity C_{ce} exceeds the average load demand, the electrical connection's allowable failure rate increases significantly; the chemical-electrical converter now is the main supplying system. It must be noted that this analysis assumes the chemical-electrical and the thermal-electrical converter to be operational with the rated capacity.

5.2 Directions for Further Work

The methods presented in chapter 3 are based on state-of-the-art reliability calculations. The major difference to existing models concerns the application for a multiple source multiple terminal system, such as the energy hub. The methods are however well established. On the other hand, the Markov model for energy storage devices, developed in chapter 4, is based on some assumptions, which could be further verified. This concerns in particular the model suggested for peak supply.

As mentioned several times throughout the thesis, the Markov model defines the failure behaviour of a storage device through its discharge behaviour. The storage device was assumed to discharge linearly, as modelled in other publications on storage devices [29, 30, 31, 32]. However, in order to be able to maintain constant transition rates for the storage device, discrete charge levels had to be introduced, approximating the gradual discharge and recharge behaviour of the storage device. It would be of interest to perform Monte Carlo reliability simulations to analyse and compare the results with those from applying the here suggested models.

In addition, the storage device has been assumed without other failure states, apart from being discharged. As indicated, a certain probability of failure while recharging the storage could be simulated by introducing a switch with a certain failure rate. Hence, the storage would be a stand-by component and if required to operate, the switch is activated. The probability of a failed recharge could be modelled by assigning a certain failure probability to the switch.

Another aspect concerns a detailed analysis of the behaviour of the supplying systems. That means to analyse the technologies using chemical and thermal energy carriers and to investigate e.g. their time dependencies, transients or the failure susceptibility and tolerance. This would help to identify interconnecting components with beneficial behaviour in terms of reliability.

5.3 Conclusion

This part of the thesis presented a model for the analysis of reliability of supply in multi-carrier energy systems. The model is based on the energy hub modelling concept, which allows the analysis of interconnections and dependencies among several energy carriers at the same time. In terms of reliability, the interconnections are meaningful both for partially redundant supply and to reduce the amount of expected energy not supplied.

In a first approach, a model was presented for analysing an energy hub with interconnections between all energy carriers. The model assumes all components to behave as Markov processes and applies state space diagrams for modelling the supply situation of each hub output. Different examples showed the applicability of the approach and verifications proved the soundness of the results.

In a second stage, a Markov model for energy storage devices was developed. The model consists of two parts to be used depending on whether the storage is providing back-up power or peak supply power. In order to simulate the charge and discharge behaviour of the storage device, discrete charge levels had to be introduced. Sensitivity analyses showed that the accuracy of the results can be improved by modelling the energy storage device with five or more discrete charge levels.

The storage models were integrated into the energy hub reliability model, giving a comprehensive model suitable for analysing energy hubs both without storage and with storage for back-up or peak supply. The model has been applied in a detailed example, identifying the value of different connections and illustrating the behaviour of the model. In terms of reliability, it is meaningful if the different energy carrier's supply systems are similarly dimensioned. Otherwise, the larger dimensioned systems will hardly profit from the interconnections.

The developed models are suitable for analysing the reliability of supply and expected energy not supplied for multi-carrier energy systems. Disadvantages and advantages of interconnections between energy carriers can be identified with the models. Hence, the models can also be applied for sensitivity analyses, giving the dependency of the reliability of supply from certain components.

Part II

IMPROVING NETWORK INFEEED RELIABILITY OF NON-DISPATCHABLE GENERATORS USING ENERGY STORAGE

Chapter 6

Combining Non-Dispatchable Generators with Energy Storage Devices

This chapter introduces the subject of the second part of the thesis, discussing different aspects of combining non-dispatchable generators with energy storage devices. The focus lies on grid-connected systems, in particular discussing potential benefits in the case of wind turbines. The principle system layout applied in the subsequent chapters is presented and a short overview of the individual chapters is given.

6.1 Introduction

The generation of electric power from renewable sources, such as wind or sun, is often difficult to predict. The reason for this is the non-deterministic nature of these energy sources, resulting in the generator output being neither deterministic nor dispatchable. This characteristic has negative consequences both in isolated systems and in grid-connected configurations.

In isolated systems, it is crucial that production and consumption match, both in dimension and in time. This is the reason why isolated systems, comprising generators that convert renewable energy sources, often also

contain conventional diesel generators. The diesel generators are operated whenever the non-dispatchable generator cannot supply the load. This operational behaviour has stimulated research on complementing isolated systems with energy storage devices [33, 34, 35, 36, 37]. The purpose of the storage device is to buffer between the non-deterministic production and the load as well as to bridge time differences between generation and consumption. The proper use of the storage results in a reduced number of operating hours of the diesel generator, i.e. lower operating costs. Furthermore, the overall reliability of supply can be improved and utilisation and value of the renewable source are increased.

In grid connected configurations, the situation is somewhat different. Depending on governmental policies, renewable energy based generators are often encouraged to feed any production at any time into the grid. The imbalance between their stochastic production and the load demand is compensated by fast responding balancing generators, connected to the grid. Thus, it does not seem necessary to combine the generators with an energy storage, with network and back-up generation having the same purpose as the storage devices in isolated networks.

However, the increasing number of grid-connected non-dispatchable generators results in cumulating infeed power fluctuations, which are difficult to predict. Thus, not the fluctuations per se are the primary issue but rather the difficulty to accurately predict them. Depending on the generation technology, already smaller forecast errors can have significant effects, leading to two major disadvantages. On the one hand, grid operators, who must place their bids in a day-ahead market – at the same time predicting the production in the respective control zone, as required e.g. in Germany –, often incur comparatively high penalties because the inaccurate forecasts make it impossible to meet the projected production profile [38]. On the other hand, several generators have to run as back-up on no-load or with throttled power, to be able to quickly ramp up and down to compensate possible deviations from the planned infeed. Usually, pumped hydro storage and gas-fired power stations are used for this purpose; throttling a thermal power plant however implies lower efficiency and hence a relatively higher amount of CO₂ released per MWh, thus reducing the positive impact of renewable-based generators in terms of emissions.

A major issue of the production from wind turbines is the forecasting of the exact timing of power changes. For safety reasons, wind turbines need to stop operation if the wind speed exceeds defined limits and re-

main turned off for a certain period of time. These safety shutdowns consequently result in significant infeed power reductions: if a gust occurs e.g. half an hour earlier than forecasted, the shutting down of the turbines results in complete loss of infeed half an hour earlier than expected. Not knowing the exact timing of these shutdowns requires the back-up generation to be ready for a period that is considerably longer than the actual infeed outage will take. This in turn results in a further increase of the mentioned emissions.

Thus, it would be favourable to alleviate or even eliminate the fluctuations and forecast uncertainties before they are imposed on the network. One option would be the installation of an energy storage device at the point of infeed, with the purpose to compensate the energy imbalances resulting from the inaccurate forecast. The question in that respect is how well such a system would perform and what the requirements for the storage device would be. Other aspects of combining grid-connected generators with energy storage devices have been addressed in few studies, investigating e.g. different operational aspects [39, 40], reduction potentials for balancing penalties [38, 29] or possible emission savings because of reduced need for conventional back-up generation [31].

This part of the thesis investigates the potential of using energy storage devices to compensate forecast errors and to consequently transform the uncertain and non-dispatchable generation into a deterministic network infeed. The fundamental approach is to define a network infeed profile for a given amount of hours in advance, based on a forecast for the renewable energy source. This infeed profile is defined to be hourly constant, according to the settlement policies of most power markets. It is important to note that the profile is not based on market prices but only on the expected output of the renewable source. Consequently, the energy storage device is used to balance the output of the non-dispatchable generator in such a way that the combined output matches the predefined network infeed profile as closely as possible.

The advantage of a deterministic infeed profile is twofold:

- Independent of market structures, a deterministic production can be incorporated reliably in the day-ahead production planning, allowing to dispatch former back-up generators for other purposes.
- In a market environment, the ability to reliably determine the near-future production enables selling and buying on the spot market with a reduced risk of incurring balancing penalties.

Generally, the storage device helps to better use the energy, converted from the renewable source, and to sell it as planned. This corresponds to a value increase for the energy source itself. The ability of the generator and the energy storage device to effectively fulfil the predefined infeed profile, depends both on the actual forecast error as well as on the characteristics of the storage. The performance will be measured according both to reliability criteria as well as to system losses and incurring balancing penalties. The results will be used to identify the relation between the magnitude of the forecast error and the capacity of the energy storage device.

6.2 System Layout

The layout of the system underlying the investigations is depicted symbolically in figure 6.1.

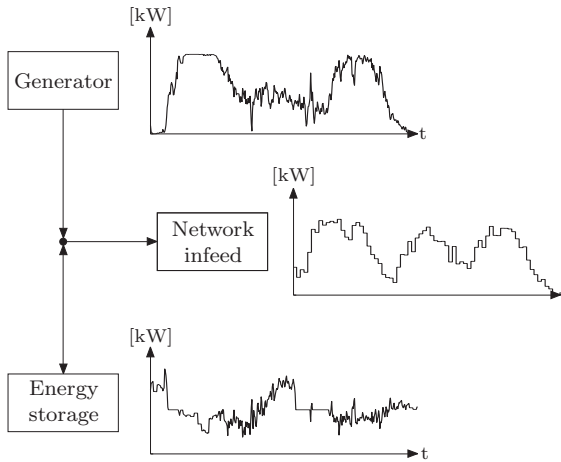


Figure 6.1: Symbolic representation of the non-dispatchable generation, the balancing storage device and the levelled network infeed profile.

This figure displays an excerpt of an output forecast for a wind turbine, the resulting infeed profile and the corresponding activities of the energy storage device. It is clearly visible how the storage balances both fluctuations within an hour as well as differences between the output

level of the generator and the targeted infeed profile. This infeed profile should be met as accurately as possible and it can be understood as the load, which the generator has to supply together with the energy storage device. In contrast to isolated system, surplus energy, i.e. energy that exceeds the targeted profile, can be fed into the grid if the storage device is already fully charged. This surplus infeed results in balancing penalties and could be avoided by having a larger storage capacity. The establishing trade-off between storage capacity and surplus energy will be discussed in the case studies in chapter 9.

To investigate the suggested configuration, a time series analysis approach has been chosen: the generator (converting power from a renewable source) is represented with a time series derived from measurements and an algorithm progresses through this time series, performing various calculations to simulate the behaviour of defined scenarios. In the underlying case, the scenario is the combining of the generator with an energy storage device. Thus, the calculations use the time series to simulate the influence of an energy storage device on the system behaviour. At the end of the simulation, results and calculations can be analysed to identify how the configuration performs. This indicates how a real system would perform, given the generator behaves exactly as in the time series.

The energy storage technology is not subject of this work, as the chosen algorithms do not depend on specific storage device parameters. It is merely identified if storage need exists and what the requirements would be. Still, both case studies will indicate possible realisation.

The next chapter discusses the chosen time series analysis in detail, suited for investigating systems, following the configuration in figure 6.1. The subsequent chapter 8 introduces different analysis procedures, suitable for assessing performance criteria, such as how accurate the profile can be met, how much energy is consumed for conversions or how much surplus energy is fed into the network. In two case studies the modelling procedure from chapter 7 will be applied and the calculations will be analysed according to the procedures proposed in chapter 8. The first case study focuses on measurement data from a 500 kWp photovoltaic installation in Switzerland and the second case study is based on wind speed measurements from Norway, for a 2 MW wind turbine. This second part of the thesis is closed with discussions and the conclusion.

Chapter 7

A Generalised Model for Time Series Analyses

This chapter presents a time series based algorithm suitable for analysing the combination of a non-dispatchable grid-connected generator with an energy storage device. The flow chart of the algorithm is introduced and selected algorithm elements are discussed in detail. The method can be used for any type of non-dispatchable generator, but the focus lies on the application of the modelling procedure for wind power and photovoltaic applications. Particularities corresponding to these types of generators are therefore discussed as well.

7.1 Algorithm

The simulation is based on a time series that is either a measurement curve or an artificially created curve, using e.g. Monte-Carlo simulations. The measurement curve's resolution and length can be of arbitrary size. Generally, the longer the time series and the higher the resolution, the more trustworthy the results will be. Depending on the measurement source, the results might not be generally valid for similar sources, as the measured time series reflects the past behaviour of the one particular source. Nevertheless, time series analysis is a well established method and the relevance of the results will be discussed in chapter 10.

Figure 7.1 shows the flowchart representing the algorithm sequence. It follows the structure of similar investigations [39] and is shortly discussed before the individual elements will be outlined in detail.

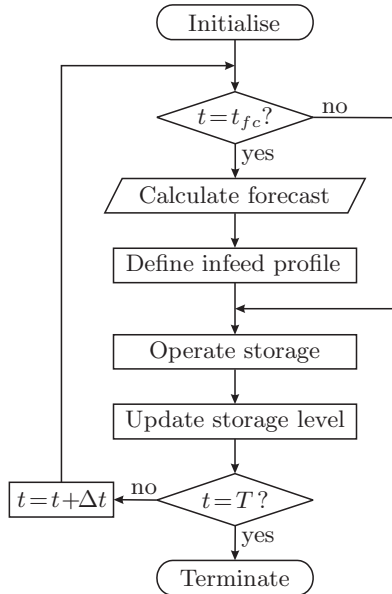


Figure 7.1: Flowchart of the simulation algorithm.

The algorithm starts with an initialisation phase, after which the actual simulation loop begins. The loop starts with a check, whether a new forecast period begins ($t = t_{fc}$). If so, the forecast for the next period is calculated, based on the parameters defined during the initialisation phase. This forecast in turn is used to define the network infeed profile, targeted for the next period. As mentioned, this profile is kept constant over the duration of one hour. The loop then continues by using the actual measurement data from the generator, trying to fulfil the targeted infeed profile as accurately as possible by operating the energy storage device. As long as no new forecast period begins, the algorithm loops through the time series, constantly operating the storage to meet the targeted infeed, always updating the charge level of the energy storage device. If the time series reaches its end ($t = T$), the loop and the algorithm terminate. During the simulation, various values are stored continuously to be analysed later-on.

7.2 Initialisation

In the initialisation phase, the time series is loaded and the simulation parameters are set. These are the forecast error, which will be discussed in section 7.3, and the storage device's power rating P_{st} , energy capacity E_{st} as well as the charge efficiency η_{ch} and the discharge efficiency η_{dch} . Depending on the storage technology used, the storage device cannot be fully discharged and also a minimum charge level $E_{st,min}$ has to be defined. A further parameter is the forecast horizon, indicating how often the infeed profile is redefined. This parameter makes little sense with photovoltaic systems as their cyclic daily behaviour suggests using 24 h horizons. With wind turbines however, different horizons are conceivable, particularly as the magnitude of forecast errors increases with increasing time horizons (see section 7.3.3). If the time series contains measurements for the renewable source, i.e. insolation or wind speed measurement, the parameters of the non-dispatchable generator also have to be defined, indicating how the source is converted. The respective case studies will discuss these parameters in more detail.

7.3 Calculation of Forecast

At the beginning of every planning period, a forecast of the stochastic generation is calculated, required for defining the hourly constant infeed profile. Various methods and approaches for the calculation of forecasts for different sources exist [41, 42, 43]. The focus of this investigation however lies not on the accuracy and advantages and disadvantages of different methods. The question addressed here, is how the magnitude of the forecast error influences the ability of the system to meet the planned generation and to what extent forecast errors can be compensated with a storage device. Therefore, not a method for forecasting is developed, but a method to simulate a certain forecast error.

The forecast error f_{RMSE} is defined as the root mean square error (RMSE) between the forecasted power output \mathbf{P}_{fc} and the actual power output \mathbf{P}_{gen} of the generator, normalised with the rated power output of the generator P_{rated} :

$$f_{RMSE} = \frac{1}{P_{rated}} \sqrt{\frac{1}{T} \sum_{t=1}^T [\mathbf{P}_{gen}(t) - \mathbf{P}_{fc}(t)]^2} \quad (7.1)$$

To analyse the relation between forecast error magnitude and storage capacity, it is necessary to be able to choose the forecast error at the beginning of a simulation run. This allows running simulations with different forecast errors and different storage capacities. The results can then be used to derive the relation between forecast accuracy and storage capacity.

As the algorithm is based on a time series, the measurements for the next planning period are already known and can be understood to represent the perfect forecast for the next period. A forecast error can thus be simulated by using this perfect forecast and by introducing a deviation. This deviation results in a deterioration of the measurement curve, and the difference to the actual measurement curve corresponds to a certain forecast error magnitude. One reference suggests to use the actual measurement and to deteriorate it by adding a normal distribution in every hour [44]. This method, however, merely generates a swing around the actual measurement, it does not show typical forecast deviations and partially ignores dependencies from one hour to the next. Therefore, a new approach was developed, based on an exponentially weighted moving average (EWMA) with a weighting factor α ($0 \leq \alpha \leq 1$) [45]: the forecast is defined by the actual measurement for the next period and a certain number of preceding periods, multiplied with an exponentially increasing weighting factor.

7.3.1 Using output power measurement data

If the measurements represent the output power of the generator (as it is the case in the first case study in section 9.2) the EWMA approach can be applied to these power measurements directly. The forecasted power $\vec{P}_{fc,n}$ for period n can be defined as the sum of the weighted actual time series \vec{P}_n of day n and the m preceding periods¹:

$$\begin{aligned} \vec{P}_{fc,n} = & \alpha \cdot \vec{P}_n + \alpha(1 - \alpha) \cdot \vec{P}_{n-1} + \dots + \\ & \alpha(1 - \alpha)^{m-1} \cdot \vec{P}_{n-(m-1)} + (1 - \alpha)^m \cdot \vec{P}_{n-m} \end{aligned} \quad (7.2)$$

Setting $\alpha = 1$ results in a perfect forecast, as equation (7.2) gives as forecast exactly the measured curve. For all other forecast error magnitudes, the corresponding values of α have to be calculated. For this

¹The vector symbol \vec{P} represents the time series for one period, whereas the bold variable \mathbf{P} is used to designate the whole time series.

purpose, forecast series need to be calculated with different values for α , using the complete time series, starting at period $m + 1$. It is not possible to start at the first period because no previous periods would be available to be used according to equation (7.2). These calculated forecast series $\mathbf{P}_{fc}(\alpha)$ are then used, together with the actual measurement series, to calculate the RMSE according to equation (7.1). This in turn allows creating a lookup table, relating the different α 's with their corresponding f_{RMSE} . During the initialisation of the simulation it is hence possible to choose a certain forecast error. The corresponding α is then applied during each 'calculate forecast' step, when calculating the next period's forecast with the targeted error.

It is important to note that α and the associated f_{RMSE} have been calculated using the complete time series. Thus, when using α during the simulation for calculating the forecast for the next period, it can happen that f_{RMSE} for certain periods deviates from the targeted f_{RMSE} . Nevertheless, the overall f_{RMSE} will correspond exactly to the chosen magnitude. Figure 7.2 shows an excerpt of the actual power output curve of a 500 kWp photovoltaic system and a forecasted power output curve, with $f_{RMSE} = 50\%$. Compared with the forecast simulation algorithm suggested by [44], this forecast curve shows typical effects as e.g. comparatively slower raise or peak mismatch.

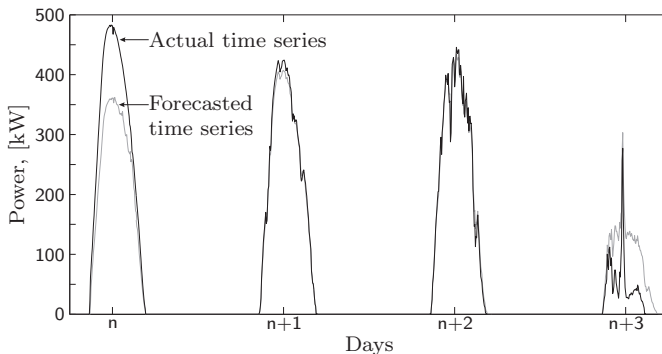


Figure 7.2: Example of the actual time series and a forecasted time series ($f_{RMSE} = 50\%$).

7.3.2 Using energy source measurement data

If the measurement data represent the actual source (as it is the case in the second case study, section 9.3), the forecast simulation procedure is slightly different. The EWMA approach has to be applied to the measurement data, but f_{RMSE} is calculated using the power output of the generator. In the case of wind speed measurements, the forecasted wind speed $\vec{V}_{fc,n}$ for period n is defined analogously to equation (7.2):

$$\begin{aligned} \vec{V}_{fc,n} = & \alpha \cdot \vec{V}_n + \alpha(1 - \alpha) \cdot \vec{V}_{n-1} + \dots + \\ & \alpha(1 - \alpha)^{m-1} \cdot \vec{V}_{n-(m-1)} + (1 - \alpha)^m \cdot \vec{V}_{n-m} \end{aligned} \quad (7.3)$$

Particularly in the case of wind turbines, it is meaningful to calculate the RMSE using the power output because of the hysteresis control, which will shortly be discussed here. Wind turbines need a certain minimum wind velocity v_{cin} in order to start operating, the so-called cut-in wind speed. They have to stop operating if the wind speed exceeds a certain maximum limit, the so-called cut-out wind speed v_{cout} . Before a wind turbine can restart operating again, after having exceeded v_{cout} , the wind speed must reduce to the so-called cut-back-in wind speed v_{cbin} and remain below this velocity for a duration of at least t_{cbin} . This measure prevents the wind turbine from turning on and off in fluctuating gusts. Consequently, wrongly predicted wind speed changes, around the cut-out wind velocity, can result in significant differences between the forecasted and the actual output power.

Figure 7.3 illustrates this behaviour with an excerpt from the data used in the wind case study, section 9.3. During day 263, the predicted wind speed raises later than the actual wind speed, consequently exceeding the cut-out wind speed v_{cout} later, suggesting a longer persisting power infeed than actually will occur. On day 265, the forecast stays below the cut-out wind speed and does not indicate an infeed outage at all.

Analogous to before, different forecast series $\mathbf{V}_{fc}(\alpha)$ have to be calculated with different values for α . These wind speed curves are then transformed into generator output power curves $\mathbf{P}_{fc}(\alpha)$, according to the characteristics of the generator (see case studies). The actual generator output curve \mathbf{P}_{gen} , derived from the actual measurement series \mathbf{V} , is then used together with each $\mathbf{P}_{fc}(\alpha)$ to calculate $f_{RMSE}(\alpha)$. This in turn allows to create the lookup table, relating α with f_{RMSE} .

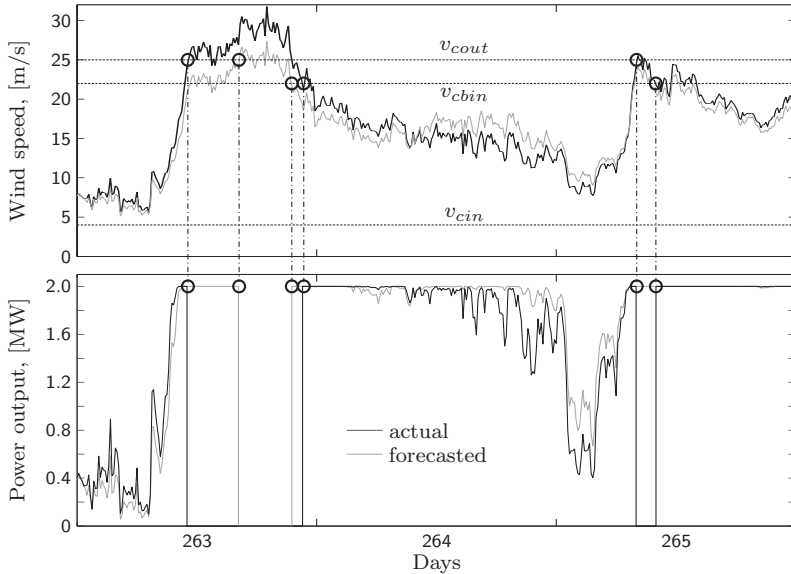


Figure 7.3: Forecasted and actual wind speed and the associated power outputs, forecast horizon $f_h = 24$ h.

The case studies later-on further discuss the creation of the lookup table. It must be noted, however, that the lookup table has to be created prior to the first simulation. Then, the simulation can be started by choosing the desired forecast error, which means implementing the corresponding α for calculating the next period's forecast with equation (7.2). This forecast then in turn serves as basis for the definition of the infeed profile, discussed in the next section. Before that section, however, the special case of time-dependent forecast errors is discussed.

7.3.3 Time dependent forecast errors

In day-ahead markets, bidding usually ends at noon and contains the bid for the following day. Thus, the production is forecasted between 12 to 36 hours in advance. For some energy sources, the forecast errors increase with an increasing forecast horizon, which has to be considered accordingly. It means that the forecasted wind speed for the first hour of the next period has a smaller f_{RMSE} than the wind speed forecast for

the last hour of the next period. Particularly for wind speed forecasts, this time-dependence significantly influences balancing penalties [38].

Forecasting methods have significantly improved over the last years [41], but the time dependence is still noticeable. A recent study from the Risø National Laboratory in Denmark [46] contains a comparison of different forecasting methods with different actual measurements. The resulting average error evolution can be identified to satisfy:

$$f_{RMSE}(t_h) = 24 + (t_h - 1) \frac{8}{35}, \text{ [%]} \quad (7.4)$$

In contrast to the otherwise used time step t , t_h represents hourly values and $f_{RMSE}(7)$ corresponds to the forecast error occurring in the 7th hour of the forecast period. As mentioned, in the day-ahead market, forecasts are calculated by noon for the next day. Hence, the forecast error of the first hour of the next day corresponds to $f_{RMSE}(13) = 7.766\%$, as the hour from 00:00 to 01:00 corresponds to the 13th hour after the forecast was made. For the simulation algorithm this means that the forecast can be calculated right at the beginning of a new period, however taking into account that the applied error corresponds to the one of the 13th hour. If the simulation is applying different forecast horizons, this time-lag can be changed accordingly. As will be seen in the case study in section 9.3, the chosen approach assumes the calculation of the forecast to take place in the middle of the previous period. That means, when using a forecast horizon of $f_h = 6$ h, the forecast is calculated 3 h in advance, i.e. the simulation uses $f_{RMSE}(4)$ for calculating the forecast for the first hour of the next period.

As the error evolves with the duration of the forecast period, for every hour of the forecasted period a different error magnitude and hence a different α has to be applied. The vector $\vec{V}_{fc,n}$, containing the forecast for the next period, has to be constructed from segments of forecasts with different errors, in order to result in a forecast with a realistically increasing forecast error. Assuming a forecast period of $f_h = 24$ h and a forecast lead of 12 h, $\vec{V}_{fc,n}$ can be defined as follows, with the indices representing the individual hours of the next period:

$$\vec{V}_{fc,n} = \begin{bmatrix} \vec{V}_{fc,n,0-1}(\alpha_{f_{RMSE}(13)}) \\ \vec{V}_{fc,n,1-2}(\alpha_{f_{RMSE}(14)}) \\ \vdots \\ \vec{V}_{fc,n,23-24}(\alpha_{f_{RMSE}(36)}) \end{bmatrix} \quad (7.5)$$

The application of equation (7.5) will be illustrated in the second case study, discussed in section 9.3, illustrated in figure 9.18.

The here described forecast simulation approach can qualitatively be justified as follows. In reality, meteorological measurements are used when calculating a forecast. Using the actual measurement for the next day, weighted with factor α , could be understood to simulate a weather forecast; it provides some knowledge on the next day's weather behaviour. In addition to that, preceding measurement periods are used in the calculation. The most simple forecast method is to use the measurements of the previous day, assuming that the next day behaves similar, i.e. that the behaviour of the source persists. This forecasting method is known as the persistence method. Considering previous periods, when calculating the forecast, can hence be understood to assume a certain persistence. Consequently, the suggested approach represents reality more than it might seem intuitively, simulating both meteorological information and persistence.

7.4 Definition of Infeed Profile

Immediately after the definition of the forecast, the infeed profile is defined. The profile is defined to be constant for the duration of one hour and it can be imagined to be the load, the generator has to supply together with the energy storage device. If the forecast for the generator output would be perfect, no storage device would be needed and the infeed profile could be defined as the hourly averaged forecast².

7.4.1 Considering non-ideal energy storage devices

According to section 7.2, the storage device is assumed to be non-ideal, characterised by charge and discharge efficiencies η_{ch} and η_{dch} , respectively (see also appendix C). This means that a portion of the originally generated electricity is consumed for conversion, whenever charging and discharging the energy storage device. Every kWh that is stored, will be reduced to $\eta_{ch} \cdot \eta_{dch}$ kWh by the time it is actually fed into the network. However, most of the generated energy is fed directly into the

²In reality, forecasts will most likely also be hourly values. The averaging is therefore just a measure within the simulation environment.

grid, without being stored at all; the infeed is planned according to a forecast for the source, and only generation that deviates from the predicted infeed profile is buffered in the storage, resulting in conversion losses. This behaviour is illustrated in figure 7.4.

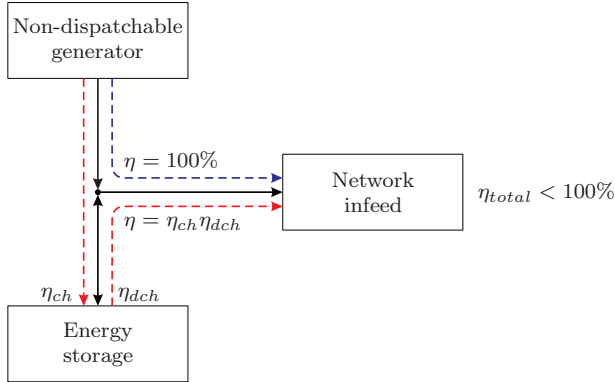


Figure 7.4: Symbolic representation of the flow and the associated efficiencies.

When planning the infeed, based on the forecast, this circumstance has to be considered. For this reason, the so-called usage factor β_{usg} is defined, indicating how much of the originally generated energy can be used, in the end, for network infeed. The usage factor relates the planned network infeed $\mathbf{P}_{planned}$ with the forecasted output of the generator \mathbf{P}_{fc} as follows:

$$\sum_{t=1}^T \mathbf{P}_{planned}(t) = \beta_{usg} \cdot \sum_{t=1}^T \mathbf{P}_{fc}(t) \quad (7.6)$$

The usage factor satisfies $0 \leq \beta_{usg} \leq 1$ and it is an efficiency factor, concerning all the energy that has to be temporarily stored. It should, however, not be mistaken for the overall storage efficiency $\eta_{ch} \cdot \eta_{dch}$. If both the forecasted output would be perfect and the energy storage device lossless, β_{usg} could be set to 1. The more the energy storage is used, continuously charging and discharging, the further the factor β_{usg} has to be reduced to take the increasing conversion losses into account.

A β_{usg} near 1 will result in a comparatively high targeted infeed profile, implying little use of the storage and good performance of the forecast.

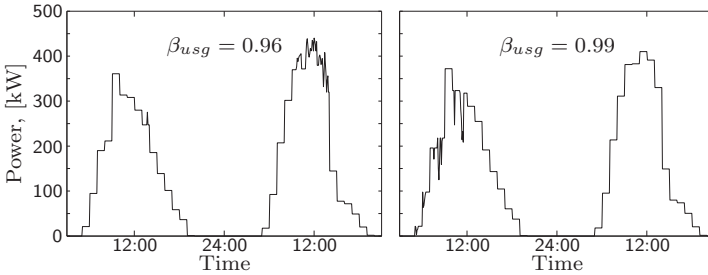


Figure 7.5: Infeed profile for $\beta_{usg} = 0.96$ and $\beta_{usg} = 0.99$. Excerpts from case study in section 9.2.

Such a profile could be difficult to fulfill, resulting in insufficient infeed P_{insuff} , which is defined as the positive difference between planned infeed $P_{planned}$ and actual infeed P_{actual} (right side of figure 7.5 and equation (7.10)). A comparatively lower β_{usg} , on the other hand, results in a lower planned infeed profile that could be satisfied often also without using the energy storage device. Depending on the storage capacity E_{st} , this strategy likely results in more surplus infeed $P_{surplus}$, defined as the positive difference between actual infeed P_{actual} and planned infeed $P_{planned}$ (left side of figure 7.5 and equation (7.8)).

Depending on the market structure, positive and negative deviations from the planned infeed result in costs for balancing energy. Accordingly, the choice of β_{usg} can also depend on these costs. More risk averse operators might desire a lower usage factor, assuming that surplus power is penalised less than insufficient power. The quantity β_{usg} hence can be defined considering both the storage device characteristics and the operation strategy. This can be achieved by incorporating an optimisation and will be discussed in section 7.4.3.

7.4.2 Incorporating the charge level in the planning

Besides the quality of the forecast, the charge level of the energy storage device also has an influence on how accurate the actual infeed matches with the planned infeed. It is therefore possible to use a dynamic usage factor $\beta_{usg}(t)$ instead of a constant β_{usg} . The dynamic $\beta_{usg}(t)$ is defined to depend on the actual content of the storage at the beginning of a planning period. In other words, if the energy storage device is

fully charged at the beginning of a forecast period (and thus at the beginning of the infeed profile planning period), a comparatively higher value for $\beta_{usg}(t)$ can be chosen, resulting in a higher targeted infeed profile. On the other hand, if the storage were only half charged or even completely discharged, an accordingly lower infeed profile would be planned, corresponding to a relatively smaller $\beta_{usg}(t)$.

In the case of a small forecast error and a fully charged storage device, it might even be beneficial to set $\beta_{usg}(t) > 1$ for the next planning period. In addition to the production from the generator, stored energy could then be fed into the network, emptying the storage to be ready to be charged again in the next period. In that next period, $\beta_{usg}(t)$ would be chosen smaller because of the lower charge level of the storage, likely resulting in energy that can be stored again. In case of a constant usage factor, such a situation would result in surplus energy, as the storage is fully charged and cannot receive any more energy. Figure 7.6 illustrates this, showing the evolution of both usage factors and the corresponding amounts of surplus and insufficient power, taken from data from the photovoltaic case study in section 9.2. The figure shows how with a dynamic usage factor the events with surplus and insufficient power are fewer and more equally distributed than with a constant usage factor.

7.4.3 Defining the usage factor

The values for the appropriate usage factor depend on the chosen forecast error f_{RMSE} and the storage capacity E_{st} . Similar to the quantity α relating to a certain f_{RMSE} , it is necessary to perform the definition of the usage factor before the first simulation. Furthermore, for the dynamic usage factor $\beta_{usg}(t)$, it is necessary to create a lookup table, indicating which value to use for $\beta_{usg}(t)$, depending on the momentary charge level of the storage device. Simple optimisation procedures can be used to find both the constant and the dynamic usage factors, as explained in the following paragraphs.

Defining the constant usage factor

The usage factor β_{usg} has a direct influence on the targeted infeed profile and thus on the ability of the system to meet this infeed profile. As mentioned above (see figure 7.5), a comparatively high β_{usg} will lead to

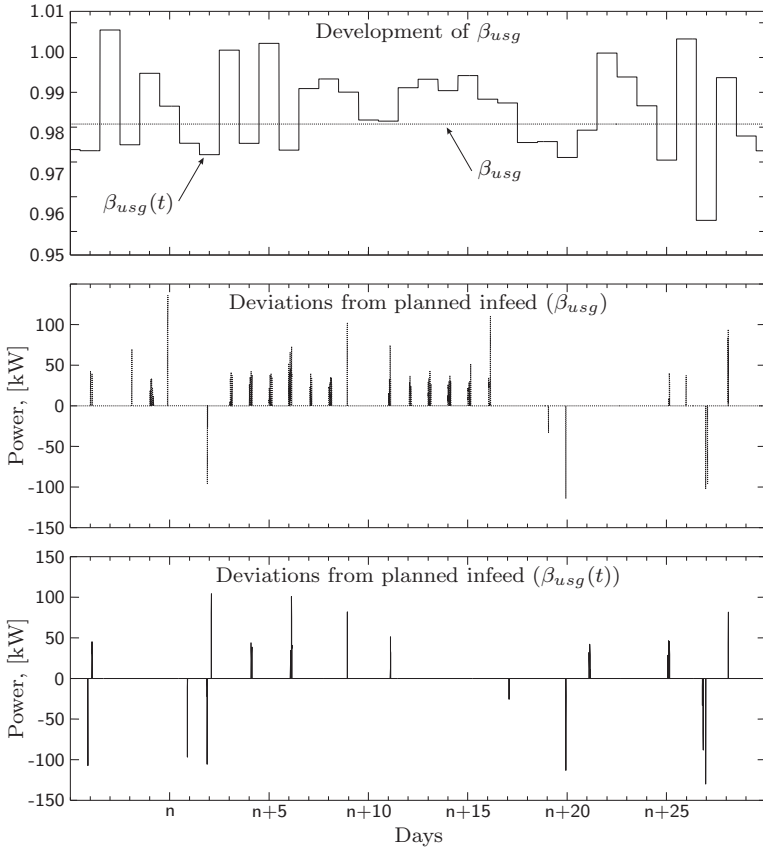


Figure 7.6: Example of the evolution of β_{usg} and $\beta_{usg}(t)$ with the corresponding deviations from the planned infeed.

more incidents with insufficient power, i.e. where the profile cannot be fulfilled, and a comparatively low β_{usg} , in turn, results in many events with surplus power. Hence, the optimal usage factor can be defined to result in a balance between surplus energy and insufficient energy.

Each time step with surplus power corresponds to a certain amount of surplus energy and their sum results in the total amount of surplus energy, fed into the grid during the time series analysis. To calculate the corresponding amount of surplus energy, surplus power must be multiplied with the relative duration of the time interval Δt . The quantity

Δt is defined relative to one hour, with an interval length of e.g. 5 min giving $\Delta t = 1/12$. Surplus power \mathbf{P}_{splus} can be defined as the positive difference between the actual infeed and the planned infeed:

$$\mathbf{P}_{splus} = \max(\mathbf{P}_{actual} - \mathbf{P}_{planned}, 0) \quad (7.7)$$

The total amount of energy that is fed into the network, exceeding the planned infeed is then defined as surplus energy E_{splus} :

$$E_{splus} = \Delta t \cdot \sum_{t=1}^T \max(\mathbf{P}_{actual}(t) - \mathbf{P}_{planned}(t), 0) \quad (7.8)$$

Analogously, insufficient power is defined as:

$$\mathbf{P}_{insuff} = \max(\mathbf{P}_{planned} - \mathbf{P}_{actual}, 0) \quad (7.9)$$

The total amount of energy that is not fed into the network, falling short the planned infeed, is accordingly the insufficient energy E_{insuff} :

$$E_{insuff} = \Delta t \cdot \sum_{t=1}^T \max(\mathbf{P}_{planned}(t) - \mathbf{P}_{actual}(t), 0) \quad (7.10)$$

Depending on the market structure, surplus and insufficient energy result in different penalties. If both cost for down regulation ($\propto E_{splus}$) and cost for up regulation ($\propto E_{insuff}$) are equal, β_{usg} can be defined to minimise the difference between E_{splus} and E_{insuff} . Otherwise, a weighting factor ω can be introduced, relating the magnitudes of cost for up regulation to those for down regulation:

$$\omega = \frac{\text{cost for up regulation per kWh}}{\text{cost for down regulation per kWh}}$$

The optimal usage factor β_{usg} is found with the following procedure:

- run simulation with $\beta_{usg} = 0.98$ ³
- calculate E_{insuff} and E_{splus}

³Starting with 0.98 was identified to result in a good performance.

- adjust β_{usg} :
 - if $(\omega \cdot E_{insuff}) > E_{splus}$, reduce β_{usg}
 - if $(\omega \cdot E_{insuff}) < E_{splus}$, increase β_{usg}
 - if $(\omega \cdot E_{insuff}) = E_{splus}$, terminate

This procedure can be performed using e.g. the `fminbnd` package in Matlab[®]. For this purpose, the simulation code has to be written as a function, taking β_{usg} as input value, and providing a return value, defined as the absolute value of the difference of $\omega \cdot E_{insuff}$ and E_{splus} :

$$\text{return value} = \text{abs}(\omega \cdot E_{insuff} - E_{splus}) + (2 - \beta_{usg}) \cdot 100$$

The second term on the righthand side can be considered as a cost function and has to be used for the following reason. For small forecast errors and large energy capacities E_{st} , different values for β_{usg} can result in $E_{insuff} = E_{splus}$. As soon as the routine `fminbnd` finds a β_{usg} that results in this equality, the routine checks the gradients and terminates if these are zero. To guarantee the largest possible value for β_{usg} to be chosen, resulting in most energy fed into the network, the second term therefore is necessary. As illustrated in figure 7.7, it is nevertheless small enough not to influence the main criterion $\omega \cdot E_{insuff} - E_{splus}$.

The disadvantage of the above optimisation criterion is the possibility of solutions, resulting in large but equal amounts for E_{insuff} and E_{splus} . Another criterion for the optimisation, i.e. the definition of the usage factor, could therefore be to minimise the total amount of energy, by which the actual infeed deviates from the planned infeed. That means, aiming to fulfill the planned infeed as closely as possible. The return value can then be defined as the sum of both deviations:

$$\text{return value} = E_{insuff} + E_{splus} + (2 - \beta_{usg}) \cdot 100$$

Again, E_{insuff} could be weighted with ω to consider different regulating penalties. Both criteria can finally also be combined to result in a β_{usg} , which minimises both the deviations from the planned infeed and the difference between the positive and negative deviations. This return value is illustrated in figure 7.7, illustrating at the same time the purpose of the cost function. Both sum and difference of E_{insuff} and E_{splus} are equal to 0 for a range of values for β_{usg} ; the cost function guarantees that β_{usg} equals the largest possible value, still fulfilling the minimisation criteria.

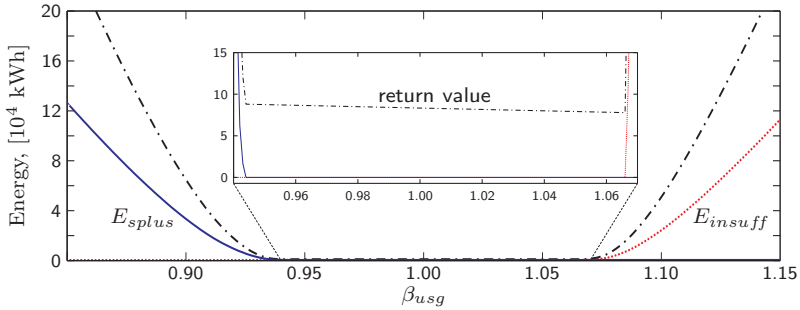


Figure 7.7: Surplus energy E_{splus} , insufficient energy E_{insuff} and return value for different usage factors β_{usg} .

Defining the dynamic usage factor

A dynamic usage factor $\beta_{usg}(t)$ is used to incorporate the charge level of the storage when planning the infeed profile. This allows a better utilisation of the stored energy and to reduce periods where the storage cannot be charged anymore because it is already full. As mentioned, a lookup table has to be created, relating the charge level of the storage device to the appropriate usage factor. At the beginning of every planning this lookup table then is consulted to apply the matching $\beta_{usg}(t)$.

To derive this table, a similar approach as before can be followed, i.e. the same optimisation criteria can be used. However, a slight adjustment has to be done to the simulation code, used for the optimisation. Basically, different charge levels of the storage device have to be simulated in order to determine the corresponding $\beta_{usg}(t)$. For this purpose, a command has to be added in the code, just before the definition of the next infeed. The command resets the momentary charge level $E_{st,ch}(t)$ to a certain level (e.g. $0.25 \cdot E_{st}$), independent of its actual charge level. Then, the above described optimisation procedure is run. The resulting β_{usg} can be assigned to the charge level, to which the storage has been constantly reset during the simulation. This procedure is recommended to be performed for different charge levels, e.g. in 20% steps from 0% to 100%. Values in between the discrete levels can be linearly interpolated and a lookup table results, relating each charge level to its appropriate $\beta_{usg}(t)$. An example of the sound performance from applying this procedure, can be identified in figure 7.6 and will be discussed in more detail in the case studies (see e.g. figures 9.3 to 9.5).

7.5 Operation of the Energy Storage

The previous two sections described procedures that are only carried out at the beginning of a new forecast period. As soon as the new infeed profile has been defined, based on the forecast, the algorithm progresses and starts with the actual operation phase. This basically means that the storage device is charged and discharged, respectively, according to the differences between the planned infeed $P_{planned}(t)$ and the actual generator output $P_{gen}(t)$.

Assuming that the storage device can switch immediately from charge to discharge state, makes it possible to define the power $P_{st,dem}(t)$, which is demanded from the energy storage device in every time step t as:

$$P_{st,dem}(t) = P_{planned}(t) - P_{gen}(t) \quad (7.11)$$

Hence, a negative $P_{st,dem}(t)$ stands for charging periods and a positive $P_{st,dem}(t)$ for discharging periods. The ability of the storage device to fulfil the required $P_{st,dem}(t)$ depends both on its power rating P_{st} and its momentary charge state $E_{st,ch}(t)$. First, it is checked whether the power rating P_{st} is lower than the required power and – if necessary – accordingly adjusted. The preliminary power flow $P_{st,prlm}(t)$ from or into the energy storage is then found as:

$$P_{st,prlm}(t) = \begin{cases} P_{st} \cdot \sigma(P_{st,dem}(t)), & |P_{st,dem}(t)| > P_{st} \\ P_{st,dem}(t), & |P_{st,dem}(t)| \leq P_{st} \end{cases} \quad (7.12)$$

Whereas $\sigma()$ represents the sign function:

$$\sigma(x) = \begin{cases} 1, & x \geq 0 \\ -1, & x < 0 \end{cases} \quad (7.13)$$

Then it is checked whether the charge state $E_{st,ch}(t)$ of the energy storage allows to deliver or absorb the required amount of power. At this point, the interval duration Δt is used to transform the power values into energy amounts and the charge and discharge efficiencies have to be considered. The charging power is multiplied with η_{ch} , resulting in the amount of energy, actually available for storing. For the charge state, i.e. $P_{st,prlm}(t) < 0$, the effective charge power flow $P_{st,eff}(t)$ is given as:

$$P_{st,eff}(t) = \begin{cases} P_{st,prlm}(t), & E_{st,ch}(t) + \phi(t) \leq E_{st} \\ -(E_{st} - E_{st,ch}(t)) \cdot \frac{1}{\Delta t} \frac{1}{\eta_{ch}}, & E_{st,ch}(t) + \phi(t) > E_{st} \end{cases} \quad (7.14)$$

Whereas the desired charge activity $\phi(t)$ is defined as:

$$\phi(t) = -\Delta t \cdot \eta_{ch} \cdot P_{st,prlm}(t) \quad (7.15)$$

If the planned charge $\phi(t)$ exceeds the rated capacity E_{st} of the storage, the charge power has to be reduced accordingly; the maximum possible charge, which the storage can still absorb $E_{st} - E_{st,ch}(t)$ is determined and multiplied with the reciprocals of the charge efficiency and Δt to result in the corresponding power value. For the discharge state, i.e. $P_{st,prlm}(t) > 0$, the according formula can be formulated as:

$$P_{st,eff}(t) = \begin{cases} P_{st,prlm}(t), & E_{st,ch}(t) - \psi(t) \geq E_{st,min} \\ (E_{st,ch}(t) - E_{st,min}) \cdot \frac{\eta_{dch}}{\Delta t}, & E_{st,ch}(t) - \psi(t) < E_{st,min} \end{cases} \quad (7.16)$$

The desired discharge activity $\psi(t)$ is defined as:

$$\psi(t) = \Delta t \cdot \frac{1}{\eta_{dch}} \cdot P_{st,prlm}(t) \quad (7.17)$$

The term $E_{st,min}$ stands for the minimum energy capacity of the storage device. Depending on the storage technology, $E_{st,min}$ is not necessarily equal to zero. In particular, kinetic storage devices as e.g. flywheels cannot be discharged below a certain level, as the remaining energy is not sufficient to reach the required level of power [47]. Equation (7.16) shows that if the energy demand $\psi(t)$ from the energy storage device exceeds the stored amount of energy, the maximum power demand is reduced to match the amount of available energy.

A short example will illustrate the operation of the energy storage device. The energy storage device is assumed to be at its minimum charge level $E_{st,min}$ at time t . The generator output is assumed to exceed the planned infeed, resulting in an available charging power $P_{st,dem}(t) = P_{st,eff}(t) = 24$ kW. Following equation (7.14), this charging power results in a charge level addition of $\phi(t) = 24 \text{ kW} \cdot \eta_{ch} \cdot \Delta t = 1.8$ kWh, with $\eta_{ch} = 0.9$ and $\Delta t = \frac{1}{12}$ h. The new charge level now is at $E_{st,ch}(t) = E_{st,min} + 1.8$ kWh. In the next time step, the generator output however decreases and cannot meet the infeed profile, resulting in a power demand of $P_{st,prlm}(t + \Delta t) = 20$ kW. This means an energy consumption of $\psi(t) = 20 \text{ kW} \cdot \eta_{dch}^{-1} \cdot \Delta t = 1.85$ kWh, with $\eta_{dch} = 0.9$.

Thus, the possible power output of the storage has to be reduced to $P_{st,eff}(t + \Delta t) = 1.8 \text{ kWh} \cdot \eta_{dch} \cdot \Delta t^{-1} = 19.44 \text{ kW}$.

The effective storage activity $\mathbf{P}_{st,eff}$ will possibly often be lower than the demanded $\mathbf{P}_{st,dem}$, particularly for smaller energy capacities E_{st} ; the planned infeed profile cannot be fully met. To incorporate this, the vector \mathbf{P}_{actual} is defined, containing the actual amount of power that is fed into the network during every time step.

Before one loop cycle terminates, with checking whether the end of the time series is reached, the storage charge level $E_{st,ch}$ has to be adjusted, according to the operation during the just passed time step. If the storage was charged, the storage power flow $P_{st,eff}(t)$ is negative, following equation (7.11), and gives:

$$E_{st,ch}(t + \Delta t) = E_{st,ch}(t) - \Delta t \cdot \eta_{ch} \cdot P_{st,eff}(t) \quad (7.18)$$

In the discharge case, the new charge level is defined as:

$$E_{st,ch}(t + \Delta t) = E_{st,ch}(t) - \Delta t \cdot \frac{1}{\eta_{dch}} \cdot P_{st,eff}(t) \quad (7.19)$$

This concludes the description and discussion of the simulation algorithm, shown in figure 7.1. During the simulation, it is important to keep track of various values to be used for the analyses, described in the next chapter. The values to continuously record and store are the forecasted generator output \mathbf{P}_{fc} , the actual generator output \mathbf{P}_{gen} , the planned network infeed $\mathbf{P}_{planned}$ and the actual network network infeed \mathbf{P}_{actual} . The actual network infeed is defined as the sum of the generator output and the effective action of the storage device; as soon as $P_{st,eff}$ differs from $P_{st,dem}$, an infeed deviation will occur. Therefore, surplus power \mathbf{P}_{splus} and insufficient power \mathbf{P}_{insuff} have to be kept track of as well. Finally, to be able to analyse the behaviour of the energy storage, the momentary charge level $E_{st,ch}$ and the actual power output $\mathbf{P}_{st,eff}$ must be recorded.

Chapter 8

Analysis Methods

In this chapter, several analysis procedures are presented and discussed. Their purpose is to investigate various aspects of combining a non-dispatchable generator with an energy storage device. The most important criterion is the performance of such a system, i.e. how well the planned infeed profile is fulfilled. Further sections provide procedures for analysing conversion losses and balancing energy requirements.

8.1 Infeed Fulfilment

In the previous chapter, a time series based modelling procedure was introduced and thoroughly discussed. The modelling procedure is intended for analysing the behaviour of a non-dispatchable generator that is operating in combination with an energy storage device. The purpose of this combined operation is to improve the network infeed accuracy of the non-dispatchable generator, resulting in a network infeed as deterministic as possible. Such combinations have several implications, which are discussed throughout this and the next sections, in order to determine the accuracy and efficiency of this approach.

The basic idea of combining the generator with a storage device is to eliminate or at least alleviate the non-deterministic fluctuations, inherent to the stochastic source. This allows to better incorporate this source into the production planning and dispatching, thus increasing the operational value of the energy, generated from that source.

Therefore, the predefined deterministic infeed profile should be fulfilled as reliably and exactly as possible. The infeed profile can be regarded as the load, which the generator has to supply together with the energy storage device, and known measures can be applied to calculate the accuracy and reliability of reaching the target. From the measurement series and the simulation output files, indices can be calculated, similar to expected energy not supplied (EENS) and to the energy indices of reliability (EIR) and unreliability (EIU) [48, 20].

Expected energy not supplied corresponds to the expected amount of energy that cannot be served if the supplying systems have an outage. In the underlying context, EENS can be understood to correspond to the insufficient energy E_{insuff} , i.e. the total amount of energy, by which the actual infeed was falling short of the planned infeed. In accordance with equation (7.10), insufficient energy is defined as:

$$E_{insuff} = \Delta t \cdot \sum_{t=1}^T \max(\mathbf{P}_{planned}(t) - \mathbf{P}_{actual}(t), 0) \quad (8.1)$$

Depending on the use of this index, it can also be put in relation to the duration of e.g. a year, suitable for comparing measurement series of different lengths. Another possibility is to express insufficient energy E_{insuff} relative to the total amount of energy planned for infeed $\Delta t \sum \mathbf{P}_{planned}$. This index then corresponds to the energy index of unreliability:

$$\text{EIU} = \frac{E_{insuff}}{\Delta t \cdot \left[\sum_{t=1}^T \mathbf{P}_{planned}(t) \right]} \quad (8.2)$$

The counterpart to this index is the energy index of reliability EIR, adding up to unity with EIU. In this context, EIR is redefined as the energy index of fulfilment EIF, designating the percentage of the planned energy that was effectively fed into the network:

$$\text{EIF} = 1 - \text{EIU} = 1 - \frac{E_{insuff}}{\Delta t \cdot \left[\sum_{t=1}^T \mathbf{P}_{planned}(t) \right]} \quad (8.3)$$

The index EIF can thus be understood as a measure, identifying how reliably the infeed plan was fulfilled. Surplus power is not considered

and the index thus only measures the share of insufficient infeed. In both case studies, this measure will be used to identify the influence of the forecast error by analysing the required energy capacity of the ESD in order to perform with an accuracy of e.g. $\text{EIF} \geq 99\%$.

8.2 Conversion Losses

The utilisation of the storage device results in a certain amount of conversion energy E_{conv} used for the conversion and storing process. This energy is basically lost for further use and can be considered as cost for using a storage device. These conversions losses are expected to increase with an increasing forecast error: the storage is not only balancing fluctuations within each hour but also compensating the differences between forecasted and actual generation series, and accordingly the storage device will be used more often. The conversion losses can be calculated with the vector containing the momentary power flows into and out of the storage $\mathbf{P}_{st,eff}$ and the efficiencies for charging and discharging η_{ch} and η_{dch} . Taking into account that negative values for $\mathbf{P}_{st,eff}$ represent charging events and positive values discharging events, gives:

$$E_{conv} = \Delta t \cdot \left[(\eta_{ch} - 1) \cdot \sum_{t=1}^T \min(\mathbf{P}_{st,eff}(t), 0) + \left(\frac{1}{\eta_{dch}} - 1 \right) \cdot \sum_{t=1}^T \max(\mathbf{P}_{st,eff}(t), 0) \right] \quad (8.4)$$

This measure can be considered as an efficiency measure. It can be applied to determine the relation between cost for using the storage (i.e. lost energy) and benefit from using the storage (i.e. avoided balancing penalties on account of the storage). However, as most of the energy generated from the stochastic source is never stored at all, but fed immediately into the network, the amount of conversion losses will take a comparatively small share of the originally generated energy $\Delta t \sum \mathbf{P}_{gen}$ (see case studies). Furthermore, assuming that all other components are lossless, the conversion losses correspond to the overall system losses. Otherwise, the losses of considered components would have to be kept track of, to be accordingly incorporated.

8.3 Infeed Accuracy

Besides the two measures conversion losses and energy index of fulfilment, a third measure can be defined, concerning the overall accuracy of the infeed. This measure is equivalent to surplus and insufficient energy, defined in equations (7.8) and (7.10) and restated here:

$$E_{\text{surplus}} = \Delta t \cdot \sum_{t=1}^T \max(\mathbf{P}_{\text{actual}}(t) - \mathbf{P}_{\text{planned}}(t), 0) \quad (8.5)$$

$$E_{\text{insuff}} = \Delta t \cdot \sum_{t=1}^T \max(\mathbf{P}_{\text{planned}}(t) - \mathbf{P}_{\text{actual}}(t), 0) \quad (8.6)$$

As outlined earlier, in section 7.4.3, choosing a comparatively low usage factor β_{usg} could result in a EIF close to 100%, however at the price of many events with surplus energy (see also figure 7.5). Consequently, the general idea of using an energy storage device would be misinterpreted if a large amount of surplus energy would result. The infeed accuracy thus is a measure to identify balanced choices for the usage factor, resulting in a reasonably planned infeed profile that is fulfilled with as little deviations as possible.

In other words, EIF indicates how reliably the projected infeed profile was met, whereas E_{surplus} designates how much energy had to be sold for a lower price, exceeding the planned infeed; it is assumed here that energy, which is sold according to a plan, generates more income than energy, which is fed in as surplus, possibly even incurring balancing penalties. Both measures can be used for analysing the already discussed trade-off between surplus energy, larger storage capacity, conversion energy and usage factor β_{usg} .

The following chapter, containing the case studies, will outline the application of the discussed analysis procedures. They will be used to determine the performance and efficiency of different configurations and to discuss the just mentioned trade-off.

Chapter 9

Case Studies

This chapter contains two case studies, applying the modelling algorithm and analysis procedures described in the previous chapters. The first case study is based on measurements from a photovoltaic system and the second case study uses data from a wind speed measurement site. Both case studies analyse various operational aspects and demonstrate the useability of the developed methods.

9.1 Outline of the Case Studies

This section gives an overview of the sequence of analyses performed throughout both case studies. After introducing the time series and defining further simulation parameters as e.g. the storage efficiency, a first simulation is done to identify a base configuration. This base configuration concerns the energy capacity and power rating of the energy storage and it is meant to be used for several comparative investigations. The first part of these comparative investigations is performed, assuming a perfect forecast, representing the ideal case. Afterwards, imperfect forecasts are introduced in the form of different forecast error magnitudes (photovoltaic case study) and different forecast horizons (wind case study). Again, the base configuration is applied to measure the performance with now imperfect forecasts. Then, the minimum required energy capacities of the storage are determined, necessary to

achieve a certain reliability of infeed, depending on the forecast imperfections. Both case studies close with a brief analysis of the performance of the system without energy storage. Short conclusions summarise each case study, with more aspects being discussed in chapter 10.

9.2 Photovoltaic System

This first case study applies the developed algorithm and analysis procedures to a measurement series from a photovoltaic (PV) installation. The purpose is to investigate whether forecast errors can be efficiently compensated with an energy storage device and what the requirements for doing so would be. Moreover, the case study demonstrates the application and usability of the presented simulation and analysis methods.

9.2.1 Characteristics of the time series and definition of the simulation parameters

The measurement series is from a 500 kWp photovoltaic system that is installed on Mont Soleil, in Switzerland. The PV array covers an area of roughly 20'000 m² and is in operation since 1992. The data series consists of various measurements (e.g. insolation, temperature, inverter losses) for every 5 min from January 2002 up to and including June 2006. The time series thus covers 4.5 years and contains 472'896 measurements. For this study, the output of the inverter is used as input data¹[49]. As outlined in chapter 7, the forecast calculations will thus be performed using equation (7.2).

The storage device is modelled with a charge efficiency $\eta_{ch} = 0.9$ and a discharge efficiency $\eta_{dch} = 0.9$, resulting in a cycle efficiency of 0.81, similar to the long run cycle efficiency of certain types of batteries [50]. The minimal energy capacity $E_{st,min}$ is set to 0 kWh. The remaining parameters are the power rating P_{st} and the energy capacity E_{st} .

9.2.2 Determination of energy and power capacity

As discussed earlier, the energy capacity is having an influence on both surplus and insufficient energy as well as on conversion losses. The first

¹The data has been kindly provided by HTA Burgdorf, Switzerland.

simulation run thus is performed to identify the influence of energy and power capacity on the energy index EIF, neglecting forecast errors. This analysis is at the same used to define the base configuration for this case study. Following section 7.4, prior to any simulation, the appropriate usage factor β_{usg} has to be determined. The purpose of this simulation is to identify the influence of E_{st} and P_{st} , which is why a constant usage factor β_{usg} was decided to be sufficiently accurate.

The usage factor was defined for energy capacities, varying from 20 kWh to 500 kWh in 20 kWh steps and for power capacities, varying from 50 kW up to 500 kW in 50 kW steps. The forecast error was set to $f_{RMSE} = 0\%$ and both surplus and insufficient energy are assumed to result in the same penalties, i.e. $\omega = 1$. The return value for the optimisation procedure can then be defined as follows, in accordance with section 7.4.3:

$$\begin{aligned} \text{return value} &= E_{insuff} + E_{splus} + \text{abs}(E_{insuff} - E_{splus}) \\ &\quad + (2 - \beta_{usg}) \cdot 100 \end{aligned}$$

An optimal β_{usg} thus results in minimal deviations and similar amounts of surplus and insufficient energy. The resulting EIF, according to equation (8.3), is shown in a surface plot in figure 9.1.

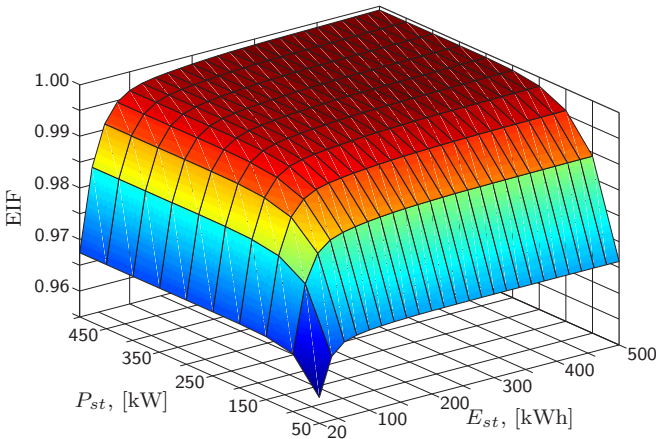


Figure 9.1: EIF for varying $E_{st} \in [20, 40, \dots, 500]$ kWh and $P_{st} \in [50, 100, \dots, 500]$ kW with $f_{RMSE} = 0\%$.

The analysis shows that both parameters have a certain influence on the fulfilment index EIF. However, the fulfilment only varies significantly for values below $P_{st} \lesssim 200$ kW and below $E_{st} \lesssim 100$ kWh. The base configuration was thus defined to have an energy capacity of $E_{st} = 100$ kWh and a power rating of $P_{st} = 500$ kW, corresponding to the rating of the PV system. The above finding is confirmed with an analysis of the discharge and charge power flows during one simulation run. The histogram illustrates in figure 9.2 that most activities have power magnitudes that are even within ± 50 kW.

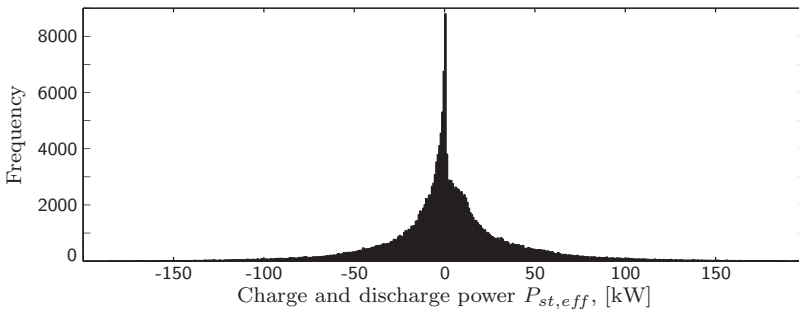


Figure 9.2: Histogram of charge and discharge power flows for an energy storage device with $P_{st} = 500$ kW and $E_{st} = 100$ kWh.

The base configuration with $P_{st} = 500$ kW and $E_{st} = 100$ kWh will be used to investigate different aspects, first without forecast error and later-on including different forecast errors.

9.2.3 Simulations with a perfect forecast

Performing simulations with a perfect forecast is a pure theoretical approach. Still, a perfect forecast can be considered to be the ideal case and consequently serves as a reference. To determine the corresponding reference values, two simulations were performed, both with a constant β_{usg} and a dynamic $\beta_{usg}(t)$. The planning period is defined to cover $f_h = 24$ h, as indicated by the daily cyclic behaviour of the source.

Before the first simulation, following the procedure outlined in section 7.4, it is necessary to define a lookup table for the dynamic usage factor. This simulation was done according to the procedure described on page

138, with discrete levels of 20% of the rated energy capacity E_{st} . To use the optimisation for studies with other energy and power capacities, it was performed as well for energy capacities, varying from 20 kWh to 500 kWh in 20 kWh steps, and for power capacities, varying from 50 kW up to 500 kW in 50 kW steps. Figure 9.3 shows the values to be used as usage factors, depending on the charge level $E_{st,ch}$ at the beginning of a planning period. Values in between the discrete 20% levels are found with a linear interpolation. The definition of the individual levels has been performed analogue to the above quoted minimisation target, as also illustrated in figure 7.7.

The subfigures contained in figure 9.3 show that the variation range is rather limited for smaller energy capacities. The larger the installed energy capacity gets, the broader the operation range for a dynamic usage factor becomes.

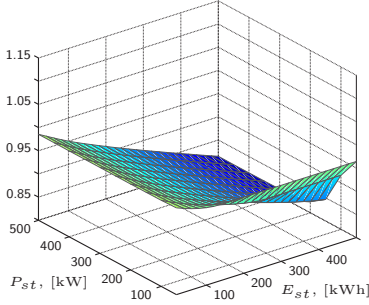
The results from both simulation runs with the base configuration are summarised in table 9.1. The table shows that incorporating the storage device's charge level into the planning process, results in a better overall performance, i.e. higher EIF and less deviations from the planned infeed. To identify the utilisation of the total generation $\Delta t \sum \mathbf{P}_{gen}$, all results are also expressed relative to this amount of energy. It is important to note that the values in the table represent the whole simulation duration of 4.5 years and not annual amounts.

In the case of a constant usage factor, the amount of energy planned for infeed $E_{planned}$ is almost identical to the actually infeed amount of energy E_{actual} . The actual infeed however also contains the amount

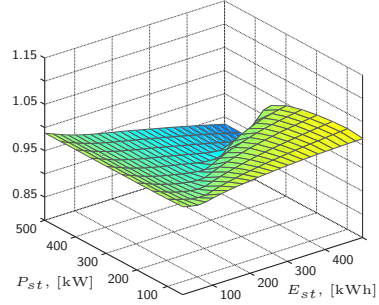
	constant β_{usg}		dynamic $\beta_{usg}(t)$	
	[kWh]	[%]	[kWh]	[%]
$E_{gen} = \Delta t \sum \mathbf{P}_{gen}$	2'640'362	100.00	2'640'362	100.00
$E_{planned} = \Delta t \sum \mathbf{P}_{planned}$	2'589'689	98.08	2'590'001	98.09
$E_{actual} = \Delta t \sum \mathbf{P}_{actual}$	2'589'690	98.08	2'588'902	98.05
E_{conv}	50'646	1.92	51'428	1.95
E_{splus}	9'517	0.36	5'598	0.21
E_{insuff}	9'517	0.36	6'697	0.25
$\emptyset \beta_{usg}$	0.9808		0.9790	
EIF	0.9963		0.9974	

Table 9.1: Simulation results for the base configuration.

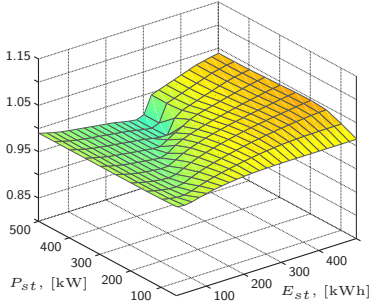
$$E_{st,ch}(t) = 0.0 \cdot E_{st}$$



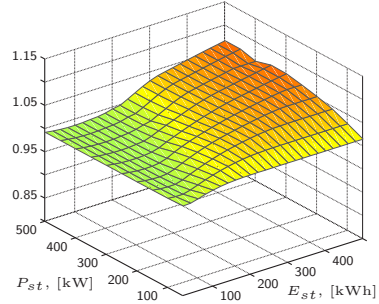
$$E_{st,ch}(t) = 0.2 \cdot E_{st}$$



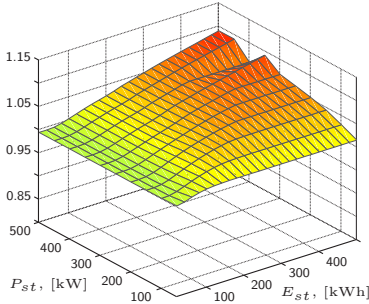
$$E_{st,ch}(t) = 0.4 \cdot E_{st}$$



$$E_{st,ch}(t) = 0.6 \cdot E_{st}$$



$$E_{st,ch}(t) = 0.8 \cdot E_{st}$$



$$E_{st,ch}(t) = 1.0 \cdot E_{st}$$

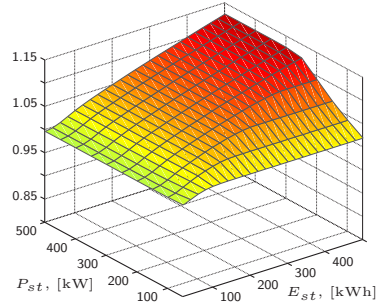


Figure 9.3: Values for $\beta_{usg}(t)$, depending on the charge level $E_{st,ch}$ at the beginning of a planning period. Values between discrete levels are interpolated.

of surplus energy E_{splus} that was fed into the network. As surplus and insufficient energy are practically identical, it looks as if the actual infeed matches with the planned infeed. This is true in terms of energy, but the fulfilment index EIF shows that during the complete simulation, 0.37% of the planned infeed was not provided. This corresponds to E_{insuff} , which sums up to 0.36% of the originally generated energy.

The benefit from incorporating the storage's charge level into the planning process is visible particularly in E_{splus} and E_{insuff} . The planned infeed is a little bit higher than with a constant usage factor and nevertheless the fulfilment is better. The positive and negative deviations from the planned infeed are significantly reduced to about two thirds. The difference between $E_{planned}$ and E_{actual} is larger than before because of the difference between surplus energy E_{splus} and E_{insuff} . Thus, it looks as if the actual infeed was higher when using a constant usage factor. If surplus energy is not considered when defining the actual infeed, an amount of 2'580'172 kWh would result, compared with 2'583'304 kWh, resulting when using a dynamic usage factor.

The only drawback of using a dynamic usage factor is visible from the increased amount of conversion energy. This increase is reasonable, as the use of a dynamic $\beta_{usg}(t)$ results in a more intensively used energy storage device. A fully charged storage device, at the beginning of a planning period, results in a higher infeed plan in order to use the stored energy. Consequently, more energy is lost for conversions, to be accurate 782 kWh. However, as outlined in the above paragraph, the amount of energy infeed as planned increases by 3'132 kWh. Furthermore, the amount of energy deviating from the infeed and resulting in balancing penalties can be reduced from totally 19'034 kWh to 12'295 kWh. Chapter 10, discussing market aspects, will indicate that the larger conversion losses are insignificant compared with the potential savings.

The following two pages contain figures further illustrating the difference between a constant and a dynamic usage factor. The curves represent a simulation with the same settings except for the energy capacity, which was increased to $E_{st} = 400$ kWh. This larger energy capacity allows to better demonstrate the flexibility of using a dynamic $\beta_{usg}(t)$, as already mentioned in the context of figure 9.3.

The left hand figure 9.4 shows days 226 to 233 from the simulation with no forecast and constant usage factor. The actual infeed matches well with the planned infeed, which in turn is well in line with the actual

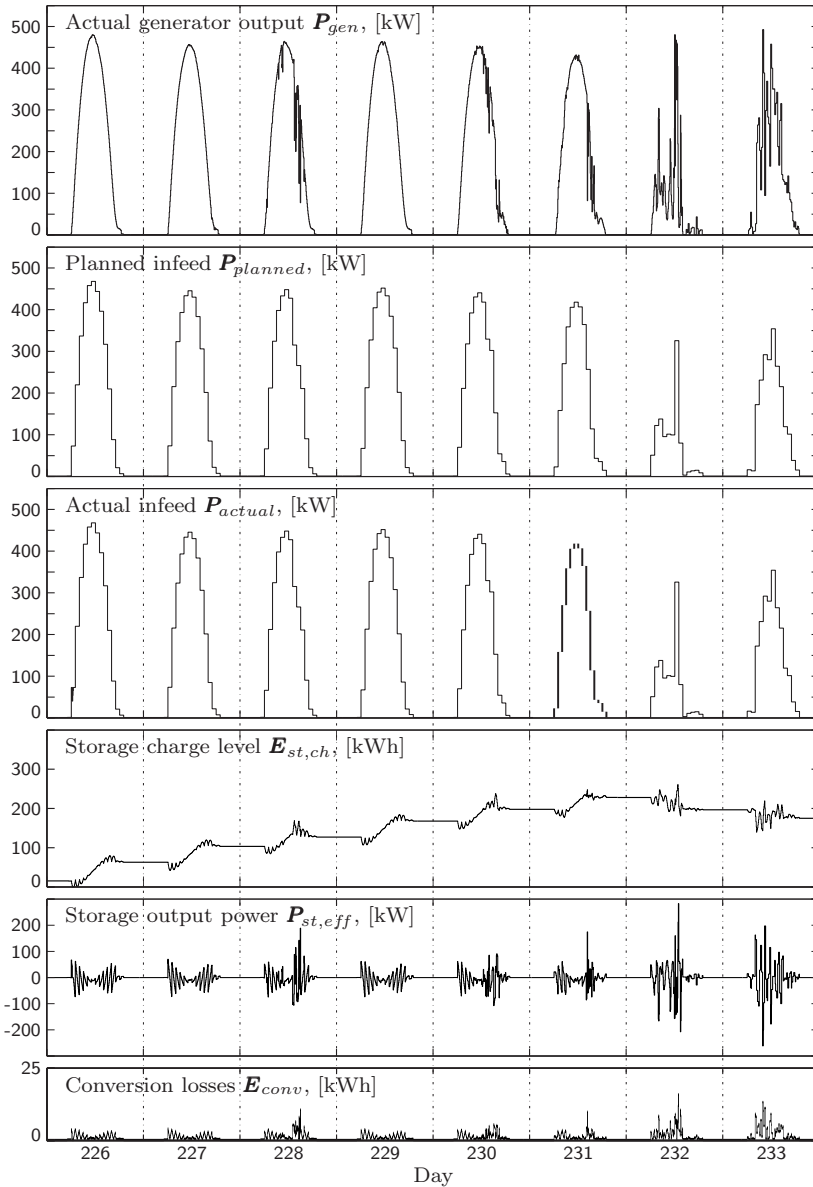


Figure 9.4: Days 226 to 233 from a simulation with the PV system base configuration with $E_{st}=400$ kWh, $f_{RMSE}=0\%$ and β_{usg} .

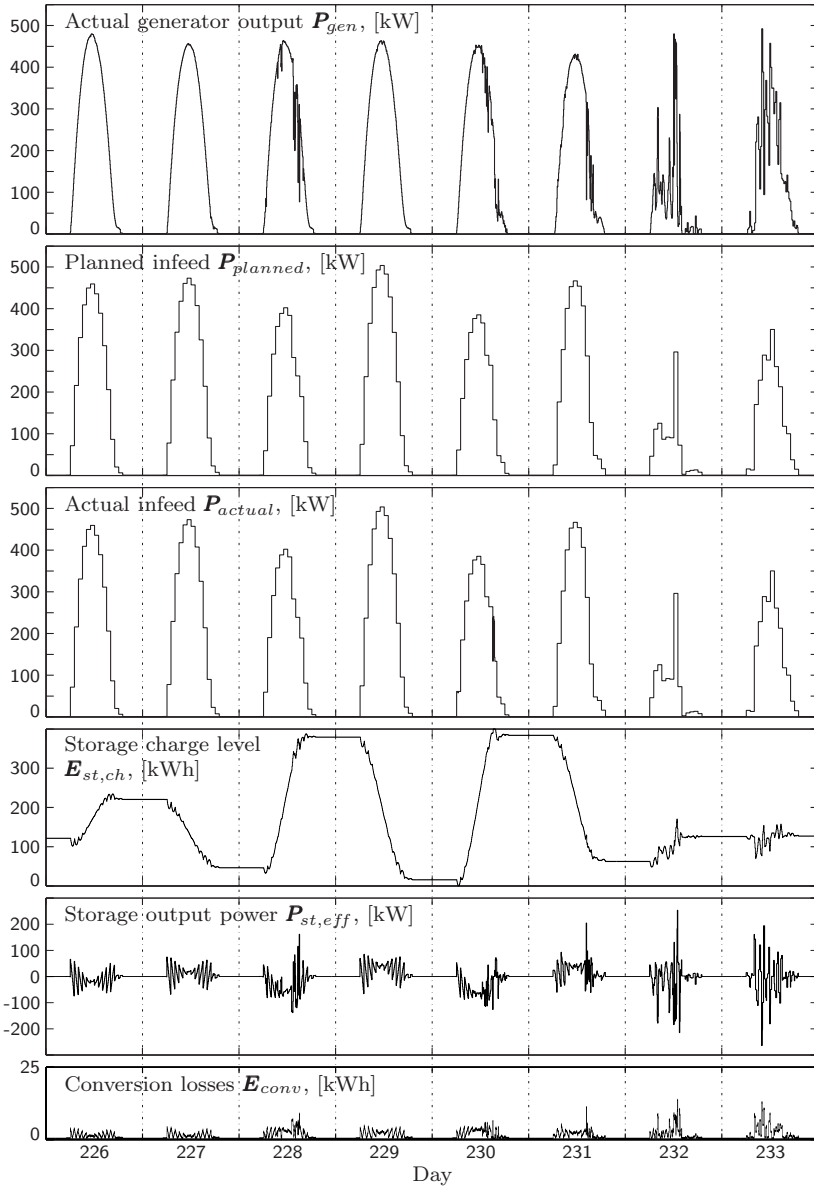


Figure 9.5: Days 226 to 233 from a simulation with the PV system base configuration with $E_{st} = 400$ kWh, $f_{RMSE} = 0\%$ and $\beta_{usg}(t)$.

generation. Over the run of these 8 days, the storage device is adding some charge every day, only a little bit balancing, mostly in between hours. This is to be expected with a perfect forecast. The right hand figure shows the same 8 days, but the power and energy values, resulting when using a dynamic usage factor $\beta_{usg}(t)$. The planned infeed is again well met with the actual infeed. However, the planned infeed is changing compared to the simulation in the left side figure. On days 229 and 231 the planned infeed clearly exceeds the actual output of the generator and on days 228 and 230 the planned infeed is below the actual generator output. This is due to the dynamically changing usage factor, whose influence is best seen in the plot with the storage charge level.

On day 228, the storage device is almost empty at the beginning of the planning period, and accordingly the infeed is planned slightly lower than with a constant usage factor. Consequently, a share of the generator's output exceeds the planned network infeed and can be stored in the energy storage device, resulting in an almost fully charged device by the end of day 228. This, in turn, leads to a comparatively high infeed target for day 229, which also requires the stored energy to be fulfilled. This behaviour results in the visible cycling of the energy storage device, explaining the additional amount of energy used for conversions. With the dynamic usage factor, the storage is hence more actively operated and not merely just used when needed.

Another interesting analysis can be performed when looking at the duration curve of the charge level of the energy storage device. If a charge level duration curve contains many entries at the minimum or the maximum, it can be understood as an indicator that the storage is not

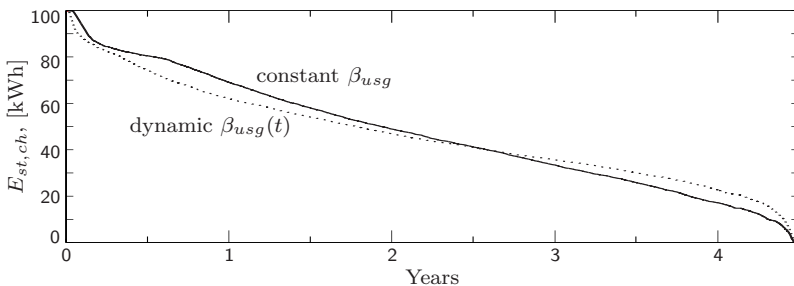


Figure 9.6: Charge level duration curve for a constant and a dynamic usage factor β_{usg} and $\beta_{usg}(t)$, respectively.

appropriately sized; it often is either empty or fully charged. This is partly the case in figure 9.6, showing that a dynamic usage factor reduces the duration the storage is full or empty (top left and bottom right corners). Furthermore, the figure shows that a dynamic usage factor leads to a flatter curve, i.e. the charge level is mostly between 20% and 80% of the rated capacity E_{st} . With the constant usage factor β_{usg} , the storage device is mostly charged between 10% and 90% of the rated capacity. Hence, the dynamic usage factor results in a better utilisation of the storage device and allows for a smaller installed energy capacity. The validity of using storage duration curves for investigating the proper E_{st} , will be discussed in more detail later-on, when comparing duration curves for different forecast error magnitudes (section 9.2.4).

A further observation can be done when looking at the histogram of the infeed deviations, i.e. the distribution of the differences between actual infeed \mathbf{P}_{actual} and planned infeed $\mathbf{P}_{planned}$. Figure 9.7 contains this distribution for capacities $E_{st} = 100$ kWh and $E_{st} = 300$ kWh. The applied usage factors satisfy $\beta_{usg,100 \text{ kWh}} = 0.980808$ and $\beta_{usg,300 \text{ kWh}} = 0.980276$; both values were determined according to the condition stated on page 149. The total number of events covered in the histogram for $E_{st} = 100$ kWh is 6'678, i.e. during 6'678 time intervals, the actual infeed deviates from the planned infeed. The total number of time intervals, during which an infeed was planned, equals 214'884. The ratio of both values equals 0.0311 and identifies the likelihood of the actual infeed not meeting the planned infeed. It does, however, not indicate the magnitude of the deviation. With $E_{st} = 300$ kWh, the number of intervals with a deviating infeed reduces to 2'254, resulting in a ratio of

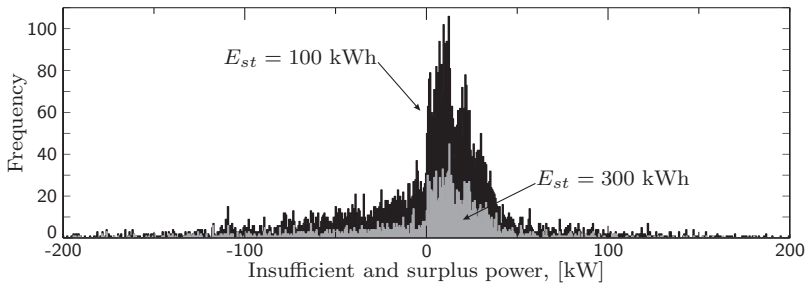


Figure 9.7: Distribution of \mathbf{P}_{plus} and \mathbf{P}_{insuff} , with $E_{st} = 100$ kWh, $E_{st} = 300$ kWh and constant β_{usg} .

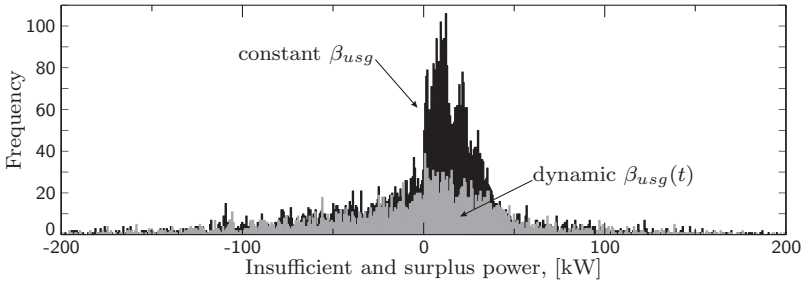


Figure 9.8: Distribution of \mathbf{P}_{plus} and \mathbf{P}_{insuff} , with $E_{st} = 100$ kWh, constant β_{usg} and dynamic $\beta_{usg}(t)$.

0.0105. In other words, with the larger storage device, the actual infeed is different in 1.1% of all intervals with a planned infeed, compared with 3.1% with the smaller storage device.

Figure 9.8 shows a similar plot, however with constant and dynamic usage factors but identical energy storage capacity $E_{st} = 100$ kWh. The shape of the distribution with the dynamic usage factor is similar to the shape obtained before, with a constant usage factor and a larger energy capacity. The number of intervals with a deviating infeed is 3'359 when applying $\beta_{usg}(t)$. In relation to all intervals, this corresponds to 0.0156, i.e. in 1.6% of all considered intervals, the infeed did not match the planned infeed. Thus, using a dynamic usage factor has a similar influence on the system behaviour as using a larger storage device. This is confirmed with the values in table 9.2, containing the energy index of fulfilment for different capacities and both versions of the usage factor.

E_{st}	100 kWh	200 kWh	300 kWh	400 kWh	500 kWh
β_{usg}	0.996325	0.998276	0.998854	0.999066	0.999260
$\beta_{usg}(t)$	0.997414	0.999660	0.999715	0.999787	0.999824

Table 9.2: EIF for different energy capacities E_{st}

It can be concluded that a well-designed infeed planning algorithm leads to slightly more conversion losses on the one hand, but on the other hand allows to accurately follow the infeed pattern with a comparatively smaller energy capacity.

9.2.4 Simulations with an imperfect forecast

The simulation results discussed so far were based on a perfect forecast and serve as reference values for the subsequent simulations. The benefit of using a dynamic usage factor has been analysed in detail and all future simulations, presented in this first case study, consequently will apply a dynamic $\beta_{usg}(t)$.

The following paragraphs contain and discuss the results from simulations with forecast error magnitudes from 0% up to 50%. Following the procedure outlined in section 7.3.1, first of all, a lookup table has to be created, relating each f_{RMSE} to its α . As the case study is based on generator output measurement data, the EWMA approach is directly applied to these power measurements, as in equation (7.2). For the underlying data, using the actual day and the seven preceding days was identified to result in useful forecasts. The formula for calculating the forecast for the next period n accordingly is:

$$\begin{aligned} \vec{P}_{fc,n} = & \alpha \cdot \vec{P}_n + \alpha(1 - \alpha) \cdot \vec{P}_{n-1} + \dots + \\ & \alpha(1 - \alpha)^6 \cdot \vec{P}_{n-6} + (1 - \alpha)^7 \cdot \vec{P}_{n-7} \end{aligned} \quad (9.1)$$

The lookup table, relating forecast error magnitude and weighting factor, can be found by applying this formula with $\alpha \in [0.50, 0.51, \dots, 1.00]$ and calculating the corresponding RMSE. The relation between both values is plotted in figure 9.9, showing an almost linear relationship.

Using this lookup table, a simulation was performed, increasing the forecast error from 0% to 50%, while keeping the storage's energy capacity constant at $E_{st} = 100$ kWh. For the planning of the infeed, the

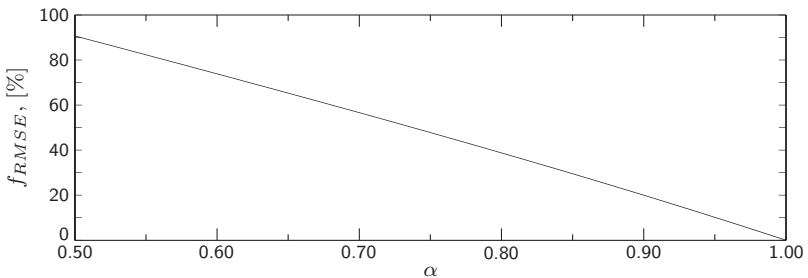


Figure 9.9: Resulting overall forecast error magnitude f_{RMSE} for different weighting factors $\alpha \in [0.50, 0.51, \dots, 1.00]$.

same $\beta_{usg}(t)$ was applied as before (figure 9.3). If $\beta_{usg}(t)$ would be determined for particular forecast error magnitudes, the factor would not anymore only represent the efficiency as depicted in figure 7.4; $\beta_{usg}(t)$ would also depend on forecast error effects, most probably distorting the true results. Consequently, the same dynamic usage factor is applied for all forecast errors, guaranteeing a fair comparison. The resulting EIF is displayed in figure 9.10, showing the influence of the forecast error. Further associated results are summarised in table 9.3.

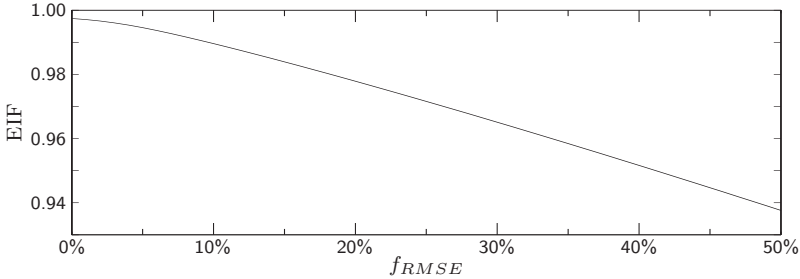


Figure 9.10: EIF for $E_{st} = 100$ kWh and different f_{RMSE} .

Figure 9.10 illustrates how the fulfilment index decreases with an increasing forecast error. At the same time, both surplus and insufficient energy are significantly increasing, as indicated by table 9.3. Besides, the growing forecast error results in more demand from the energy storage device, which is obviously not able to meet this requirement: the decreasing conversion energy indicates a reduced utilisation of the storage. This occurs usually because the storage device cannot be operated anymore, which is the case if it is either fully charged or discharged. The

f_{RMSE}		0%	10%	20%	30%	40%	50%
$E_{planned}$	[MWh]	2'590	2'586	2'589	2'591	2'593	2'595
E_{actual}	[MWh]	2'589	2'591	2'593	2'596	2'598	2'560
E_{conv}	[kWh]	51'428	49'448	46'997	44'763	42'702	40'874
E_{splus}	[kWh]	5'598	31'391	61'810	94'664	129'960	166'849
E_{insuff}	[kWh]	6'697	26'934	57'314	90'466	125'439	161'884
$\emptyset E_{st,ch}(t)$	[kWh]	46.33	40.03	40.40	41.17	41.81	42.34
$\emptyset \beta_{usg}(t)$		0.9790	0.9753	0.9758	0.9765	0.9770	0.9775
EIF		0.9974	0.9896	0.9779	0.9651	0.9516	0.9376

Table 9.3: Simulation results for $E_{st} = 100$ kWh and different f_{RMSE} .

charge level duration curve, displayed in figure 9.11, confirms this interpretation. Charge level duration curves have already been mentioned to be useful for analysing the system's capability of appropriately utilising the energy storage device. The charge level should be equally distributed if – as it is the case here – no particular control algorithm is applied; the duration curve should linearly decrease from the maximum to the minimum charge level, indicating an even use at all levels.

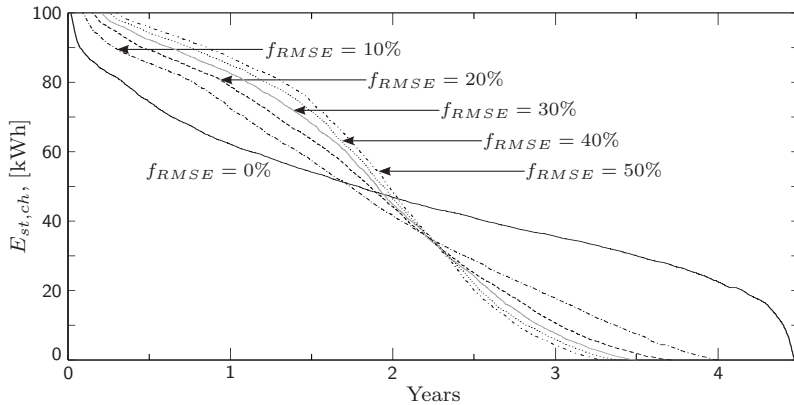


Figure 9.11: Charge level duration curve for $E_{st} = 100$ kWh and different f_{RMSE} , covering the total data length of 4.5 years.

The duration curve illustrates the increasing durations with fully charged or discharged storage device for growing f_{RMSE} . With a forecast error magnitude of $f_{RMSE} = 50\%$, the storage device is at either the lower or upper limit during totally 547 days, i.e. 1.5 years. In other words, during a third of the total simulation duration, the storage device cannot be disposed as desired, because its charge level is at the limits. This, in turn, results in fewer operations with the storage and in the decreasing amount of conversion energy, shown in table 9.3. Consequently, the storage device's energy capacity $E_{st} = 100$ kWh is too small to be of proper use with increased forecast error magnitudes.

Figure 9.10 shows a flatter decline in the EIF for small f_{RMSE} . This fact can be understood as an indicator that the system is capable of achieving a high infeed fulfilment with $E_{st} = 100$ kWh and $f_{RMSE} \lesssim 5\%$. This finding is confirmed with the duration curves in figure 9.11, indicating $E_{st} = 100$ kWh to be the appropriate size for a system with a forecast error somewhere between 0% and 10%.

f_{RMSE}		0%	10%	20%	30%	40%	50%
Min E_{st}	[kWh]	56	104	245	475	1'174	1'652
$E_{planned}$	[MWh]	2'595	2'586	2'577	2'576	2'579	2'570
E_{actual}	[MWh]	2'593	2'591	2'584	2'574	2'557	2'545
E_{conv}	[kWh]	47'406	49'742	56'413	66'553	82'667	94'660
E_{spplus}	[kWh]	23'548	30'280	32'194	23'402	3'918	1'187
E_{insuff}	[kWh]	25'152	25'818	25'701	25'687	27'784	25'697
$\emptyset E_{st, ch}(t)$	[kWh]	23.5	41.7	98.7	173.9	293.0	396.0
$\emptyset \beta_{usg}(t)$		0.9817	0.9750	0.9655	0.9571	0.9439	0.9275

Table 9.4: Minimum required E_{st} to achieve an $EIF \geq 0.99$.

The investigations so far have demonstrated that the forecast error has an influence on the overall system performance and that the base configuration with $E_{st} = 100$ kWh is not sufficient to be beneficially used with increasing forecast errors. The following investigation hence analyses the minimum required E_{st} in order to achieve an $EIF \geq 0.99$. In other words, during the 4.5 years covered in the simulation, the actual infeed amount is accepted to be below the planned infeed amount by 1%. The simulation results are compiled in table 9.4 and should be put in relation to the total generation $E_{gen} = 2'640'362$ kWh.

The table shows significantly increased minimum required energy capacities for growing forecast errors. With the energy capacity, also the conversion losses E_{conv} increase; in order to achieve the aimed for fulfilment ≥ 0.99 , the storage device has to be utilised more often. The large capacities required for forecast errors $f_{RMSE} \geq 40\%$ result in almost no surplus energy, as the storage obviously is capable of absorbing most of the generation exceeding the planned infeed.

A larger E_{st} offers a wider spectrum for usage factors, as discussed in the context of defining $\beta_{usg}(t)$ in figure 9.3. According to table 9.4, the average charge level is approximately a third of the respective rated energy capacities. Consequently, the average usage factors decrease with increasing f_{RMSE} , as shown in the table.

Concluding, the charge level duration curves are displayed again, for the different forecast errors and the respective calculated minimum energy capacities (according to table 9.4). Figure 9.12 shows rather linear duration curves for forecast errors up to 30%. The duration curves corresponding to forecast errors of 40% and 50%, however, show an interesting behaviour: the storage device is comparatively seldom fully charged. Obviously, the large capacity is necessary to meet $EIF \geq 0.99$,

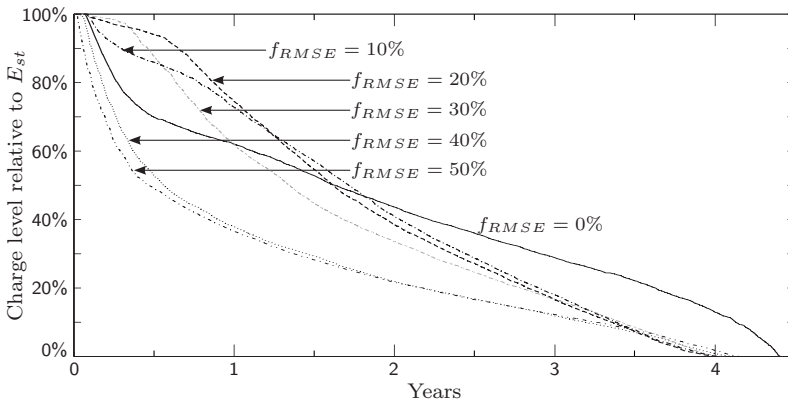


Figure 9.12: Charge level duration curve for the minimum required E_{st} , depending on f_{RMSE} as defined in table 9.4, covering the total data length of 4.5 years.

but only because of relatively few extreme events. If the required fulfilment index would be set to $EIF \geq 0.985$, the required capacity would decrease to 1'246 kWh in the case of $f_{RMSE} = 50\%$ and to 812 kWh in the case of $f_{RMSE} = 40\%$.

To identify the improvements stemming from using an energy storage device, simulations were performed without incorporating storage at all. In other words, the usage factor was set to $\beta_{usg} = 1$ and the storage capacity to 0 kWh. The key results are displayed in table 9.5.

f_{RMSE}		0%	10%	20%	30%	40%	50%
E_{splus}	[kWh]	247'726	258'446	276'555	299'079	324'877	353'456
E_{insuff}	[kWh]	247'727	258'367	276'393	298'827	324'524	352'955
EIF		0.9062	0.9021	0.8953	0.8868	0.8771	0.8663

Table 9.5: Simulation results without energy storage device.

Comparing these results with the values in table 9.4 indicates large quantities of surplus and insufficient energy. This is reflected as well in the fulfilment index, being around 90% and less, with increasing forecast error magnitude. While the presence of the energy storage device results in a significant amount of energy lost for conversion processes, it nevertheless increases the amount of energy to be fed into the network as planned. Comparing the deviations and conversion losses, shows

that in the perfect forecast case, additional 446'753 kWh can be fed into the network as planned and not as surplus or insufficient energy. This amount increases to 679'527 kWh for $f_{RMSE} = 50\%$. These numbers can be considered as the benefit, stemming from the utilisation of the energy storage device. Without a storage, these amounts of energy would have resulted in overshoots and undershoots compared to the planned infeed, possibly even resulting in balancing penalties.

9.2.5 Case study summary

The simulations performed with the 500 kW PV system showed both the applicability of the proposed algorithms and their usefulness for investigating the possibilities of beneficially operating an energy storage device.

The major finding is that it is possible to use an energy storage device to transform the non-deterministic output into a determinist network infeed with a high reliability of success. For small forecast errors, already energy capacities around 100 kWh lead to significant improvements. If the forecast error magnitudes increase beyond 40%, the energy storage device must however be capable of storing more than two hours of production from the PV system, i.e. more than 1'000 kWh. Despite the overall efficiency of 81% of the energy storage device, the total system losses sum up to only approximately 2% to 4%, depending on f_{RMSE} . The reason is that most energy is fed directly into the network, with the infeed plan being based on a forecast for the energy source.

As a comparison, the battery energy storage system (BESS) at the Golden Valley Electric Association in Alaska is capable of providing 27 MW during 15 min or 46 MW during 5 min [51, 52]. For this purpose, the BESS consists of 13'760 Ni-Cd batteries, with a total capacity of 3680 Ah at the nominal voltage of 5000 V. Comparing with these values shows that an energy capacity in the range of a few 100 kWh could be achieved with a comparatively small battery cluster. In order to reduce the required energy capacity of the storage device, it is important to incorporate the energy storage's charge level into the planning process. The benefits of doing so have been demonstrated with several investigations throughout the case study.

Further discussions concerning the value of the energy storage device can be found in chapter 10.

9.3 Wind-Turbine System

This case study applies the developed algorithm and analysis procedures to a measurement series from a wind speed measurement site in Norway. In contrast to the first case study, the influence of a time-dependent forecast error and the impact of different forecast horizons are analysed. Most algorithm related aspects, like definition of the usage factor or differences between constant and dynamic usage factor, have already been discussed in the first case study. This second case study therefore focuses on the identification of the storage requirements for this particular measurement series, only discussing specific wind related algorithm issues.

9.3.1 Characteristics of the time series and definition of the simulation parameters

The measurement series stems from a wind speed measurement site in northern Norway. The series covers one year of measurements, consisting of 10 min measurement intervals, i.e. the data series contains 52'560 entries. The measurements concern the energy source, which is why it is necessary to transform the wind speed values into the appropriate power output values of the wind turbine. For this purpose, a wind turbine was simulated, corresponding to a state-of-the-art model with a rated power output of $P_{rated} = 2$ MW. A model of this size is offered by most manufacturers with hysteresis characteristics similar to the ones applied here: cut-in wind speed $v_{cin} = 4$ m/s, cut-out wind speed $v_{cout} = 25$ m/s, cut-back-in wind speed $v_{cbin} = 22$ m/s and the hysteresis duration $t_{cbin} = 10$ min.

Besides the hysteresis characteristics, the wind turbine is defined through its power curve, relating wind speed to power output [39]. The implemented power curve is depicted in figure 9.13, equivalent to the power curve of a state-of-the-art wind turbine. The cut-out limit results in zero output for wind speeds exceeding $v_{cout} = 25$ m/s.

Prior to applying the power curve, however, the wind speed measurement must be adjusted to the height of the wind turbine's hub [39]. Wind speed measurements are usually taken some 10 to 20 m above ground. As wind speed increases with increasing height above ground, the measurement values have to be adjusted to match the height of the

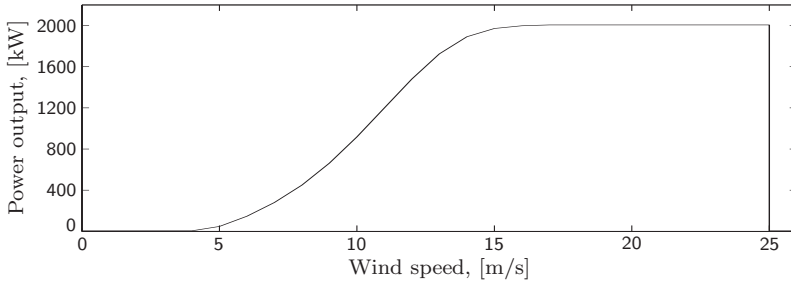


Figure 9.13: Power curve of the wind turbine, transforming the wind speed into the turbine’s output power.

turbine’s hub. The underlying measurements were taken at $h_{meas} = 20$ m and the turbine is defined to have its hub at $h_{hub} = 100$ m above ground. The terrain of this particular measurement site is rather flat, which is represented with a roughness factor of $z_0 = 0.03$ m [39]. The relation between the measured speed $v_{h_{meas}}$ at height h_{meas} and the speed $v_{h_{hub}}$ at hub height h_{hub} can be approximated as follows [39]:

$$v_{h_{hub}} = v_{h_{meas}} \cdot \frac{\log\left(\frac{h_{hub}}{z_0}\right)}{\log\left(\frac{h_{meas}}{z_0}\right)} \quad (9.2)$$

The translation of the height-adjusted wind speed into the corresponding power output is then achieved by applying the power curve of the wind turbine, displayed in figure 9.13.

9.3.2 Determination of energy and power capacity

As in the first case study, the initial simulation is meant for defining a base configuration. Charge and discharge efficiency of the storage device are both set to $\eta_{ch} = \eta_{dch} = 0.9$ and the minimum energy capacity is defined as $E_{st,min} = 0$ kWh. To identify suitable values for power rating and energy capacity, a simulation is run with energy capacities, varying from 100 kWh to 2000 kWh in steps of 100 kWh, and power ratings, varying from 100 kW to 2000 kW in 100 kW steps. The parameters were chosen larger than in the first case study, displayed in figure 9.1, because of the larger rating of the wind turbine, being 4 times higher

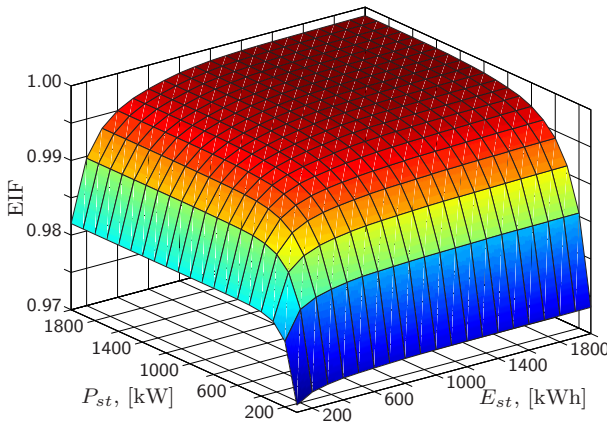


Figure 9.14: Energy index EIF for $E_{st} \in [100, 200, \dots, 2000]$ kWh and $P_{st} \in [100, 200, \dots, 2000]$ kW with $f_{RMSE} = 0\%$.

with its power output of 2 MW. Prior to this simulation, the optimal usage factor β_{usg} had to be identified as well. The optimal factor is again defined as the factor reducing both the sum and the differences of surplus and insufficient energy. The resulting fulfilment is displayed in figure 9.14, calculated with a constant β_{usg} .

According to figure 9.14, in this case study the power rating P_{st} is the limiting parameter rather than the energy capacity E_{st} . For storage device characteristics of $E_{st} \gtrsim 800$ kWh and $P_{st} \gtrsim 1'000$ kW, the fulfilment index does not anymore change significantly. Obviously, the power demand from the storage is often above approximately 1'000 kW; with a power rating smaller than that, the demand can only be partly satisfied (equation (7.12)), resulting in insufficient energy and thus a decreased fulfilment. Figure 7.3 showed that already small time differences of the predicted wind speed near the cut-out velocity v_{cout} can result in a power demand equal to the rated power of the wind turbine, i.e. equal to 2 MW.

On the other hand, a power demand from the storage device of e.g. 1'000 kW during one time interval, requires the amount of 185 kWh to be stored in the energy storage device, considering the discharge efficiency. Because of such considerable amounts of energy, an energy capacity of $E_{st} \approx 800$ kWh is required in order to operate with a reasonable EIF, according to figure 9.14. The base configuration was therefore

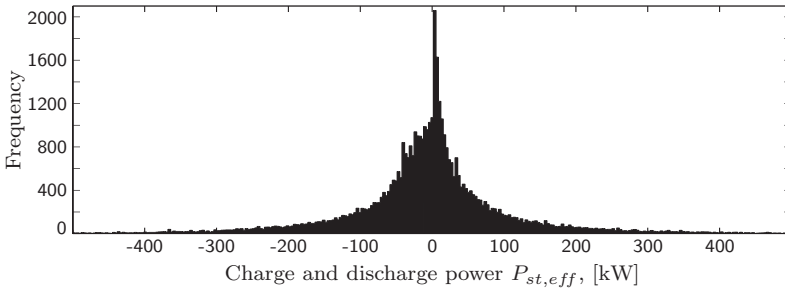


Figure 9.15: Histogram of charge and discharge power flows for a storage device with $P_{st} = 2'000$ kW and $E_{st} = 800$ kWh.

chosen with $E_{st} = 800$ kWh and $P_{st} = 2'000$ kW, corresponding to the rating of the wind turbine.

The charge and discharge power flows at the storage interface are displayed in figure 9.15 for the base configuration, this time applying a dynamic usage factor. The histogram shows most activities to have power magnitudes within ± 400 kW. Furthermore, similar to the PV case study, the power demand is significantly lower than the rated capacity of the generator. The data series in this case study covers only 1 year and consists of 6 measurements per hour. This explains the differently scaled ordinate, compared with the first case study.

It is important to note that the measured values represent average wind velocities during 10 min intervals. The fluctuations within these intervals might be fairly strong and would also have to be balanced with the energy storage. Thus, with higher resolved data, representing these fluctuations more accurately, the conversion losses can be expected to be larger than with 10 min intervals.

9.3.3 Simulations with a perfect forecast

This section discusses the results from simulations where the forecast is assumed to be perfect. As mentioned, these results represent the ideal case and serve as reference values for analyses with imperfect forecasts. Section 9.2 demonstrated the advantages when applying a dynamic usage factor. All subsequent simulations are therefore exclusively applying dynamic usage factors. Figure 9.16 is only used to demonstrate that ap-

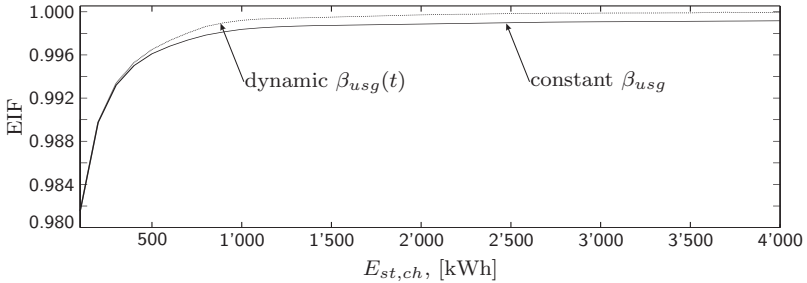


Figure 9.16: EIF for different energy capacities E_{st} and both constant and dynamic usage factors.

plying a dynamic usage factor, instead of a constant usage factor, leads to similar improvements as in the PV case study. It is interesting, however, to note that the dynamic usage factor $\beta_{usg}(t)$ has an influence for energy capacities above 500 kWh only. Below this capacity, the charge margin is obviously too small to be beneficially used by adapting the usage factor. Table 9.6 summarises the results from a simulation with a perfect forecast, applying a dynamic usage factor.

A perfect forecast corresponds to the hourly mean values of the actual generation. In this context, the storage device is only used to balance the differences between the hourly constant infeed profile and the varying output of the generator. This results in high fulfilment index values. Nevertheless, more than 1% of the total generation is consumed for conversions in the storage device. Figures 9.20 and 9.21 show that,

	$f_h = 6$ h		$f_h = 12$ h		$f_h = 24$ h	
	[kWh]	[%]	[kWh]	[%]	[kWh]	[%]
E_{gen}	5'699'634	100.00	5'699'634	100.00	5'699'634	100.00
$E_{planned}$	5'618'264	98.57	5'630'164	98.78	5'629'768	98.77
E_{actual}	5'621'264	98.63	5'628'241	98.75	5'629'014	98.76
E_{conv}	77'944	1.37	70'853	1.24	70'063	1.23
E_{splus}	8'789	0.15	2'181	0.04	5'686	0.10
E_{insuff}	5'789	0.10	4'104	0.07	6'440	0.11
$\varnothing\beta_{usg}$	0.9788		0.9839		0.9856	
EIF	0.9989		0.9993		0.9989	

Table 9.6: Results for the base configuration simulation with perfect forecast and dynamic usage factor.

compared with the PV case study, the storage device is used more or less constantly. This is one reason for the significantly higher amount of lost energy E_{conv} . Another reason is the higher rating of the generator of $P_{rated} = 2$ MW: a mismatch between forecasted and actual generation requires accordingly more power and energy from the storage device. The presence of the energy storage device, however, results in an accurately matching infeed, as indicated by the high fulfilment and the insignificant amounts of E_{splus} and E_{insuff} . The shorter planning horizons with $f_h = 6$ h and $f_h = 12$ h result in more conversion losses, as the system can better react to changing charge levels.

When comparing results from table 9.6 with results from the base configuration analysis of the PV case study, summarised in table 9.1, it is important to consider the mentioned differences between the generators' power ratings and between the length of the data series. The same holds true when comparing the results from simulations with imperfect forecasts, discussed in the following section.

9.3.4 Simulations with an imperfect forecast

Following to the procedures discussed in chapter 7, prior to the calculation of a forecast series, the appropriate weighting factor α has to be determined. This case study is based on measurement data for the energy source, which is why the procedures from section 7.3.2 are applied. For the underlying measurement data, it was identified to be appropriate to use the measurements for the actual day and the preceding day to be applied with the EWMA approach. The forecast for period n is thus calculated as follows, according to equation (7.3):

$$\vec{V}_{fc,n} = \alpha \cdot \vec{V}_n + (1 - \alpha) \cdot \vec{V}_{n-1} \quad (9.3)$$

Similar to the first case study, this equation is applied to calculate forecast series with varying $\alpha \in [0.00, 0.01, \dots, 1.00]$. To determine the corresponding forecast error, the resulting wind speed curves $\mathbf{V}_{fc}(\alpha)$ have to be translated into power output series, according to the power curve of the wind turbine (figure 9.13). These output power forecasts $\mathbf{P}_{fc}(\alpha)$ are then used together with the original power output curve (which is determined by applying the power curve to the original measurement data) to calculate the corresponding RMSE, according to equation (7.1). The resulting relation between α and f_{RMSE} is displayed in figure 9.17.

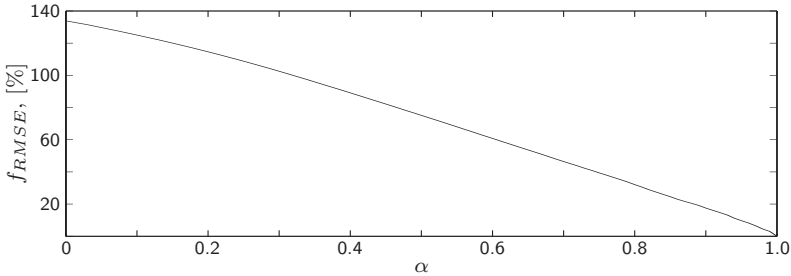


Figure 9.17: Resulting forecast errors f_{RMSE} for different weighting factors $\alpha \in [0.00, 0.01, \dots, 1.00]$.

Choosing $\alpha = 0$ results in an $f_{RMSE} \approx 134\%$ between the original and the forecasted generator output. Looking at equation (9.3), shows that this case corresponds to a forecast, applying the persistence method, as discussed at the end of section 7.3. In other words, applying persistence as forecast technique for the underlying measurement series, results in an average error of 134%. The corresponding analysis done for the PV case study and displayed in figure 9.9, showed a slightly different relation: a value of $\alpha = 0.5$ resulted in forecast errors around 90%. The reason for this is the larger number of preceding days, considered for forecasting in the PV case study, resulting in a forecast, being the sum of 8 exponentially weighted periods.

While the first case study investigated the influence of constant forecast error magnitudes, this second case study analyses the influence of time dependent forecast errors, as discussed in section 7.3.3. Following the reasoning of that section, the forecast error increases, the further the forecasted period lies in the future. A relation between forecast horizon t_h and forecast error $f_{RMSE}(t_h)$ was found and compiled as discussed in the context of equation (7.4), based on [41, 46]:

$$f_{RMSE}(t_h) = 24 + (t_h - 1) \frac{8}{35}, \quad [\%] \quad (9.4)$$

Based on studies, concerning potential balancing penalty savings [38, 53], it was decided to investigate the implications of three different forecast horizons with $f_h = 6$ h, $f_h = 12$ h and $f_h = 24$ h. According to equation (9.4), the actual forecast for one period (6, 12 or 24 h) is a compilation of forecast curves with increasing forecast errors, as

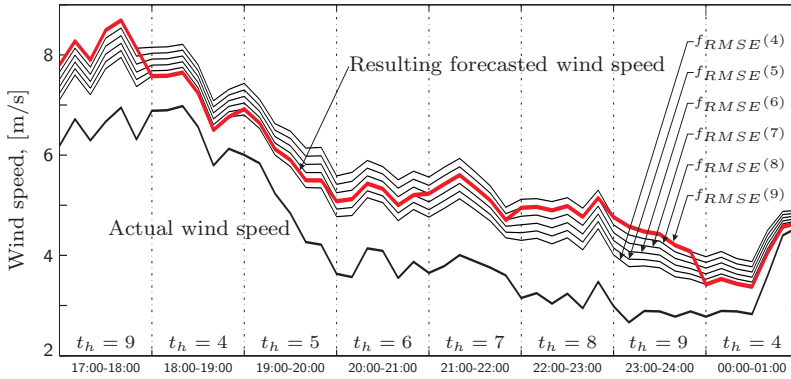


Figure 9.18: Compilation of a wind speed forecast with $f_h = 6$ h from constant forecast curves with different f_{RMSE} .

outlined in equation (7.5). As discussed in section 7.3, it is assumed that the forecast takes place in advance, exactly in the middle of the preceding period. That means a forecast with a horizon of $f_h = 6$ h is performed 3 h in advance. Thus, the first hour in a 6 h forecast corresponds to the fourth hour in equation (9.4) with $f_{RMSE}(t_h = 4) = 24.7\%$, which in turn corresponds to $\alpha = 0.8491$ (see figure 9.17). The previous day consequently is weighted with approximately 15.1% for the wind speed forecast simulation. The forecast series for the second hour uses $\alpha = 0.8477$, corresponding to $f_{RMSE}(t_h = 5) = 24.9\%$. For the second hour, the previous days' wind speed is thus weighted slightly more, with roughly 15.2%, leading to an overall increased RMSE. Hour by hour the forecast can be assembled like this, with an increasing f_{RMSE} and corresponding α . This procedure is illustrated in figure 9.18. Every sixth hour, the forecasted wind speed gets closer again to the actual generation, reflecting the smaller RMSE at the beginning of the next forecast. The reason for all forecast curves to be above the actual curve is the wind speed being higher the previous day at the same time. Following the modelling procedure, the resulting wind speed forecast is translated into the forecast for the power output of the turbine, used in turn to define the infeed for the next period.

Comparing the different forecast horizons means comparing different forecast error ranges. In the case of a 6 h forecast, the last hour of the forecasted period corresponds to the 9th hour in equation (9.4). The

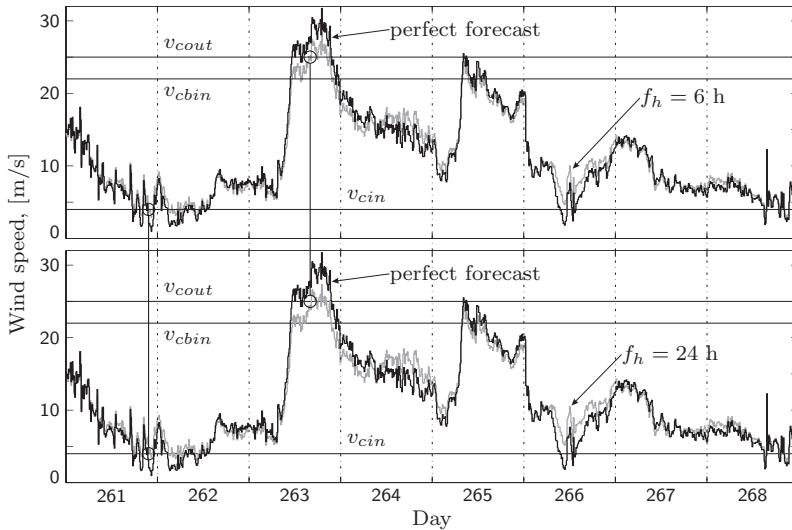


Figure 9.19: Forecasted ($f_h = 6$ h and $f_h = 24$ h) and actual wind speed on days 261 to 268, corresponding to figures 9.20 and 9.21.

forecast error magnitude thus evolves from 24.7% to 25.8%. With the forecast covering $f_h = 24$ h, the error evolves from 26.7% to 32% in the 36th hour. Compared with the PV case study, the differences thus are relatively small in terms of the forecast error magnitude. Figure 9.19 shows a comparison of forecasts with $f_h = 6$ h and $f_h = 24$ h. The differences between both forecasts are small but visible nevertheless. The two marked cases show events, where the forecast with $f_h = 6$ h compared with $f_h = 24$ h first goes beyond v_{cin} and then later-on also crosses the cut-out wind speed v_{cout} first.

Similar to figures 9.4 and 9.5, the following two pages contain excerpts from the simulation, this time showing the influence of the different forecast horizons. Figure 9.20 on the left shows the situation with a forecast horizon of $f_h = 6$ h and figure 9.21 the case with $f_h = 24$ h, on the right hand. Looking at the planned infeed $\mathbf{P}_{planned}$ indicates how the shorter periods on the left allow to better adjust the infeed, actually rather to the storage level than to the forecasted generation. The forecasted generator output on day 264 is similar with both forecasts, but the shorter planning period allows to faster react to mismatches between forecasted and actual generation, utilising the storage accordingly.

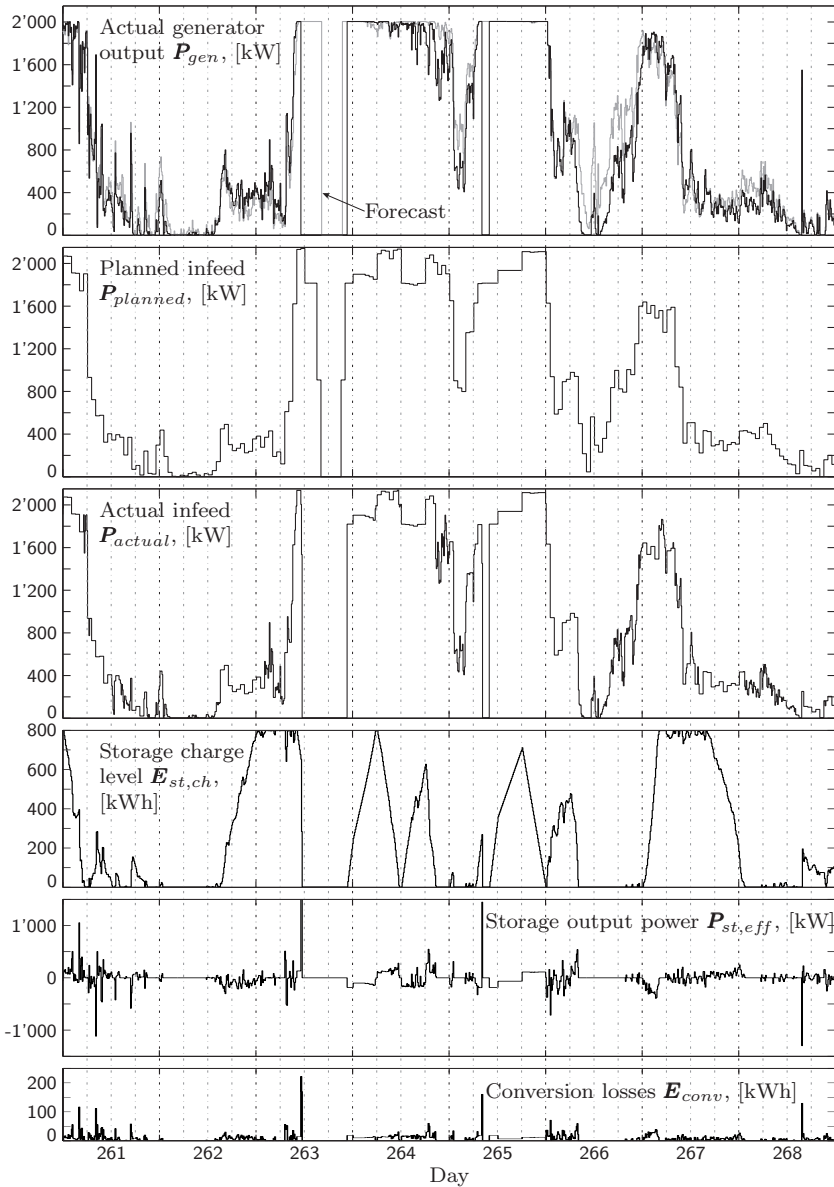


Figure 9.20: Days 261 to 268 from a simulation with the wind system base configuration with $E_{st} = 800$ kWh and $f_h = 6$ h.

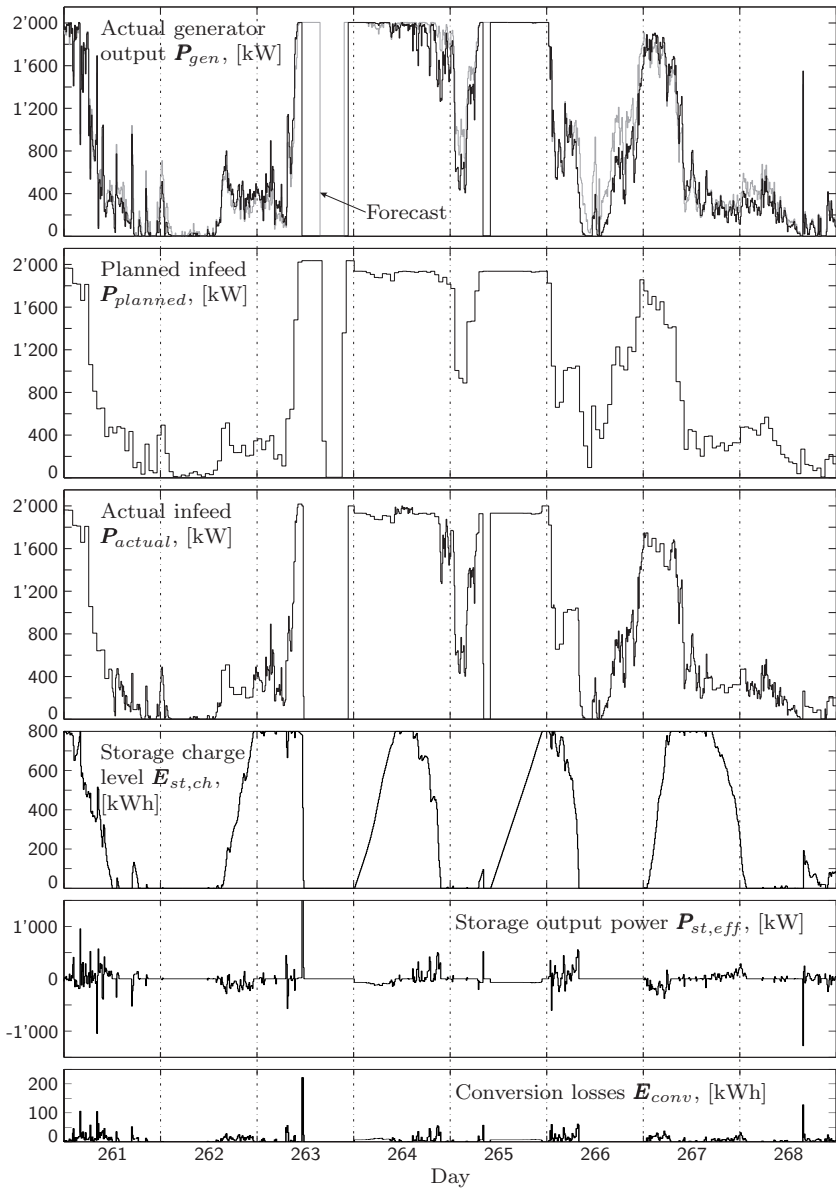


Figure 9.21: Days 261 to 268 from a simulation with the wind system base configuration with $E_{st} = 800$ kWh and $f_h = 24$ h.

Because of the shorter period, the storage device is faster recharged, due to a lower planned infeed from 00:00 to 06:00 on day 264. The second 6 h period on the same day consequently is planned with a higher infeed, according to the fully charged storage. The storage charge level plots confirm this behaviour as well. With the longer forecast horizon, the storage cannot be cycled as much, resulting in many incidents with full or empty storage device. This, in turn, results in less conversion energy consumed, compared with the case with $f_h = 6$ h.

The wrongly forecasted transition across the cut-out wind speed v_{cout} during day 263 (see also figure 9.19) also shows how comparatively small a capacity of $E_{st} = 800$ kWh is. In both figures, the storage device is almost immediately discharged, with a power demand of 2000 kW during 10 min requiring 370 kWh, i.e. almost half of the charged energy.

Table 9.7 shows the results from both simulations together with those from a simulation with $f_h = 12$ h. The table confirms some of the above made observations and displays some interesting results. First of all, the observation concerning the decreasing amount of conversion energy E_{conv} is confirmed. Often, the energy storage device is at the upper or lower limit and cannot be used further. With the shorter forecast horizon, the infeed plan can accordingly be adjusted, resulting however in more lost energy. Considering again how fast the energy storage device is discharged in case of prediction errors also indicates a inappropriate capacity E_{st} ; obviously the energy capacities are insufficient for cases with forecasts. The charge level duration curve, displayed in figure 9.22, confirms this finding. As duration curves have been dis-

	$f_h = 6$ h		$f_h = 12$ h		$f_h = 24$ h	
	[kWh]	[%]	[kWh]	[%]	[kWh]	[%]
E_{gen}	5'699'634	100.00	5'699'634	100.00	5'699'634	100.00
$E_{planned}$	5'737'078	100.66	5'738'839	100.69	5'738'818	100.67
E_{actual}	5'630'394	98.76	5'641'627	98.98	5'647'184	99.08
E_{conv}	68'713	1.21	57'593	1.01	51'877	0.91
E_{splus}	153'086	2.69	215'578	3.78	294'928	5.17
E_{insuff}	259'769	4.56	312'789	5.49	386'562	6.78
f_{RMSE} range	24.7%-25.8%		25.4%-27.9%		26.7%-32.0%	
$\varnothing\beta_{usg}$	0.9923		0.9923		0.9922	
EIF	0.9574		0.9455		0.9326	

Table 9.7: Simulation results for the base configuration, applying the forecast function from (9.4).

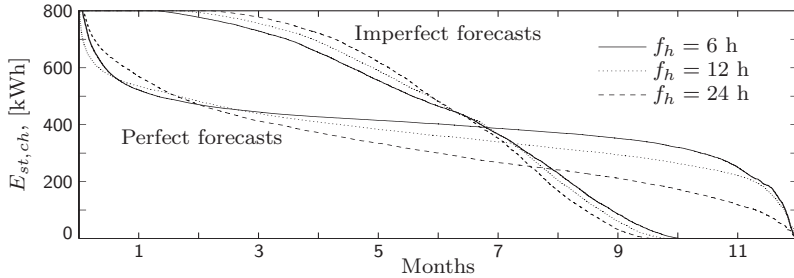


Figure 9.22: Charge level duration curves for perfect and imperfect forecasts and different forecast horizons, base configuration.

cussed thoroughly in the previous case study, the figure is only displayed here to confirm the interpretation of the decreasing conversion losses.

The most interesting observation, however, is the planned infeed exceeding the actual generation. This behaviour results from the usage factor β_{usg} obviously being chosen too high. The discrepancy between E_{splus} and E_{insuff} indicates non-optimal usage factors as well. A detailed analysis of the optimisation results and procedure however confirmed the optimisation to have one local minimum, which is found at all times. Hence, the usage factors are correct, but the large amounts of energy, required to be stored in or discharged from the energy storage device, cannot be handled by the system. For example, a discharged storage device will result in a lower infeed plan for the next period. This guarantees a certain amount of surplus generation, which can be used for charging the storage. Because of the often large power discrepancies between forecasted and actual generation, the storage device is probably sooner charged than expected, resulting in surplus network infeed. Nevertheless, at the beginning of the subsequent planning period, the storage device is fully charged and results in a comparatively high infeed profile. Most probably, similar to the charging, the storage device is also discharged too early, and a certain insufficient network infeed results. Days 263 and 264 in figures 9.20 and 9.21 illustrate this behaviour. The duration curves in figure 9.22 confirm this reasoning: with imperfect forecasts, the storage device is at either limit during approximately a quarter of the whole simulation.

Following the sequence of the first case study, the minimum required energy capacities are determined now, in order to achieve a fulfilment

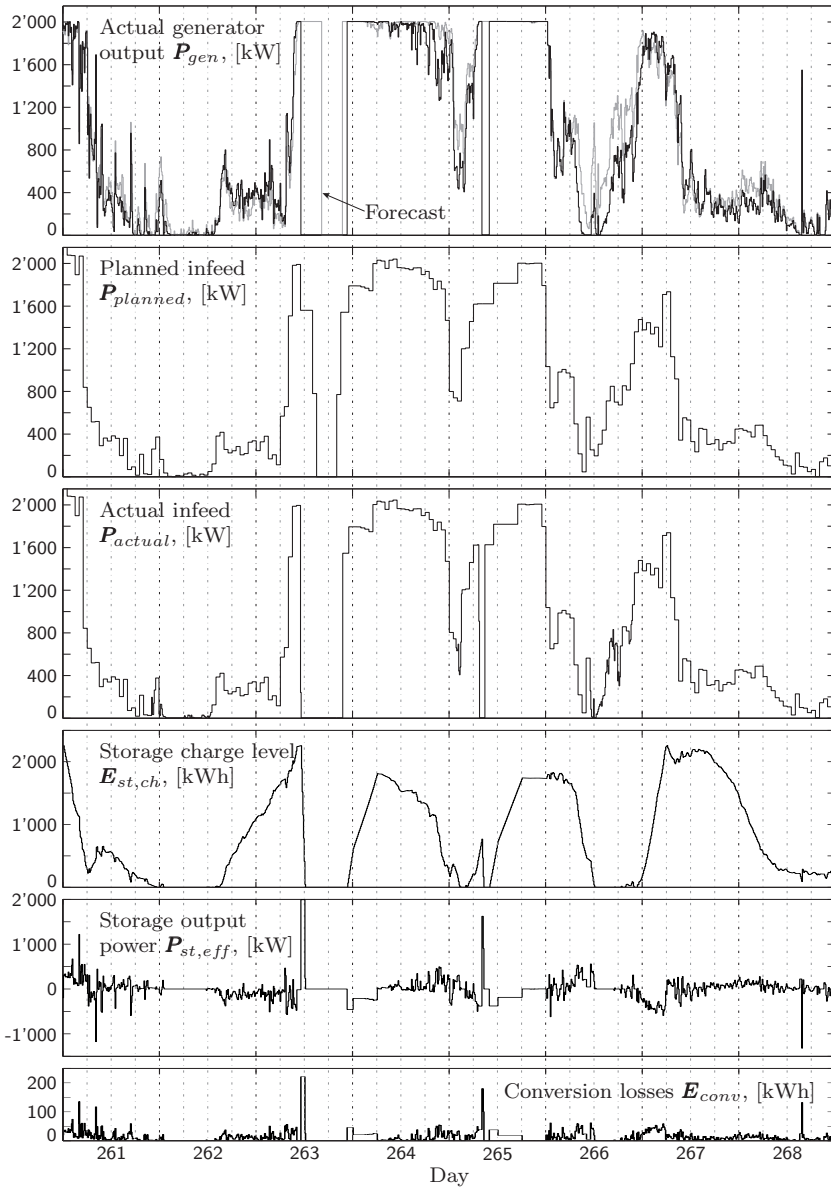


Figure 9.23: Days 261 to 268 from a simulation with the wind system base configuration with $E_{st} = 2'319$ kWh and $f_h = 6$ h.

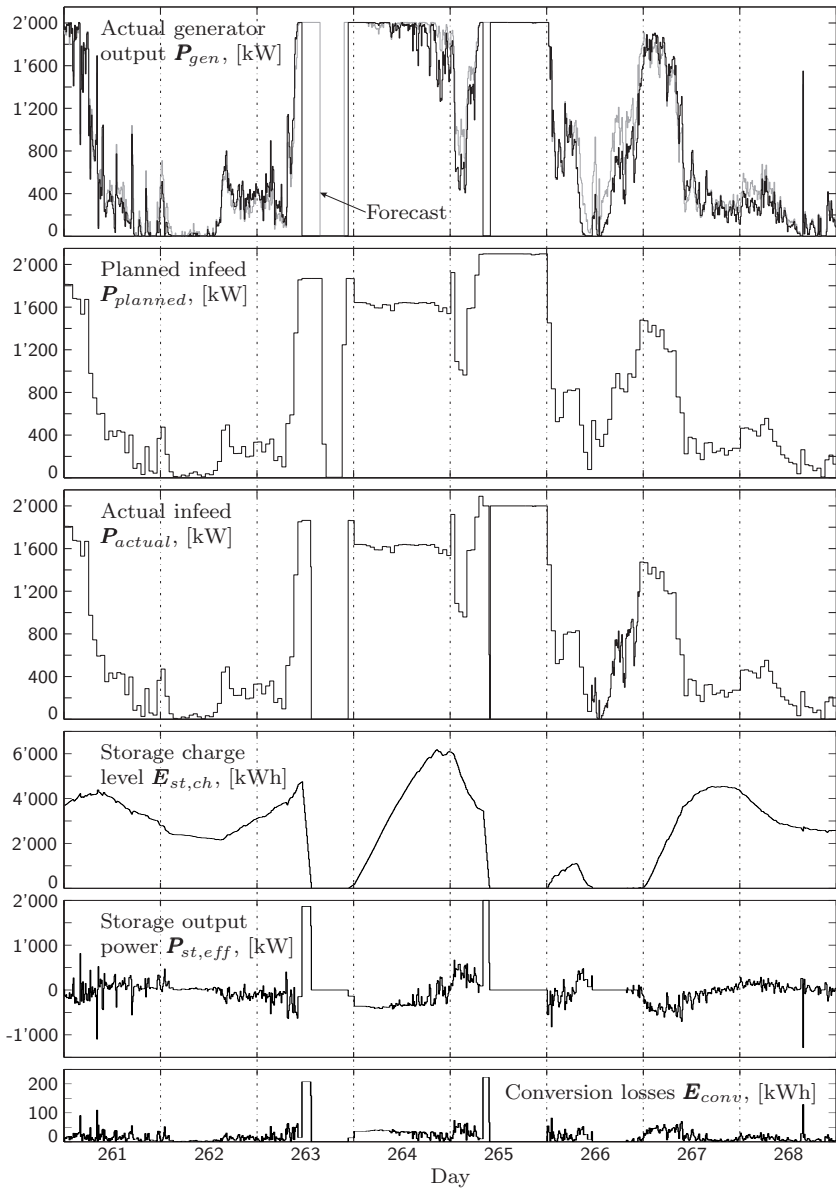


Figure 9.24: Days 261 to 268 from a simulation with the wind system base configuration with $E_{st} = 7'529$ kWh and $f_h = 24$ h.

	$f_h = 6$ h		$f_h = 12$ h		$f_h = 24$ h	
	[kWh]	[%]	[kWh]	[%]	[kWh]	[%]
Min E_{st}	2'319		4'232		7'529	
E_{gen}	5'699'634	100.00	5'699'634	100.00	5'699'634	100.00
$E_{planned}$	5'672'025	99.52	5661'727	99.33	5'643'194	99.01
E_{actual}	5'597'012	98.20	5'581'880	97.93	5'569'526	97.72
E_{conv}	100'801	1.77	115'049	2.02	124'123	2.18
E_{splus}	38'417	0.67	33'383	0.59	39'188	0.69
E_{insuff}	113'430	2.00	113'230	1.99	112'857	1.98
$\varnothing E_{st,ch}(t)$	1'316		2'359		4'151	
$\varnothing \beta_{usg}$	0.9783		0.9816		0.9785	

Table 9.8: Minimum required E_{st} to achieve $EIF \geq 0.98$.

index of $EIF \geq 0.98$. This target is chosen lower on purpose, to not result in infeasible capacities required. The results are given in table 9.8 and applied in figures 9.23 and 9.24. These figures show the same excerpts as figures 9.20 and 9.21, illustrating the different behaviour with the larger storage capacities. The actual infeed P_{actual} shows few deviations only from the planned infeed $P_{planned}$ in both cases. Furthermore, the storage output power shows how the not predicted supply outage on day 265 can almost be bridged in the case of $f_h = 24$ h. The storage charge levels also lack the cyclic behaviour, seen in figures 9.20 and 9.21; the available capacity seems to be appropriately used, in turn resulting in higher conversion losses.

Table 9.8 shows minimum required energy capacities that are significantly larger than in the first case study. As already discussed throughout this case study, the major reasons are the larger capacity of the turbine and the cut-out cut-back-in hysteresis, which does not exist in a similar form for photovoltaic installations. In other words, the risk of a sudden and total production outage, as it happens because of a gust with wind turbines, is non-existent in PV systems and consequently, the storage device seldom must take over the nominal output of the generator. Although the usage factors are optimised to balance surplus and insufficient energy, surplus energy is significantly smaller. The reason for this is the large amount of energy capacity available. In the case of $f_h = 24$ h, the capacity of $E_{st} = 7'529$ kWh represents a charge equivalent to 4 h rated generator output. This capacity is quite linearly utilised through the simulation duration, as indicated by the duration curves in figure 9.25, and surplus production hence mostly can be stored for later use and rarely must be fed into the network.

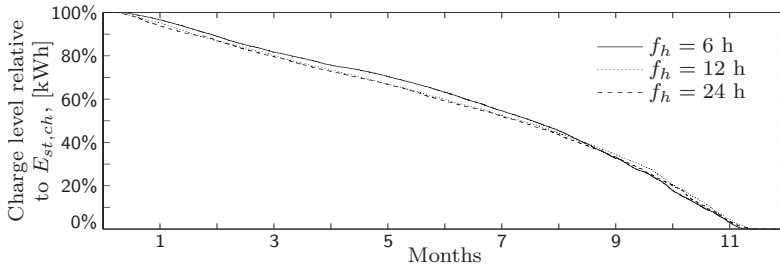


Figure 9.25: Charge level duration curves for the minimum required E_{st} , depending on f_{RMSE} as defined in table 9.8.

The duration curves indicate appropriately sized energy storage capacities, with the charge levels distributed evenly over a large period of the time. Nevertheless, during approximately 1 month, the storage device is at either limit. Despite this, each configuration is capable of reaching the aimed for fulfilment of 98%.

To provide reference values and to identify the benefits of the energy storage device, simulations were performed without an energy storage device. The forecast is calculated as before, used to determine an infeed profile, applying $\beta_{usg} = 1$ and $E_{st} = 0$ kWh. The positive differences between the planned infeed $\mathbf{P}_{planned}$ and the original generation \mathbf{P}_{gen} then correspond to E_{insuff} and the negative differences accordingly to E_{splus} . Table 9.9 lists the resulting values and fulfilment indices.

		$f_h = 6$ h	$f_h = 12$ h	$f_h = 24$ h
E_{splus}	[kWh]	473'731	493'170	535'833
E_{insuff}	[kWh]	543'508	568'345	616'323
EIF		0.9058	0.9016	0.8934

Table 9.9: Simulation results without energy storage device.

Closing, it is interesting to note how the large amounts of deviating energy, up to 535 MWh surplus and 616 MWh insufficient energy, can be reduced to less than a fifth by utilising an energy storage device, when comparing with table 9.8. Put differently, in the case of $f_h = 24$ h, the use of the energy storage device results in additional 1'000'111 kWh that are fed into the network as planned. This amount corresponds to the difference between the sum of surplus and insufficient energy

without storage and the sum of surplus and insufficient energy with storage. Hence, roughly 1'000 MWh of power can be sold as projected and do not anymore result in balancing penalties. With $f_h = 12$ h the equivalent amount is 915 MWh and with $f_h = 6$ h it adds up to 865 MWh. All in all, the presence of an energy storage device allows to reliably decrease the mismatch between planned and actual infeed by more than 10% of the original production.

9.3.5 Case study summary

The simulation performed with wind speed measurements, translated into the power output of a 2 MW wind turbine, proved the usability of the developed methods and algorithms. The simulation results show the feasibility of improving the network infeed by combining the wind turbine with an energy storage device.

The algorithm is useful for determining suitable energy capacities of the energy storage device. The resulting capacities, however, are comparatively large when looking at battery systems. Again comparing with the BESS of the Golden Valley Electric Association, identifies a battery of similar size when planning with 24 h horizons. In other words, combining a wind turbine with an energy storage device would improve the infeed quality significantly. The energy demand is however substantial and not feasible with today's battery technologies.

Looking at pumped hydro storage power plants however puts the energy capacities in a different relation. Thus, applying the concept of virtual power plants seems to be an option. Still, one idea of combining the renewables based generator with a storage was to avoid unpredicted line-loading. This effect would not be alleviated when applying the virtual power plant concept; this concept only allows to act on markets with a reduced risk of incurring balancing penalties.

Comparing the results for the three different forecast horizons leads to a similar conclusion as in [53]. There, the shorter forecast horizons were showed to result in significantly smaller sums of balancing penalties. In this study, the shorter forecast horizons show significant benefits as well. Comparing 6 h periods with 24 h periods identifies a considerable smaller required energy capacity and reduced conversion losses. Thus, for the overall system performance, a shorter forecast horizon would be advantageous.

The power market of the Nordic countries, Nordpool², recognised this disadvantage inherent to day-ahead markets and founded an intraday spot market, the so-called ELBAS. Participants in this market can trade power up to 1 h before physical delivery, allowing to accurately adjust their day-ahead profile. Analogously, the European Power Exchange (EEX)³ in Germany started an intraday market on September 25, 2006.

²<http://www.nordpool.com>

³<http://www.eex.com>

Chapter 10

Discussion and Conclusion

This chapter addresses several aspects, which have been mentioned or partly discussed throughout the previous chapters of this part of the thesis. First, an approach to determine the value of the energy storage device is discussed, followed by some thoughts on how to incorporate price signals into the analysis. Afterwards, the usefulness and the meaningfulness of results from time series analyses is outlined. The chapter closes with a short conclusion, summing up part II.

10.1 Value of the Energy Storage Device

So far, costs for the installation and operation of the energy storage device have not been discussed, nor have financial benefits stemming from the utilisation of the energy storage device. This section therefore outlines how the value of the energy storage device can be identified. The suggested procedure works for all types of non-dispatchable generators. However, with 1 MWh being the smallest traded unit on power markets, these concepts apply to wind turbines rather than photovoltaic installations, simply because of the power ratings.

One of the reasons for looking at combining a non-dispatchable generator with an energy storage device was the idea of reducing the risk of incurring balancing penalties due to wrongly predicted infeed profiles. In other words, the storage device should help to increase the infeed

accuracy from the non-dispatchable generator, resulting in fewer events with unexpected overshoots and undershoots; every MWh that is fed into the network as planned results in cost savings. Consequently, the reduction in expenditures for balancing penalties can be put in relation to the investment necessary for installing and operating the energy storage device. The investment is done once, whereas the operation of the storage results in cost reductions during several years. A basic cash flow analysis can thus be applied to determine the net present value of the energy storage device.

Let κ_{up} define the cost for up-regulation per MWh of insufficient infeed. Analogously, κ_{down} represents the cost or penalty for down-regulation per MWh of surplus energy. The amount of surplus energy, which would be fed into the network without an energy storage device, is designated as $E_{splus,ns}$. The amount of insufficient energy accordingly $E_{insuff,ns}$. With the storage device present, the surplus infeed is designated as $E_{splus,ws}$ and the insufficient infeed as $E_{insuff,ws}$. The operation of the energy storage device results in both savings in surplus energy ΔE_{splus} and savings in insufficient energy ΔE_{insuff} , defined as:

$$\begin{aligned}\Delta E_{splus} &= E_{splus,ns} - E_{splus,ws} \\ \Delta E_{insuff} &= E_{insuff,ns} - E_{insuff,ws}\end{aligned}\quad (10.1)$$

With all energy values expressed in [MWh], the amount of saved costs π can now be calculated as follows:

$$\pi = \kappa_{down} \cdot \Delta E_{splus} + \kappa_{up} \cdot \Delta E_{insuff}\quad (10.2)$$

The first term represents costs saved because of a smaller amount of surplus infeed, requiring down regulation. Analogously, the second term represents the cost saved because of fewer periods, with the actual infeed falling short of the planned infeed, which would have otherwise resulted in cost for up regulation.

Figures 10.1 and 10.2 contain values from tables 9.4 and 9.5 as well as 9.8 and 9.9. The figures show the evolvement of surplus and insufficient energy both with and without energy storage. The applied energy capacities correspond to those which have been determined required for $EIF \geq 0.99$ in the PV case and for $EIF \geq 0.98$ in the wind case.

Figure 10.1 displays the results from the PV case study. These values have to be understood to cover the savings in surplus and insufficient

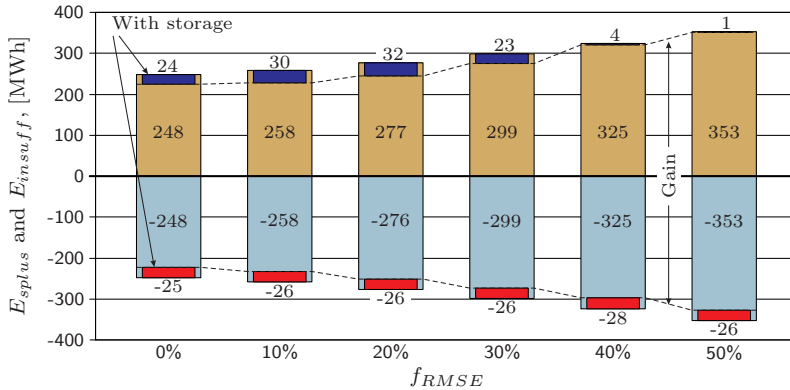


Figure 10.1: Surplus and insufficient energy with and without storage device; PV case study, according to tables 9.4 and 9.5.

energy over a period of 4.5 years. The annual contribution is thus modest. The gain, i.e. the increased amount that is infed as planned, is visible to increase with an increasing forecast error. The results from the wind case study are displayed in figure 10.2 and only represent one year, showing considerable savings of up to 1 GWh. Again, the amount of energy that is fed into the network as planned, increases with increasing forecast horizon. For both cases, the surplus energy is diminishing as the larger energy capacities can absorb most of the surplus generation.

The investment for an energy storage device depends both on the technology but moreover on the installed energy capacity and power rating. With different new storage technologies emerging and maturing, it is difficult to assume certain costs. Nevertheless, the approach in equation (10.2) can be applied to determine the potential savings over a certain amount of years. If these discounted savings outnumber the investment cost, the net present value of the energy storage investment is positive and the investment considered profitable. In other words, this approach allows to define what the investment can cost at maximum.

Equation (10.2) is however only a simple and rough approximation. Depending on the market, the penalties are differently handled [53, 54], as also visible on the homepage of the Nordic power market Nordpool¹. There are occasions where surplus or insufficient infeed is not penalised

¹<http://www.nordpool.com>

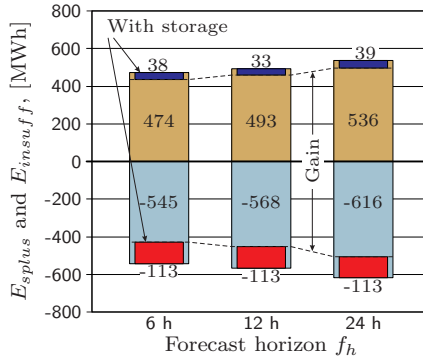


Figure 10.2: Surplus and insufficient energy with and without storage device; wind case study, according to tables 9.8 and 9.9.

at all; if the system is e.g. overloaded and the forecast overestimated the network infeed, the actually lower infeed is beneficial for the system. In this context, e.g. Norway and Denmark have different approaches to balancing penalties, varying from sometimes even negative costs, i.e. rewarding for beneficially deviating infeed, up to several times the price one MWh would cost on the spot market. In addition, the valuation suggested in equation (10.2) is based on an average return only. A more accurate procedure would be to incorporate the amounts of energy sold as base load and as peak load or even using the hourly prices. Still, this is only meaningful if a group of wind turbines is considered or if the turbine is part of a portfolio. Otherwise, the hourly amount often will be below the traded unit of 1 MWh.

Just to get an impression of the monetary amount these savings correspond to, the balancing prices from the last three month of the year 2006 were taken from the Nordpool spot market. The used measurements are from a measurement site in Northern Norway and consequently, the prices for regulating power in the corresponding market region Norway-3 were taken. The price per MWh is the same for up and down regulation and satisfies $\kappa_{up} = \kappa_{down} = 50.90 \text{ €/MWh}$. Looking at the 24 h forecast horizon gives the following income, resulting from the operation of the storage:

$$\begin{aligned} \pi &= 37.25 \text{ €} \cdot 497 \text{ MWh} + 37.25 \text{ €} \cdot 503 \text{ MWh} \\ &= 50'900 \text{ €} \end{aligned}$$

The average prices for up and down regulation in the Eastern Denmark region are at $\kappa_{up} = 49.25$ €/MWh and $\kappa_{down} = 44.03$ €/MWh. The resulting cost reduction then equals to $\pi = 46'656$ €/MWh. This indicates the variations depending on the policy concerning costs for up and down regulation.

If the storage would operate for e.g. 10 years, the same calculation would have to be performed, assuming prices for the next 10 years and discounting the resulting values with an appropriate discount rate. The sum of the 10 discounted values then gives the maximum allowable investment cost.

10.2 Incorporating Price Signals

The presented algorithms define the network infeed exclusively based on the forecast for the energy source. Thus, the primary subject is to best utilise the available amount of energy. However, the idea of using an energy storage device to bridge the differences between forecasted and actual generation also triggers the thought of using price signals to operate the storage device. The question can be raised if it would be beneficial to install a capacity even larger than actually required, according to the above calculations. The larger capacity would allow to purposely store energy during low price hours, to be supplied to the network later-on, during high price hours. This section therefore discusses how price signals could be incorporated into the algorithm.

In order to be able to react to changing market prices during the day, it must be possible to influence both the storage charge level and the planned infeed. Figures 9.5, 9.23 and 9.24 show segments of the time series, illustrating that this is possible, with the planned infeed being adjusted to the momentary charge level of the energy storage device.

A straight forward approach would be to use a curve, representing the daily relative price signals. The average daily price corresponds to 1 and the price levels of the other hours would be accordingly below or above 1. This is illustrated using the relative hourly price curve from January 1, 2006 up to November 20, 2006 from the European Power Exchange (EEX)², displayed in figure 10.3. This figure contains the

²<http://www.eex.com>

average hourly prices divided by the mean value. Hours with values above 1 thus are hours with prices above average and vice versa.

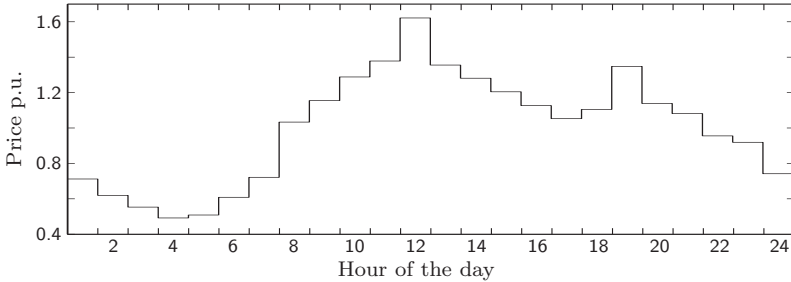


Figure 10.3: Relative hourly price curve of the European Power Exchange, based on 2006 market data.

Similar to the dynamic usage factor, this profile can be superimposed to the daily profile, increasing or decreasing the planned infeed accordingly. Thus, the planned infeed for the first hour of the day would be reduced to 71.2%, according to figure 10.3. Looking at the wind turbine from the second case study, this would mean that, with nominal turbine output of 2 MW, 576 kWh of energy would have to be stored to be used later-on, between the hours 8 and 21, where the price is above average and an infeed is favourable. This has to be considered for every hour, where the infeed is reduced because of the price signal, summing up to a maximum required energy capacity of 6'339 kWh, not considering the charge and discharge efficiencies.

With the applied overall efficiency of 81% considered, the maximum available amount of 6'339 kWh would thus only result in 5'134 kWh available for infeed, with an effectively required storage capacity of 5'705 kWh. The non-ideality of the energy storage device can thus be considered by multiplying the profile in figure 10.3 with 0.9. During charging hours, i.e. hours with the profile below 1, the infeed is reduced by 10% to consider the charging efficiency η_{ch} . During discharge hours, i.e. hours with the profile above 1, the infeed is reduced by 10% as well, to take into account the discharge efficiency η_{dch} . Another possibility is to optimise the usage factor, incorporating the price signal and the hence more intensively used storage device. In any case, it is recommended to apply a constant usage factor, as a dynamic one would most probably interfere with the price signal.

To see the influence of incorporating the price signal, an analysis is performed, using the wind turbine from the case study, assuming a forecast horizon of $f_h = 24$ h and the determined energy capacity of $E_{st} = 7529$ kWh. This case has been chosen because of the large energy capacity. Nevertheless, the above determined required capacity of 5'705 kWh is necessary only for shifting the production within one day. To be able to do so and at the same time compensate forecast errors, the total required energy capacity might even be higher.

The simulation with the price signal is performed applying a constant usage factor $\beta_{usg} = 0.965066$, optimised according to the earlier applied criteria. Thus, the price curve has been applied as defined in figure 10.3, without explicitly considering the storage efficiency. The here applied usage factor considers not only the conversion losses from compensating planning errors but also from shifting the production from low price to high price periods. As this results in more conversion losses, the applied usage factor $\beta_{usg} = 0.965066$ is smaller than the equivalent constant one, which would be used without price signals, $\beta_{usg} = 0.986330$.

	without price signal		with price signal	
	[kWh]	[%]	[kWh]	[%]
E_{gen}	5'699'634	100.00	5'699'634	100.00
$E_{planned}$	5'643'194	99.01	5'624'293	98.68
E_{actual}	5'569'526	97.72	5'531'778	97.05
E_{conv}	124'123	2.18	167'856	2.95
E_{splus}	39'188	0.69	150'014	2.63
E_{insuff}	112'857	1.98	242'530	4.26
$\varnothing E_{st,ch}(t)$	4'151		3'610	
$\varnothing \beta_{usg}$	0.9785		0.9651	
EIF	0.9800		0.9568	

Table 10.1: Simulation results with and without price signal, $E_{st} = 7'529$ kWh, $f_h = 24$ h.

Figure 10.4 shows the average daily network infeed with and without considering the price curve and table 10.1 displays the results from the same simulations. The simulation results for the case without price signals were calculated applying a dynamic usage factor. This allows to compare the network infeed optimised for the utilisation of the energy source with the network infeed optimised for the price signals. According to figure 10.4, the average daily network infeed is changed

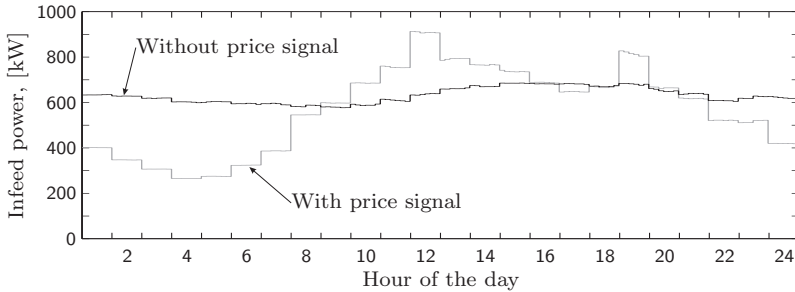


Figure 10.4: Average daily infeed with and without considering the price signal from figure 10.3.

considerably when applying the price signal. The relative improvement can now be identified from multiplying the average daily curve with the price curve from figure 10.3. It must be noted that this does not result in a double weighting with the price curve; during the simulation, the price curve is only used to shift the production from low price hours to high price hours. To identify the benefit of doing so, the shifted profile however still has to be weighted with the relative price of the individual hours.

Thus, if the price signal would not be considered in the planning, the average daily infeed, multiplied with the price curve, results in an average daily income of 792.78 €/day. This value was calculated with the price curve containing the absolute values, i.e. the relative price curve multiplied with the mean market price of 51.97 €/MWh. With the price signal incorporated into the planning, the average daily income increases by 5.93% to 839.80 €/day.

Without following the price signal, the average infeed power equals 631 kW. This infeed power reduces to 614 kW when considering the price information. Thus, the average infeed is reduced, but the shifting to the higher price periods still results in an overall higher income. Looking at the charge level duration curves, shows further that the capacity of 7529 kWh is too small to be handled by the system. Obviously, following the price signals results in many events with a fully charged storage device, see figure 10.5. Increasing the energy capacity to 15 MWh, results in slightly lower deviations from the planned infeed but almost 200 MWh conversion losses. The average daily income however increases to 850.28 €/day.

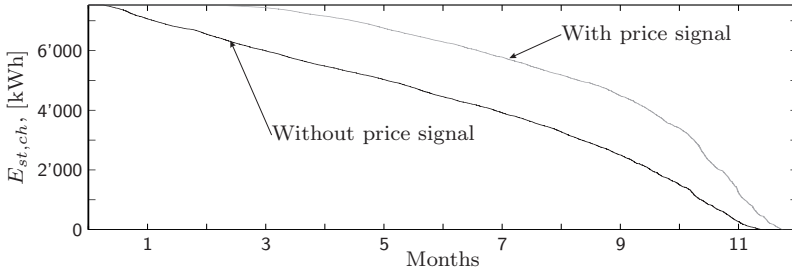


Figure 10.5: Charge level duration curves with and without considering the price signal from figure 10.3, $E_{st} = 7'529$ kWh.

This short investigation shows the ability of the system to react to price signals. So far, however the increase in income is not outstanding, particularly as it results in more conversion losses and more deviations from the planned infeed. Hence, the increased balancing penalties should be taken into account as well, when analysing the true value of incorporating prices. So far, the major driver for the infeed profile definition is still the forecast for the renewable source; the price signal is only superimposed. Thus, a more price fundamental infeed planning process is likely to move more generation from low price to high price periods, resulting in more income. Figure 10.6 shows a price curve, where the hours with prices below average are set to 0. The remaining hours, i.e. from hours 8 to 21, are increased such that the mean is equal to the curve from figure 10.3. The resulting average hourly infeed is shown in figure 10.7, for a storage capacity of both $E_{st} = 7'529$ kWh and $E_{st} = 15'000$ kWh.

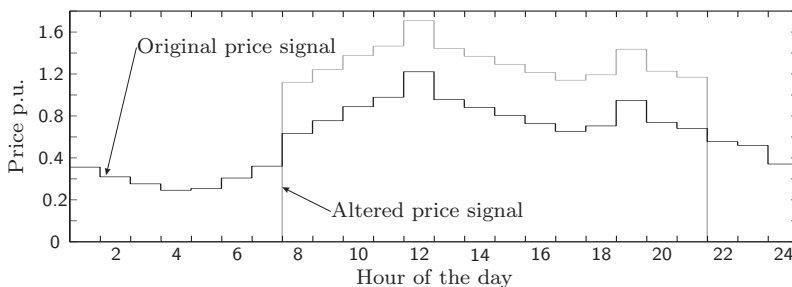


Figure 10.6: Relative hourly price curves of the European Power Exchange, based on 2006 market data.

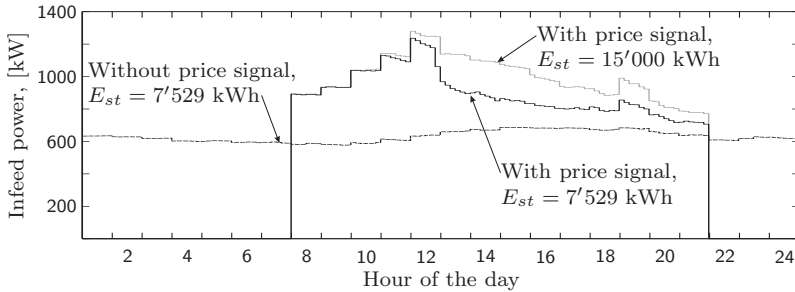


Figure 10.7: Average daily infeed with and without considering the price signal from figure 10.6.

With the smaller energy capacity, the average daily income decreases to 809.36 €/day and it increases to 900.30 €/day with $E_{st} = 15'000$ kWh. The stronger differentiating price signals results in an infeed shift to the hours with higher prices. However, the fulfillment decreases to $EIF = 0.8905$, the conversion losses increase to $E_{conv} = 406'666$ kWh, the surplus infeed to $E_{splus} = 207'190$ kWh and insufficient energy to $E_{insuff} = 625'550$ kWh. Hence, as already discussed, the expenditures for balancing penalties are likely to increase, with the amounts getting similar to the amounts that were determined for the case without energy storage device, listed in table 9.9.

The above discussion showed the feasibility of influencing the infeed profile according to price signals. The brief analysis indicated considerable energy capacities required to achieve a significant return. Furthermore, distinct profile alterations result in increasing amounts of surplus and insufficient energy. This is a contradiction to the original premise, which was to improve not primarily the income but the infeed reliability. Nevertheless, it is interesting to note how the presence of a comparatively large energy storage device allows to increase the income, while still reducing overshoots and undershoots from the planned infeed profile.

10.3 Relevance of Time Series Models

The measurement data used in the photovoltaic case study has been applied earlier, for a similar case study using the same models [55]. The measurement data are exactly the same, but only cover the years 2002 to 2004, while this study uses data from the year 2002 up to June 2006. Hence, the earlier presented case study contains results based on a section of the measurement data used here. Most interestingly, these results are very similar to the results obtained in this case study. This fact is the subject of the next few pages, discussing the relevance of results obtained with time series models in contrast to results obtained with probabilistic models.

Renewable energy sources, such as wind or sun, are often referred to as stochastic energy sources. Consequently, the generators, converting energy from these sources into electrical energy, are considered to operate stochastically as well. However, the behaviour of a process is often just claimed to be stochastic if the process cannot be described with deterministic models. Looking e.g. at the production from a photovoltaic system shows that the output cannot be considered stochastic but rather non-deterministic or semi-deterministic. That means, the production of a photovoltaic system follows certain physical rules, which cannot be ignored. For example, in Central Europe, a PV system's output at midnight cannot be higher than at noon, just given by the sun's insolation angle and power.

Hence, the energy source's output follows certain physical boundaries, within which the behaviour can be considered stochastic with the proviso that a truly stochastic process is memoryless. Looking again at renewable sources, such as wind or sun, indicates a dependency to exist: given by physical laws, it is impossible to have wind speed completely cease from one second to the next or to have clouds move in from one instant to the next, completely shading a PV array. Thus, the energy source's output follows a certain dependency within the aforementioned given enfolding. This behaviour is often modelled with Markov chains, defining the probability of the system moving from one state to another. One example are cloud models, defining the transition probabilities between different levels of clouded skies, e.g. the likelihood of a clouded sky to be free of clouds in the next interval, as applied e.g. in [33].

Time series analyses, which are based on measurement data, are thus often criticised to not provide any information on the future behaviour

of the considered energy source. Following the reasoning assuming the energy source to behave stochastically would mean that the measured time series only represents one snapshot out of a large amount of possible realisations. Hence, using a measured time series for investigations would lead to results, which are only valid for that explicit time series.

Still assuming the behaviour of the energy source to be stochastic, a further approach is to define the probability density function, describing the behaviour of the considered energy source. This density function or distribution is used as basis for e.g. a Monte Carlo simulation. Several 1'000 simulations are performed, always drawing from the distributions, resulting in various different possible realisations of the signal. Thus, instead of using one measurement series, representing the true sequence, many hundreds of artificial sequences are applied.

Usually, however, the probability density functions, used for the probabilistic analyses, are derived from measurements of the considered source, e.g. wind speed measurements. Thus, a measurement series is applied to derive the probability distribution of e.g. the wind speed. This distribution then in turn is used to calculate new wind speed sequences. The discrepancy of this approach is two-fold. On the one hand, the distribution itself is based on a measurement series. This series however is claimed only to be a snapshot of all possible realisations. Consequently, the distribution cannot be assumed to be representative, as long as the time series is claimed not to be representative. On the other hand, as mentioned, stochastic processes do not have a memory. Strictly spoken, the distribution derived from a historic measurement cannot be assumed to represent the distribution of the future behaviour of the energy source; theoretically, the future behaviour of the source could follow a completely different pattern. Besides, the reduction of a time series to its probability functions, results in a loss of the time information. In particular for applications with energy storage devices, however, the sequence of the behaviour of the energy source is crucial for identifying e.g. the charge behaviour of the energy storage device.

In this context, it is interesting to end up with almost identical results from the two case studies, applying time series analyses. The first conclusion is that the three year measurement series contains all representative cases such that the additional 1.5 years do not effectively alter the results and conclusions. Hence, for this very measurement series, looking at three years of data seems to be sufficient. The following paragraphs will further investigate the sensitivities, related to this con-

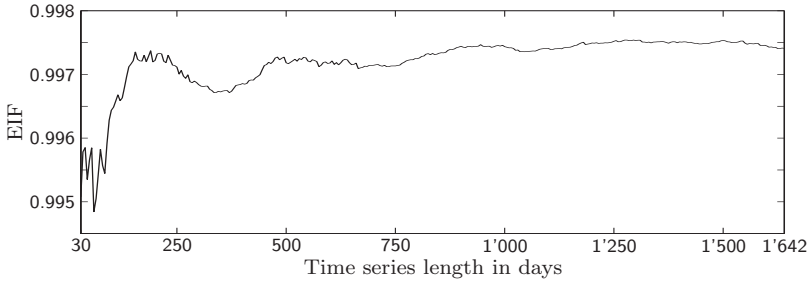


Figure 10.8: EIF for increasing time series length.

clusion. The investigated configuration is the base configuration with no forecast error and $E_{st} = 100$ kWh and $P_{st} = 500$ kW; this configuration is sufficient to analyse the steadiness of the results.

The first analysis investigates after which length of the measurement series the results become stable. With the overall target of improving the network infeed accuracy, the important parameters are the energy index of fulfilment EIF and the deviations from the planned infeed E_{splus} and E_{insuff} . Figure 10.8 shows the evolvement of the fulfilment index for an increasing simulation duration, from 30 days up to the full length of 1642 days, representing the 4.5 years. For the same simulation durations, figure 10.9 shows the development of the average daily surplus and insufficient energy. Both figures show the respective values to stop changing significantly after about 2 years, i.e. approximately 750 days. If comparing with other fulfilment plots, as e.g. figures 9.1 and 9.14, it must be noted that the ordinate of figure 10.8 covers only a small range.

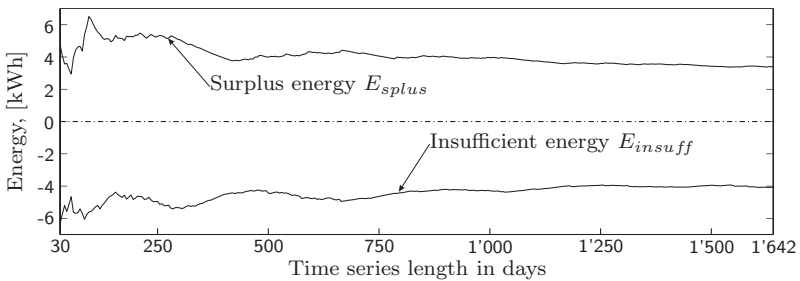


Figure 10.9: Daily E_{splus} and E_{insuff} for increasing time series length.

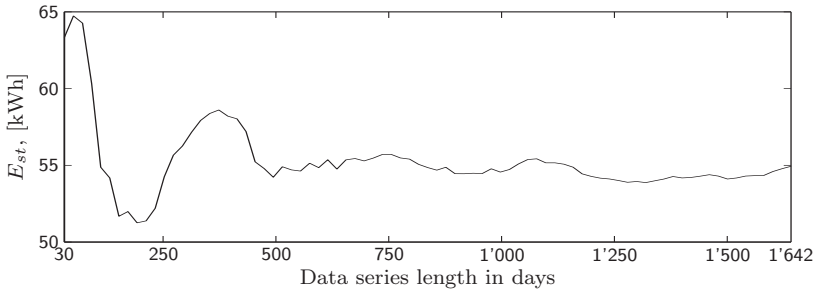


Figure 10.10: Evolvement of the minimum required E_{st} for $f_{RMSE} = 0\%$.

Besides the fulfilment and the deviations from the planned infeed, one of the major investigations of the analyses in the case studies concerned the minimum required energy capacity, required for the system to achieve a certain level of infeed reliability. Hence, a simulation was performed with an increasing simulation duration to identify the resulting energy capacity, both with a perfect forecast and an imperfect forecast with $f_{RMSE} = 20\%$. The energy capacities, resulting when targeting $\text{EIF} \geq 0.99$, are displayed in figures 10.10 and 10.11. These figures prove the above stated conclusion that the range of the results does not anymore change, when using more than 2 years of measurements; the values converge to the values determined in table 9.4. Renewable energy sources often show seasonality effects and it is likely that the duration of two years is sufficient to incorporate most of the crucial seasonal effects.

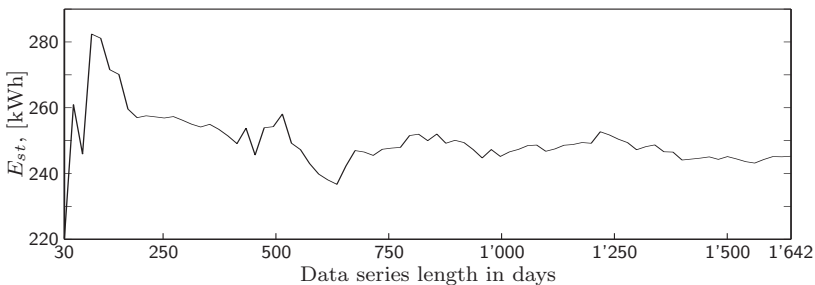


Figure 10.11: Evolvement of the minimum required energy capacity E_{st} for $f_{RMSE} = 20\%$.

The investigations so far showed that the measurement data from the photovoltaic measurement site are consistent and that it would have been sufficient to use measurements from two years; taking longer time series does not affect the conclusions. Consequently, the time series analysis lead to results that can be regarded as valid for future periods as well. The question remains however, whether the first two years happen to be incidentally representative or if generally any two-years data set from this energy source is sufficient. A last analysis therefore is performed with a simulation duration of two years, moving through the measurement series of 4.5 years in monthly intervals. That means, the simulation starts with the years 2002 and 2003 and ends with the data from July 2004 up to June 2006. The resulting energy indices of fulfilment are displayed in figure 10.12.

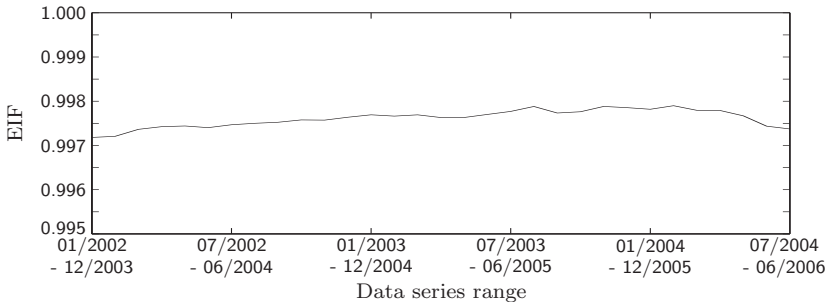


Figure 10.12: Evolvement of EIF for moving measurement series windows of length of 2 years.

This last investigation verifies that any excerpt, covering 2 years of the measurement data, results in almost identical results. It can also be stated that it would be appropriate to use 2 years of measurement data to determine a probability density function to be used in probabilistic analyses. Nevertheless, the sensitivity analyses performed in this chapter proved a time series analysis to be a valid way for identifying energy storage capacities for the intended purpose of improving the network infeed reliability.

10.4 Conclusion

This part of the thesis discussed various issues of combining grid-connected non-dispatchable generators with energy storage devices. The purpose of the energy storage device is to compensate differences between the forecasted and the actual infeed, in order to improve the reliability of the non-dispatchable generator. A modelling algorithm, suitable for time series analyses, was presented, including a new approach for the simulation of forecasts. Together with analysis procedures, this modelling algorithm was then applied in two case studies. The purpose of the case studies was both to discuss and demonstrate the usability of the developed procedures and to investigate the storage requirements and the system performance.

The first case study analysed 4.5 years of measurement data from a 500 kW photovoltaic installation in Switzerland. The applicability of the methods was demonstrated and it was shown to be beneficial to include the charge level of the storage device into the operation planning process. The combination of the PV system with energy storage devices transforms the generator's output into a reliable and deterministic infeed profile. This is particularly useful for incorporating the PV system into the planning and scheduling process. For smaller forecast errors, the energy capacities, required to achieve an infeed reliability close to 100%, are in the range of few 100 kWh. The power rating of the photovoltaic system does not suggest incorporating market aspects; the smallest traded unit on most European electricity markets is 1 MWh, exceeding the rated hourly production from the PV system.

The second case study analysed 1 year of wind speed measurement data from Norway, used to operate a 2 MW turbine. Because of the large rating of the wind turbine and the possible continuous production from the turbine, the storage requirements are considerably larger. The larger rating of the wind turbine also allows the consideration of market aspects when analysing the performance. In this context, a reliably deterministic infeed profile facilitates the accurate production scheduling of other generators. But, it also allows to buy and sell accordingly on the market, with a significantly lower risk of incurring balancing penalties. The case study indicates that shorter forecast horizons would be beneficial for the system behaviour, in particular concerning conversion losses and storage capacity requirements.

The developed forecast simulation algorithm, based on an EWMA approach resulted in appropriate forecast simulations, both in the PV case study for different forecast error magnitudes and in the wind case study for a time evolving forecast error with different forecast horizons. This can be derived from the circumstance that the conclusions from the wind data case study comply with other studies looking at forecast issues with wind power.

In conclusion, a way for determining the value of the energy storage device was proposed and the consistency of the applied time series analysis was discussed and demonstrated with the photovoltaic measurement data. In addition, the extension of the proposed models with price signals was outlined and the ability of the system to follow these price signals was demonstrated. This allows to plan the network infeed not only based on forecasts for the energy source but also based on market signals. The suggested approach could be extended to analyse the trade-off between more income from shifting the network infeed from low price periods to high price periods and the accordingly higher investment costs required for the larger energy capacity.

The developed algorithm proved useful for the targeted type of analysis. Its application showed that energy storage devices at the point of network infeed result in considerable improvements of the dependability and reliability of the forecasted network infeed.

Appendix

Basic Concepts of Reliability Modelling

This chapter contains a general overview and introduction into the reliability modelling of energy systems. It basically is a compilation of sections from four comprehensive books on the subject of reliability in engineering and power systems [18, 19, 20, 21]. The focus lies on reliability block diagrams and on Markov processes, used for state space diagram analyses.

A.1 Reliability Block Diagrams

Reliability block diagrams are used to illustrate the influence and dependence of single components on the reliability of supply. The basic example consists of two independent repairable components. Depending on the needs of the system, these components are either crucial or redundant for the success of the system.

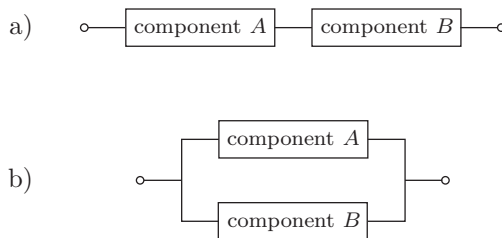


Figure A.1: Reliability block diagram of a system with two components.

Figure A.1 shows the reliability block diagram for both situations. It is important to note that these diagrams do not represent physical connections; they represent functionality in terms of reliability. Figure A.1a) represents the case where both components are crucial for the operation; they form a series connection in terms of reliability; if either one of the components fails, the connection is broken and system success cannot be achieved. Figure A.1b) displays the case where each component can fulfill the required task on its own. In terms of reliability the two components form a parallel or redundant connection; if one component fails, the system is still successful.

Let R_A and R_B denote the probability of successful operation of components A and B , respectively, and Q_A and Q_B the corresponding probability of failure. With success and failure being mutually exclusive, the following relations hold true:

$$R_A + Q_A = 1 \quad (\text{A.1})$$

$$R_B + Q_B = 1 \quad (\text{A.2})$$

A.1.1 Series systems

For the case of the series connection (figure A.1a)), both components must be operating for success and the corresponding probability R_{series} can be written as:

$$R_{series} = R_A \cdot R_B \quad (\text{A.3})$$

For a system consisting of n components in series, equation (A.3) can be generalised to:

$$R_{series} = \prod_{i=1}^n R_i \quad (\text{A.4})$$

The probability of failure for the series system is accordingly defined as:

$$\begin{aligned} Q_{series} &= 1 - R_{series} \\ &= 1 - R_A \cdot R_B \\ &= Q_A + Q_B - Q_A \cdot Q_B \end{aligned} \quad (\text{A.5})$$

For the system consisting of n components in series, it can be generalised as:

$$Q_{series} = 1 - \prod_{i=1}^n R_i \quad (\text{A.6})$$

A.1.2 Parallel systems

If the components form a parallel or redundant system, the probability of success is defined vice-versa:

$$\begin{aligned} R_{parallel} &= 1 - Q_{parallel} \\ &= R_A + R_B - R_A \cdot R_B \end{aligned} \quad (\text{A.7})$$

For n components the relation is accordingly:

$$R_{parallel} = 1 - \prod_{i=1}^n Q_i \quad (\text{A.8})$$

The probability of failure finally is defined similarly to the probability of success for the series system. For the parallel system to fail, both components must fail; they form a series system:

$$Q_{parallel} = Q_A \cdot Q_B \quad (\text{A.9})$$

A.1.3 Combinations of series and parallel systems

Most systems consist of more than 2 components and their reliability block diagrams are not necessarily purely series or parallel connections. Such systems are usually analysed by combining appropriate series and parallel connections and replacing them with a single component with equivalent characteristics. The following small example illustrates this process [19]. For the system given in figure A.2, calculate the probability of success.

Components C and D can be summarised with component F, as illustrated in figure A.3a). The probability of component F being operating can be found as:

$$R_F = R_C + R_D - R_C R_D$$

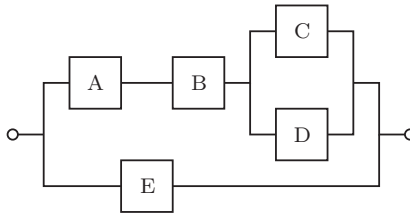


Figure A.2: Basic case for example of parallel and series system.

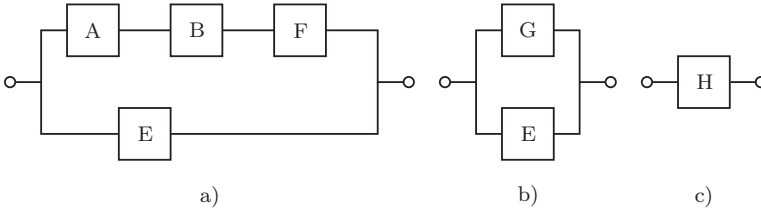


Figure A.3: Reduction of system from figure A.2. a) first reduction, b) second reduction, c) third reduction.

Components A, B and F now form a series system, which can be represented by component G, as illustrated in figure A.3b). The probability of success of component G is:

$$\begin{aligned}
 R_G &= R_A R_B R_F \\
 &= R_A R_B (R_C + R_D - R_C R_D)
 \end{aligned}$$

The system in figure A.3b) forms a parallel system and can be combined to a single component H as shown in figure A.3c):

$$\begin{aligned}
 R_H &= R_E + R_G - R_E R_G \\
 &= R_E + R_A R_B (R_C + R_D - R_C R_D) \\
 &\quad - R_A R_B R_E (R_C + R_D - R_C R_D)
 \end{aligned}$$

The probability of failure can be found accordingly as:

$$\begin{aligned}
 Q_H &= Q_E (Q_A + Q_B + Q_C Q_D - Q_A Q_B \\
 &\quad - Q_B Q_C Q_D - Q_A Q_C Q_D + Q_A Q_B Q_C Q_D)
 \end{aligned}$$

A.1.4 Standby redundant systems

In the previous sections it was assumed that all present components are operating. Sometimes however, components are ready to start operating, but they need to be switched on first. These systems are called standby redundant systems, as the redundancy relates to the stand-by component.

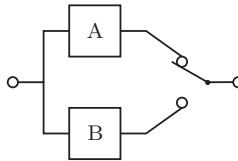


Figure A.4: Standby redundant systems.

With such a configuration, two cases can be distinguished: perfect switching and imperfect switching. Perfect switching means that the switch-over happens 100% reliably. Furthermore it is assumed that component B is not failed while in the standby position. The probability of failure hence is the probability of failure of component A and the probability of failure Q_B of component B, given that component A has failed:

$$Q = Q(A) \cdot Q(B|\bar{A}) \quad (\text{A.10})$$

If both components are independent, this relation reduces to:

$$Q = Q_A \cdot Q_B \quad (\text{A.11})$$

It is important to note that this equation is similar to equation (A.9), but the used values will be divergent: a component residing mostly in standby will have different reliability characteristics than a component that is in continuous operation.

Imperfect switching means that the switch itself has a certain probability of failure. This failure potential can show both while switching but also after switching, during normal operation. The left component S in figure A.5, labelled with P_S , denotes the probability of a changeover failure. The probability of system failure is then given as follows, assuming

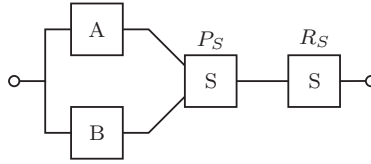


Figure A.5: Standby redundant systems with an imperfect switch.

independence of all components:

$$\begin{aligned}
 Q &= Q_A Q_B P_S + Q_A \bar{P}_S \\
 &= Q_A Q_B P_S + Q_A - Q_A P_S \\
 &= Q_A - Q_A P_S (1 - Q_B)
 \end{aligned} \tag{A.12}$$

The system fails if the changeover is successful but component B fails or if component A fails and the changeover is not successful. In addition, as indicated in figure A.5 by the right component S, labelled with R_S , the system additionally fails if the switch itself fails during normal operation, i.e. not during the changeover. The resulting failure probability is found as:

$$\begin{aligned}
 Q &= [Q_A - Q_A P_S (1 - Q_B)] + Q_S (1 - [Q_A - Q_A P_S (1 - Q_B)]) \\
 &= 1 - [R_S (1 - (Q_A - Q_A P_S (1 - Q_B)))]
 \end{aligned} \tag{A.13}$$

The disadvantage of the so far presented models is the assumption of a known, single value probability of failure and success. This is not valid as component reliability usually follows a certain probability distribution. The referenced books [18, 19, 20, 21] discuss these aspects.

These concepts however have to be further extended, as they usually assume instantaneous repairs, which is in turn unlikely. One important and useful technique covering these requirements, is the so-called Markov approach, which will be the subject of the second part of this appendix.

A.2 Markov Processes

The techniques and modelling approaches described in this chapter apply to systems, which have the properties of a so-called stationary

Markov process. Before the models are introduced, the properties of such processes are thus discussed.

Generally, a process is considered to be a stationary Markov process if it fulfills two properties:

- The process does not have a memory. The future development is independent of past developments and only depends on the present state.
- The process must be stationary. The probability of a transition from one state to the other is independent of the time; it is the same at all times in the past and in the future.

Mathematically, these properties can be described by assuming a stochastic process $\{X(t), t \geq 0\}$ with continuous time and state space $\mathcal{X} = \{1, 2, \dots, r\}$. At time s the process resides in state $X(s) = i, i \in \mathcal{X}$ and the probability of the process being in state j at time $s + t$ is:

$$P(X(s+t) = j | X(s) = i, X(u) = x(u), 0 \leq u < s) \quad (\text{A.14})$$

Whereas the expression $\{x(u), 0 \leq u < s\}$ represents the history of the process up to but not including s . The process $X(t)$ satisfies the Markov property of having no memory if the following relation holds true:

$$\begin{aligned} P(X(s+t) = j | X(s) = i, X(u) = x(u), 0 \leq u < s) \\ = P(X(s+t) = j | X(s) = i, \forall x(u), 0 \leq u < s) \end{aligned} \quad (\text{A.15})$$

This means that when the present state of the process is known, i.e. $X(s) = i$, the future development is independent of the history, i.e. of previous states of the process. The stationarity criterion, i.e. the criterion that the transition rates are constant at all times, can be described formally as:

$$P(X(s+t) = j | X(s) = i) = P(X(t) = j | X(0) = i), \forall s, t \geq 0 \quad (\text{A.16})$$

In other words, the probability of a transition from state i to state j is independent of how long the process has been residing in state i .

A.2.1 Failure and repair rates

Components present in power systems can be understood to satisfy Markov properties and can thus be modelled accordingly. Throughout this thesis, a single repairable component is assumed to have two operating states: it is either in the up state, i.e. working, or it is in the failed or down state, i.e. not working because of a failure. Power systems are continuous in time and discrete in space, which means they reside continuously in an identifiable state until a transition to another state occurs. The transitions between the states happen with a certain frequency or rate, whereas the transition rate from the up state to the down state is usually designated as failure rate λ and the transition rate from the failed state back to the operating state as repair rate μ . Figure A.6 shows this for one component with a so-called state space diagram.

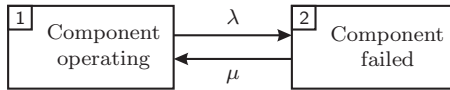


Figure A.6: Basic reliability block diagram for a single component with failure rate λ and repair rate μ .

The failure rate λ is defined as the reciprocal of the mean time to failure (MTTF). Analogously, the repair rate μ is defined as the reciprocal of the mean time to repair (MTTR).

$$\lambda = \frac{1}{\text{MTTF}} \quad (\text{A.17})$$

$$\mu = \frac{1}{\text{MTTR}} \quad (\text{A.18})$$

Usually, both rates are expressed relative to the duration of a year. If MTTF is 1 year, the failure rate thus is:

$$\lambda = \frac{1}{8760 \text{ h}} \cdot \frac{8760 \text{ h}}{8760 \text{ h}} = \frac{1}{\text{yr}} \quad (\text{A.19})$$

For a MTTR of e.g. 24h, the repair rate is:

$$\mu = \frac{1}{24 \text{ h}} \cdot \frac{8760 \text{ h}}{8760 \text{ h}} = \frac{365}{\text{yr}} \quad (\text{A.20})$$

Assuming the process to be in state 1, i.e. operating, the probability that the process will be in state 1 after the time interval dt can be defined as:

$$P_1(t + dt) = P_1(t) \cdot (1 - \lambda dt) + P_2(t)(1 - \mu dt) \quad (\text{A.21})$$

The time interval dt is chosen sufficiently small such that the probability of two or more events occurring during this interval can be considered to be zero. Applying a Laplace transformation, the probabilities for both states for the component in figure A.6 can be found as [19]:

$$P_1(t) = \frac{\mu}{\lambda + \mu} + \frac{\lambda e^{-(\lambda + \mu)t}}{\lambda + \mu} \quad (\text{A.22})$$

$$P_2(t) = \frac{\lambda}{\lambda + \mu} - \frac{\lambda e^{-(\lambda + \mu)t}}{\lambda + \mu} \quad (\text{A.23})$$

The steady state probabilities are then found by letting $t \rightarrow \infty$:

$$P_1(t \rightarrow \infty) = \frac{\mu}{\lambda + \mu} \quad (\text{A.24})$$

$$P_2(t \rightarrow \infty) = \frac{\lambda}{\lambda + \mu} \quad (\text{A.25})$$

It is important to note that these relations hold true independent of the state the systems was residing in at $t = 0$. Using the definitions from equations (A.17) and (A.18), the limiting probabilities can also be written as:

$$P_1 = \frac{\text{MTTF}}{\text{MTTF} + \text{MTTR}} \quad (\text{A.26})$$

$$P_2 = \frac{\text{MTTR}}{\text{MTTF} + \text{MTTR}} \quad (\text{A.27})$$

If the component is non-repairable, i.e. $\mu = 0$, the probability of being in the up state, also called availability, is defined as $P_1(t) = \lambda e^{\lambda t}$. This relation coincides with the survivor function of the component. Figure A.7 shows the evolution of the survivor function and the associated availability, both approaching their steady state value for increasing time [18].

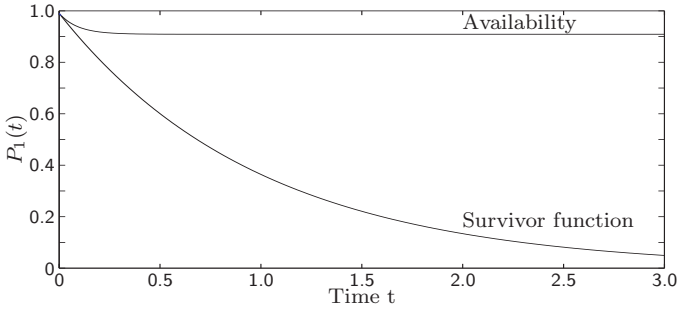


Figure A.7: Availability and survivor function of a single component ($\lambda = 1, \mu = 10$)

A.2.2 Transition rate matrix

The probabilities for the up and down state can also be found through the transition rate matrix. This matrix contains the transition rates from one state to the other states as entries. The transition from state 1 to state 2 is then associated with the matrix entry a_{12} , which for the state space diagram in figure A.6 corresponds to λ :

$$\mathbb{A} = \begin{bmatrix} 1 - \lambda & \lambda \\ \mu & 1 - \mu \end{bmatrix} \tag{A.28}$$

With the limiting state probability vector $\mathbf{P}^T = [P_1 \ P_2]$ the state equations for the Markov process can be found as:

$$\mathbf{P}^T(t) \cdot \mathbb{A} = \dot{\mathbf{P}}^T(t) \tag{A.29}$$

These equations can be solved through a Laplace transformation, as discussed in the referenced books. For the underlying thesis, however only the limiting state probabilities are of interest. Accordingly, the states will not anymore change during a small time step and equation (A.29) can be written as:

$$\mathbf{P}^T \cdot \mathbb{A} = \mathbf{P}^T \tag{A.30}$$

$$P_1(1 - \lambda) + P_2\mu = P_1 \tag{A.31}$$

$$P_1\lambda + P_2(1 - \mu) = P_2 \tag{A.32}$$

Equations (A.31) and (A.32) are linearly dependent. To solve the linear system, one of these equations has to be replaced with the relation:

$$P_1 + P_2 = 1 \tag{A.33}$$

Solving these equations then results in equations (A.24) and (A.25) again:

$$P_1 = \frac{\mu}{\lambda + \mu} \tag{A.34}$$

$$P_2 = \frac{\lambda}{\lambda + \mu} \tag{A.35}$$

A.2.3 Larger systems

With each component either being operating or in failure mode, the number of possible system states increases to 2^n states for n components. Accordingly, the solution of the linear systems gets more complex. To close this appendix, an example with a system consisting of 3 components is displayed and the different results are discussed, depending on whether the three components form series or parallel combination.

The example is displayed in figure A.8, whereas the symbol '✓' designates an operating component and the symbol '×' a failed component.

As mentioned above, the single matrix entries a_{ij} correspond to the transition from state i to state j . The diagonal elements contain all transitions leaving the particular state, including the option to stay in the state, e.g. a_{22} then is equal to $a_{22} = 1 - \mu_A - \lambda_B - \lambda_C$.

The complete transition rate matrix for the system in figure A.8 can be found as:

$$\mathbb{A} = \begin{bmatrix} a_{11} & \lambda_A & \lambda_B & \lambda_C & 0 & 0 & 0 & 0 \\ \mu_A & a_{22} & 0 & 0 & \lambda_B & 0 & \lambda_C & 0 \\ \mu_B & 0 & a_{33} & 0 & \lambda_A & \lambda_C & 0 & 0 \\ \mu_C & 0 & 0 & a_{44} & 0 & \lambda_B & \lambda_A & 0 \\ 0 & \mu_B & \mu_A & 0 & a_{55} & 0 & 0 & \lambda_C \\ 0 & 0 & \mu_C & \mu_B & 0 & a_{66} & 0 & \lambda_A \\ 0 & \mu_C & 0 & \mu_A & 0 & 0 & a_{77} & \lambda_B \\ 0 & 0 & 0 & 0 & \mu_C & \mu_A & \mu_B & a_{88} \end{bmatrix} \tag{A.36}$$

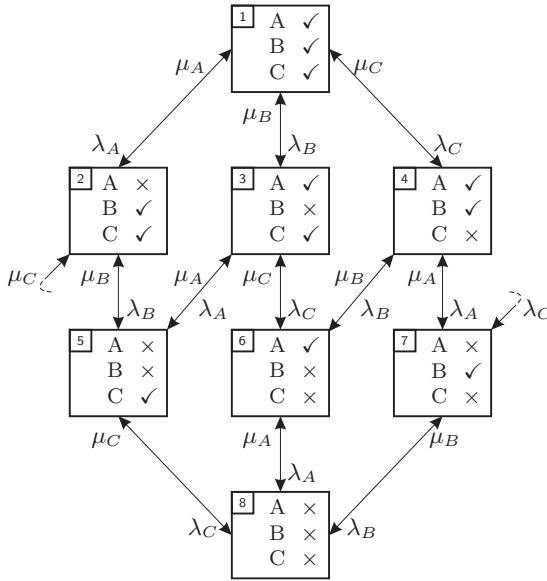


Figure A.8: State space diagram of a system consisting of $n = 3$ component with $2^n = 8$ states.

The diagonal elements are:

$$\begin{aligned}
 a_{11} &= 1 - \lambda_A - \lambda_B - \lambda_C & a_{22} &= 1 - \mu_A - \lambda_B - \lambda_C \\
 a_{33} &= 1 - \lambda_A - \mu_B - \lambda_C & a_{44} &= 1 - \lambda_A - \lambda_B - \mu_C \\
 a_{55} &= 1 - \mu_A - \mu_B - \lambda_C & a_{66} &= 1 - \lambda_A - \mu_B - \mu_C \\
 a_{77} &= 1 - \mu_A - \lambda_B - \mu_C & a_{88} &= 1 - \mu_A - \mu_B - \mu_C
 \end{aligned}$$

The validity of the matrix can be checked by summing up each row. Each row contains the state and all the transitions leaving this particular state and thus the sum must be equal to unity:

$$\sum_{j=1}^r P_{ij} = 1, \forall i \in \mathcal{X} \tag{A.37}$$

Following equation (A.30), the system can be written with the following set of linear equations:

$$\begin{aligned}
-(\lambda_A + \lambda_B + \lambda_C)P_1 + \mu_A P_2 + \mu_B P_3 + \mu_C P_4 &= 0 \\
\lambda_A P_1 - (\mu_A + \lambda_B + \lambda_C)P_2 + \mu_B P_5 + \mu_C P_7 &= 0 \\
\lambda_B P_1 - (\lambda_A + \mu_B + \lambda_C)P_3 + \mu_A P_5 + \mu_C P_6 &= 0 \\
\lambda_C P_1 - (\lambda_A + \lambda_B + \mu_C)P_4 + \mu_B P_6 + \mu_A P_7 &= 0 \\
\lambda_B P_2 + \lambda_A P_3 - (\mu_A + \mu_B + \lambda_C)P_5 + \mu_C P_8 &= 0 \\
\lambda_C P_3 + \lambda_B P_4 - (\lambda_A + \mu_B + \mu_C)P_6 + \mu_A P_8 &= 0 \\
\lambda_C P_2 + \lambda_A P_4 - (\mu_A + \lambda_B + \mu_C)P_7 + \mu_B P_8 &= 0 \\
\lambda_C P_5 + \lambda_A P_6 + \lambda_B P_7 - (\mu_A + \mu_B + \mu_C)P_8 &= 0
\end{aligned} \tag{A.38}$$

The equations in the set of equations (A.38) are linearly dependent, which is why one of them has to be substituted with the following relation:

$$P_1 + P_2 + P_3 + P_4 + P_5 + P_6 + P_7 + P_8 = 1 \tag{A.39}$$

This set of equations can be solved to give the following result:

$$\begin{aligned}
P_1 &= \frac{\mu_A \mu_B \mu_C}{(\mu_A + \lambda_A)(\mu_B + \lambda_B)(\mu_C + \lambda_C)} \\
P_2 &= \frac{\lambda_A \mu_B \mu_C}{(\mu_A + \lambda_A)(\mu_B + \lambda_B)(\mu_C + \lambda_C)} \\
P_3 &= \frac{\mu_A \lambda_B \mu_C}{(\mu_A + \lambda_A)(\mu_B + \lambda_B)(\mu_C + \lambda_C)} \\
P_4 &= \frac{\mu_A \mu_B \lambda_C}{(\mu_A + \lambda_A)(\mu_B + \lambda_B)(\mu_C + \lambda_C)} \\
P_5 &= \frac{\lambda_A \lambda_B \mu_C}{(\mu_A + \lambda_A)(\mu_B + \lambda_B)(\mu_C + \lambda_C)} \\
P_6 &= \frac{\mu_A \lambda_B \lambda_C}{(\mu_A + \lambda_A)(\mu_B + \lambda_B)(\mu_C + \lambda_C)} \\
P_7 &= \frac{\lambda_A \mu_B \lambda_C}{(\mu_A + \lambda_A)(\mu_B + \lambda_B)(\mu_C + \lambda_C)} \\
P_8 &= \frac{\lambda_A \lambda_B \lambda_C}{(\mu_A + \lambda_A)(\mu_B + \lambda_B)(\mu_C + \lambda_C)}
\end{aligned} \tag{A.40}$$

In the first part of this appendix, reliability block diagrams have been introduced, used for determining how the individual components contribute to system success. This approach can now be used to calculate

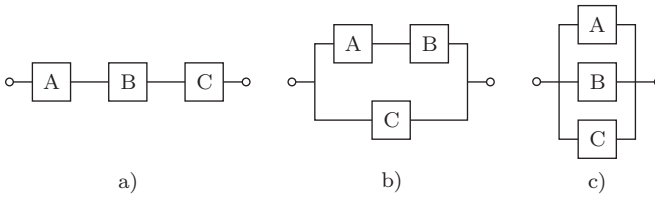


Figure A.9: Possible reliability block diagrams for the components represented with the state space diagram in figure A.8.

the probability of success and failure for particular configuration. Figure A.9 shows three possible configurations for which the corresponding probabilities for success and failure will be discussed.

Figure A.9a) shows a configuration where the successful operation depends on all three components; they form a series system. Thus, the process is only successful as long as it resides in state 1 and consequently:

$$R = P_1$$

$$Q = P_2 + P_3 + P_4 + P_5 + P_6 + P_7 + P_8$$

Figure A.9c) shows the counter part to figure A.9a); the components form a doubly redundant parallel configuration. Accordingly, the process is successful unless it resides in state 8:

$$R = P_1 + P_2 + P_3 + P_4 + P_5 + P_6 + P_7$$

$$Q = P_8$$

Figure A.9b) shows a combination of parallel and series structures. Obviously, the process is successful whenever component C is operating, i.e. states 1, 2, 3 and 5. It is also successful as long as both component A and B are operating, i.e. states 1 and 4. Thus, as long as the process resides in any of the states 1, 2, 3, 4 and 5, the system is successful:

$$R = P_1 + P_2 + P_3 + P_4 + P_5$$

$$Q = P_6 + P_7 + P_8$$

This example closes the introduction into reliability modelling basics; for more in-depth background information and further models and methods, the interested reader is recommended to consult the books, underlying this appendix [18, 19, 20, 21].

Kronecker Products and Sums

This chapter contains a short definition and overview of Kronecker products, following the book by Rausand [18].

With matrix \mathbb{A} of dimension $m \times n$ and matrix \mathbb{B} of dimension $p \times q$, the Kronecker product, designated with the symbol \otimes , is given as:

$$\mathbb{A} \otimes \mathbb{B} = \begin{bmatrix} a_{11}\mathbb{B} & a_{12}\mathbb{B} & \cdots & a_{1n}\mathbb{B} \\ a_{21}\mathbb{B} & a_{22}\mathbb{B} & \cdots & a_{2n}\mathbb{B} \\ \vdots & \vdots & \ddots & \vdots \\ a_{m1}\mathbb{B} & a_{m2}\mathbb{B} & \cdots & a_{mn}\mathbb{B} \end{bmatrix} \quad (\text{B.1})$$

Hence, the Kronecker product of both matrices results in a matrix of dimension $mp \times nq$. The Kronecker sum of two matrices is defined as follows, for square matrices \mathbb{A} and \mathbb{B} :

$$\mathbb{A} \oplus \mathbb{B} = \mathbb{A} \otimes \mathbb{I}_q + \mathbb{I}_n \otimes \mathbb{B} \quad (\text{B.2})$$

The matrix \mathbb{I}_x is the identity matrix of dimension x . For more than two matrices, associativity holds true:

$$\mathbb{A} \otimes (\mathbb{B} \otimes \mathbb{C}) = (\mathbb{A} \otimes \mathbb{B}) \otimes \mathbb{C} \quad (\text{B.3})$$

To illustrate the application, the transition rate matrix from section [A.2.3](#) is defined using Kronecker sums and products.

For this purpose, three individual and independent systems are as-

summed, represented with the following state transition matrices:

$$\vec{P}_A \cdot \mathbb{A} = \begin{bmatrix} P_{A1} & P_{A2} \end{bmatrix} \cdot \begin{bmatrix} -\lambda_A & \lambda_A \\ \mu_A & -\mu_A \end{bmatrix} = 0 \quad (\text{B.4})$$

$$\vec{P}_B \cdot \mathbb{B} = \begin{bmatrix} P_{B1} & P_{B2} \end{bmatrix} \cdot \begin{bmatrix} -\lambda_B & \lambda_B \\ \mu_B & -\mu_B \end{bmatrix} = 0 \quad (\text{B.5})$$

$$\vec{P}_C \cdot \mathbb{C} = \begin{bmatrix} P_{C1} & P_{C2} \end{bmatrix} \cdot \begin{bmatrix} -\lambda_C & \lambda_C \\ \mu_C & -\mu_C \end{bmatrix} = 0 \quad (\text{B.6})$$

First, the systems A and B are combined, as follows:

$$\begin{aligned} \mathbb{A} \oplus \mathbb{B} &= \begin{bmatrix} -\lambda_A & \lambda_A \\ \mu_A & -\mu_A \end{bmatrix} \otimes \begin{bmatrix} 1 & 0 \\ 0 & 1 \end{bmatrix} + \begin{bmatrix} 1 & 0 \\ 0 & 1 \end{bmatrix} \otimes \begin{bmatrix} -\lambda_B & \lambda_B \\ \mu_B & -\mu_B \end{bmatrix} \\ &= \begin{bmatrix} -\lambda_A & 0 & \lambda_A & 0 \\ 0 & -\lambda_A & 0 & \lambda_A \\ \mu_A & 0 & -\mu_A & 0 \\ 0 & \mu_A & 0 & -\mu_A \end{bmatrix} + \begin{bmatrix} -\lambda_B & \lambda_B & 0 & 0 \\ \mu_B & -\mu_B & 0 & 0 \\ 0 & 0 & -\lambda_B & \lambda_B \\ 0 & 0 & \mu_B & -\mu_B \end{bmatrix} \\ &= \begin{bmatrix} -(\lambda_A + \lambda_B) & \lambda_B & \lambda_A & 0 \\ \mu_B & -(\lambda_A + \mu_B) & 0 & \lambda_A \\ \mu_A & 0 & -(\mu_A + \lambda_B) & \lambda_B \\ 0 & \mu_A & \mu_B & -(\mu_A + \mu_B) \end{bmatrix} \end{aligned}$$

Adding the transition rate matrix of system C gives the new transition rate matrix \mathbb{D} as:

$$\begin{aligned} \mathbb{D} &= \mathbb{A} \oplus \mathbb{B} \oplus \mathbb{C} \\ &= (\mathbb{A} \oplus \mathbb{B}) \otimes \begin{bmatrix} 1 & 0 \\ 0 & 1 \end{bmatrix} + \begin{bmatrix} 1 & 0 & 0 & 0 \\ 0 & 1 & 0 & 0 \\ 0 & 0 & 1 & 0 \\ 0 & 0 & 0 & 1 \end{bmatrix} \otimes \begin{bmatrix} -\lambda_C & \lambda_C \\ \mu_C & -\mu_C \end{bmatrix} \\ &= \begin{bmatrix} a_{11} & \lambda_C & \lambda_B & 0 & \lambda_A & 0 & 0 & 0 \\ \mu_C & a_{22} & 0 & \lambda_B & 0 & \lambda_A & 0 & 0 \\ \mu_B & 0 & a_{33} & \lambda_C & 0 & 0 & \lambda_A & 0 \\ 0 & \mu_B & \mu_C & a_{44} & 0 & 0 & 0 & \lambda_A \\ \mu_A & 0 & 0 & 0 & a_{55} & \lambda_C & \lambda_B & 0 \\ 0 & \mu_A & 0 & 0 & \mu_C & a_{66} & 0 & \lambda_B \\ 0 & 0 & \mu_A & 0 & \mu_B & 0 & a_{77} & \lambda_C \\ 0 & 0 & 0 & \mu_A & 0 & \mu_B & \mu_C & a_{88} \end{bmatrix} \end{aligned}$$

The diagonal elements are:

$$\begin{aligned}
 a_{11} &= -(\lambda_A + \lambda_B + \lambda_C) & a_{22} &= -(\lambda_A + \lambda_B + \mu_C) \\
 a_{33} &= -(\lambda_A + \mu_B + \lambda_C) & a_{44} &= -(\lambda_A + \mu_B + \mu_C) \\
 a_{55} &= -(\mu_A + \lambda_B + \lambda_C) & a_{66} &= -(\mu_A + \lambda_B + \mu_C) \\
 a_{77} &= -(\mu_A + \mu_B + \lambda_C) & a_{88} &= -(\mu_A + \mu_B + \mu_C)
 \end{aligned}$$

The corresponding state probability vector is found as:

$$\vec{P} = \vec{P}_A \otimes \vec{P}_B \otimes \vec{P}_C = \begin{bmatrix} P_{A1}P_{B1}P_{C1} \\ P_{A1}P_{B1}P_{C2} \\ P_{A1}P_{B2}P_{C1} \\ P_{A1}P_{B2}P_{C2} \\ P_{A2}P_{B1}P_{C1} \\ P_{A2}P_{B1}P_{C2} \\ P_{A2}P_{B2}P_{C1} \\ P_{A2}P_{B2}P_{C2} \end{bmatrix}^T$$

The transition rate matrix \mathbb{D} and the state probability vector \vec{P} now define the the new system as:

$$\vec{P} \cdot \mathbb{D} = 0 \tag{B.7}$$

Compared with the state space diagram in figure A.8, some states are defined differently, i.e. state 4 from figure A.8 corresponds to the 2nd entry in the state probability vector, with component A and B being operating while C is down. However, matrix \mathbb{D} is consistent with vector \vec{P} and they represent the same system as in section A.2.3.

Characteristics of Energy Storage Devices

As outlined in section 4.1, storage devices can be represented as systems with failure and repair rates. These rates depend directly on the charge and discharge behaviour of the individual storage technologies and implementations (equations (4.3), (4.5)). This chapter therefore shortly discusses the general approach for modelling energy storage devices.

A storage device can be said to be charged with a certain charge efficiency $\eta_{ch}(t)$ and to be discharged with a certain discharge efficiency $\eta_{dch}(t)$. Detailed models [56, 57] show that these efficiencies depend on the momentary charge power $P_{st}(t)$ and the momentary charge level $E_{st}(t)$. The relation for the charging situation, where $E_{st}(t_2) > E_{st}(t_1)$ with $t_2 > t_1$, is defined as:

$$E_{st}(t_2) = E_{st}(t_1) + \int_{t=t_1}^{t_2} P_{st}(t) \cdot \eta_{ch}(E_{st}(t), P_{st}(t)) dt \quad (\text{C.1})$$

For the discharge situation, where $E_{st}(t_2) < E_{st}(t_1)$ with $t_2 > t_1$, the relation is given as:

$$E_{st}(t_2) = E_{st}(t_1) - \int_{t=t_1}^{t_2} P_{st}(t) \cdot \frac{1}{\eta_{dch}(E_{st}(t), P_{st}(t))} dt \quad (\text{C.2})$$

However, many system level investigations using energy storage devices, assume constant charge and discharge efficiencies [29, 30, 31, 32]. Thus,

equations (C.1) and (C.2) can be written as:

$$E_{st}(t_2) = E_{st}(t_1) + \eta_{ch} \cdot \int_{t=t_1}^{t_2} P_{st}(t) dt \quad (\text{C.3})$$

$$E_{st}(t_2) = E_{st}(t_1) - \frac{1}{\eta_{dch}} \cdot \int_{t=t_1}^{t_2} P_{st}(t) dt \quad (\text{C.4})$$

The behaviour of electrical energy storage devices has been investigated thoroughly in various studies, both on the technological level [56, 57, 58, 59, 60] as well as on the system level [29, 30, 31, 32, 61, 62, 63]. Usually, the studies are performed with discrete time series and the integration can then be replaced by a summation. Fewer publications exist on the modelling and integration of energy storage devices for chemical and thermal energy [13, 64, 65, 66, 67, 68, 69, 70]. In contrast to electricity, gaseous and liquid energy carriers can be stored either in the transportation facility itself or in locally concentrated storage facilities such as tanks or caverns. The process of increasing the pressure levels at both ends of the pipeline, allowing to store energy in the pipeline segment, is usually referred to as line pack [68].

Bibliography

- [1] R. C. Dugan and T. E. McDermott, “Distributed generation”, *Industry Applications Magazine, IEEE*, vol. 8, no. 2, p. 19, 2002, 1077-2618.
- [2] W. Patterson and M. Grubb, “Liberalizing European electricity: Impacts on generation and environment”, *Royal Institute of International Affairs Briefing Paper No. 34*, 1996.
- [3] N. Wohlgemuth, “Renewable energy and energy efficiency in liberalized European electricity markets”, *European Environment*, vol. 10, no. 1, pp. 1–11, 2000.
- [4] Great Britain Office of Gas and Electricity Markets, “Annual report 2005-2006”, 2006.
- [5] Great Britain Dept. of Trade and Industry, “Secretary of state’s second report to parliament on security of gas and electricity supply in Great Britain”, 2006.
- [6] European Commission, “The support of electricity from renewable energy sources”, *Communication from the Commission COM(2005) 627*. Commission of the European Communities, 2005.
- [7] R. Dugan and T. McDermott, “Operating conflicts for distributed generation on distribution systems”, *Rural Electric Power Conference, 2001*, 2001, pp. A3/1–A3/6.
- [8] UCTE, “Annual report 2005”, <http://www.ucte.org>, 2006.
- [9] Z. Li, “Natural gas for generation: a solution or a problem?”, *Power and Energy Magazine, IEEE*, vol. 3, no. 4, pp. 16–21, 2005.

-
- [10] M. Vignolo and R. Zeballos, “Transmission networks or distributed generation?”, *First International Symposium on Distributed Generation*. Stockholm: Royal Institute of Technology, 2001.
- [11] M. Shahidehpour, Y. Fu, and T. Wiedman, “Impact of natural gas infrastructure on electric power systems”, *Proceedings of the IEEE*, vol. 93, no. 5, pp. 1042–1056, 2005.
- [12] M. Geidl and G. Andersson, “Operational and structural optimization of multi-carrier energy systems”, *European Transactions on Electrical Power*, vol. 16, no. 5, pp. 463–477, 2006.
- [13] S. An, Q. Li, and T. W. Gedra, “Natural gas and electricity optimal power flow”, *IEEE/PES Transmission and Distribution Conference*, Dallas TX, 2003.
- [14] J. Munoz, *et al.*, “Natural gas network modeling for power systems reliability studies”, *Power Tech Conference Proceedings, 2003 IEEE Bologna*, vol. 4, p. 8, 2003.
- [15] A. Helseth and A. Holen, “Reliability modeling of gas and electric power distribution systems; similarities and differences”, *9th International Conference on Probabilistic Methods Applied to Power Systems*, Stockholm, Sweden, 2006.
- [16] B. H. Bakken and A. T. Holen, “Energy service systems: integrated planning case studies”, *Power Engineering Society General Meeting*, Denver, Colorado USA, 2004, p. 2068.
- [17] M. Geidl and G. Andersson, “Optimal power flow of multiple energy carriers”, *Power Systems, IEEE Transactions on*, vol. 22, no. 1, 2007.
- [18] M. Rausand and A. Høyland, *System reliability theory: models, statistical methods, and applications*, 2nd ed., Hoboken, NJ: Wiley-Interscience, 2004.
- [19] R. Billinton and R. N. Allan, *Reliability evaluation of engineering systems: concepts and techniques*, 2nd ed., New York: Plenum Press, 1992.
- [20] —, *Reliability Evaluation of Power Systems*, 2nd ed., New York: Plenum Press, 1996.

-
- [21] W. Li, *Risk assessment of power systems: models, methods, and applications*, IEEE Press series on power engineering. Piscataway, NJ: IEEE Press: Wiley-Interscience, 2005.
- [22] R. N. Allan, *et al.*, “Bibliography on the application of probability methods in power system reliability evaluation: 1987-1991,” *Power Systems, IEEE Transactions on*, vol. 9, no. 1, p. 41, 1994.
- [23] —, “Bibliography on the application of probability methods in power system reliability evaluation,” *Power Systems, IEEE Transactions on*, vol. 14, no. 1, p. 51, 1999.
- [24] R. Billinton, M. Fotuhi-Firuzabad, and L. Bertling, “Bibliography on the application of probability methods in power system reliability evaluation 1996-1999,” *Power Systems, IEEE Transactions on*, vol. 16, no. 4, p. 595, 2001.
- [25] C. Fünfgeld and R. Tiedermann, “Anwendung der repräsentativen VDEW-Lastprofile - step-by-step”, VDEW Materialien m05/2000, Brandenburgische Technische Universität, 2000.
- [26] W. Krewitt, *et al.*, “Market perspectives of stationary fuel cells in a sustainable energy supply system—long-term scenarios for Germany”, *Energy Policy*, vol. 34, no. 7, p. 793, 2006.
- [27] S. B. Riffat and X. Ma, “Thermoelectrics: a review of present and potential applications”, *Applied Thermal Engineering*, vol. 23, no. 8, p. 913, 2003.
- [28] M. Tanrioven and M. S. Alam, “Reliability modeling and analysis of stand-alone pem fuel cell power plants”, *Renewable Energy*, vol. 31, no. 7, p. 915, 2006.
- [29] G. N. Bathurst and G. Strbac, “Value of combining energy storage and wind in short-term energy and balancing markets”, *Electric Power Systems Research*, vol. 67, no. 1, p. 1, 2003.
- [30] Bagen and R. Billinton, “Incorporating well-being considerations in generating systems using energy storage”, *Energy Conversion, IEEE Transactions on*, vol. 20, no. 1, pp. 225–230, 2005.
- [31] M. Black and G. Strbac, “Value of storage in providing balancing services for electricity generation systems with high wind penetration”, *Journal of Power Sources*, vol. 162, no. 2, p. 949, 2006.

-
- [32] M. Korpås, R. Hildrum, and A. Holen, “Optimal operation of hydrogen storage for energy sources with stochastic input”, *Power Tech Conference Proceedings, 2003 IEEE Bologna*, vol. 4, p. 8, 2003.
- [33] S. J. Ehnberg and M. H. Bollen, “Reliability of a small power system using solar power and hydro”, *Electric Power Systems Research*, vol. 74, no. 1, pp. 119–127, 2005.
- [34] Bagen and R. Billinton, “Evaluation of different operating strategies in small stand-alone power systems”, *Energy Conversion, IEEE Transactions on*, vol. 20, no. 3, pp. 654–660, 2005.
- [35] R. Billinton and Bagen, “Incorporating reliability index distributions in small isolated generating system reliability performance assessment”, *Generation, Transmission and Distribution, IEE Proceedings-*, vol. 151, no. 4, pp. 469–476, 2004.
- [36] A. G. Bakirtzis, “A probabilistic method for the evaluation of the reliability of stand alone wind energy systems”, *Energy Conversion, IEEE Transactions on*, vol. 7, no. 1, p. 99, 1992.
- [37] X. Liu and S. Islam, “Reliability evaluation of a wind-diesel hybrid power system with battery bank using discrete wind speed frame analysis”, *9th International Conference on Probabilistic Methods Applied to Power Systems*, Stockholm, Sweden, 2006.
- [38] H. Holttinen, G. Giebel, and T. Nielsen, “Wind energy in the liberalised market - forecast errors in a day-ahead market compared to a more flexible market mechanism”, *2nd International Symposium on Distributed Generation*. Stockholm: Royal Institute of Technology, 2002.
- [39] M. Korpås, “Distributed energy systems with wind power and energy storage”, Ph.D. dissertation, 2004:39, Norwegian University of Science and Technology, 2004.
- [40] J. Matevosyan and L. Söder, “Optimal daily planning for hydro power system coordinated with wind power in areas with limited export capability”, *9th International Conference on Probabilistic Methods Applied to Power Systems*, Stockholm, Sweden, 2006.

- [41] G. Giebel, R. Brownsword, and G. Kariniotakis, “The state-of-the-art in short-term prediction of wind power - a literature overview”, ANEMOS (EU Framework 5) Development of a Next Generation Wind Resource Forecasting System for the Large-Scale Integration of Onshore and Offshore Wind Farms, 2003.
- [42] T. H. M. El-Fouly, E. F. El-Saadany, and M. M. A. Salama, “One day ahead prediction of wind speed using annual trends”, *Power Engineering Society General Meeting*, Montreal, Canada, 2006.
- [43] G. Kariniotakis, *et al.*, “Next generation forecasting tools for the optimal management of wind generation”, *9th International Conference on Probabilistic Methods Applied to Power Systems*, Stockholm, Sweden, 2006.
- [44] E. Castronuovo and J. Lopes, “On the optimization of the daily operation of a wind-hydro power plant”, *Power Systems, IEEE Transactions on*, vol. 19, no. 3, pp. 1599–1606, 2004.
- [45] J. Hull, *Options, futures, and other derivatives*, 6th ed., Upper Saddle River, NJ: Pearson, Prentice Hall, 2005.
- [46] G. Giebel, *et al.*, “Wind power prediction using ensembles”, Risø National Laboratory, Risø-R-1527(EN), 2005.
- [47] R. Hebner, J. Beno, and A. Walls, “Flywheel batteries come around again”, *IEEE Spectrum*, vol. 39, pp. 46–51, 2002.
- [48] R. Allan and R. Billinton, “Probabilistic assessment of power systems”, *Proceedings of the IEEE*, vol. 88, no. 2, p. 140, 2000.
- [49] Hochschule Burgdorf, <http://www.pvtest.ch>
- [50] S. Lemofouet and A. Rufer, “A hybrid energy storage system based on compressed air and supercapacitors with maximum efficiency point tracking (mept)”, *Industrial Electronics, IEEE Transactions on*, vol. 53, no. 4, p. 1105, 2006.
- [51] B. Roberts and J. McDowall, “Commercial successes in power storage”, *Power and Energy Magazine, IEEE*, vol. 3, no. 2, p. 24, 2005.
- [52] J. McDowall, “High power batteries for utilities - the world’s most powerful battery and other developments”, *Power Engineering Society General Meeting*, Denver, Colorado USA, 2004.

-
- [53] H. Holttinen, “Optimal electricity market for wind power”, *Energy Policy*, vol. 33, no. 16, p. 2052, 2005.
- [54] —, “The impact of large scale wind power production in the nordic electricity system”, Ph.D. dissertation, Helsinki University of Technology, 2004.
- [55] G. Koeppel and M. Korpås, “Using storage devices to compensate uncertainties caused by non-dispatchable generators”, *9th International Conference on Probabilistic Methods Applied to Power Systems*, Stockholm, 2006.
- [56] T. Christen and M. W. Carlen, “Theory of ragone plots”, *Journal of Power Sources*, vol. 91, no. 2, p. 210, 2000.
- [57] T. Christen and C. Ohler, “Optimizing energy storage devices using ragone plots”, *Journal of Power Sources*, vol. 110, no. 1, p. 107, 2002.
- [58] A. Schweiger, “Beiträge der Energiespeicherung für künftige, innovative Energiesysteme”, *IEWT 2003, 3. Internationale Energiewirtschaftstagung: Die Zukunft der Energiewirtschaft im liberalisierten Markt*, Vienna, 2003.
- [59] P. Ribeiro, *et al.*, “Energy storage systems for advanced power applications”, *Proceedings of the IEEE*, vol. 89, no. 0018-9219, pp. 1744–1756, 2001.
- [60] L. Chen, *et al.*, “Detailed modeling of superconducting magnetic energy storage (smes) system”, *Power Delivery, IEEE Transactions on*, vol. 21, no. 2, p. 699, 2006.
- [61] P. Barker, “Ultracapacitors for use in power quality and distributed resource applications”, *Power Engineering Society Summer Meeting, 2002 IEEE*, vol. 1, 2002, pp. 316–320 vol.1.
- [62] S. Kolluri, “Application of distributed superconducting magnetic energy storage system (d-smes) in the energy system to improve voltage stability vo - 2”, *Power Engineering Society Winter Meeting, 2002. IEEE*, vol. 2, 2002, pp. 838–841 vol.2.
- [63] C. A. Luongo, *et al.*, “A 100 mj smes demonstration at fsu-caps”, *Applied Superconductivity, IEEE Transactions on*, vol. 13, no. 2, p. 1800, 2003.

-
- [64] R. G. Carter and H. H. Rachford Jr., “Optimizing line-pack management to hedge against future load uncertainty”, *Pipeline Simulation Interest Group*, Berne, Switzerland, 2003.
- [65] W. J. van Rooyen, *et al.*, “Simulation and optimisation of gas storage tanks filled with heat sink”, *Nuclear Engineering and Design*, vol. 236, no. 2, p. 156, 2006.
- [66] H. Tanaka, T. Tomita, and M. Okumiya, “Feasibility study of a district energy system with seasonal water thermal storage”, *Solar Energy*, vol. 69, no. 6, p. 535, 2000.
- [67] M. Mohitpour, J. Szabo, and T. V. Hardeveld, *Pipeline operation and maintenance: a practical approach*, New York: ASME Press, 2005.
- [68] E. S. Menon, *Gas pipeline hydraulics*, Boca Raton, FL: Taylor & Francis, 2005.
- [69] A. Carpignano, *et al.*, “Reliability and availability evaluation for highly meshed network systems: status of the art and new perspectives”, *Proceedings of the Annual Reliability and Maintainability Symposium, 2002*, 2002.
- [70] D. Röttsch, *Zuverlässigkeit von Rohrleitungssystemen, Fernwärme und Wasser*, Berlin: Springer, 1999.

Curriculum vitae

- May 28, 1976 Born in Remagen, Germany
- 1983 – 1988 Primary school: Schulhaus Rütönen,
Windisch, Switzerland
- 1988 – 1992 Secondary school: Bezirksschule,
Windisch, Switzerland
- 1992 – 1996 Highschool: Alte Kantonsschule Aarau,
Aarau, Switzerland
- June 1996 Matura Type B
- 1996 – 2002 Study of Electrical Engineering
at ETH Zurich, Switzerland
- March 2002 Diploma in Electrical Engineering
at ETH Zurich, Switzerland
- 2002 – 2006 Assistant at the Power Systems Laboratory,
ETH Zurich;
PhD thesis under the supervision of
Prof. Dr. G. Andersson